Insights into the evolution and ecology of mammals from the Hell Creek region of northeastern Montana

Jordan R. Claytor

A dissertation

submitted in partial fulfillment of the

requirements for the degree of

Doctor of Philosophy

University of Washington

2023

Reading Committee:

Gregory P. Wilson Mantilla, Chair

Caroline A. E. Strömberg

Christian A. Sidor

Program Authorized to Offer Degree:

Biology

University of Washington

Abstract

Insights into the evolution and ecology of mammals from the Hell Creek region of northeastern Montana

Jordan R. Claytor

Chair of the Supervisory Committee:
Gregory P. Wilson Mantilla
Department of Biology

The Cretaceous-Paleogene (K-Pg) mass extinction event has historically been viewed as the catalyst for the radiation of mammals, with marked increases in body mass, taxonomic richness, and ecological disparity during the Paleocene biotic recovery. The majority of studies during this interval have focused on taxonomic proxies rather than ecological ones and applied the proxies over coarse spatiotemporal scales, potentially obscuring local patterns. Moreover, the taxonomic and ecological aspects of recovery often proceed at differing rates, thus interpretations based solely on taxonomic proxies may miss important details. In addition, recent analyses have demonstrated that several mammal groups began diversifying ecologically prior to the K-Pg mass extinction, changing how we view Mesozoic mammal communities. This dissertation seeks to add to our understanding of (i) the biotic recovery of mammals through

analyses of the taxonomic and ecological aspects of recovery in a limited spatiotemporal window (ii) the ecological diversity of Late Cretaceous mammals through an investigation of the ecology of the metatherian *Didelphodon*. My first study details the mammalian faunal assemblages from three vertebrate microfossil assemblages, the deposition of which we constrained to the first 28 ka to 80 ka of the Paleocene using new stratigraphic observations. Through quantitative and qualitative comparisons with other local faunas from the Hell Creek region and Denver Basin, we proposed a new model of biotic recovery that subdivides the already established 'disaster' and 'recovery' phases into early and late sub-phases, each characterized by differences in taxonomic composition. My second study utilized the new model to compare the taxonomic and ecological aspects of biotic recovery. We investigated both aspects over a large temporal interval, ~1 million years following the Cretaceous-Paleogene boundary (KPB), utilizing 2-dimensional ecospace models with estimates for body mass and dietary ecology for each taxon. Our results showed a concordance in taxonomic and ecological recovery, both reaching pre-mass-extinction levels 500–900 ka following the KPB. Moreover, there was increased ecological redundancy during the early phases of recovery, potentially related to abiotic or biotic factors, such as the environmental instability related to Deccan volcanism and the recovery of angiosperms, respectively. The last study used stable isotope analyses to investigate the ecology of *Didelphodon*. Using isotopes of oxygen ($\delta^{18}O$), and carbon ($\delta^{13}C$) derived from enamel and the established relationship between these values and numerous ecological factors, we determined that *Didelphodon* was likely the earliest known semiaquatic therian mammal. This finding adds to our understanding of the ecological diversity of Mesozoic mammals and provides a framework for future isotopic analyses. Overall, my results add to our understanding of the

ecology and evolution of mammals from the Hell Creek region and are potentially applicable to other studies of mammalian recovery patterns and ecological diversity

.TABLE OF CONTENTS

LIST OF FIGURES

CHAPTER 2: NEW MAMMALIAN LOCAL FAUNAS FROM THE FIRST CA. 80 KA OF THE PALEOCENE IN NORTHEASTERN MONTANA AND A REVISED MODEL OF BIOTIC RECOVERY FROM THE CRETACEOUS-PALEOGENE MASS EXTINCTION

LIST OF TABLES

ACKNOWLEDGMENTS

None of this work would be possible without the support of my amazing mentors, collaborators, friends, and family. I would first like to thank my advisor, Greg Wilson Mantilla, for his continued support throughout my graduate career. Over the course of the last six years, Greg has taught me how to be a diligent, meticulous researcher and a confident science communicator. I want to thank him for taking a chance on accepting me into the lab and letting me explore a wide range of interests, both scientific and otherwise. I'd also like to thank the rest of my committee, Chris Sidor, Caroline Strömberg, and Patricia Kramer, for their thoughtful feedback throughout my graduate career that was vital to my development as a researcher. Additionally, I'd like to thank the late Bill Clemens, whose expansive career built the foundation for my research. I was incredibly fortunate to have had many conversations with Bill early in my graduate career, many of which helped shape who I am as a researcher. I'd like to thank my research collaborators, Tom Tobin, Andy Schauer, and Kate Huntington, for their assistance in various research projects. Thank you, Tom, for helping me understand the geology and stratigraphy of the Hell Creek region; Andy for helping me fight Boris, the most temperamental mass spectrometer known to man; and Kate for giving me access to your lab space.

Outside of research, teaching has been a major portion of my graduate and subsequent professional careers, and I was fortunate to find unofficial advisors in both Elli Theobald and Ben Wiggins. Thank you, Elli, for hiring me as a TA for BIOL180. I truly treasured our conversations during weekly meetings or side conversations before lectures, and your advice for applying for teaching positions was invaluable. And thank you, Ben, for showing me what kind of educator, mentor, and friend I want to be. Ben has taken me under his wing and given me numerous opportunities to hone my skills. Additionally, he has been there for me during difficult periods, and it truly means the world to me. I'd also like to thank the rest of the UW Biology teaching staff and faculty: John Parks, Jon Herron, Scott Freeman, Christine Savolainen, Liz Warfield, Abby Gilbert, and Kyle Loucks. I've had a great time getting to know and learn from each of you.

The UW Biology community has been an incredible support system. Big thanks to the Biology administrative staff, both past and present: Marissa Heringer, Sarah O'Hara, Yen Lai, Davis Chong, Michele Conrad, Brianna Divine, Eddie Sabiniano, Alex Hansen, Dave Hurley, Ron Killman, Andrea Pardo, and Jeannette Takashima. I'd also like to thank Ben Kerr, Jennifer Nemhauser, and Karen Peterson for their guidance and support throughout my graduate career; I've learned valuable skills from each of them related to navigating academia and standing up for what I believe in. Additionally, I want to thank the larger graduate community within the Biology Department; it has been an honor to work alongside you all. I'd specifically like to thank the UW PaleoPod, both past and present, including Brandon Peecook, Meg Whitney, Savannah Olroyd, Elliot Armour Smith, Anna Brant, Bryan Gee, Camilla Crifó, Will Brightly, Alex Lowe, Elena Stiles, Ben Lloyd, and Chris Schiller. I've learned so much about paleontology and research more broadly from all of you and made some lifelong friends as well.

Outside of the University of Washington, I want to thank my mentors from Elon University, Antonio Izzo, Michael Kingston, and Kathy Galluci. Thank you, Antonio, for the help navigating the world of graduate school applications; Michael for being a great advisor and support system; and Kathy for hiring me as a TA for my junior year of college and introducing me to the world of teaching. I'd also like to thank Matt Carrano, who served as my advisor during an internship at the Smithsonian Museum of Natural History, where I was first introduced to paleontology. Thank you for bringing me into the world of paleontology, helping me find and get into a graduate program, and for your continued support during my time at UW.

I'd like to thank everyone at the Burke Museum who helped support my research and professional development as well. Specifically, Katie Anderson, Ron Eng, Meredith Rivin, and Jeff Bradley for helping with any of my collections or photography questions; Michael Holland and Kelsie Abrams for teaching me the ways of molding and casting; and Burke Operations for logistical help. I'd also like to thank the Burke Education and Outreach team for allowing me to participate in programs and helping to build professional skills. A special thank you to Alvin Logan for his advice, both personal and professional. I'd also like to thank the Burke field crews who assisted in the collection of my numerous fossils, with a special shoutout to Logan Knowles for being my field assistant for three seasons. I'd like to thank the Wilson Mantilla Lab undergraduates who worked hard to sort, identify, and catalog my fossils, with a special shoutout to Blake Knobbe, Eddy Armstrong, and Keith Sanderson for their help with other aspects of my dissertation. Lastly, I'd like to thank the ranchers, Jane and Dale Tharp, who allowed access to their land, without which none of this work would be possible.

I'd like to thank my funding sources and permitting agencies, without whom none of this work would have been completed. This includes the UW Biology Department, the Colorado

Scientific Society, the Society of Vertebrate Paleontology, the Paleontological Society, the North American Paleontological Conference, the National Science Foundation Graduate Research Fellowship Program along with the Bureau of Land Management, the Charles M. Russell Wildlife Refuge, the Army Corps of Engineers, and the state of Montana.

I have been fortunate to have worked with a great group of graduate and postdoctoral researchers in the Wilson Mantilla lab. The more senior members, Steph Smith, Dave Grossnickle, Alex Brannick, Luke Weaver, Brody Hovatter, and Paige Wilson Diebel, each took me under their wing and taught me important skills that have served me well throughout graduate school. I really appreciate all the time you each have taken to help me out and all the good times we've had together outside of research. And thanks to the junior members of the lab: Eddy Armstrong, Kirsten Meltesen, Jacqueline Silvira, and Isiah Newbins. I've really enjoyed watching you each come into your own as researchers, and I have appreciated all the help, jokes, and enthusiasm you've brought to the lab. I also want to thank the Wilson Mantilla lab management, Amanda Peng, Henry Fulghum, Dave DeMar, and Logan Knowles, for keeping the lab running smoothly.

A very special thank you to my cohort: Kavya Pradhan, Zoe Kulik, Marina Watowich, Jackson Tonnies, Aji John, Jazzmine Waugh, and Ashley Paynter. Our cohort was instantly a close-knit group and has remained that way throughout the last six years. Thank you all for all the support with research, academics, teaching, personal life drama, and so much more. I really couldn't have asked for a better group of people to have gone through this process with. Even though we're all going in different directions post-graduation I hope we remain as close-knit as we are now. You have truly been my Seattle family, and I'm going to miss you. Also, a big thanks to the cohort partners, Tim Slesinger, Guillermo Vera, Carly Busch, and Claudia Lopez,

for helping to keep us all sane and grounded. And a big thank you to my other friends who have been the best cheerleaders on the sidelines: Gaby Chiongbian, Tim Gagnon, Chris Tarpley, Dom Cadet, Justin Vieira, Carly Ackerman Canning, Franklin Kramer, Allie Duncan, Eddie and Ana Montero-Valdez and many more. Thank you to Nickolas Valentine for being the most supportive, caring, patient, and funny partner anyone could ask for. You've helped me immensely over the last few years, and I truly appreciate it. And thanks to the Uncles for taking me into your family during quarantine and introducing me to the cutest doodles in the world.

I'd lastly like to thank my family back in Maryland and Virginia. I'd specifically like to thank my parents, Hope Hall, and Bobby Claytor, for always supporting my passions and nurturing my love for science from a very young age. I am truly fortunate to have parents who go above and beyond to help make my dreams come true, and I love you both so much. I'd also like to thank Wyndy Webb for taking me in as her own son, helping me out throughout college and graduate school, and Ian Doanes for being a great little brother. Lastly, I want to thank my grandmother, Barbara Ann Hall, and my late grandfather, Earl Emory Hall. They both dedicated so much of their time to taking care of me as a kid; I wouldn't be the person I am today without you both.

CHAPTER 1: INTRODUCTION

The Cretaceous-Paleogene (K-Pg, hereafter) mass extinction 66 million years ago (MA) was a watershed moment in the evolution of life on Earth, marking the demise of the non-avian dinosaur and the formation of modern, mammalian-dominated terrestrial ecosystems (Simpson, 1937). The subsequent biotic recovery of mammals has historically been viewed as the beginning of an evolutionary radiation associated with increases in body mass, taxonomic richness, and ecological disparity (Lillegraven, 1972; Maas and Krause, 1994; Alroy, 1999; Smith et al., 2010; Wilson, 2013, 2014; Grossnickle and Newham, 2016; Halliday and Goswami, 2016; Chen et al., 2019; Wilson et al., 2021). However, the majority of these studies utilize taxonomic proxies and, to a lesser extent, ecological proxies, both of which are often applied over coarse spatiotemporal scales (i.e., regional-to-continental and hundreds of thousands to millions of years). As a result, mainly local, ecologically relevant patterns may have been obscured, limiting our understanding of the post-K-Pg biotic recovery. The first two studies presented here aim to address these issues through (i) detailed descriptions of multiple fossil assemblages and their geological context within a limited spatiotemporal framework and (ii) comparisons of the taxonomic and ecological aspects of biotic recovery.

Chapter Two of this dissertation focuses on novel descriptions of fossil assemblages and using the data to establish a new framework for biotic recovery within the Hell Creek region of northeastern Montana. The Hell Creek region features extensive exposures of the Hell Creek Formation and the Tullock Member, which preserve vertebrate fossil assemblages that sample a 3-Ma window spanning the K-Pg boundary (KPB; Swisher et al., 1993; Clemens, 2002; Renne et al., 2013; Sprain et al., 2015, 2018). Previous geological studies have resulted in a high-

resolution temporal framework that researchers have integrated fossil assemblages into (Archibald, 1982; Swisher et al., 1993; Wilson, 2005, 2014; Renne et al., 2013; Smith et al., 2018; Sprain et al., 2015, 2018; Weaver et al., 2022). Here I provided revised stratigraphy and faunal descriptions of three localities—Morales 1, Herpijunk Promontory, and Carrie Padgett 6—that allow for better integration into the established high-resolution temporal framework (Archibald, 1982). The age of the localities was constrained to the first 28 ka to 80 ka after the KPB, providing a high-resolution view into the biotic recovery of mammals. Along with detailed descriptions of the three local faunas, I also made quantitative and qualitative comparisons to other Hell Creek local faunas—Worm Coulee 1, Z-Line, and Luck O Hutch—resulting in a new model for biotic recovery within the Hell Creek region (Archibald, 1982; Lofgren, 1995; Clemens, 2002; Wilson, 2014; Sprain et al., 2018). I then tested the new model and explored potential heterogeneity in mammalian recovery through additional quantitative and qualitative comparisons with local faunas from the Denver Basin (Eberle, 2003; Middleton and Dewar, 2004; Dahlberg et al., 2016).

Chapter Three of this dissertation utilizes the new framework from *Chapter Two* to explore differences in the progression between the taxonomic and ecological aspects of biotic recovery. Studies investigating biotic recovery often rely on taxonomic proxies (i.e., taxonomic richness and evenness; Niklas et al., 1983; Benton, 1995; Wilson, 2014) and, to a lesser extent, ecological proxies (i.e., ecological diversity and disparity, or morphospace occupation; Sahney and Benton, 2008; Wilson, 2013; Grossnickle and Newham, 2016). However, the few studies to investigate both aspects show that they are often temporally decoupled, with either taxonomic or ecological outpacing the other (Foote, 1999; Erwin, 2007; Edie et al., 2018; Cole and Hopkins, 2021). If these two facets of biotic recovery are truly decoupled, then previous interpretations of

recovery patterns based solely on taxonomic proxies may be failing to capture the full picture. Moreover, understanding these dynamics may also inform us about the origin and maintenance of diversity and the assembly of communities.

In *Chapter Three*, I tested the possible decoupling of taxonomic and ecological recovery using an expanded version of the biotic recovery framework established in *Chapter Two*. I expanded the framework to capture the pre-extinction community along with the first 1.01 million years of the Paleocene (Sprain et al. 2018). I defined an ecosystem as fully recovered when the community had reached or surpassed levels of pre-extinction richness, either taxonomic or ecological. To investigate taxonomic recovery, I used taxonomic richness. For ecological recovery, I constructed two-dimensional ecospace models that allow for insights into how the combination of different ecological factors (body size and diet) influence the patterns of ecospace occupation. From the constructed ecospace models, I was able to calculate ecological richness, disparity, and functional evenness. These analyses allowed for direct comparisons of the tempo of taxonomic and ecological recovery and insights into how mammals occupied ecospace in the post-extinction communities.

Recent analyses and fossil discoveries suggest that several groups of mammals, including multituberculates, metatherians, and possibly placental eutherians, began diversifying both taxonomically and ecologically prior to the K-Pg (Wilson et al., 2012; Grossnickle and Polly, 2013; dos Reis et al., 2014; Grossnickle et al., 2019; Brannick and Wilson, 2020). *Chapter Four* focuses on investigating the ecology of a member of the metatherians, the stem-based clade that includes marsupials and their closest relatives, *Didelphodon*, using stable isotope analyses (Clemens, 1968; Rougier et al., 1998; Sereno, 2006; Wilson et al., 2016). *Didelphodon* is part of a clade of metatherians called the Stagodontidae, and members of the clade, including

Didelphodon, possess dentocranial characteristics that imply a durophagous ecology (Clemens, 1966; Lofgren, 1992; Fox and Naylor, 2006; Wilson et al., 2016; Cohen, 2017; Brannick and Wilson, 2020). In addition, the limited post-cranial remains referred to *Didelphodon* suggest a semiaquatic ecology, potentially making *Didelphodon* the earliest known semiaquatic and possibly molluscivorous therian (Salazy, 1994; Longrich, 2004; Borths, 2008; though see Fox and Naylor, 2006, for different interpretations). However, the limited post-cranial material presents a problem for understanding the ecology of *Didelphodon*. As such, for *Chapter Four*, I applied a morphology-independent technique, stable isotope analyses, to help elucidate the ecology of *Didelphodon*.

Stable isotope analyses have been utilized to answer numerous questions about the ecology of both extant and extinct mammals (Koch et al., 1989; Clementz and Koch, 2001; Thewissen et al., 2007; Secord et al., 2008; Clemens et al., 2019, 2020). Specifically, the majority of studies focus on the ratios of diagenetically resistant isotopes of oxygen ($\delta^{18}O$), and carbon ($\delta^{13}C$) derived from the carbonate component of enamel (Kohn and Cerling, 2002). $\delta^{18}O$ can be used as a proxy for understanding paleoclimates and habitat use (Koch et al., 1989, Clementz and Koch, 2001; Thewissen et al., 2007). Meanwhile, $\delta^{13}C$ can give insights into dietary ecology (Cerling and Ehleringer, 2000; Secord et al., 2008; Cullen et al., 2019, 2020). Utilizing the established relationships between the $\delta^{18}O$ and $\delta^{13}C$ values and different ecological factors, I conducted the first stable isotope analysis of enamel from *Didelphodon* to help better infer its ecology.

Chapter Five consists of concluding remarks and major takeaway from the previous three chapters.

Overall, this dissertation utilizes novel techniques and data to help further our understanding of the ecology of Mesozoic mammals and the biotic recovery of mammals following the K-Pg mass extinction event. *Chapter Two* establishes a novel framework for investigating the biotic recovery of mammals within the Hell Creek region and further afield to other Western Interior regions. *Chapter Three* provides new insights into the progression of biotic recovery within terrestrial communities, specifically the timing of recovery for both taxonomic and ecological metrics. *Chapter Four* establishes a novel line of evidence for the ecology of *Didelphodon* and adds to our growing understanding of Mesozoic mammal ecological diversity. Future collection efforts should aim to continually test and refine the framework and models established in *Chapters Two* and *Three.* Moreover, the methodology used in *Chapter Four* should be utilized as a means to investigate the ecology of other Mesozoic mammals that lack abundant post-cranial remains

1.1 REFERENCES CITED.

Alroy, J. (1999). The Fossil Record of North American Mammals: Evidence for a Paleocene Evolutionary Radiation. *Systematic Biology*, *48*(1), 107–118. https://doi.org/10.1080/106351599260472

Archibald, J. D. (1982). *A Study of Mammalia and Geology Across the Cretaceous-tertiary Boundary in Garfield County, Montana*. University of California Press.

Benton, M. J. (1995). Diversification and Extinction in the History of Life. *Science*, *268*(5207), 52–58. https://doi.org/10.1126/science.7701342

Brannick, A. L., & Wilson, G. P. (2020). New Specimens of the Late Cretaceous Metatherian Eodelphis and the Evolution of Hard-Object Feeding in the Stagodontidae. *Journal of Mammalian Evolution*, *27*(1), 1–16. https://doi.org/10.1007/s10914-018-9451-z

Cerling, T. E., & Ehleringer, J. R. (2000). Welcome to the C4 World. *The Paleontological Society Papers*, *6*, 273–286. https://doi.org/10.1017/S1089332600000802

Chen, M., Strömberg, C. A. E., & Wilson, G. P. (2019). Assembly of modern mammal community structure driven by Late Cretaceous dental evolution, rise of flowering plants, and dinosaur demise. *Proceedings of the National Academy of Sciences*, *116*(20), 9931–9940. https://doi.org/10.1073/pnas.1820863116

Clemens, W. A. (1966). *Fossil Mammals, Type Lance Formation, Wyoming. Part II. Marsupialia*. University of California Publications in Geological Sciences.

Clemens, W. A. (1968). Origin and Early Evolution of Marsupials. *Evolution*, *22*(1), 1–18. https://doi.org/10.2307/2406645

Clemens, W. A. (2002). Evolution of the mammalian fauna across the Cretaceous-Tertiary boundary in northeastern Montana and other areas of the Western Interior. In J. H. Hartman,

K. R. Johnson, & D. J. Nichols, *The Hell Creek Formation and the Cretaceous-Tertiary boundary in the northern Great Plains: An Integrated continental record of the end of the Cretaceous*. Geological Society of America. https://doi.org/10.1130/0-8137-2361-2.217

Clementz, M. T., & Koch, P. L. (2001). Differentiating aquatic mammal habitat and foraging ecology with stable isotopes in tooth enamel. *Oecologia*, *129*(3), 461–472. https://doi.org/10.1007/s004420100745

Cohen, J. E. (2018). Earliest Divergence of Stagodontid (Mammalia: Marsupialiformes) Feeding Strategies from the Late Cretaceous (Turonian) of North America. *Journal of Mammalian Evolution*, *25*(2), 165–177. https://doi.org/10.1007/s10914-017-9382-0

Cole, S. R., & Hopkins, M. J. (2021). Selectivity and the effect of mass extinctions on disparity and functional ecology. *Science Advances*, *7*(19), eabf4072. https://doi.org/10.1126/sciadv.abf4072

Cullen, T. M., Longstaffe, F. J., Wortmann, U. G., Goodwin, M. B., Huang, L., & Evans, D. C. (2019). Stable isotopic characterization of a coastal floodplain forest community: A case study for isotopic reconstruction of Mesozoic vertebrate assemblages. *Royal Society Open Science*, *6*(2), 181210. https://doi.org/10.1098/rsos.181210

Cullen, T. M., Longstaffe, F. J., Wortmann, U. G., Huang, L., Fanti, F., Goodwin, M. B., Ryan, M. J., & Evans, D. C. (2020). Large-scale stable isotope characterization of a Late Cretaceous dinosaur-dominated ecosystem. *Geology*, *48*(6), 546–551. https://doi.org/10.1130/G47399.1

Dahlberg, E. L., Eberle, J. J., Sertich, J. J. W., & Miller, I. M. (2016). A new earliest Paleocene (Puercan) mammalian fauna from Colorado's Denver Basin, U.S.A. *Rocky Mountain Geology*, *51*(1), 1–22. https://doi.org/10.2113/gsrocky.51.1.1

dos Reis, M., Donoghue, P. C. J., & Yang, Z. (2014). Neither phylogenomic nor palaeontological data support a Palaeogene origin of placental mammals. *Biology Letters*, *10*(1). https://doi.org/10.1098/rsbl.2013.1003

Eberle, J. J. (2003). Puercan mammalian systematics and biostratigraphy in the Denver Formation, Denver Basin, Colorado. *Rocky Mountain Geology*, *38*(1), 143–169. https://doi.org/10.2113/gsrocky.38.1.143

Edie, S. M., Jablonski, D., & Valentine, J. W. (2018). Contrasting responses of functional diversity to major losses in taxonomic diversity. *Proceedings of the National Academy of Sciences*, *115*(4), 732–737. https://doi.org/10.1073/pnas.1717636115

Erwin, D. H. (2007). Disparity: Morphological Pattern and Developmental Context. *Palaeontology*, *50*(1), 57–73. https://doi.org/10.1111/j.1475-4983.2006.00614.x

Foote, M. (1999). Morphological diversity in the evolutionary radiation of Paleozoic and post-Paleozoic crinoids. *Paleobiology*, *25*(sp1), 1–116. https://doi.org/10.1666/0094-8373(1999)25[1:MDITER]2.0.CO;2

Fox, R. C., & Naylor, B. G. (2006). Stagodontid marsupials from the Late Cretaceous of Canada and their systematic and functional implications. *Acta Palaeontologica Polonica*, *51*(1). https://bibliotekanauki.pl/articles/23125

Grossnickle, D. M., & Newham, E. (2016). Therian mammals experience an ecomorphological radiation during the Late Cretaceous and selective extinction at the K–Pg boundary. *Proceedings of the Royal Society B: Biological Sciences*, *283*(1832), 20160256. https://doi.org/10.1098/rspb.2016.0256

Grossnickle, D. M., & Polly, P. D. (2013). Mammal disparity decreases during the Cretaceous angiosperm radiation. *Proceedings of the Royal Society B: Biological Sciences*, *280*(1771), 20132110. https://doi.org/10.1098/rspb.2013.2110

Grossnickle, D. M., Smith, S. M., & Wilson, G. P. (2019). Untangling the Multiple Ecological Radiations of Early Mammals. *Trends in Ecology & Evolution*, *34*(10), 936–949. https://doi.org/10.1016/j.tree.2019.05.008

Halliday, T. J. D., & Goswami, A. (2016). Eutherian morphological disparity across the end-Cretaceous mass extinction. *Biological Journal of the Linnean Society*, *118*(1), 152–168. https://doi.org/10.1111/bij.12731

Koch, P. L., Fisher, D. C., & Dettman, D. (1989). Oxygen isotope variation in the tusks of extinct proboscideans: A measure of season of death and seasonality. *Geology*, *17*(6), 515–519. https://doi.org/10.1130/0091-7613(1989)017<0515:OIVITT>2.3.CO;2

Kohn, M. J., & Cerling, T. E. (2002). Stable Isotope Compositions of Biological Apatite. *Reviews in Mineralogy and Geochemistry*, *48*(1), 455–488. https://doi.org/10.2138/rmg.2002.48.12

Lillegraven, J. A. (1972). Ordinal and Familial Diversity of Cenozoic Mammals. *TAXON*, *21*(2–3), 261–274. https://doi.org/10.2307/1218194

Lofgren, D. L. (1992). Upper Premolar Configuration of Didelphodon vorax (Mammalia, Marsupialia, Stagodontidae). *Journal of Paleontology*, *66*(1), 162–164.

Lofgren, D. L. (1995). *The Bug Creek Problem and the Cretaceous-Tertiary Transition at McGuire Creek, Montana*. University of California Press.

Maas, M. C., & Krause, D. W. (1994). Mammalian turnover and community structure in the Paleocene of North America. *Historical Biology*, *8*(1–4), 91–128. https://doi.org/10.1080/10292389409380473

Middleton, M. D., & Dewar, E. W. (2016). New Mammals from the Early Paleocene Littleton Fauna (Denver Formation, Colorado). *Rocky Mountain Geology*, *51*(1), 1–22.

Niklas, K. J., Tiffney, B. H., & Knoll, A. H. (1983). Patterns in vascular land plant diversification. *Nature*, *303*(5918), Article 5918. https://doi.org/10.1038/303614a0

Renne, P. R., Deino, A. L., Hilgen, F. J., Kuiper, K. F., Mark, D. F., Mitchell, W. S., Morgan, L. E., Mundil, R., & Smit, J. (2013). Time Scales of Critical Events Around the Cretaceous-Paleogene Boundary. *Science*, *339*(6120), 684–687. https://doi.org/10.1126/science.1230492

Sahney, S., & Benton, M. J. (2008). Recovery from the most profound mass extinction of all time. *Proceedings of the Royal Society B: Biological Sciences*, *275*(1636), 759–765. https://doi.org/10.1098/rspb.2007.1370

Secord, R., Wing, S. L., & Chew, A. (2008). Stable isotopes in early Eocene mammals as indicators of forest canopy structure and resource partitioning. *Paleobiology*, *34*(2), 282–300. https://doi.org/10.1666/0094-8373(2008)034[0282:SIIEEM]2.0.CO;2

Sereno, P. C. (2006). Shoulder girdle and forelimb in multituberculates: Evolution of parasagittal forelimb posture in mammals. *Amniote Paleobiology: Perspectives on the Evolution of Mammals, Birds, and Reptiles*, 315–366.

Simpson, G. G. (1937). The Beginning of the Age of Mammals. *Biological Reviews*, *12*(1), 1–46. https://doi.org/10.1111/j.1469-185X.1937.tb01220.x

Smith, F. A., Boyer, A. G., Brown, J. H., Costa, D. P., Dayan, T., Ernest, S. K. M., Evans, A. R., Fortelius, M., Gittleman, J. L., Hamilton, M. J., Harding, L. E., Lintulaakso, K., Lyons, S. K., McCain, C., Okie, J. G., Saarinen, J. J., Sibly, R. M., Stephens, P. R., Theodor, J., & Uhen, M. D. (2010). The Evolution of Maximum Body Size of Terrestrial Mammals. *Science*, *330*(6008), 1216–1219. https://doi.org/10.1126/science.1194830

Smith, S. M., Sprain, C. J., Clemens, W. A., Lofgren, D. L., Renne, P. R., & Wilson, G. P. (2018). Early mammalian recovery after the end-Cretaceous mass extinction: A high-resolution view from McGuire Creek area, Montana, USA. *GSA Bulletin*, *130*, 2000–2014. https://doi.org/10.1130/B31926.1

Sprain, C. J., Renne, P. R., Clemens, W. A., & Wilson, G. P. (2018). Calibration of chron C29r: New high-precision geochronologic and paleomagnetic constraints from the Hell Creek region, Montana. *GSA Bulletin*, *130*(9–10), 1615–1644. https://doi.org/10.1130/B31890.1

Sprain, C. J., Renne, P. R., Wilson, G. P., & Clemens, W. A. (2015). High-resolution chronostratigraphy of the terrestrial Cretaceous-Paleogene transition and recovery interval in the Hell Creek region, Montana. *Geological Society of America Bulletin*, *127*(3–4), 393–409. https://doi.org/10.1130/B31076.1

Swisher III, C. C., Dingus, L., & Butler, R. F. (1993). 40Ar/39Ar dating and magnetostratigraphic correlation of the terrestrial Cretaceous–Paleogene boundary and Puercan Mammal Age, Hell Creek – Tullock formations, eastern Montana. *Canadian Journal of Earth Sciences*, *30*(9), 1981–1996. https://doi.org/10.1139/e93-174

Thewissen, J. G. M., Cooper, L. N., Clementz, M. T., Bajpai, S., & Tiwari, B. N. (2007). Whales originated from aquatic artiodactyls in the Eocene epoch of India. *Nature*, *450*(7173), 1190–1194. https://doi.org/10.1038/nature06343

Weaver, L. N., Tobin, T. S., Claytor, J. R., Wilson Deibel, P. K., Clemens, W. A., & Wilson Mantilla, G. P. (2022). Revised Stratigraphic Relationships Within the Lower Fort Union Formation (Tullock Member, Garfield County, Montana, U.S.A.) Prodive a New Framework for Examining Post-KPG Mammalian Recovery Dynamics. *PALAIOS*, *37*(4), 104–127. https://doi.org/10.2110/palo.2021.011

Wilson, G. P. (2005). Mammalian Faunal Dynamics During the Last 1.8 Million Years of the Cretaceous in Garfield County, Montana. *Journal of Mammalian Evolution*, *12*(1–2), 53–76. https://doi.org/10.1007/s10914-005-6943-4

Wilson, G. P. (2013). Mammals across the K/Pg boundary in northeastern Montana, U.S.A.: Dental morphology and body-size patterns reveal extinction selectivity and immigrant-fueled ecospace filling. *Paleobiology*, *39*(3), 429–469. https://doi.org/10.1666/12041

Wilson, G. P. (2014). Mammalian extinction, survival, and recovery dynamics across the Cretaceous-Paleogene boundary in northeastern Montana, USA. In G. P. Wilson, W. A. Clemens, J. R. Horner, & J. H. Hartman, *Through the End of the Cretaceous in the Type Locality of the Hell Creek Formation in Montana and Adjacent Areas*. Geological Society of America. https://doi.org/10.1130/2014.2503(15)

Wilson, G. P., Ekdale, E. G., Hoganson, J. W., Calede, J. J., & Vander Linden, A. (2016). A large carnivorous mammal from the Late Cretaceous and the North American origin of marsupials. *Nature Communications*, *7*(1), Article 1. https://doi.org/10.1038/ncomms13734

Wilson, G. P., Evans, A. R., Corfe, I. J., Smits, P. D., Fortelius, M., & Jernvall, J. (2012). Adaptive radiation of multituberculate mammals before the extinction of dinosaurs. *Nature*, *483*(7390), 457–460. https://doi.org/10.1038/nature10880

CHAPTER 2: NEW MAMMALIAN LOCAL FAUNAS FROM THE FIRST CA. 80 KA OF THE PALEOCENE IN NORTHEASTERN MONTANA AND A REVISED MODEL OF BIOTIC RECOVERY FROM THE CRETACEOUS-PALEOGENE MASS EXTINCTION

Claytor, J.R., Weaver, L.N., Tobin, T.S., Wilson Mantilla, G.P. New mammalian local faunas from the first ca. 80 ka of the Paleocene in northeastern Montana and a revised model of biotic recovery from the Cretaceous-Paleogene mass extinction. Accepted in the Journal of Vertebrate Paleontology.

2.1 AUTHOR CONTRIBUTIONS

JRC and GPWM conceived of the project; JRC, LNW, TST and GPWM conducted fieldwork related to the project, both specimen collections and stratigraphic observations, and contributed to the manuscript; JRC identified specimens, took photographs, conducted analyses, made figures, and wrote the main body of text.

2.2 ABSTRACT

The earliest phases of mammalian recovery following the Cretaceous-Paleogene (K-Pg) mass extinction are incompletely known but crucial to understanding the development of modern terrestrial ecosystems. Here we report new mammalian faunal data from three vertebrate microfossil assemblages in the Hell Creek region of northeastern Montana, the deposition of which we constrain to within the first 28 ka to 80 ka of the Paleocene using new stratigraphic observations within a high-resolution chronostratigraphic framework. We quantified the taxonomic diversity among these three assemblages and five other assemblages from both the Hell Creek region and Denver Basin, together spanning the first ca. 300 ka post-K-Pg mass

extinction. Our results allowed us to sub-divide the established 'disaster' and 'recovery' phases of recovery into the following sub-phases: (i) early disaster, characterized by the presence of 'dead clades walking,' high relative abundance of bloom taxa, and the appearance of post-extinction immigrants, (ii) late disaster, characterized by a reduction in the number of 'dead clades walking,' continued high relative abundance of 'bloom taxa', and a more diverse assemblage of immigrants (iii) early recovery, characterized by decreased relative abundance of bloom taxa, and continued immigration (iv) late recovery, characterized by the onset of in-situ diversification. We note important differences in the pattern and timing of mammalian faunal succession between the Hell Creek and Denver Basin, suggesting that post-K-Pg mammalian recovery was spatially heterogeneous. Our results provide a new model for post-K-Pg mammalian biotic recovery that can now be tested with other earliest Paleocene assemblages across western North America.

2.3 Introduction

The Cretaceous-Paleogene (K-Pg) mass extinction 66 million years ago (Ma) is a pivotal event in evolutionary history, resulting in the formation of the mammalian-dominated terrestrial ecosystems present today (Simpson, 1937). The Paleocene biotic recovery of mammals transitioned into an evolutionary radiation, particularly of placentals (but see dos Reis et al., 2014 for discussion of molecular evidence suggesting a latest Cretaceous radiation for placental mammals), associated with increases in body mass (Alroy, 1999; Smith et al., 2010; Wilson, 2013), taxonomic richness (Lillegraven, 1972; Maas and Krause, 1994; Wilson, 2014; Wilson et al., 2021), and ecological disparity (Wilson, 2013; Grossnickle and Newham, 2016; Halliday and Goswami, 2016; Chen et al., 2019; Grossnickle et al., 2019). This important interval in

mammalian history has been studied using a variety of taxonomic and, to a lesser extent, ecological proxies (e.g., Archibald, 1983a; Maas and Krause, 1994; Lillegraven and Eberle, 1999; Wilson, 2013, 2014; DeBey and Wilson, 2014; DeBey and Wilson, 2017; Smith et al., 2018; Lyson et al., 2019). However, those proxies have often been applied over coarse spatiotemporal scales (i.e., regional-to-continental and hundreds of thousands to millions of years), such that local, ecologically relevant patterns of interest are obscured because they are aggregated across biogeographic provinces, environmental gradients, and long temporal intervals. A key step toward obtaining higher-resolution patterns of the K-Pg biotic recovery and radiation of mammals is the detailed description of multiple fossil assemblages and their geological context (sedimentology, stratigraphy, and geochronology) within a single, local framework.

Here, we describe mammalian assemblages from three vertebrate microfossil localities from the lowermost Paleocene Tullock Member of the Fort Union Formation (Tullock Member, hereafter) in the Hell Creek region of northeastern Montana. The Hell Creek region is among the best places in the world to study the K-Pg mass extinction event and the subsequent biotic recovery and radiation from a terrestrial perspective. Extensive exposures of the Hell Creek Formation and the Tullock Member in Garfield and McCone County, Montana preserve vertebrate micro- and macrofossil assemblages that sample a ca. 3-Ma window spanning the K-Pg boundary (KPB) (Swisher et al., 1993; Clemens, 2002; Renne et al., 2013; Wilson et al., 2014; Sprain et al., 2015, 2018; see Clemens and Hartman, 2014 for a historical review). Paleontological studies of the mammalian assemblages from this region document a sequence of local faunas that encompass the Lancian, Puercan (Pu1 and Pu3 subzones), and earliest Torrejonian (To1 subzone) North American Land Mammal ‘ages ’(NALMAs, hereafter;

Archibald, 1982; Lofgren, 1995; Clemens, 2002; Wilson, 2005; Clemens and Wilson, 2009; Wilson, 2014; Smith et al., 2018). Geological studies have constructed a high-resolution temporal framework from magneto-, litho-, chemo-, and biostratigraphy and radioisotopic ages (Archibald et al., 1987; Swisher et al., 1993; LeCain et al., 2014; Renne et al., 2013; Moore et al., 2014; Hartman et al., 2014; Ickert et al., 2015; Sprain et al., 2015, 2018). With careful stratigraphic correlation, researchers have integrated the fossil assemblages from the region into that framework (Archibald, 1982; Lofgren, 1995; Clemens, 2002; Wilson, 2005, 2014; Smith et al., 2018; Weaver et al., 2022a).

The localities in this study—Morales 1, Herpijunk Promontory, and Carrie Padgett 6—are briefly mentioned by Archibald (1982), but paleontological and geological fieldwork conducted in the last 12 years has led to larger fossil sample sizes from these localities, refined understanding of their stratigraphic relationships, and better integration of their fossil assemblages into the high-resolution geochronological framework for the study areas. Indeed, we constrain the age of these localities, which are all located within a ~2 km^2 area, to the first ca. 80 ka after the KPB within C29r; this offers the highest resolution view yet known of the initial phase of post-K-Pg mammalian recovery in the Western Interior of North America. To better understand the temporal pattern of post-K-Pg mammalian recovery, we quantify the taxonomic diversity of these fossil assemblages and compare them to those from other early Puercan (Pu1) local faunas from the Hell Creek region (Archibald, 1982; Lofgren, 1995; Clemens, 2002; Wilson, 2014; Sprain et al., 2018), which have been integrated into the same geochronological framework. We also make comparisons to fossil assemblages from the farther afield Denver Basin (Eberle, 2003; Middleton and Dewar, 2004; Dahlberg et al., 2016) to explore the heterogeneity of biotic recovery patterns across the Western Interior.

Biotic Recovery. Biotic recovery is a complex evolutionary and ecological process that lacks a single, clear definition. We broadly describe biotic recovery as the return to pre-mass-extinction or similar levels of diversity (Kauffman and Harries, 1996; Erwin, 1998; Sahney and Benton, 2008). This process of biotic recovery is often characterized as a three-phase model derived from marine settings (Erwin, 1998). Phase 1, often referred to as the 'lag,' 'survival,' or 'disaster phase,' is the immediate aftermath characterized by low evenness and low taxonomic richness, along with high relative abundance of ecological generalist bloom taxa and low relative abundance of immigrant refugia species, taxa that were likely present nearby but did not appear in the fossil record until after the disaster (Harries and Kauffman, 1990; Schindler, 1990; Schubert and Bottjer, 1992; Erwin, 1993; Kauffman and Harries, 1996; Erwin, 1998; Smith et al., 2018). Phase 2, the 'recovery phase,' typically characterized by the appearance of new taxa that are phylogenetically closely related to previously documented taxa (presumably byproducts of in-situ diversification of refugia taxa or local survivors), a continued increase in taxonomic richness and relative abundance of non-bloom taxa, a decreased relative abundance of bloom taxa, and the reappearance of Lazarus taxa (Kauffman and Harries, 1996). Lastly, Phase 3, the 'recovered phase,' marks the return to, or exceeding of, pre-mass-extinction levels of richness and evenness (Kauffman and Harries, 1996; Erwin, 1998). We acknowledge that the previous descriptions of the three-phase model were derived from marine settings, and as such, the patterns observed may differ from those observed in the terrestrial realm. Therefore, we refine this model of biotic recovery to better fit the patterns observed in our terrestrial communities. We refer to the refugia species as immigrant taxa, due to the lack of resolution on their origins and the possible reoccupation of their original habitat (see the Faunal Recovery Groups section for information on taxonomic groupings; see Kauffman and Harries, 1996, for a more in-depth

assessment of refugia species). Moreover, we subdivide the phases based on our diversity analysis and stratigraphic interpretations of the three described localities, along with other localities from the Hell Creek region and the Denver Basin (chosen because its chronostratigraphic framework is comparable to that of the Hell Creek).

2.4 MATERIALS AND METHODS

Field Methods. The University of California Museum of Paleontology (UCMP) and the University of Washington Burke Museum of Natural History and Culture (UWBM) field crews collected the fossils included in this study over the last 40 years. Bulk sediment samples were collected from the fossiliferous horizons of the three vertebrate microfossil localities: Morales 1 (UCMP locality V77128 = UWBM locality C1671), Herpijunk Promontory (UCMP V77129 = UWBM C1153), and Carrie Padgett 6 (UCMP V77124 = UWBM C1360). The UWBM field crews collected over 2,000 kg of bulk sediment across all three localities; mass estimates of the bulk sediment collected by the UCMP crews are not available but are likely comparable. The bulk sediment samples were underwater screen-washed both in the field and then in the laboratory, using nested boxes with #18- and #30-size meshes (0.98-mm and 0.54-mm openings, respectively) and following procedures in Cifelli et al. (1996). Volunteers and students picked fossils from the resulting sediment concentrate with the aid of dissecting microscopes (10x magnification) at the UCMP and UWBM facilities (Cifelli et al., 1996). Here, we describe 398 mammalian specimens from these collections; specifically, those isolated premolars and molars and a few dentary- and maxillary fragments that are identifiable to the genus level or lower. Other mammalian specimens (189), mainly premolars and tooth fragments, were found as well.

Specimen descriptions and images can be found in Supplemental Materials. The geological descriptions for the localities are based mainly on our own field observations and measurements but also on the published literature (e.g., Archibald, 1982; Smit and Van der Kaars, 1984). We measured stratigraphic sections for the localities using a Jacob's staff and Abney level. When beds could not be physically traced on foot, we calculated stratigraphic distances from marker beds (e.g., coal layers) using high-resolution (< 1 m accuracy) Trimble R2 GNSS receivers (Wide Area Augmentation System enabled).

Taxonomic Metrics. Relative abundance and other taxonomic metrics were calculated to allow for quantitative comparisons across localities. Relative abundance was calculated as the number of identifiable specimens (NISP) of a taxon divided by the total number of specimens (identifiable to genus or lower) in the assemblage. We used NISP to represent individuals because the vertebrate microfossil assemblages described here were transported at least some distance by fluvial action prior to deposition and association of elements from the same individual is unlikely (Badgley, 1986; Rogers and Brady, 2010). Taxonomic richness was assessed using three metrics: raw richness, rarefied richness, and shareholder quorum subsampling (SQS) (Alroy, 2010). For each metric, richness was calculated at both the species and genus level to account for difficulties in assigning species-level identifications to certain isolated specimens. We compared the richness values of the three assemblages described in this paper with those from the latest Cretaceous Flat Creek local fauna (combined assemblages from Flat Creek 3 and 5; Wilson, 2014) along with three other earliest Paleocene assemblages from the Hell Creek region (Z-Line and Luck O Hutch [Smith et al., 2018] and Worm Coulee 1 [Wilson, 2014]) and two from the Denver Basin (Gars Galore [Dahlberg et al., 2016] and Littleton [Middleton and Dewar, 2004]), all of similar age.

To correct for differences in sampling intensity of assemblages, we calculated rarefied richness with 95% confidence intervals for each assemblage using the function rarefy() from the R package *vegan*, which uses the subsampling methodology of Hurlbert (1971). We ran rarefaction with sampling level N = (smallest sample size – 1). To account for differences in evenness structure of assemblages, we also subsampled with SQS following Holland (2015) based on Alroy (2010). To further account for differences in evenness, we ran SQS excluding the most common taxon (Alroy, 2010) and chose our quorum level (q) based on the assemblage with the lowest value (Luck O Hutch in all cases).

We calculated two other taxonomic diversity indices at genus level that incorporate both richness and relative abundance of taxa in each assemblage: Simpson's evenness (1-D; Simpson, 1949) and Pielou's evenness (J'; Pielou, 1966). These indices were chosen due to their relative ease of interpretation and emphasis on different aspects of relative abundance; Simpson's evenness emphasizes abundant taxa, whereas Pielou's evenness emphasizes rare taxa (Magurran, 2004). We also assessed faunal dissimilarity between assemblages at the genus level using the Bray-Curtis dissimilarity metric (BC) (Lance and Williams, 1967). BC performs well with small sample sizes but tends to emphasize abundant taxa (Krebs, 1989). We followed the double standardization method outlined in Donohue et al. (2013) and Smith et al. (2018) to balance the influence of abundant and rare taxa (Faith et al., 1987; Krebs, 1989). We conducted non-metric multidimensional scaling using Bray-Curtis dissimilarity at the genus level using abundance data to visualize the associations between assemblages and genera.

Institutional Abbreviations. **DMNH**, Denver Museum of Nature & Science, Denver, Colorado, U.S.A.; **UCM**, University of Colorado Museum, Boulder, Colorado, U.S.A.; **UCMP**, the University of California Museum of Paleontology, Berkeley, California, U.S.A.; **UW**, the

University of Washington, Seattle, Washington, U.S.A.: **UWBM**, the University of Washington Burke Museum of Natural History and Culture, Seattle, Washington, U.S.A.

Faunal Recovery Groups. We categorized each taxon from the post-KPB mammalian local faunas into one of four faunal recovery groups: dead clades walking, bloom taxa, immigrant taxa, or byproducts of in-situ diversification (see Supplemental Table 22). The term 'dead clades walking' (DCW; Jablonski, 2002) refers to taxa whose survival across an extinction event was short-lived. We define DCW as taxa present in the Lancian that locally survived the K-Pg mass extinction but attained only low relative abundance in the Pu1 and did not persist beyond that subinterval (e.g., *Cimexomys* spp.). Bloom taxa were also local survivors, typically ecological generalists, but found in high relative abundance during the disaster stage of biotic recovery (Kauffman and Harries, 1996; Erwin, 1998). We follow Wilson (2014) in categorizing *Mesodma* spp., *Thylacodon montanensis*, and *Procerberus formicarum* as bloom taxa. Immigrant taxa are defined as having made their first local appearance post-KPB and lacking a probable ancestor among Lancian local faunas in the same region (Weil and Clemens, 1998; Clemens, 2002, 2010). The archaic ungulates *Baioconodon*, *Protungulatum*, *Oxyprimus*, and *Mimatuta* and the eucosmodontid multituberculate *Stygimys*, all of which first appeared immediately after the KPB, are considered immigrants (but see Archibald et al., 2011 and Kelly, 2014 for possible pre-KPB immigration events of certain archaic ungulates). The byproducts of in-situ diversification are taxa (e.g., *Procerberus* cf. *P. grandis*) that are probable descendants of immigrant taxa or local survivors (Weil, 1998; Eberle, 2003; Clemens, 2010). This group includes members of clades that appear after the first appearance of the clade (e.g., eucosmodontid multituberculates, arctocyonid and periptychid archaic ungulates). Although these taxa could possibly represent later immigration events rather than in-situ diversification, they differ from the taxa that we

designate as ‘immigrants’ because they have congeners present in older local faunas from the region and in certain cases a demonstrated phylogenetic connection (Weil, 1999; McComas and Eberle, 2016). Although categorization of taxa into faunal recovery groups is imperfect, it provides a useful means to characterize the phases of post-KPB biotic recovery.

2.5 GEOLOGICAL BACKGROUND OF THE HELL CREEK REGION

The Hell Creek region of Garfield and McCone counties in northeastern Montana has exposures of the Hell Creek Formation (mostly uppermost Cretaceous) and Tullock Member of the Fort Union Formation (lower Paleocene). In this region, the Hell Creek Formation is ~90 m thick and is characterized by drab-colored (e.g., gray, purple) mudstones and sandstones, typically with gradational contacts between meter-scale strata (Archibald, 1982; Fastovsky, 1987; Hartman et al., 2014). The Tullock Member is ~80 m thick and is characterized by bright-colored (e.g., yellow, tan) mudstones and sandstones with sharp, clearly defined contacts between decimeter-scale strata and by common and laterally continuous low-grade coal or lignite layers (coals, hereafter) (Archibald et al., 1982; Fastovsky, 1987; Fastovsky and Bercovici, 2016). The contact between the Hell Creek and Fort Union formations is defined as the base of the stratigraphically lowest, laterally continuous coal layer, which is termed the ‘Z coal’ (Calvert, 1912; Collier and Knechtel, 1939; Brown, 1952; Moore et al., 2014; however, note the presence of the Null Coal [or Tonstein Lignite] in the Hell Creek Formation, ~25–30 m below the formational contact in some sections in eastern Garfield and western McCone counties [Rigby and Rigby, 1990; Lofgren, 1995; Sprain et al., 2015]). At many sites in central Garfield County, including our study areas, the Z coal immediately overlies the ‘impact claystone’ associated with the Chicxulub bolide impact, characterized by some combination of an iridium anomaly, shocked

quartz, and glassy spherules (Alvarez et al., 1980; Clemens and Hartman, 2014; Moore et al., 2014). As such, in our study areas the Z coal is referred to as the Iridium Z (IrZ) coal, and the Hell Creek-Fort Union contact is considered roughly coincident with the KPB (see Moore et al., 2014 for a review). In eastern Garfield County and western McCone County, the KPB impact layer has not been identified, and the uppermost ~1 m of the Hell Creek Formation is interpreted as early Paleocene in age (see Lofgren [1995] and Smith et al. [2018] for discussion; see also Tobin et al. [2021] for possible boundary identification).

2.6 GEOLOGY OF THE VERTEBRATE MICROFOSSIL LOCALITIES

The fossil localities described herein are vertebrate microfossil bonebeds (VMBs; Rogers and Brady, 2010)—accumulations of disarticulated and dissociated vertebrate hardparts (e.g., teeth, scales, and scutes), with elements predominantly in the millimeter to centimeter size range (≥ 75% of bioclasts ≤ 5 cm maximum dimension). Morales 1 (UCMP loc. V77128 = UWBM loc. C1671) and Herpijunk Promontory (UCMP loc. V77129 = UWBM loc. C1153) are in the Hauso Flats area within 750 m of each other, and Carrie Padgett 6 (UCMP loc. V77124 = UWBM loc. C1360) is in the adjacent Hell Hollow area, ~2 km to the east of Herpijunk Promontory (Fig. 2.1; Archibald, 1982). Previous work in the Hell Hollow area has mainly focused on the description of two fossil localities, Hell Hollow Channel and Worm Coulee 1 (UCMP locs. V74110 and V74111, respectively), their mammalian assemblages (Archibald, 1982; Wilson 2014), and, more recently, the sedimentology, stratigraphy, and geochronology of this area (Sprain et al., 2015, 2018; Weaver et al., 2022a). In contrast, the mammalian assemblages from the Hauso Flats area have not previously been described; rather, attention has focused on geological descriptions of KPB sections (Alvarez, 1983; Smit and van der Kaars,

1984) and related geochronology and geochemistry (e.g., Arens and Jahren, 2000, 2014; Renne et al., 2013; Tobin et al., 2021). Below, we revise the descriptions of the lithology and stratigraphy of the localities and discuss their ages on the basis of recent geochemical and geochronological studies (Renne et al., 2013; Moore et al., 2014; Hartman et al., 2014; Ickert et al., 2015; Sprain et al., 2018) and updates to the stratigraphic relationships in the lower Tullock Member (Weaver et al., 2022a).

Morales 1. This locality occurs on a ~3-m-tall, isolated hillock in the Hauso Flats area (Figs. 1 and 2). Vertebrate microfossils and gastropod and bivalve fossil shell fragments are found as surface float on the hillock slope and the surrounding flat at ground level. The basal 175 cm of the hillock is a dark gray, massive, silty claystone with irregular, iron staining (orange-red) and carbonized plant debris (~0.1–1.0 cm maximum dimension) (Fig. 2.3, Unit 1). Overlying this basal unit is a 30-cm-thick, greenish-gray, silty claystone characterized by iron staining, slickensides, sparse 5–20-cm-deep root traces with minimal branching, and sparse carbonized plant debris (~0.1–0.5 cm in maximum dimension)—all of these features are characteristic of the hydromorphic paleosols found in other nearby sections of the Hell Creek Formation (Fig. 2.3, Unit 2; Fastovsky and McSweeney, 1987). Vertebrate microfossils are hosted within a generally subangular, very-fine-grained sandstone with rare fine to medium-sized grains; the sandstone forms an irregular contact with the underlying green-gray, silty claystone unit of the Hell Creek Formation. The vertebrate microfossil-bearing sandstone also incorporates lenses of bivalve/gastropod shell-hash, carbonized plant debris, and abundant, pebble-sized mud rip-up clasts. This layer varies in thickness laterally from 1 cm to 10 cm (~5 cm on average) and thins to the southwest, consistent with the dip direction of the overlying strata (Fig. 2.2A; Fig. 2.3, Unit 3). Above the fossil-bearing unit is a 20-cm-thick, thinly laminated, silty claystone unit with

carbonized plant debris (Fig. 2.3, Unit 4). Overlying Unit 4 is a 30-cm-thick layer alternating every ~5 cm between a yellow, very-fine sandstone, similar to the fossil-bearing horizon though it lacks fossils, and a laminated, silty claystone (Fig. 2.3, Unit 5). These alternating coarse-to-fine lithologic units dip at an angle of ~5° to the southwest, consistent with lateral accretion surfaces that characterize point bar deposits (Fig. 2.2A; Thomas et al., 1987; Rogers, 1998). The uppermost unit is a 45-cm-thick, black-dark gray, thinly laminated claystone that also dips at an angle of ~5° to the southwest. This unit is characterized by abundant carbonized plant debris and becomes more fissile upsection.

Approximately 150 m north-northwest of Morales 1 across a flat is Iridium Hill (Fig. 2.1 and 2.2 B), where Alvarez (1983) and colleagues identified an iridium anomaly in a thin, reddish claystone (i.e., 'impact claystone') immediately underlying the Z coal (IrZ coal). The dark gray and greenish-gray, silty claystone units that underlie the IrZ coal and impact claystone at Iridium Hill can be traced laterally to the Morales 1 hillock (Fig. 2.2, Unit 2). The IrZ coal is not present in the hillock at Morales 1, although we would expect its presence based on a horizontal projection of the layer from Iridium Hill. We interpret the fossiliferous unit of Morales 1 and the overlying strata to represent channel-point-bar deposition during channel migration in the earliest Paleocene. In this model, the channel scoured through the IrZ coal and uppermost Hell Creek Formation at that location. This interpretation is consistent with previous stratigraphic interpretations of the strata near the KPB in the Hell Hollow and Hauso Flats areas (Archibald, 1982; Smit & van der Kaars, 1984), and to date no definitively Cretaceous-aspect fossils have been recovered from Morales 1.

Herpijunk Promontory. This vertebrate microfossil locality (Herpijunk, hereafter) occurs on a ledge, ~5 m above the base of a thick exposure of upper Hell Creek and lower Tullock sediments

approximately 700 m east-southeast of Morales 1 (Figs. 1 and 2). Vertebrate microfossils weather out onto the ledge, with some fossils eroding down the hillside onto the sandy flat below (Fig. 2.4A).

The fossil-bearing unit at Herpijunk is a 15-cm-thick clay-pebble conglomerate that forms the base of a 1.5-m-thick sequence of alternating ~10-cm-thick sandstone and ~0.5–1-cm-thick mudstone beds that dip ~5° to the west, consistent with lateral accretion bedding (Fig. 2.4 and Fig. 2.5, Units 9–11). The fossil-bearing horizon forms a sharp, irregular (and likely erosional) contact with an underlying 20-cm-thick, massive, light green-gray silty-claystone that is rich with carbonized plant debris and root traces (Fig. 2.5, Unit 8). Above the basal fossil-bearing pebble conglomerate, the coarse-grained units fine upwards vertically from medium-grained sands to very fine sands and up-dip from medium-grained sands to sandy siltstones. The entire lateral accretion deposit is overlain by a 1.2-m section of thinly laminated, black (with rust staining) silty claystone (Fig. 2.5, Unit 12). For a full stratigraphic log of the Herpijunk locality see Figure 5.

The Herpijunk locality is one point along the base of a laterally extensive channel deposit recognized by a lateral accretional surface in the outcrop across its extent (Fig. 2.4). Tracing the base of these deposits ~65 m to the northeast, this unit eventually crosscuts an exposure of the IrZ coal (Fig. 2.4B)—which hosts a confirmed impact claystone and has yielded the highest iridium anomaly in the region (~11.2 ppb; Smit and van der Kaars, 1984)—and the lateral extension of the MCZ coal (see ‘Geochronological framework for Hell Hollow and Hauso Flats areas’ section below), before grading upwards into horizontal beds ~2 m above the IrZ coal. On the basis of this sedimentological and stratigraphic evidence, we interpret the Herpijunk fossiliferous horizon as a lag or single-event deposit near the base of a point bar formed by an

earliest Paleocene channel as it scoured through the IrZ and MCZ coals and into underlying Hell Creek Formation strata, supporting the interpretation of Smit and van der Kaars (1984; Fig. 2.4B).

The inclined, lateral-accretion beds that characterize both Morales 1 and Herpijunk and crosscut the IrZ coal are present at lowermost Tullock exposures across the Hauso Flats area (along a nearly E-W transect) and can be traced to other vertebrate microfossil-bearing exposures geographically intermediate between those two localities. Given that (i) the depositional scenario for Herpijunk is nearly identical to that for Morales 1, (ii) both localities were deposited in the lowest portions of the Tullock Member, (iii) they are less than 1 km from each other, and (iv) we are able to trace the same point bar facies from Morales 1 to Herpijunk, we hypothesize that both vertebrate microfossil localities were formed in meanders of the same channel complex, which we term the Hauso Flats channel.

Carrie Padgett 6. This locality is at the base of a ~8-m-high and ~7-m-diameter grass-covered knob of fine-to-medium-grained, moderately well-indurated sandstone (Fig. 2.6); vertebrate microfossils are found as surface float near the base of this exposure and on the surrounding flat. The stratigraphically lowest unit exposed at Carrie Padgett 6 (Unit 1) is a 60-cm-thick, dark gray, silty claystone with popcorn weathering (Fig. 2.7, Unit 1). That same dark gray claystone can be physically traced to exposures ~100 m northwest of Carrie Padgett 6, where it is overlain by the Z coal and underlain by green-gray, silty claystone with light orange mottling (~5–10 cm in diameter) and abundant ~20-cm-deep root traces (Fig. 2.6). The Z coal (see Tobin et al., 2021 for further discussion) has been traced laterally across the Hell Hollow area and hosts a bentonite that has been radioisotopically and geochemically correlated with the bentonite from the IrZ coal at Iridium Hill in the adjacent Hauso Flats area (Renne et al., 2013; Ickert et al., 2015; Sprain et

al., 2015 and 2018). The fossil-bearing unit is a 15-cm-thick, very-fine- to fine-grained sandstone that hosts abundant pebble-sized, mud rip-up clasts, sulfur nodules (likely secondary modification of organic precursors), and 0.5–2.0-cm-diameter coal fragments (Fig. 2.7, Unit 2). This fossiliferous unit forms an abrupt, likely erosional contact with the dark gray claystone below. Overlying the fossiliferous unit is a white, fine-to-medium grained sandstone with 0.25–0.50-m-thick trough cross beds. We interpret this unit, which is 8-m-thick and extends to the top of the section at this outcrop (Fig. 2.7, Unit 6), as a channel deposit. Because this channel deposit overlies Hell Creek muds and the IrZ coal is missing in this section, we interpret the Carrie Padgett 6 locality as a channel-lag or single-event deposit at the base of an early Paleocene channel that scoured through the IrZ coal and into underlying Hell Creek strata. This interpretation is consistent with previous studies (Archibald, 1982; Weaver et al., 2022a) that showed that the Carrie Padgett channel deposit crosscuts both the older, early Paleocene-age Hell Hollow channel deposit, which hosts the Worm Coulee 1 vertebrate microfossil locality (UCMP V74111), and the IrZ coal. The Carrie Padgett channel deposit hosts several other vertebrate microfossil localities, of which only the Carrie Padgett 1 locality (UCMP V79100) has thus far yielded mammalian fossils. Eight mammalian fossils have been identified and cataloged from the site (UCMP 294522, 294524, and 294525: *Mesodma* sp.; UCMP 294523, and 294527: *Mesodma thompsoni*; UCMP 294526 *Mesodma formosa*; UCMP 150007: *Procerberus formicarum*; and UCMP 150027: *Mimatuta minuial*), although we have not had the opportunity to confirm the taxonomic identifications of the latter two specimens. Because the Carrie Padgett 1 locality is in close geographic proximity to Carrie Padgett 6 locality (~135 m northeast), is from the base of the same channel deposit, and is sedimentologically identical to the fossiliferous horizon at Carrie Padgett 6, we add its eight specimens to the Carrie Padgett 6 fossil assemblage and

hereafter treat the combined assemblage as the Carrie Padgett local fauna. Although the channel cut into latest Cretaceous-age Hell Creek strata, no definitively Cretaceous-aspect fossils have been recovered in our samples; thus, we consider the Carrie Padgett local fauna as early Paleocene in age.

Geochronological framework for Hell Hollow and Hauso Flats areas. The coal beds distributed throughout the Tullock Member typically contain multiple, sanidine-rich bentonites. Many of these bentonites have been sampled in the Hell Hollow and Hauso Flats areas and have yielded high-precision $^{40}Ar/^{39}Ar$ ages (Swisher et al., 1993; Renne et al., 2013; Sprain et al., 2015, 2018). The distinct Pb isotopic composition of the coal bentonites sometimes allow for even more precise correlations of potentially discontinuous coal layers than is possible from radioisotopic ages alone (Ickert et al., 2015). There has also been a significant amount of high-resolution paleomagnetic work in the Hell Hollow and Hauso Flats areas (Swisher et al., 1993; LeCain et al., 2014; Sprain et al., 2018). The impact claystone, characterized by an iridium anomaly and associated with the bolide impact, has been identified in the Hauso Flats area and potentially in the Hell Hollow area (see Tobin et al., 2021 for further discussion; Alvarez et al., 1980; Clemens and Hartman, 2014; Moore et al., 2014). We use the results of those studies and the observed stratigraphic relationships (Weaver et al., 2022a) of the relevant beds to constrain the depositional ages of the fossil localities in this study.

Three dated marker beds, or their lateral equivalents, are preserved in our study areas: the Iridium Z (IrZ), McGuire Creek Z (MCZ), and Hauso Flats Z (HFZ) coals. Those marker beds allow us to arrange the deposits hosting the mammalian fossil assemblages of interest (Morales 1, Herpijunk, and Carrie Padgett) in relative temporal order and to place them within the first ca. 28 to 80 ka after the KPB (Fig. 2.8). A bentonite within the IrZ coal, stratigraphically a few

centimeters above the impact claystone, has yielded a pooled mean $^{40}Ar/^{39}Ar$ age of 66.052 ± 0.008/0.043 Ma, which is treated as the age of the KPB (Swisher et al., 1993; Renne et al., 2013; Sprain et al., 2018). The MCZ coal, which was first identified ~75 km to the east of our study areas in the McGuire Creek area of McCone County (Lofgren, 1995), hosts a bentonite that has yielded a slightly younger (28 ± 18 ka) pooled mean age of 66.024 ± 0.014/0.044 Ma (Sprain et al., 2018). The MCZ bentonite from McCone County has been correlated to exposures in Garfield County based on a distinct Pb isotope signature that was detected by Ickert and colleagues (2015) in a carbonaceous-shale-hosted bentonite exposed in and around the Hauso Flats area; we call this the 'MCZ lateral extension' (see Fig. 2.1, square symbols). The highest relevant marker bed is the HFZ coal. This ~1.5–2-m-thick coal is exposed in both the Hauso Flats and Hell Hollow areas (among other places) and can be visually traced between those two study areas (Figs. 2, 4, and 6). Bentonites hosted within the HFZ coal have been correlated, both geochemically and radioisotopically, across areas where it is exposed and have yielded an age of 65.973 ± 0.020/0.047 Ma (Ickert et al., 2015; Sprain et al., 2015, 2018; Fendley et al., 2019).

Depositional age of the vertebrate microfossil localities in the Hell Hollow and Hauso Flats areas. We interpret all three of the focal localities in this study as hosted within channel deposits that scoured through, and are thus geologically younger than, the IrZ coal (and by extension the KPB). At the Herpijunk locality section, the Hauso Flats channel also scoured through a stratigraphically higher, ~10-cm-thick carbonaceous shale that can be laterally traced to the MCZ lateral extension at the Nirvana section ~830 m to the east-southeast (Ickert et al., 2015; Sprain et al., 2018; Figs. 3 and 8). Given that the top of the Hauso Flats channel lies only ~2 m above the IrZ and ~10–20 cm above the MCZ lateral extension, we interpret the deposition of the Herpijunk fossiliferous horizon to have been shortly after the deposition of the MCZ coal. Thus,

we bracket the age of the deposition of the Herpijunk fossiliferous horizon between the ages of the MCZ and HFZ coals but recognize that it is likely towards the older end of that age bracket, as suggested by the stratigraphic proximity of the top of the Hauso Flats channel and the MCZ coal (Fig. 2.8; 66.024 ± 0.014/0.044 Ma and 65.973 ± 0.020/0.047, respectively; Sprain et al., 2018). The Morales 1 locality section does not preserve the MCZ lateral extension, presumably because there are not enough overlying strata preserved on the hillock or because the Hauso Flats channel scoured through the MCZ lateral extension locally. Nevertheless, because we interpret this vertebrate microfossil concentration, like Herpijunk, as having been deposited in the Hauso Flats channel complex, we also bracket the age of the deposition of the Morales 1 fossiliferous horizon between the ages of the MCZ and HFZ coals and likely towards the older end of that age bracket (Fig. 2.8; 66.024 ± 0.014/0.044 Ma and 65.973 ± 0.020/0.047, respectively). The Carrie Padgett 6 locality is at the base of the much thicker Carrie Padgett channel complex (Archibald, 1982; Weaver et al., 2022a), the top of which is ~8 m above the IrZ coal (and thus stratigraphically above the top of the Hauso Flats channel deposits). An MCZ-equivalent coal or carbonaceous shale has not yet been identified in the Hell Hollow area. However, at the Herpijunk locality section in the Hauso Flats area, there is a ~6.4-m-thick sandstone bed that is lithologically nearly identical to the Carrie Padgett sandstone (as described in Weaver et al., 2022a), the base of which is ~4 m above the MCZ-equivalent carbonaceous shale and the Hauso Flats channel (Fig. 2.5). This extension of the Carrie Padgett channel in the Hauso Flats area does not scour the MCZ lateral extension, which implies that either (1) the Carrie Padgett channel deposit in Hauso Flats is younger than that exposed in Hell Hollow or (2) the Carrie Padgett channel did not scour as deeply in Hauso Flats as it did in Hell Hollow. In either case, we interpret the Carrie Padgett channel as having been formed after deposition of the Hauso

Flats channel, MCZ coal, and IrZ coal given its stratigraphic position above those three units. Previous work has also demonstrated that the Carrie Padgett channel crosscut, and was thus deposited after, the Hell Hollow channel (Weaver et al., 2022a), which is the sedimentary unit that hosts the well-sampled Worm Coulee 1 vertebrate microfossil locality (Archibald, 1982; Wilson, 2014). Nonetheless, in the Hell Hollow area, the Hell Hollow channel deposit, host to the Worm Coulee 1 local fauna, spans the same stratigraphic interval as the Carrie Padgett channel, and therefore it too likely formed after the deposition of the MCZ coal and Hauso Flats channel (Weaver et al., 2022a; but see Archibald, 1982 for a different interpretation). We interpret the depositional age of the Carrie Padgett fossiliferous horizon as younger than the Hauso Flats channel but still bracketed between the ages of the MCZ and HFZ coals (Fig. 2.8; 66.024 ± 0.014/0.044 Ma and 65.973 ± 0.020/0.047, respectively; Sprain et al., 2018).

Taken together, all the localities in our study and some of those previously studied from these areas (Archibald, 1982; Wilson, 2014) were deposited between 28 ka and 80 ka after the KPB. We can arrange them into a temporal succession from oldest to youngest: (1) Herpijunk and Morales 1, (2) Worm Coulee 1, and (3) Carrie Padgett (Weaver et al., 2022a; Fig. 2.8). Note that the fossil concentrations associated with channel deposits may have been sourced from any of the strata (and possibly multiple strata) within the stratigraphic interval of the channel deposit (Rogers and Brady, 2010; Weaver et al., 2022a). Thus, the temporal constraints of the fossil assemblages may differ from the temporal constraints of the channel deposits discussed here. Because the paleochannels associated with our fossil concentrations scoured into underlying Hell Creek strata, although not deeply (0.5–1 m), latest Cretaceous fossils might have been incorporated into our assemblages; however, thus far we have not documented any definitively

Cretaceous-aspect fossils in them to indicate reworking of vertebrate remains from below the KPB.

Other Pu1 Western Interior localities. From adjacent western McCone County come two additional points of faunal comparison: the Z-Line local fauna (from UCMP locs. V84193 and V84194) and the Luck O Hutch (LOH, hereafter) local fauna (from UCMP loc. V88036). The taxonomic composition and diversity of both local faunas have previously been described in detail (Lofgren, 1995; Smith et al., 2018). Their localities are near each other in the McGuire Creek area and have been integrated into their local chronostratigraphic framework (Sprain et al., 2015, 2018; Smith et al., 2018). The KPB impact claystone has not been identified in McCone County, but a carbonaceous shale that underlies the Z-Line localities is interpreted as the KPB on the basis of vertebrate biochronology and carbon isotope stratigraphy (Arens et al., 2014; but see Tobin et al., 2021 for an alternative view on identification of the KPB using carbon isotopes). The Z-Line localities are thus bracketed between the KPB and the MCZ coal (Fig. 2.8; Smith et al., 2018) and are the oldest localities considered in this study. The LOH locality is stratigraphically above the MCZ coal and below the C29r/C29n boundary (65.724 ± 0.013/0.044 Ma; Sprain et al., 2018). Thus, it is younger than the Z-Line localities, but it is not yet possible to definitively determine the age of LOH relative to the Worm Coulee 1 and Carrie Padgett localities—their corresponding bracketed temporal intervals overlap substantially (Fig. 2.8; Smith et al., 2018). Nevertheless, because the channel deposits, which host the localities, only slightly overlap in stratigraphic position (Fig. 2.8), we suggest that the LOH local fauna is probably younger than the Hell Hollow and Carrie Padgett local faunas.

More geographically distant points of faunal comparison come from the Denver Basin's Gars Galore and Littleton local faunas (DMNH loc. 2560 and UCM locs. 77267 and 77283,

respectively). Gars Galore yields a Pu1 local fauna that is from 9 m above the locally identified KPB (Dahlberg et al., 2016). The estimated age of the Gars Galore locality is ca. 65.893 Ma or ~128 ka after the KPB, based on the median sediment accumulation rate derived from the new age model in Clyde et al. (2016); this age is within the age range of LOH in the Hell Creek region. The Littleton local fauna has been interpreted as 100–300 ka after the KPB (Lyson et al., 2019), which is younger than all the Hell Creek region local faunas discussed in this study, except possibly LOH (Smith et al., 2018).

2.7 RESULTS

Raw and Subsampled Richness. To compare taxonomic richness among the local faunas of interest, we calculated raw richness, rarefied richness, and shareholders quorum subsampling (SQS) at both the species (see Supplemental Information) and genus level (Fig. 2.9). Out of the newly described local faunas Herpijunk has the highest values (13 spp., 9 gen.; Fig. 2.9), similar to those from other Pu1 local faunas from both the Hell Creek region (Worm Coulee 1 and Luck O Hutch) and Denver Basin (Gars Galore; Fig. 2.9). Z-Line and Carrie Padgett have the lowest raw species- and generic-richness values (10 spp., 8 gen. and 10 spp., 7 gen. respectively; Fig. 2.9). The Littleton local fauna, which is likely the youngest of the Pu1 local faunas included here, has substantially higher richness values for all metrics at both the species and genus level (raw richness: 20 spp., 15 gen.; Fig. 2.9). The rarefied and SQS values of all the Pu1 local faunas, except the Littleton local fauna, are much lower compared to the values of the Lancian Flat Creek local fauna (28 spp., 21 gen.).

Evenness Metrics. We calculated Simpson's evenness (Fig. 2.10) and Pielou's evenness (Supplementary Information) at the genus level to investigate changes in community structure of

the local faunas, specifically the relative abundance structure. Higher values for these indices indicate a local fauna with a more even distribution of relative abundances across its constituent taxa; whereas lower values indicate a local fauna with an uneven distribution of relative abundances (i.e., predominated by a few taxa). The Lancian Flat Creek local fauna has high evenness (0.85 for Simpson's evenness), whereas the Pu1 local faunas values have mostly lower evenness and fall into three groups: (1) the five local faunas deposited in the earliest Paleocene (< 130 ka post-KPB, ca. 65.893 Ma) except Worm Coulee l have low evenness (0.30–0.40 for Simpson's evenness; Fig. 2.10), significantly less than that for Flat Creek; (2) the LOH local fauna (ca. 28–328 ka post-KPB) has moderate evenness (0.50 for Simpson's evenness; Fig. 2.10), although not significantly greater than the values in Group 1; and (3) the Worm Coulee 1 and the Littleton local faunas have higher evenness (0.75 and 0.89 for Simpson's evenness, respectively; Fig. 2.10), significantly greater than those for all the other Pu1 local faunas and, in the case of the Littleton local fauna (ca.100–300 ka post-KPB), statistically indistinguishable from that for the Lancian Flat Creek local fauna. Thus, the Pu1 local faunas had low evenness through the first 80 to 100 ka post-KPB except for the anomalously high evenness for Worm Coulee 1, and there was an increase in evenness between 100 and 300 ka post-KPB, with higher values for both Luck O Hutch and the Littleton local fauna (nonsignificant and significant, respectively). Values for Pielou's evenness largely follow the same pattern (see Supplemental Information).

Faunal Dissimilarity Metrics. The Bray Curtis (BC) dissimilarity values indicate how dissimilar two local faunas are in taxonomic composition and relative abundance structure. Higher values indicate a greater degree of dissimilarity between local faunas. The Littleton local fauna is the most dissimilar among our selected Pu1 local faunas (BC: 0.67–0.81 at the genus

level; Table 2.1). This pattern is not driven by inter-basin distance—the Littleton and Gars Galore local faunas are highly dissimilar from each other as well (0.77 at the genus level). Worm Coulee 1 is also highly dissimilar to the other assemblages (BC: 0.44–0.74; see Discussion for more detailed explanation). Comparisons among all other Pu1 local faunas yield low to moderate dissimilarity, indicating similar taxonomic composition and relative abundance structure (BC: 0.17–0.46; Table 2.1).

These results are graphically reflected in the non-metric multidimensional scaling (NMDS) analysis (Fig. 2.11). Coordinate 1 shows the high dissimilarity between the Littleton local fauna (Fig. 2.11, far right) and all other Pu1 local faunas (center). Coordinate 2 does not segregate among the other Pu1 local faunas; however, some genera that are found exclusively at Worm Coulee (*Prodiacodon* and *Acheronodon*) and Luck O Hutch (*Prodiacodon* and Periptychidae indet.) plot in the upper quadrant. Moreover, genera found exclusively at Morales 1 (*Puercolestes)* and Gars Galore (*Mairoana)* plot towards the lower margin.

2.8 DISCUSSION

Newly Described Local Faunas. We assign all three mammalian local faunas described here—Morales 1, Herpijunk, and Carrie Padgett—to the Pu1 interval zone of the Puercan NALMA based on the presence of characteristic taxa (Table 2.2, e.g., *Stygimys kuszmauli*, *Procerberus formicarum*, *Thylacodon montanensis*, *Oxyprimus erikseni*, *Protungulatum donnae*; Lofgren et al., 2004). Previous work also supports this designation (Archibald, 1982; Archibald et al., 1987; Wilson, 2014). The Pu1 interval zone constrains these local faunas to the first ca. 300 ka of the Paleocene (Lofgren et al., 2004). Using the chronostratigraphic framework for the Hell Creek region, we further constrain the deposition of these mammalian fossil assemblages between the

first ca. 28 ka and 80 ka of the Paleocene; this offers the highest resolution view yet known of the initial phase of post-K-Pg mammalian recovery (Fig. 2.8). These local faunas resemble each other and previously described post-KPB 'disaster' local faunas including Z-Line and Worm Coulee 1 (Wilson, 2014; Smith et al., 2018). The taxonomic composition is fairly consistent among them, as shown by the low taxonomic dissimilarity values and clustering in the NMDS plot (Table 2.1 and Fig. 2.11). Each of the three local faunas has low evenness, particularly at the genus level, which is typical of 'disaster' local faunas (Harries and Kauffman, 1990; Erwin, 1993; Wilson, 2014; Smith et al., 2018). This pattern is driven by the high relative abundance of the multituberculate genus *Mesodma* (> 70% of the individuals in each assemblage; Fig.11 and Table 2.2). *Mesodma* has been interpreted as a local survivor of the K-Pg mass extinction that proliferated in the aftermath with increases in relative abundance from ~20–40% pre-K-Pg to ~70–80% post-K-Pg (bloom taxon); its numerical abundance was perhaps due to some combination of its small body size, generalized diet, and reproductive strategy (Clemens, 2002; Wilson et al., 2012; Wilson, 2013, 2014; Weaver et al., 2022b). Two other taxa previously identified as post-KPB mammalian bloom taxa, the metatherian *Thylacodon montanensis* and the eutherian cimolestid *Procerberus formicarum* (Wilson, 2013; Wilson, 2014), occur in the three local faunas described here but in low relative abundances (< 5% and 10%, respectively) inconsistent with their bloom taxon designation. Immigrant taxa, including the archaic ungulate genera *Baioconodon*, *Protungulatum*, *Oxyprimus*, and *Mimatuta* and the eucosmodontid multituberculate *Stygimys kuszmauli*, also occur in low relative abundances (each < 5% of individuals) like in other Pu1 'disaster' faunas (Lofgren, 1995; Wilson, 2014; Smith et al., 2018). The high relative abundance of the bloom taxon *Mesodma*, the high degree of similarity among the Morales 1, Herpijunk, and Carrie Padgett local faunas, and their low evenness suggest that

they sample what has broadly been termed the disaster interval of the post-KPB biotic recovery (Fig. 2.13).

From Post-KPB Disaster to Recovery Phase in the Hell Creek Region. The Worm Coulee 1 local fauna has long stood as the standard-bearer for the post-KPB disaster phase of the recovery in the Hell Creek region (Archibald, 1982; Archibald et al., 1987; Clemens, 2002; Wilson, 2014). By comparison with the pre-KPB Lancian local faunas (e.g., Flat Creek 5), the disaster-phase mammalian fauna has thus been characterized as having (i) low species richness (Fig. 2.9; Wilson, 2014), (ii) substantial taxonomic turnover (e.g., disappearance of ≥ 75% of Lancian taxa, Wilson, 2014), and (iii) highly uneven community structure (Fig. 2.10; Wilson, 2014), driven by a few local bloom taxa (*Mesodma thompsoni*, *Procerberus formicarum*, and *Thylacodon montanensis*) with high relative abundances and a substantial number of immigrant taxa (seven archaic ungulate species and *Stygimys kuszmauli*) with low relative abundances (Clemens, 2002; Clemens, 2010; Wilson, 2014). Now, with additional sampling and description of mammalian assemblages from the lowermost Paleocene, greater precision on the age of these assemblages, and quantitative analysis of the diversity of these and other assemblages from the first 300 ka post-KPB (= Pu1 interval zone), we can refine our model of the disaster and recovery phases of mammalian recovery in the Hell Creek region. We focus on the following Pu1 local faunas from the region: Morales 1, Herpijunk, and Carrie Padgett (this study) as well as Z-Line and Luck O Hutch (Lofgren, 1995; Smith et al., 2018) and Worm Coulee 1 (Archibald, 1982; Wilson, 2014).

Early Disaster Sub-Phase. The Z-Line local fauna from the McGuire Creek area is from the oldest deposits among the Hell Creek region Pu1 local faunas (Fig. 2.8). It is distinct from the Worm Coulee 1 local fauna as well as the other Pu1 local faunas. The Z-Line local fauna has some of the lowest richness values, although not significantly less, for all three metrics at the

genus level (raw = 6 genera, rarefied = 4.8 genera, and SQS = 2.6 genera; Fig. 2.9). Among the immigrant taxa that characterize the Pu1 (*Protungulatum donnae*, *Baioconodon* spp., *Mimatuta* spp., *Oxyprimus erikseni*, and *Stygimys kuszmauli*), only *Mimatuta* sp. is present in the Z-Line local fauna; whereas at least three are present in each of the other Pu1 local faunas included in this study. Additionally, the Z-Line local fauna is the only Pu1 local fauna to have multiple Lancian-aspect taxa including several metatherians (*Leptalestes*, two specimens referred to Alphadontidae indet., and four referred to Metatheria indet.), which Smith et al. (2018) classified as 'dead clades walking' (Jablonski, 2002). Nonetheless, in our NMDS plot the local fauna does not segregate from other Pu1 local faunas, driven primarily by the abundance of *Mesodma* (Fig. 2.11). We hypothesize that these faunal differences are evolutionarily significant, reflecting an earlier stage of post-KPB recovery than do the other Pu1 local faunas. Several of the following hypotheses could explain some or all these faunal differences, but we contend that they are not as well supported by the available data: (i) sampling of the Z-Line local fauna is still relatively incomplete; (ii) there is a taphonomic bias against larger-bodied archaic ungulates at Z-Line; and/or (iii) as the easternmost of the Hell Creek localities, Z-Line captures a distinct depositional environment. Indeed, the combined sample size of the Z-Line assemblages (N = 116) is considerably less than those of Morales 1 (N = 248) and Worm Coulee 1 (N = 920); nevertheless, we largely discount the sampling hypothesis (i) because the rarefaction curve for Z-Line (Smith et al., 2018:Fig. 2.5) is nearly asymptotic compared to those for other local faunas with similar sample sizes, indicating that more sampling probably would not substantially alter the faunal composition. The size-bias hypothesis (ii) does not seem likely considering that *Mimatuta* sp., which is similar in size to the other archaic ungulates, and other larger vertebrate fossils (e.g., champsosaur vertebrae) have been recovered from the Z-Line localities. Addressing

hypothesis (iii) the Z-Line localities are hosted in a fine-to-medium-grained channel deposit, which is lithologically similar to the depositional environments of all the other localities under consideration here, and the size and taxonomic makeup of their vertebrate microfossil assemblages are consistent with the other Pu1 localities reported here, suggesting they had similar taphonomic origins (Rogers and Brady, 2010; Rogers et al., 2017). Thus, although it is impossible to entirely reject that the distinctness of the Z-line local fauna simply reflects paleoenvironmental heterogeneity, those paleoenvironmental differences must have been subtle enough so as not to leave an appreciable impression on the sedimentology of the site. Therefore, our working hypothesis is that the Z-Line local fauna represents the earliest documented stage of post-KPB recovery, which we refer to as the 'early disaster sub-phase' and bracket between 66.052 ± 0.008/0.043 and 66.024 ± 0.014/0.044 Ma or the first 28 ka following the KPB (Sprain et al., 2018; Fig. 2.13). We characterize the early disaster sub-phase by the presence of multiple dead clades walking, a high relative abundance of bloom taxa (specifically *Mesodma*), and very low richness and relative abundance of immigrant taxa (Fig. 2.13). However, another mammalian assemblage in the Hell Creek region, Constenius (UCMP loc. V96268), may sample the same temporal interval as Z-Line. Emphasizing that this assemblage has not been fully examined and described, preliminary inspection by one of us (GPWM) suggests it has better representation of immigrant taxa than does Z-Line. Comprehensive study of the Constenius assemblage and its local stratigraphy as well as additional sampling at Z-Line will be critical to sharpening our view of the early disaster sub-phase and the possibility of spatial heterogeneity within the Hell Creek region.

Late Disaster Sub-Phase. The Morales 1, Herpijunk, Carrie Padgett, and Worm Coulee 1 local faunas are all from deposits between the MCZ and HFZ coals and are all interpreted to be

younger than the Z-Line local fauna (Fig. 2.8; 66.024 ± 0.014/0.044 Ma and 65.973 ± 0.020/0.047, respectively). The genus *Mesodma* is the most common taxon in all four local faunas. Moreover, only one dead clade walking is present (*Cimexomys* spp.), and at least three of the characteristic Pu1 immigrant taxa (*Protungulatum donnae*, *Baioconodon* spp., *Mimatuta* spp., *Oxyprimus erikseni*, and *Stygimys kuszmauli*) are present in low relative abundance in all the local faunas. The four local faunas also plot near each other in our NMDS plot, a pattern driven by similarities in taxonomic composition and relative abundances (Fig. 2.11). We interpret the faunal similarities among these four local faunas to mean that they represent the same phase of post-KPB recovery. We refer to it as the 'late disaster sub-phase' as it is further along the process of biotic recovery than the early disaster sub-phase represented by the Z-Line local fauna (Fig. 2.13). The late disaster sub-phase is characterized by the continued high relative abundance of bloom taxa, reduction in the number of dead clades walking, and the first appearance of a more taxonomically rich assemblage of immigrant taxa.

Although we assign the Worm Coulee 1 local fauna to the late disaster sub-phase, it differs from other late-disaster local faunas in several ways. The bloom taxa *Thylacodon montanensis* and *Procerberus formicarum* (Fig. 2.11) have higher relative abundance in Worm Coulee 1 (18% and 32%, respectively; Wilson, 2014) than in Morales 1, Herpijunk, and Carrie Padgett (< 10% for both taxa). Also, the Worm Coulee 1 local fauna records the presence of taxa that are otherwise only known from younger deposits, including an undescribed periptychid (Periptychidae indet.) and the multituberculates *Catopsalis alexanderi* and *Acheronodon garbani* (but see Lofgren 1995 for other possible early immigration events of *Catopsalis alexanderi*). Several hypotheses could explain some or all of these faunal differences: (i) Worm Coulee 1 has a taphonomic bias towards smaller-bodied mammalian taxa; (ii) the Hell Hollow channel, which

hosts the Worm Coulee 1 assemblage, incorporated fossils from across multiple heterogenous paleoenvironments; (iii) Worm Coulee 1 potentially sampled a younger vertebrate microfossil source than Morales 1, Herpijunk, and Carrie Padgett 6; and (iv) the differences are an artifact of differences in sampling intensity. We reject the size-sorting hypothesis (i) based on the presence of a broad size range of fossils from mammalian and non-mammalian taxa. The high relative abundance of bloom taxa suggests that the Worm Coulee 1 local fauna is of similar age to the other late disaster local faunas (Fig. 2.13). However, the early appearances of younger aspect taxa (Periptychidae indet., *Catopsalis alexanderi*, and *Acheronodon garbani*) and differences in the most abundant bloom taxa suggest a potentially younger age that prevents us from fully rejecting hypothesis (iii). We are also unable to reject hypothesis (ii) and (iv). Worm Coulee 1 is within a more laterally expansive channel complex than Morales 1, Herpijunk, and Carrie Padgett, which are all found within relatively narrow meander belts (Weaver et al., 2022a). If the meander belt that makes up the Hell Hollow channel deposit reworked underlying sediments from a broader geographic area, then it is possible that the difference in faunal composition is the result of Worm Coulee 1 hosting fossil concentrations accumulated from a wider array of different paleoenvironments (Hypothesis [ii]; Rogers and Brady, 2010; Weaver et al., 2022a This could potentially explain the differences in abundance of bloom taxa (*Thylacodon montanensis* and *Procerberus formicarum*) and the early appearances of younger aspect taxa that potentially resided in more fringe environments not sampled by other channels. Moreover, Worm Coulee 1 has the largest sample size (N = 920) of all the Hell Creek region Pu1 localities, potentially more closely approximating the true relative abundance structure of Pu1 local faunas and the first appearances of younger-aspect taxa (Hypothesis [iv]). Despite these differences, we still attribute Worm Coulee 1 to the late-disaster subphase due to the high relative abundance of bloom taxa,

the presence of dead clades walking, and overall faunal similarity with other late-disaster local faunas (Fig. 2.11). Continued collecting and taphonomic study of Morales 1, Herpijunk, and Carrie Padgett and other spatially adjacent localities will allow more robust testing of these hypotheses.

Early Recovery Sub-Phase? The Luck O Hutch (LOH) local fauna is bracketed between 66.024 ± 0.014/0.044 Ma and 65.724 ± 0.013/0.044 Ma (ca. 28–328 ka post-KPB; Sprain et al., 2018). These temporal brackets overlap those of the Carrie Padgett and Worm Coulee 1 local faunas, but we interpret LOH as likely younger based on the depth of the channel deposit (see 'Other Pu1 Western Interior localities' and Fig. 2.8). We must also acknowledge that the low sample size of LOH (55 specimens) reduces our ability to fully characterize the early recovery subphase. Nevertheless, like the other Pu1 local faunas, LOH has a high relative abundance of the bloom taxon *Mesodma* (Smith et al., 2018) and, in turn, clusters with the late-disaster sub-phase local faunas in the NMDS plot (Fig. 2.11). Of the other recognized bloom taxa, *Thylacodon montanensis* is absent and *Procerberus formicarum* is very rare (2% relative abundance) in the LOH local fauna. Additionally, the evenness of the LOH local fauna is greater than that of the other Pu1 local faunas in the region, except for Worm Coulee 1, although this difference is only statistically significant relative to Morales 1 ($p = 0.006$; Fig. 2.10). Younger-aspect taxa, such as Periptychidae indet. (not *Mimatuta* spp.) and ?*Prodiacodon crustulum*, occur in the LOH local fauna as well. Accordingly, Smith et al. (2018) proposed that LOH represents a later stage of post-KPB recovery than the other Pu1 local faunas, the 'early recovery sub-phase,' which is characterized by lower relative abundance of bloom taxa and higher evenness (Kauffman and Harries, 1996; Erwin, 1998; Smith et al., 2018). The Harley's Point locality (UCMP V77087) from Garfield County temporally overlaps the LOH locality, bracketed

between 65.946 Ma and 65.912 Ma (ca. 105–139 ka post-KPB; Wilson Mantilla et al., 2021). Although the Harley's Point local fauna has not been fully described, the appearance of two purgatoriid plesiadapiform species suggests that it might also represent the early recovery sub-phase (Wilson Mantilla et al., 2021). Likewise, the Coke's Clemmys locality (UCMP V88046) from McCone County also temporally overlaps the LOH locality, bracketed between 65.802 ± 0.116/0.125 and 65.724 ± 0.013/0.044 Ma (ca. 250–328 ka post-KPB; Sprain et al., 2018; Smith et al., 2018). Similar to LOH, Coke's Clemmys sample size is small (58 specimens) but the appearance of the purgatoriid plesiadapiform species *Purgatorius* cf. *P. coracis* suggests it also represents the early recovery sub-phase (Smith et al., 2018). Formal descriptions of the Harley's Point local fauna and additional sampling at LOH and Coke's Clemmys will allow us to better understand and provide a formal designation for the early recovery sub-phase. Until then, we refer to the LOH local fauna as tentatively representing the early recovery sub phase due to presence of the younger aspect taxa Periptychidae indet. and ?*Prodiacodon crustulum* along with the fact that it was likely deposited after the late disaster sub-phases localities (Smith et al., 2018).

Late Recovery Sub-Phase. In the Hell Creek region, there is a 231-ka temporal gap between the well-documented local faunas of the disaster phase (e.g., Worm Coulee 1) that are less than 80 ka post-KPB and the previously studied local faunas of the recovered phase (e.g., Garbani local fauna; Weaver et al. 2022a) that are 512 to 934 ka post-KPB. This gap is partly filled by the tentative early-recovery local faunas like LOH, Coke's Clemmys, and Harley's Point, although these local faunas would benefit from additional sampling or in the case of Harley's Point formal study. We suspect that within the rest of that gap lies what we call the 'late recovery sub-phase,' which represents the faunal transition from the early recovery sub-phase to

the recovered phase (more detailed explanation in forthcoming section). We infer that this sub-phase would be characterized by the onset of in-situ diversification, absent in the LOH local fauna, along with continued immigration. Through ongoing targeted fossil prospecting, geochronological sampling, and description of existing fossil collections, we aim to fill this gap in the Hell Creek region. As discussed below, we assign the Littleton local fauna from the Denver Basin to this late recovery sub-phase, although we acknowledge that compositional differences with older Hell Creek region local faunas could reflect differences in biogeography as well as recovery sub-phase (see Denver Basin Late Recovery Sub-Phase below). Moreover, it is possible that the localities described herein simply reflect 'disaster' and 'recovery' phases and that the taxonomic differences among the local faunas are driven by sampling of spatial heterogeneity. Nonetheless, these differences occur more or less in stratigraphic order and fit logically with the expectations of ecological recovery theory. We expect that this is not the case and that the local faunas represent different sub-phases of biotic recovery.

Testing the Generality of the Mammalian Recovery Model. Although the Hell Creek region has become a focal point for studies of the K-Pg mass extinction and biotic recovery, we recognize that it is a single location and may not accurately reflect patterns more broadly at the continental or global scale. However, there are few places in the world with the fossil record and geochronological framework to permit comparisons of high-resolution patterns of post-KPB mammalian recovery (see reviews of global records in Clemens, 2001, 2010). Thus, we investigate the generality of our model of biotic recovery in the Western Interior using the Denver Basin as a single point of comparison but hope that in the coming years we can expand those comparisons. The Denver Basin is located ~920 km south of the Hell Creek region and

hosts multiple well-described Pu1 local faunas within a comparable geochronological framework (e.g., Clyde et al., 2016; Fuentes et al., 2019; Lyson et al., 2019). We focus on the Gars Galore local fauna (Dahlberg et al., 2016) and the Littleton local fauna (Middleton, 1983; Eberle, 2003; Middleton and Dewar, 2004) because both have been interpreted as representing Pu1 faunas but differing in their relative ages.

Denver Basin Late Disaster Sub-Phase. The Gars Galore mammalian assemblage (DMNH loc. 2560) consists of 108 specimens, of which 69 are identifiable to genus level or lower (Dahlberg et al., 2016). The age of the Gars Galore locality is ca. 128 ka (ca. 65.893 Ma) after the KPB, based on its stratigraphic height above the locally identified KPB and application of a median sediment accumulation rate (Clyde et al., 2016). This age falls within the tentative early recovery sub-phase of our new model; however, the Gars Galore local fauna differs substantially from the Luck O Hutch local fauna. The Gars Galore local fauna has lower species richness (9 spp.), lower evenness, and a very high relative abundance of the bloom taxon *Mesodma* (81%), all of which are more in line with early-disaster and late-disaster sub-phase local faunas from the Hell Creek region (Figs. 9 and 10). The Gars Galore local fauna is also distinct in that it lacks cimolestids (e.g., *Procerberus formicarum* or *Puercolestes simpsoni*), which are common in Pu1 local faunas from the Hell Creek region (Archibald, 1982; Wilson, 2014) and in other, younger Pu1 local faunas from the Denver Basin (Eberle, 2003; Middleton and Dewar, 2004). It is unlikely that their absence in the assemblage reflects a taphonomic size bias, given that taxa both smaller (e.g., *Mesodma)* and larger (e.g., *Baioconodon)* than the common Pu1 cimolestids are present. Moreover, specimens from Gars Galore were collected using screen-washing equipment and techniques similar to those used in the Hell Creek region (Dahlberg et al., 2016), and the depositional environment is a fluvial system similar to the

localities in the Hell Creek region (Dahlberg et al., 2016). The Gars Galore local fauna also lacks the appearance of multiple younger-aspect taxa found at the tentative early recovery local faunas (e.g. *Conacodon)*. Overall, the Gars Galore local fauna, despite its younger age, is more similar in composition to the Hell Creek region disaster phase local faunas than to the tentatively early recovery local fauna of Luck O Hutch (Fig. 2.9 and 10). These differences with the early-recovery sub-phase local fauna from the Hell Creek region might reflect spatial heterogeneity of the biotic recovery process, uncertainty in the age estimate of Gars Galore, the incomplete sampling of the Gars Galore local fauna, or some combination of those factors. Until those factors are more fully evaluated, we provisionally assign the Gars Galore local fauna to the late disaster sub-phase.

Denver Basin Late Recovery Sub-Phase. The Littleton local fauna consists of assemblages from two localities, the Alexander locality (UCM loc. 77267) and South Table Mountain (UCM loc. 77283) (see Middleton and Dewar, 2004 for a discussion of whether these two localities should be combined into a single local fauna). These localities fall within magnetochron C29r, like other Pu1 localities in the Hell Creek region and Denver Basin (Eberle, 2003; Middleton and Dewar, 2004; Lyson et al., 2019). The age of the local fauna is otherwise poorly constrained but has been interpreted to be 100–300 ka after the KPB (Lyson et al., 2019), likely younger than Gars Galore and almost all the selected Hell Creek region local faunas, except perhaps Luck O Hutch (though we interpret the LOH as older than Littleton). We would thus expect the Littleton local fauna to represent either the early recovery or late recovery sub-phase of biotic recovery. Indeed, it preserves the bloom taxon *Mesodma* but in much lower relative abundance than any of the other Pu1 local faunas (< 3%; Eberle, 2003; Middleton and Dewar, 2004). It has higher evenness and taxonomic richness (20 spp.) than the older Pu1 local

faunas in the Denver Basin and Hell Creek region and is comparable in those metrics to the latest Cretaceous (Lancian) Flat Creek local fauna (Figs. 9 and 10). The Littleton local fauna also has a greater species richness of multituberculates and archaic ungulates than the other Pu1 local faunas, and many of those taxa are more derived representatives of the mammalian families that characterize older Pu1 local faunas. For example, *Conacodon* of the Littleton local fauna is a more derived periptychid than either *Mimatuta* or *Maiorana* (Archibald et al., 1983b), of which the latter two are present among most of the older Pu1 local faunas examined here; this implies either in-situ diversification or an immigration event (Archibald, 1982; Archibald 1983b). We interpret this higher taxonomic richness and evenness, higher relative abundance of immigrant taxa, and byproducts of in-situ diversification of the Littleton local fauna as indicators of a more advanced sub-phase of biotic recovery—the late recovery sub-phase (Fig. 2.13). We also acknowledge that, as is the case for Gars Galore, some differences with Hell Creek region local faunas might also reflect spatial heterogeneity in the biotic recovery process. Other studies have shown that by the early Paleocene there were patterns of north-south provincialism (e.g., Weil, 1999; Smith et al., 2018; Hovatter et al., 2019) as well as diversity gradients related to topography (Johnson et al., 2003). For example, floras in the western portion of the Denver Basin closer to the foothills of the Rocky Mountains tend to be more taxonomically rich than their more eastern, coastally adjacent counterparts (Johnson et al., 2003). Thus, the greater taxonomic richness and evenness of the Littleton local fauna relative to more northern and eastern local faunas like Luck O Hutch could relate to latitudinal and/or paleoenvironmental differences as well. The high richness of archaic ungulates in the Pu1 local fauna of the Great Divide Basin in Wyoming might also reflect a closer proximity to upland environments (McComas and Eberle, 2016; Atteberry and Eberle, 2021). That said, we underscore that these

faunas have wide age brackets that might give a false sense of contemporaneity. Along with the need for additional sampling of these local faunas, higher precision geochronology is required to further resolve our understanding of the heterogeneity in these patterns.

2.9 CONCLUSION

Taken together, our new model (Fig. 2.13) proposes a more granular look at the disaster and recovery phases of post-KPB biotic recovery in mammalian communities. Analyses of the Morales 1, Herpijunk, and Carrie Padgett local faunas along with other recently described local faunas within a high-resolution chronostratigraphic framework allowed us to identify key sub-phases of biotic recovery: early disaster, late disaster, early recovery, and late recovery. We suggest that immigrants began colonizing vacated ecospace immediately after the KPB (early disaster) but did not fully establish themselves across the region until after the disappearance of most genera classified as 'dead clades walking' (late disaster; Fig. 2.12). The disaster phase in total spans at least the first 80 ka following the KPB and possibly up to 128 ka in the Denver Basin. One possible explanation for the length of the disaster phase includes environmental instability related to Deccan Trap volcanism, supported by evidence of a pulse in volcanic activity that roughly coincides with the interval (Schoene et al., 2019, 2021; but see Sprain et al., 2019 for a different interpretation). The length of instability is also supported by the paleobotanical record, which shows a return to pre-KPB levels of taxonomic richness in the region after 80 ka, suggesting a return of stable environmental conditions (Wilson Deibel, 2022). Moreover, the difference in the length of the disaster phase in the Hell Creek region and Denver Basin may be a result of spatial variability in the return to pre-KPB levels of floral richness (Lyson et al., 2019).

Our results suggest that the transition between the disaster phase and recovery phase occurred between 100 ka and 300 ka following the KPB and was mostly driven by increases in both generic richness and relative abundance of immigrant taxa, displacing bloom taxa and 'dead clades walking.' In-situ diversification of taxa likely lagged, only ramping up after the first 300 ka following the KPB. Ultimately, our study underscores the importance of evaluating biotic recovery at finer temporal and geographic scales such that local, ecologically relevant patterns of interest are discernible. This was highlighted by the comparisons with the Denver Basin local faunas, which suggest biotic recovery was not spatially uniform. Comparisons with other regions within the Western Interior, including the Hanna and Great Divide Basins of Wyoming, could further test the generality of the model and explore how differences in regional landscapes, climate, or other environmental variables (e.g., vegetation) might have influenced the timing of post-KPB mammalian recovery and give us a more complete view of what led to the mammalian-dominated terrestrial ecosystems that characterize the modern world.

2.10 ACKNOWLEDGEMENTS

We acknowledge that the fossils in this paper were collected on lands that are the traditional territory of the Fort Belknap Assiniboine & Gros Ventre Tribes and Fort Peck Assiniboine & Sioux Tribes. Future field trips will be respectful to the original peoples and sovereignty.

We would like to express our deep gratitude to our late mentor and friend W. A. Clemens; without his contributions to the study of the Hell Creek region's fossil and rock record none of this work would have been possible. We also thank the people of Jordan, Montana for welcoming us into their community each summer, Jane and Dale Tharp for granting access to these field areas, I. Fendley and C. Sprain for discussions on Hell Creek chronostratigraphy, S. Smith for help with

taxon identifications and discussions about recovery, current and former members of the Wilson Mantilla Lab (A. Brannick, H. Fulghum, D. Grossnickle, B. Hovatter, A. Peng, and P. Wilson Deibel) for field work assistance and feedback throughout the writing process, current and former undergraduate assistants E. Armstrong, B. Knobbe, L. Knowles, B. LeFevre, and S. Majidi for help in both the field and the lab, P. Holroyd for providing access to UCMP collections, former UCMP field crews for vertebrate microfossil collecting, Katherine Anderson for managing the UWBM vertebrate paleontology collections, the UW PaleoPod for fruitful discussions and support, the U.S. Bureau of Land Management and the Montana State Department of Natural Resources and Conservation for providing paleontological permits, and Greg Liggett, Doug Melton, and Patrick Rennie for facilitating those permits. Financial support of the Hell Creek Project was provided by the Myhrvold and Havranek Charitable Family Fund, the David B. Jones Foundation, the University of Washington Department of Biology, and the Burke Museum of Natural History and Culture. Financial support was also provided to JRC and LNW through National Science Foundation Graduate Research Fellowships and LNW through NSF EAR-PF 2052992.

2.11 REFERENCES CITED

Alroy, J. (1999). The Fossil Record of North American Mammals: Evidence for a Paleocene Evolutionary Radiation. *Systematic Biology*, *48*(1), 107–118. https://doi.org/10.1080/106351599260472

Alroy, J. (2010). Fair Sampling of Taxonomic Richness and Unbiased Estimation of Origination and Extinction Rates. *The Paleontological Society Papers*, *16*, 55–80. https://doi.org/10.1017/S1089332600001819

Alvarez, L. W., Alvarez, W., Asaro, F., & Michel, H. V. (1980). Extraterrestrial Cause for the Cretaceous-Tertiary Extinction. *Science*, *208*(4448), 1095–1108. https://doi.org/10.1126/science.208.4448.1095

Alvarez, L. W., Alvarez, W., Asaro, F., & Michel, H. V. (1981). Extraterrestrial cause for the Cretaceous-Tertiary extinction: experiment and theory. In *Applications of Space Developments* (pp. 241–271). Elsevier. https://doi.org/10.1016/B978-0-08-026729-6.50022-8

Archibald, J. D. (1982). *A Study of Mammalia and Geology Across the Cretaceous-Tertiary Boundary in Garfield County, Montana*. University of California Press.

Archibald, J. D. (1983). Structure of the K-T mammal radiation in North America: Speculations on turnover rates and trophic structure. *Acta Palaeontologica Polonica*, *28*(1–2), 11.

Archibald, J. D., Gingerich, P. D., Lindsay, E. H., Clemens, W. A., Krause, D. W., & Rose, K. D. (1987). First North American Land Mammal Ages of the Cenozoic Era. In M.O. Woodburne (Ed.), *Cenozoic Mammals of North America*. University of California Press.

Archibald, J. D., Schoch, R. M., & Rigby, J. K. (1983). A new subfamily, Conacodontinae, and new species, Conacodon kohlbergeri, of the Periptychidae (Condylarthra, Mammalia). *Postilla*, *191*, 1–24.

Archibald, J. D., Zhang, Y., Harper, T., & Cifelli, R. L. (2011). Protungulatum, Confirmed Cretaceous Occurrence of an Otherwise Paleocene Eutherian (Placental?) Mammal. *Journal of Mammalian Evolution*, *18*(3), 153–161. https://doi.org/10.1007/s10914-011-9162-1

Arens, N. C., & Jahren, A. H. (2000). Carbon Isotope Excursion in Atmospheric CO2 at the Cretaceous-Tertiary Boundary: Evidence from Terrestrial Sediments. *PALAIOS*, *15*(4), 314–322. https://doi.org/10.1669/0883-1351(2000)015<0314:CIEIAC>2.0.CO;2

Arens, N. C., Jahren, A. H., & Kendrick, D.C. (2014). Carbon isotope stratigraphy and correlation of plant megafossil localities in the Hell Creek Formation of eastern Montana, USA. In G. P. Wilson, W. A. Clemens, J. R. Horner, & J. H. Hartman (Eds.), *Through the End of the Cretaceous in the Type Locality of the Hell Creek Formation in Montana and Adjacent Areas*. Geological Society of America. https://doi.org/10.1130/2014.2503(07)

Atteberry, M. R., & Eberle, J. J. (2021). New earliest Paleocene (Puercan) periptychid 'condylarths' from the Great Divide Basin, Wyoming, USA. *Journal of Systematic Palaeontology*, *19*(8), 565–593. https://doi.org/10.1080/14772019.2021.1924301

Badgley, C. (1986). Counting Individuals in Mammalian Fossil Assemblages from Fluvial Environments. *PALAIOS*, *1*(3), 328. https://doi.org/10.2307/3514695

Brown, R. W. (1952). Tertiary strata in eastern Montana and western North and South Dakota. *Montana Geological Society*, 89–92.

Calvert, W. R. (1912). Geology of certain lignite fields in eastern Montana. *U.S. Geological Survey Bulletin*, *471*, 187–201.

Chen, M., Strömberg, C. A. E., & Wilson, G. P. (2019). Assembly of modern mammal community structure driven by Late Cretaceous dental evolution, rise of flowering plants, and dinosaur demise. *Proceedings of the National Academy of Sciences*, *116*(20), 9931–9940. https://doi.org/10.1073/pnas.1820863116

Cifelli, R. L. (1996). *Techniques for Recovery and Preparation of Microvertebrate Fossils* (Vols. 96–4). Oklahoma Geological Survey Special Publication.

Clemens, W. A. (2001). Patterns of mammalian evolution across the Cretaceous-Tertiary boundary. *Zoosystematics and Evolution*, *77*(2), 175–191. https://doi.org/10.1002/mmnz.20010770204

Clemens, W. A. (2002). Evolution of the mammalian fauna across the Cretaceous-Tertiary boundary in northeastern Montana and other areas of the Western Interior. In J. H. Hartman, K. R. Johnson, & D. J. Nichols (Eds.), *The Hell Creek Formation and the Cretaceous-Tertiary boundary in the northern Great Plains: An Integrated continental record of the end of the Cretaceous*. Geological Society of America. https://doi.org/10.1130/0-8137-2361-2.217

Clemens, W. A. (2010). Were immigrants a significant part of the earliest Paleocene mammalian fauna of the North American western interior. *Vertebrata Palasiatica*, *48*, 285–307.

Clemens, W. A., & Hartman, J. H. (2014). From Tyrannosaurus rex to asteroid impact: Early studies (1901–1980) of the Hell Creek Formation in its type area. In G. P. Wilson, W. A. Clemens, J. R. Horner, & J. H. Hartman (Eds.), *Through the End of the Cretaceous in the Type Locality of the Hell Creek Formation in Montana and Adjacent Areas*. Geological Society of America. https://doi.org/10.1130/2014.2503(01)

Clyde, W. C., Ramezani, J., Johnson, K. R., Bowring, S. A., & Jones, M. M. (2016). Direct high-precision U–Pb geochronology of the end-Cretaceous extinction and calibration of Paleocene astronomical timescales. *Earth and Planetary Science Letters*, *452*, 272–280. https://doi.org/10.1016/j.epsl.2016.07.041

Collier, A. J., & Knechtel, M. M. (1939). *The Coal Resources of McCone County, Montana*. U.S. Government Printing Office.

Dahlberg, E. L., Eberle, J. J., Sertich, J. J. W., & Miller, I. M. (2016). A new earliest Paleocene (Puercan) mammalian fauna from Colorado's Denver Basin, U.S.A. *Rocky Mountain Geology*, *51*(1), 1–22. https://doi.org/10.2113/gsrocky.51.1.1

DeBey, L. B., & Wilson, G. P. (2014). Mammalian femora across the Cretaceous–Paleogene boundary in eastern Montana. *Cretaceous Research*, *51*, 361–385. https://doi.org/10.1016/j.cretres.2014.06.001

DeBey, L., & Wilson, G. (2017). Mammalian distal humerus fossils from eastern Montana, USA with implications for the Cretaceous-Paleogene mass extinction and the adaptive radiation of placentals. *Palaeontologia Electronica*. https://doi.org/10.26879/694

Donohue, S. L., Wilson, G. P., & Breithaupt, B. H. (2013). Latest Cretaceous multituberculates of the Black Butte Station local fauna (Lance Formation, southwestern Wyoming), with implications for compositional differences among mammalian local faunas of the Western Interior. *Journal of Vertebrate Paleontology*, *33*(3), 677–695. https://doi.org/10.1080/02724634.2013.745416

dos Reis, M., Donoghue, P. C. J., & Yang, Z. (2014). Neither phylogenomic nor palaeontological data support a Palaeogene origin of placental mammals. *Biology Letters*, *10*(1). https://doi.org/10.1098/rsbl.2013.1003

Eaton, J. G. (1995). Cenomanian and Turonian (Early Late Cretaceous) Multituberculate Mammals from Southwestern Utah. *Journal of Vertebrate Paleontology*, *15*(4), 761–784.

Eberle, J. J. (2003). Puercan mammalian systematics and biostratigraphy in the Denver Formation, Denver Basin, Colorado. *Rocky Mountain Geology*, *38*(1), 143–169. https://doi.org/10.2113/gsrocky.38.1.143

Eriksson, O. (2016). Evolution of angiosperm seed disperser mutualisms: The timing of origins and their consequences for coevolutionary interactions between angiosperms and frugivores: Coevolution between angiosperms and frugivores. *Biological Reviews*, *91*(1), 168–186. https://doi.org/10.1111/brv.12164

Erwin, D. H. (1993). *The Great Paleozoic Crisis: Life and Death in the Permian*. Columbia University Press.

Erwin, D. H. (1998). The end and the beginning: Recoveries from mass extinctions. *Trends in Ecology & Evolution*, *13*(9), 344–349. https://doi.org/10.1016/S0169-5347(98)01436-0

Faith, D. P., Minchin, P. R., & Belbin, L. (1987). Compositional dissimilarity as a robust measure of ecological distance. *Vegetatio*, *69*(1), 57–68. https://doi.org/10.1007/BF00038687

Fastovsky, D. E. (1987). Paleoenvironments of Vertebrate-Bearing Strata during the Cretaceous-Paleogene Transition, Eastern Montana and Western North Dakota. *PALAIOS*, *2*(3), 282. https://doi.org/10.2307/3514678

Fastovsky, D. E., & Bercovici, A. (2016). The Hell Creek Formation and its contribution to the Cretaceous–Paleogene extinction: A short primer. *Cretaceous Research*, *57*, 368–390. https://doi.org/10.1016/j.cretres.2015.07.007

Fastovsky, D. E., & McSweeney, K. (1987). Paleosols spanning the Cretaceous-Paleogene transition, eastern Montana and western North Dakota. *GSA Bulletin*, *99*(1), 66–77. https://doi.org/10.1130/0016-7606(1987)99<66:PSTCTE>2.0.CO;2

Fendley, I. M., Mittal, T., Sprain, C. J., Marvin-DiPasquale, M., Tobin, T. S., & Renne, P. R. (2019). Constraints on the volume and rate of Deccan Traps flood basalt eruptions using a combination of high-resolution terrestrial mercury records and geochemical box models. *Earth and Planetary Science Letters*, *524*, 115721. https://doi.org/10.1016/j.epsl.2019.115721

Fuentes, A. J., Clyde, W. C., Weissenburger, K., Bercovici, A., Lyson, T. R., Miller, I. M., Ramezani, J., Isakson, V., Schmitz, M. D., & Johnson, K. R. (2019). Constructing a time

scale of biotic recovery across the Cretaceous–Paleogene boundary, Corral Bluffs, Denver Basin, Colorado, U.S.A. *Rocky Mountain Geology*, *54*(2), 133–153. https://doi.org/10.24872/rmgjournal.54.2.133

Grossnickle, D. M., & Newham, E. (2016). Therian mammals experience an ecomorphological radiation during the Late Cretaceous and selective extinction at the K–Pg boundary. *Proceedings of the Royal Society B: Biological Sciences*, *283*(1832), 20160256. https://doi.org/10.1098/rspb.2016.0256

Grossnickle, D. M., Smith, S. M., & Wilson, G. P. (2019). Untangling the Multiple Ecological Radiations of Early Mammals. *Trends in Ecology & Evolution*, *34*(10), 936–949. https://doi.org/10.1016/j.tree.2019.05.008

Halliday, T. J. D., & Goswami, A. (2016). Eutherian morphological disparity across the end-Cretaceous mass extinction. *Biological Journal of the Linnean Society*, *118*(1), 152–168. https://doi.org/10.1111/bij.12731

Harries, P. J., & Kauffman, E. G. (1990). Patterns of survival and recovery following the Cenomanian-Turonian (Late Cretaceous) mass extinction in the Western Interior Basin, United States. In E. G. Kauffman & O. H. Walliser (Eds.), *Extinction Events in Earth History* (pp. 277–298). Springer. https://doi.org/10.1007/BFb0011152

Hartman, J., Butler, R., Weiler, M., & Schumaker, K. (2014). Context, naming, and formal designation of the Cretaceous Hell Creek Formation lectostratotype, Garfield County, Montana. *Special Paper of the Geological Society of America*, *503*, 89–121. https://doi.org/10.1130/2014.2503(02)

Holland, S. (2015). *Data Analysis in the Geosciences*. Retrieved August 22, 2022, from https://strata.uga.edu/8370/rtips/shareholderQuorumSubsampling.html

Hovatter, B. T., & Wilson, G. P. (2019). *Composition of newly described earliest Torrejonian (To1) fauna from northeastern Montana, U.S.A. reveals taxonomic differences among early Paleocene faunas in the western interior of North America and highlights north-south provinciality*. Society of Vertebrate Paleontology, Brisbane.

Hurlbert, S. H. (1971). The Nonconcept of Species Diversity: A Critique and Alternative Parameters. *Ecology*, *52*(4), 577–586. https://doi.org/10.2307/1934145

Ickert, R. B., Mulcahy, S. R., Sprain, C. J., Banaszak, J. F., & Renne, P. R. (2015). Chemical and Pb isotope composition of phenocrysts from bentonites constrains the chronostratigraphy around the Cretaceous-Paleogene boundary in the Hell Creek region, Montana: Chemistry of bentonites at Hell Creek. *Geochemistry, Geophysics, Geosystems*, *16*(8), 2743–2761. https://doi.org/10.1002/2015GC005898

Jablonski, D. (2002). Survival without recovery after mass extinctions. *Proceedings of the National Academy of Sciences*, *99*(12), 8139–8144. https://doi.org/10.1073/pnas.102163299

Jepsen, G. L. (1940). Paleocene Faunas of the Polecat Bench Formation, Park County, Wyoming: Part I. *Proceedings of the American Philosophical Society*, *83*(2), 217–340.

Johnson, K. R., Reynolds, M. L., Werth, K. W., & Thomasson, J. R. (2003). Overview of the Late Cretaceous, early Paleocene, and early Eocene megafloras of the Denver Basin, Colorado. *Rocky Mountain Geology*, *38*(1), 101–120. https://doi.org/10.2113/gsrocky.38.1.101

Kauffman, E. G., & Harries, P. J. (1996). The importance of crisis progenitors in recovery from mass extinction. *Geological Society, London, Special Publications*, *102*(1), 15–39. https://doi.org/10.1144/GSL.SP.1996.001.01.02

Kelly, T. S. (2014). Preliminary report on the mammals from Lane's Little Jaw site quarry: a latest Cretaceous (earliest Puercan?) local fauna, Hell Creek Formation, southeastern Montana. Paludicola, 10(1), 42.

Kielan, Z. (2004). A new reconstruction of multituberculate endocranial casts and encephalization quotient of Kryptobaatar. *Acta Palaeontologica Polonica*, 12.

Krebs, C. (1989). *Ecological methodology*. Harper Collins Publishers (1967).

Lance, G. N., & Williams, W. T. (1967). A General Theory of Classificatory Sorting Strategies: 1. Hierarchical Systems. *The Computer Journal*, *9*(4), 373–380. https://doi.org/10.1093/comjnl/9.4.373

LeCain, R., Clyde, W., Wilson Mantilla, G., & Riedel, J. (2014). Magnetostratigraphy of the Hell Creek and lower Fort Union Formations in northeastern Montana. *Special Paper of the Geological Society of America*, *503*, 137–147. https://doi.org/10.1130/2014.2503(04)

Lillegraven, J. A. (1972). Ordinal and familial diversity of Cenozoic mammals. *TAXON*, *21*(2–3), 261–274. https://doi.org/10.2307/1218194

Lillegraven, J. A., & Eberle, J. J. (1999). Vertebrate faunal changes through Lancian and Puercan time in southern Wyoming. *Journal of Paleontology*, *73*(4), 691–710. https://doi.org/10.1017/S0022336000032510

Lofgren, D. L. (1995). *The Bug Creek Problem and the Cretaceous-Tertiary Transition at McGuire Creek, Montana*. University of California Press.

Lofgren, D. L., Lillegraven, J. A., Clemens, W. A., Gingerich, P. D., & Williamson, T. E. (2004). 3. Paleocene Biochronology: The Puercan Through Clarkforkian Land Mammal Ages. In M. O. Woodburne (Ed.), *Late Cretaceous and Cenozoic mammals of North America* (pp. 43–105). Columbia University Press. https://doi.org/10.7312/wood13040-005

Lowery, C. M., & Fraass, A. J. (2019). Morphospace expansion paces taxonomic diversification after end Cretaceous mass extinction. *Nature Ecology & Evolution*, *3*(6), 900–904. https://doi.org/10.1038/s41559-019-0835-0

Lyson, T. R., Miller, I. M., Bercovici, A. D., Weissenburger, K., Fuentes, A. J., Clyde, W. C., Hagadorn, J. W., Butrim, M. J., Johnson, K. R., Fleming, R. F., Barclay, R. S., Maccracken, S. A., Lloyd, B., Wilson, G. P., Krause, D. W., & Chester, S. G. B. (2019). Exceptional continental record of biotic recovery after the Cretaceous–Paleogene mass extinction. *Science*, *366*(6468), 977–983. https://doi.org/10.1126/science.aay2268

Maas, M. C., & Krause, D. W. (1994). Mammalian turnover and community structure in the Paleocene of North America. *Historical Biology*, *8*(1–4), 91–128. https://doi.org/10.1080/10292389409380473

MacLeod, K. G., Quinton, P. C., Sepúlveda, J., & Negra, M. H. (2018). Postimpact earliest Paleogene warming shown by fish debris oxygen isotopes (El Kef, Tunisia). *Science*, *360*(6396), 1467–1469. https://doi.org/10.1126/science.aap8525

Magurran, A. E. (2004). Measuring biological diversity. *African Journal of Aquatic Science*, *29*(2), 285–286.

McComas, K. M., & Eberle, J. J. (2016). A new earliest Paleocene (Puercan) arctocyonid mammal from the Fort Union Formation, Great Divide Basin, Wyoming, and its phylogenetic position among early 'condylarths.' *Journal of Systematic Palaeontology*, *14*(6), 445–459. https://doi.org/10.1080/14772019.2015.1066886

Middleton, M. D. (1982). A New Species and Additional Material of Catopsalis (Mammalia, Multituberculata) from the Western Interior of North America. *Journal of Paleontology*, *56*(5), 1197–1206.

Middleton, M. D., & Dewar, E. W. (2016). New mammals from the early Paleocene Littleton fauna (Denver Formation, Colorado). *Rocky Mountain Geology*, *51*(1), 1–22.

Moore, J. R., Wilson, G. P., Sharma, M., Hallock, H. R., Braman, D. R., & Renne, P. R. (2014). Assessing the relationships of the Hell Creek-Fort Union contact, Cretaceous-Paleogene boudnary, and Chicxulub impact ejecta horizon at the Hell Creek Fromation lectostratotype. *Special Paper of the Geological Society of America*, *503*, 123–135. https://doi.org/10.1130/2014.2503(04)

Novacek, M., & Clemens, W. A. (1977). Aspects of Intrageneric Variation and Evolution of Mesodma (Multituberculata, Mammalia). *Journal of Paleontology*, *51*(4), 701–717.

Pielou, E. C. (1966). The measurement of diversity in different types of biological collections. *Journal of Theoretical Biology*, *13*, 131–144. https://doi.org/10.1016/0022-5193(66)90013-0

Renne, P. R., Deino, A. L., Hilgen, F. J., Kuiper, K. F., Mark, D. F., Mitchell, W. S., Morgan, L. E., Mundil, R., & Smit, J. (2013). Time Scales of Critical Events Around the Cretaceous-Paleogene Boundary. *Science*, *339*(6120), 684–687. https://doi.org/10.1126/science.1230492

Rigby, J. K., & Rigby Jr, J. K. (1990). Geology of the Sand Arroyo and Bug Creek Quadrangles, McCone County, Montana. *Brigham Young University Geology Studies*, *36*, 69–134.

Rogers, R. R. (1998). Sequence analysis of the Upper Cretaceous Two Medicine and Judith River formations, Montana; nonmarine response to the Claggett and Bearpaw marine cycles. *Journal of Sedimentary Research*, *68*(4), 615–631. https://doi.org/10.2110/jsr.68.604

Rogers, R. R., & Brady, M. E. (2010). Origins of microfossil bonebeds: Insights from the Upper Cretaceous Judith River Formation of north-central Montana. *Paleobiology*, *36*(1), 80–112. https://doi.org/10.1666/0094-8373-36.1.80

Rogers, R. R., Carrano, M. T., Curry Rogers, K. A., Perez, M., & Regan, A. K. (2017). Isotaphonomy in concept and practice: An exploration of vertebrate microfossil bonebeds in the Upper Cretaceous (Campanian) Judith River Formation, north-central Montana. *Paleobiology*, *43*(2), 248–273. https://doi.org/10.1017/pab.2016.37

Sahney, S., & Benton, M. J. (2008). Recovery from the most profound mass extinction of all time. *Proceedings of the Royal Society B: Biological Sciences*, *275*(1636), 759–765. https://doi.org/10.1098/rspb.2007.1370

Schindler, E. (1990). The late Frasnian (Upper Devonian) Kellwasser Crisis. In E. G. Kauffman & O. H. Walliser (Eds.), *Extinction Events in Earth History* (pp. 151–159). Springer. https://doi.org/10.1007/BFb0011143

Schoene, B., Eddy, M. P., Keller, C. B., & Samperton, K. M. (2021). An evaluation of Deccan Traps eruption rates using geochronologic data. *Geochronology*, *3*(1), 181–198. https://doi.org/10.5194/gchron-3-181-2021

Schoene, B., Eddy, M. P., Samperton, K. M., Keller, C. B., Keller, G., Adatte, T., & Khadri, S. F. R. (2019). U-Pb constraints on pulsed eruption of the Deccan Traps across the end-Cretaceous mass extinction. *Science*, *363*(6429), 862–866. https://doi.org/10.1126/science.aau2422

Schubert, J. K., & Bottjer, D. J. (1992). Early Triassic stromatolites as post-mass extinction disaster forms. *Geology*, *20*(10), 883–886. https://doi.org/10.1130/0091-7613(1992)020<0883:ETSAPM>2.3.CO;2

Simpson, E. H. (1949). Measurement of Diversity. *Nature*, *163*(4148), 688–688. https://doi.org/10.1038/163688a0

Simpson, G. G. (1937). The Beginning of the Age of Mammals. *Biological Reviews*, *12*(1), 1–46. https://doi.org/10.1111/j.1469-185X.1937.tb01220.x

Smit, J., & van der Kaars, S. (1984). Terminal Cretaceous Extinctions in the Hell Creek Area, Montana: Compatible with Catastrophic Extinction. *Science*, *223*(4641), 1177–1179. https://doi.org/10.1126/science.223.4641.1177

Smith, F. A., Boyer, A. G., Brown, J. H., Costa, D. P., Dayan, T., Ernest, S. K. M., Evans, A. R., Fortelius, M., Gittleman, J. L., Hamilton, M. J., Harding, L. E., Lintulaakso, K., Lyons, S. K., McCain, C., Okie, J. G., Saarinen, J. J., Sibly, R. M., Stephens, P. R., Theodor, J., & Uhen, M. D. (2010). The Evolution of Maximum Body Size of Terrestrial Mammals. *Science*, *330*(6008), 1216–1219. https://doi.org/10.1126/science.1194830

Smith, S. M., Sprain, C. J., Clemens, W. A., Lofgren, D. L., Renne, P. R., & Wilson, G. P. (2018). Early mammalian recovery after the end-Cretaceous mass extinction: A high-resolution view from McGuire Creek area, Montana, USA. *GSA Bulletin*, *130*, 2000–2014. https://doi.org/10.1130/B31926.1

Sprain, C. J., Renne, P. R., Clemens, W. A., & Wilson, G. P. (2018). Calibration of chron C29r: New high-precision geochronologic and paleomagnetic constraints from the Hell Creek region, Montana. *GSA Bulletin*, *130*(9–10), 1615–1644. https://doi.org/10.1130/B31890.1

Sprain, C. J., Renne, P. R., Vanderkluysen, L., Pande, K., Self, S., & Mittal, T. (2019). The eruptive tempo of Deccan volcanism in relation to the Cretaceous-Paleogene boundary. *Science*, *363*(6429), 866–870. https://doi.org/10.1126/science.aav1446

Sprain, C. J., Renne, P. R., Wilson, G. P., & Clemens, W. A. (2015). High-resolution chronostratigraphy of the terrestrial Cretaceous-Paleogene transition and recovery interval in the Hell Creek region, Montana. *Geological Society of America Bulletin*, *127*(3–4), 393–409. https://doi.org/10.1130/B31076.1

Swisher III, C. C., Dingus, L., & Butler, R. F. (1993). 40Ar/39Ar dating and magnetostratigraphic correlation of the terrestrial Cretaceous–Paleogene boundary and Puercan Mammal Age, Hell Creek – Tullock formations, eastern Montana. *Canadian Journal of Earth Sciences*, *30*(9), 1981–1996. https://doi.org/10.1139/e93-174

Thomas, R. G., Smith, D. G., Wood, J. M., Visser, J., Calverley-Range, E. A., & Koster, E. H. (1987). Inclined heterolithic stratification—Terminology, description, interpretation and significance. *Sedimentary Geology*, *53*(1), 123–179. https://doi.org/10.1016/S0037-0738(87)80006-4

Tiffney, B. H. (1984). Seed Size, Dispersal Syndromes, and the Rise of the Angiosperms: Evidence and Hypothesis. *Annals of the Missouri Botanical Garden*, *71*(2), 551–576. https://doi.org/10.2307/2399037

Tobin, T. S., Honeck, J. W., Fendley, I. M., Weaver, L. N., Sprain, C. J., Tuite, M. L., Flannery, D. T., Mans, W. W., & Wilson Mantilla, G. P. (2021). Analyzing sources of uncertainty in terrestrial organic carbon isotope data: A case study across the K-Pg boundary in Montana, USA. *Palaeogeography, Palaeoclimatology, Palaeoecology*, *574*, 110451. https://doi.org/10.1016/j.palaeo.2021.110451

Weaver, L. N., Fulghum, H. Z., Grossnickle, D. M., Brightly, W. H., Kulik, Z. T., Wilson Mantilla, G. P., & Whitney, M. R. (2022). Multituberculate Mammals Show Evidence of a

Life History Strategy Similar to That of Placentals, Not Marsupials. *The American Naturalist*. https://doi.org/10.1086/720410

Weaver, L. N., Tobin, T. S., Claytor, J. R., Wilson Deibel, P. K., Clemens, W. A., & Wilson Mantilla, G. P. (2022). Revised stratigraphic relationships within the lower Fort Union Formation (Tullock member, Garfield County, Montana, U.S.A.) provide a new framework for examining post K–Pg mammalian recovery dynamics. *PALAIOS*, *37*(4), 104–127. https://doi.org/10.2110/palo.2021.011

Weil, A. I. (1999). *Multituberculate phylogeny and mammalian biogeography in the Late Cretaceous and earliest Paleocene Western Interior of North America* [Ph.D., University of California, Berkeley]. Retrieved July 25, 2022, from https://www.proquest.com/docview/304497245/abstract/C4E6A1E3F3EF4CDFPQ/1

Weil, A. I., & Clemens, W. A. (1998). Aliens in Montana: Phylogenetically and biogeographically diverse lineages contributed to an earliest Cenozoic community. *Cordilleran Section*, *30*.

Wilson Deibel, P. (2022). *Vegetation and Environmental Changes Across the Cretaceous-Paleogene (K-Pg) Boundary in Northeastern Montana* [Thesis]. https://digital.lib.washington.edu:443/researchworks/handle/1773/48392

Wilson, G. P. (2005). Mammalian Faunal Dynamics During the Last 1.8 Million Years of the Cretaceous in Garfield County, Montana. *Journal of Mammalian Evolution*, *12*(1–2), 53–76. https://doi.org/10.1007/s10914-005-6943-4

Wilson, G. P. (2013). Mammals across the K/Pg boundary in northeastern Montana, U.S.A.: Dental morphology and body-size patterns reveal extinction selectivity and immigrant-fueled ecospace filling. *Paleobiology*, *39*(3), 429–469. https://doi.org/10.1666/12041

Wilson, G. P. (2014). Mammalian extinction, survival, and recovery dynamics across the Cretaceous-Paleogene boundary in northeastern Montana, USA. In G. P. Wilson, W. A. Clemens, J. R. Horner, & J. H. Hartman, *Through the End of the Cretaceous in the Type Locality of the Hell Creek Formation in Montana and Adjacent Areas*. Geological Society of America. https://doi.org/10.1130/2014.2503(15)

Wilson, G. P., Evans, A. R., Corfe, I. J., Smits, P. D., Fortelius, M., & Jernvall, J. (2012). Adaptive radiation of multituberculate mammals before the extinction of dinosaurs. *Nature*, *483*(7390), 457–460. https://doi.org/10.1038/nature10880

Wilson Mantilla, G. P., Chester, S. G. B., Clemens, W. A., Moore, J. R., Sprain, C. J., Hovatter, B. T., Mitchell, W. S., Mans, W. W., Mundil, R., & Renne, P. R. (2021). Earliest Palaeocene purgatoriids and the initial radiation of stem primates. *Royal Society Open Science*, *8*(2), rsos.210050, 210050. https://doi.org/10.1098/rsos.210050

2.12 FIGURES

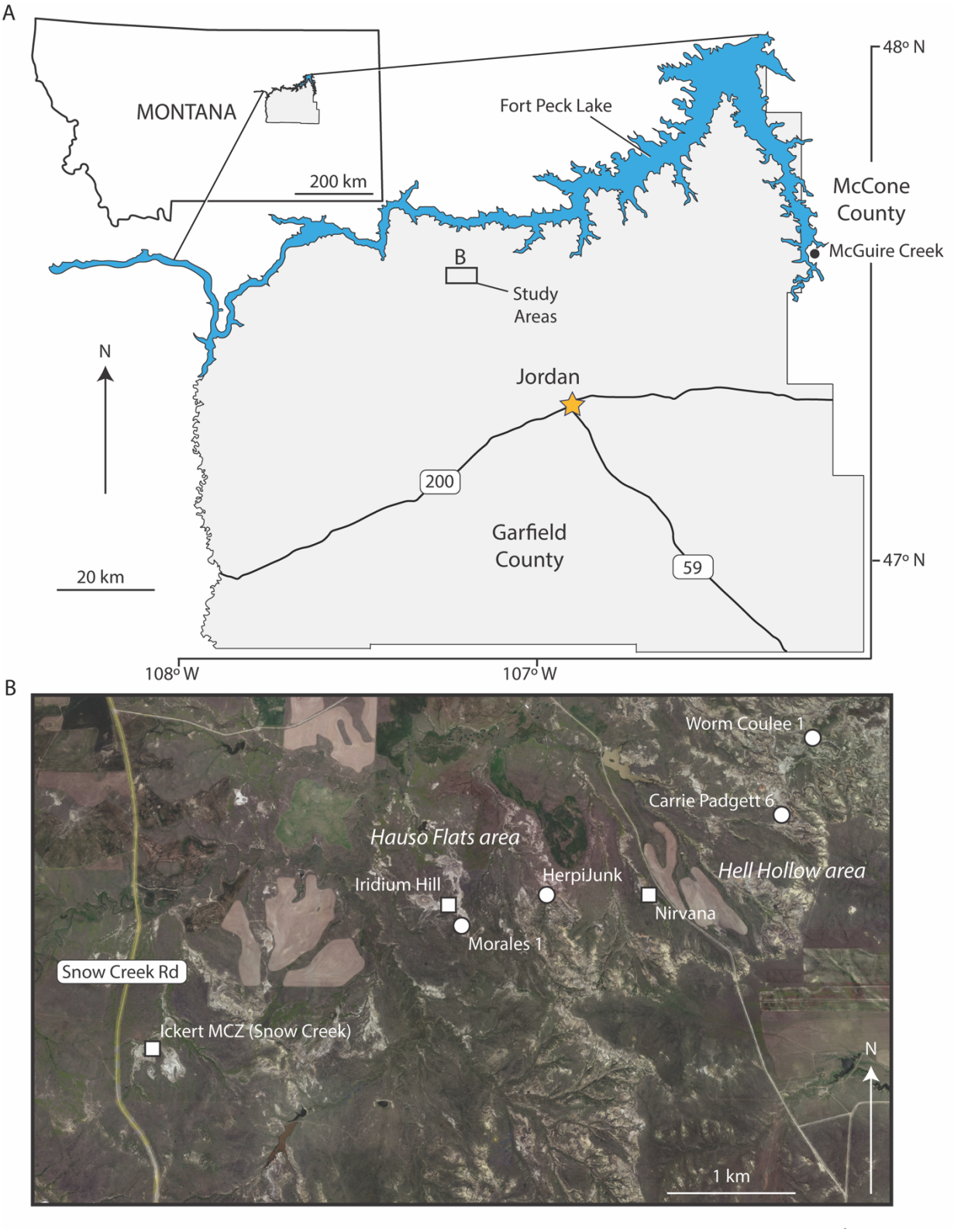

Figure 2.1 A, Map of the Hell Creek region in Garfield and McCone counties, Montana, U.S.A. (modified from Weaver et al., 2022a). Both Z-Line (UCMP V84193 and V84194) and Luck O

Hutch (UCMP V88036) are located at McGuire Creek. **B**, Satellite imagery of the study areas (Google Earth) showing the fossil localities Morales 1 (UCMP V77128), Herpijunk (UCMP V77129), Carrie Padgett 6 (UCMP V77124), and Worm Coulee 1 (UCMP V74111) (circles) and relevant geochronology localities (squares). The Ickert MCZ square marks the location of the MCZ lateral extension identified by Ickert et al. (2015). The Iridium Hill square marks the location of a KPB section with a so-called 'impact claystone' layer, which is characterized by an iridium anomaly that is associated with the bolide impact (Alvarez et al., 1980). The Nirvana square marks an additional location of the MCZ lateral extension identified by Ickert et al. (2015) and a location of a KPB section. The road running northwest between Nirvana and Carrie Padgett 6 separates the Hauso Flats and Hell Hollow study areas. MCZ— McGuire Creek Z.

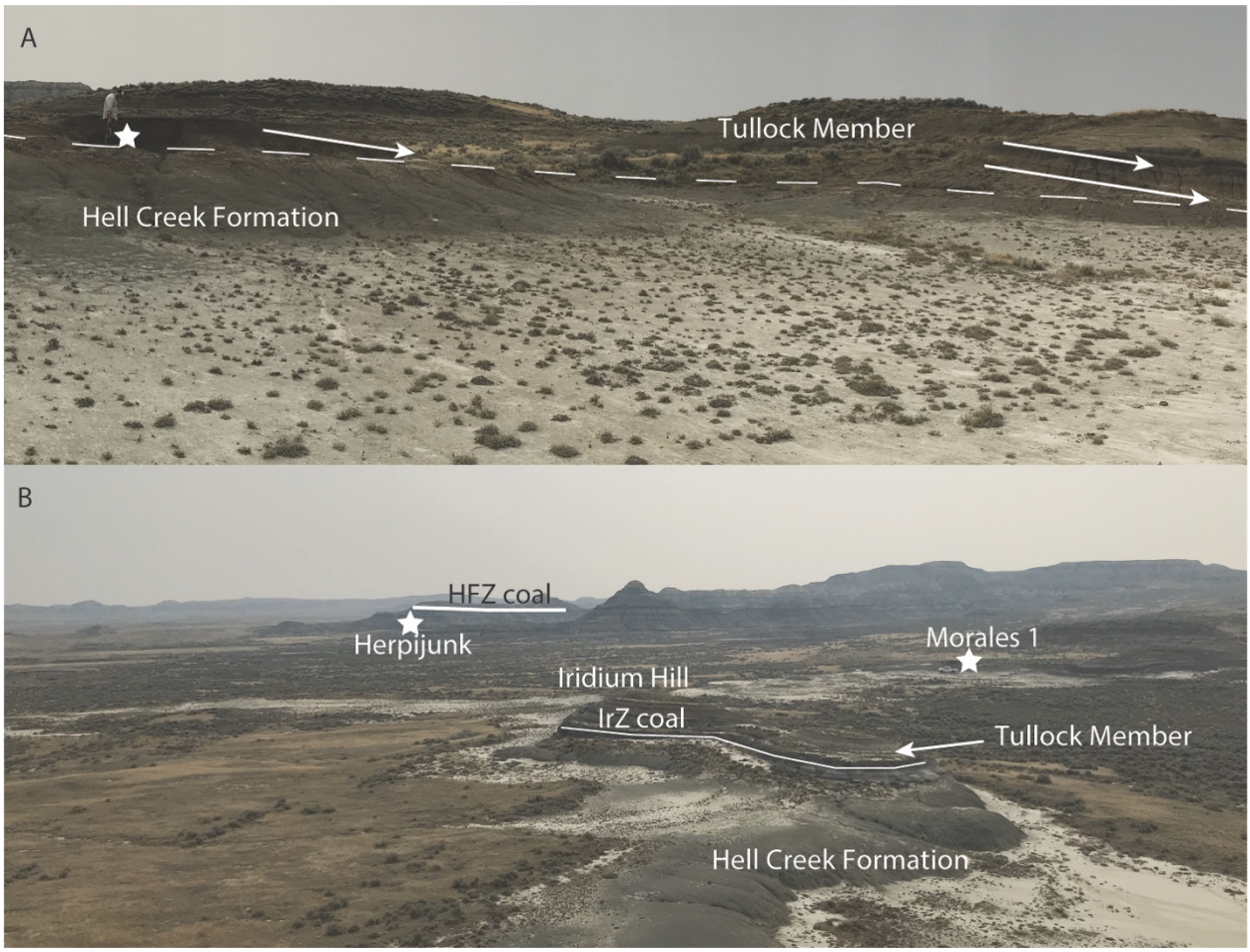

Figure 2.2 A, A south-facing view of the hillock containing the Morales 1 (UCMP V77128; white star) vertebrate microfossil locality and surrounding stratigraphy (person for scale). The white arrows highlight the ~5° southwest dip of the unit containing the Morales 1 vertebrate microfossils, which we interpret as the basal Tullock Member locally. **B**, A wide east-southeast view of the Hauso Flats area and stratigraphy relevant to our interpretations of the vertebrate microfossil locality and the Herpijunk vertebrate microfossil locality (UCMP V77129). Morales 1 and Iridium Hill are roughly 150 meters apart. Haziness in the photographs is due to smoke from nearby wildfires during the 2021 summer field season.

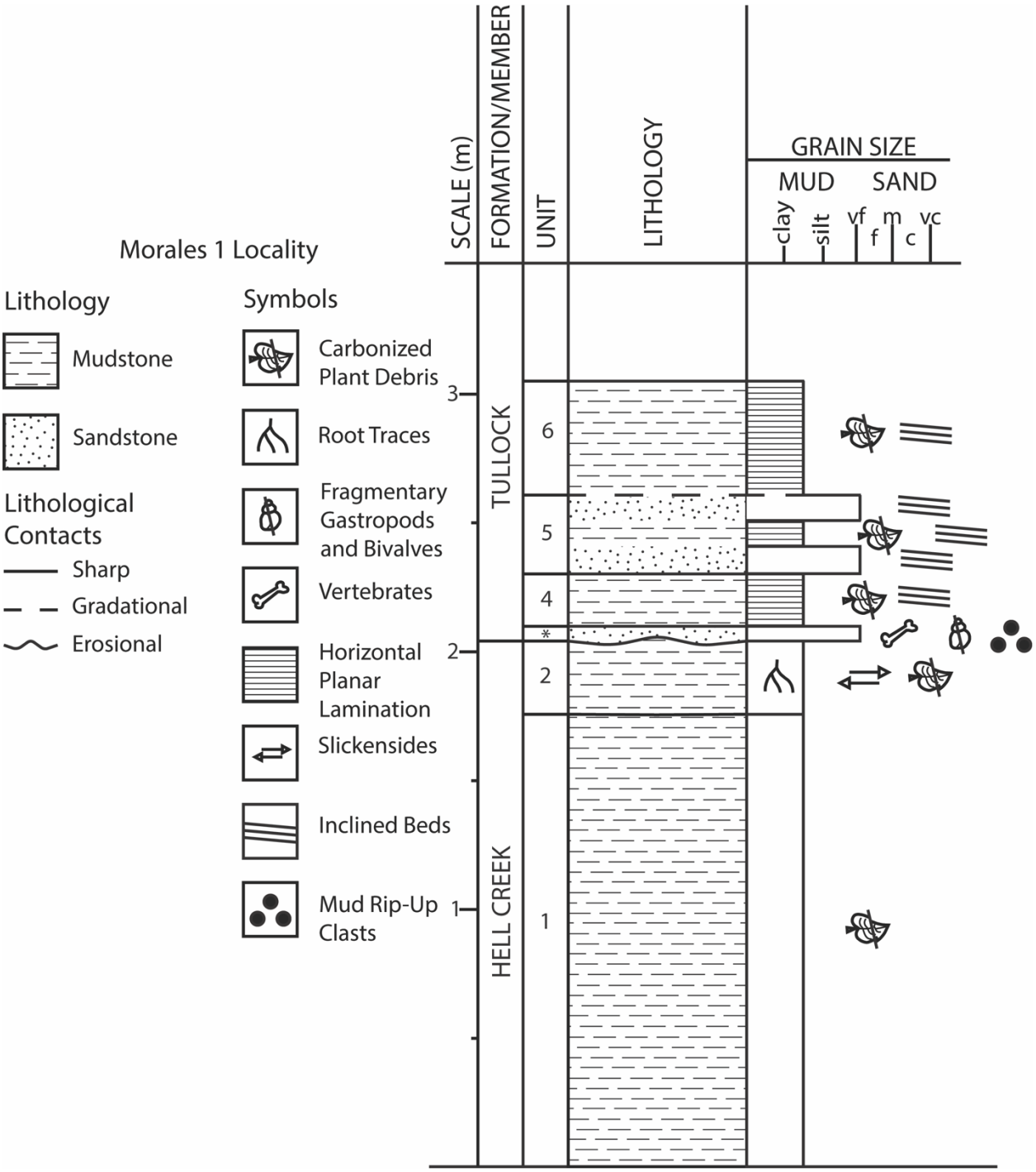

Figure 2.3 Stratigraphic section of the vertebrate microfossil locality Morales 1 (UCMP loc. V77128 = UWBM loc. C1671). The asterisk (*) indicates Unit 3. The top of the stratigraphic section indicates the top of the local stratigraphy.

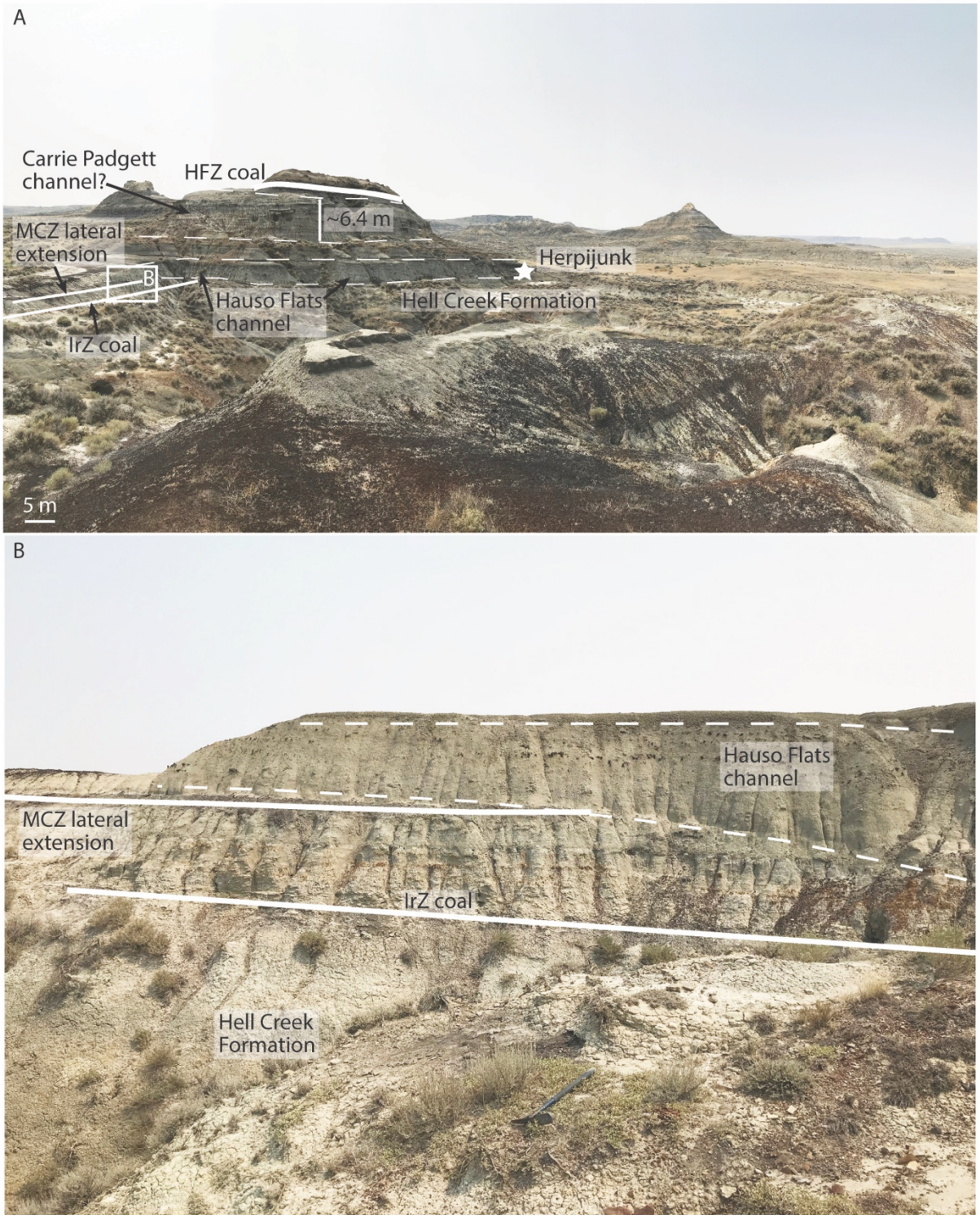

Figure 2.4 A, A south-facing view of the outcrop containing the Herpijunk Promontory vertebrate microfossil locality (white star). The ~6.4-m-thick sandstone unit that is ~5.5 m above the locality is interpreted as the Carrie Padgett channel complex. The Herpijunk microfossil locality is within the Hauso Flats channel deposit that crosscuts both the MCZ and IrZ coals and sits below a sandstone bed that is lithologically nearly identical to the sandstone characteristic of the Carrie Padgett channel deposit (Weaver et al. 2022a). **B**, Close-up, east-facing view of the

section highlighted with a box in A, showing the Hauso Flats channel deposit that hosts the Herpijunk vertebrate microfossil locality scouring the MCZ coal. Although not shown, the Hauso Flats channel also crosscuts the IrZ coal to the right. See pickaxe in the foreground for scale.

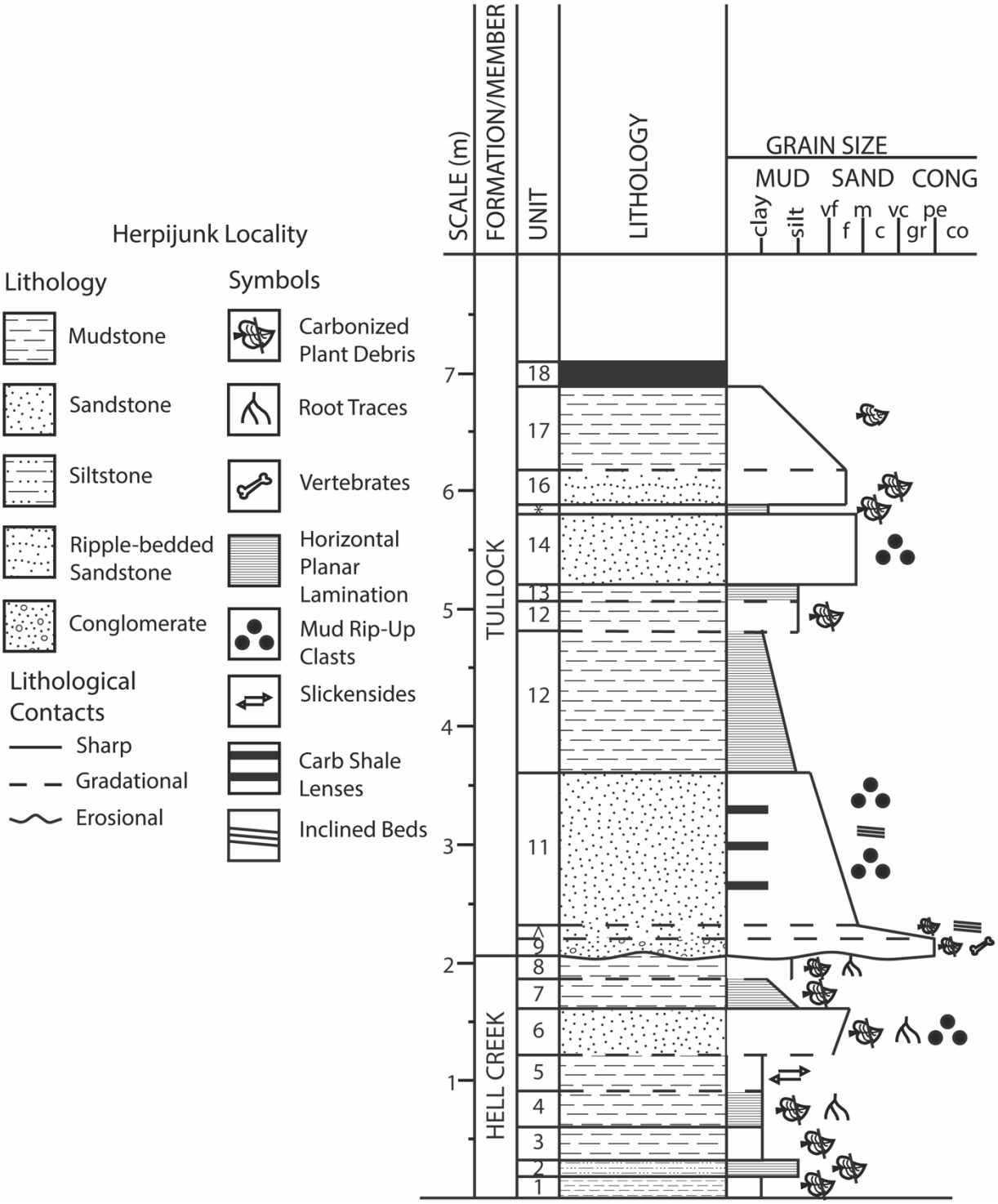

Figure 2.5 Stratigraphic section of the vertebrate microfossil locality Herpijunk (UCMP loc. V77129 = UWBM loc. C1153). The carrot (^) indicates Unit 10. The asterisk (*) indicates Unit

15. The top of the stratigraphic section does not indicate the top of the local stratigraphy but rather the end of stratigraphic logging.

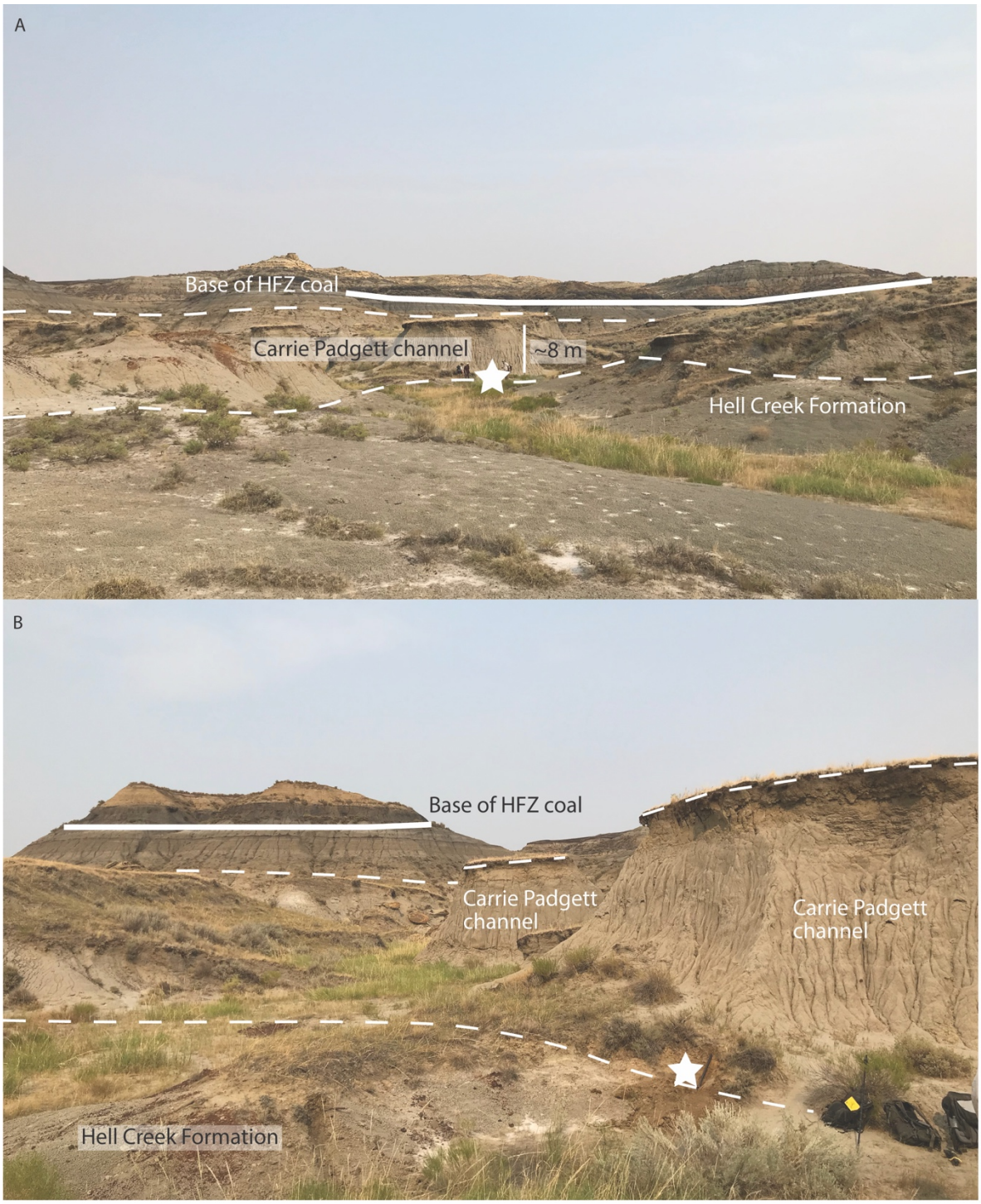

Figure 2.6 A, An east-southeast-facing view of the outcrop containing the Carrie Padgett 6 vertebrate microfossil locality (white star), the Carrie Padgett channel, and the overlying HFZ coal. **B**, An east-facing view of the outcrop containing the Carrie Padgett 6 vertebrate microfossil locality (white star), the Carrie Padgett channel, and the overlying HFZ coal.

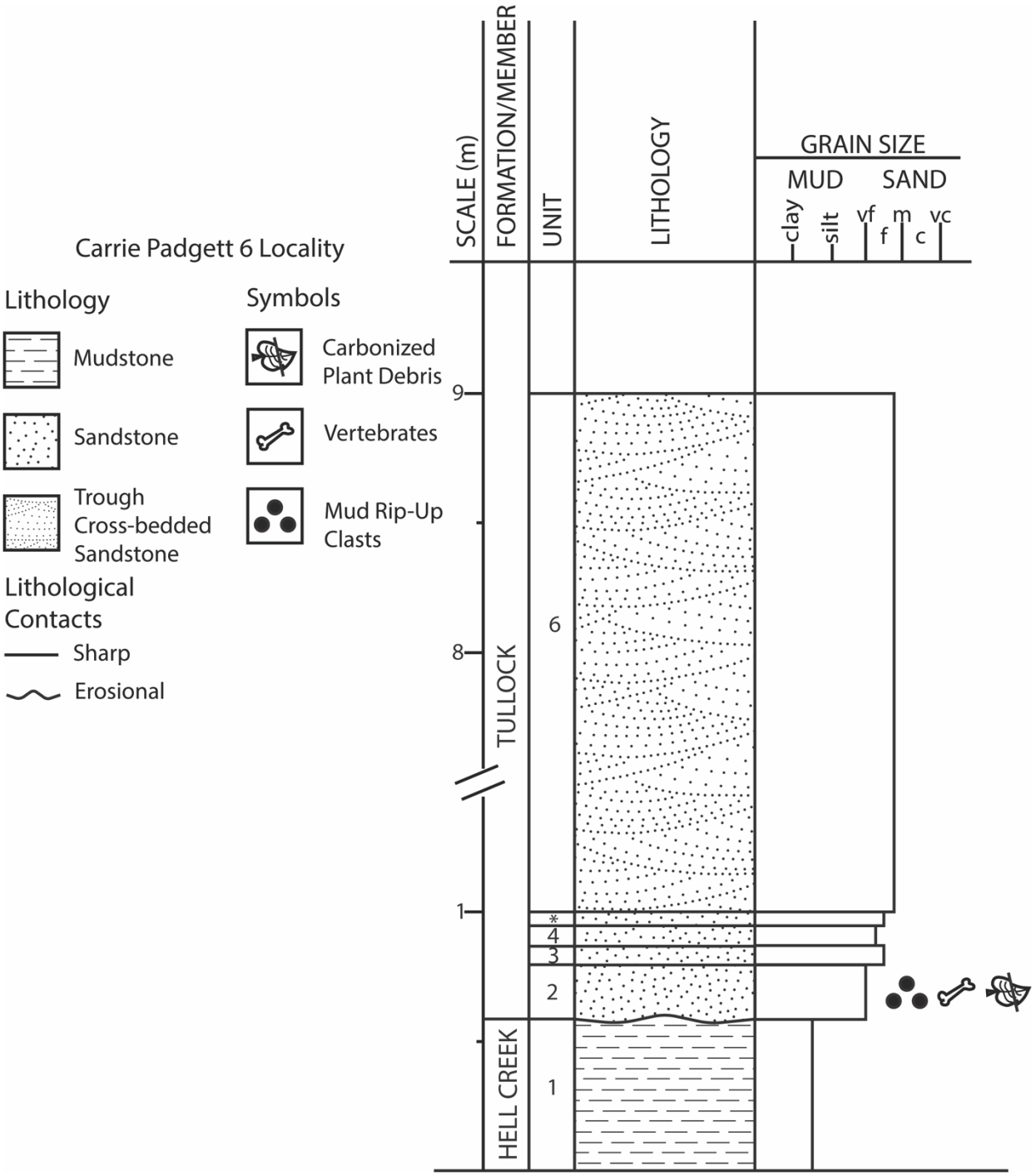

Figure 2.7 Stratigraphic section of the vertebrate microfossil locality Carrie Padgett 6 (UCMP loc. V77124 = UWBM loc. C1360). The asterisk (*) indicates Unit 5. Note the vertical scale break between 1 m and 8 m. The top of the stratigraphic section indicates the top of the local stratigraphy.

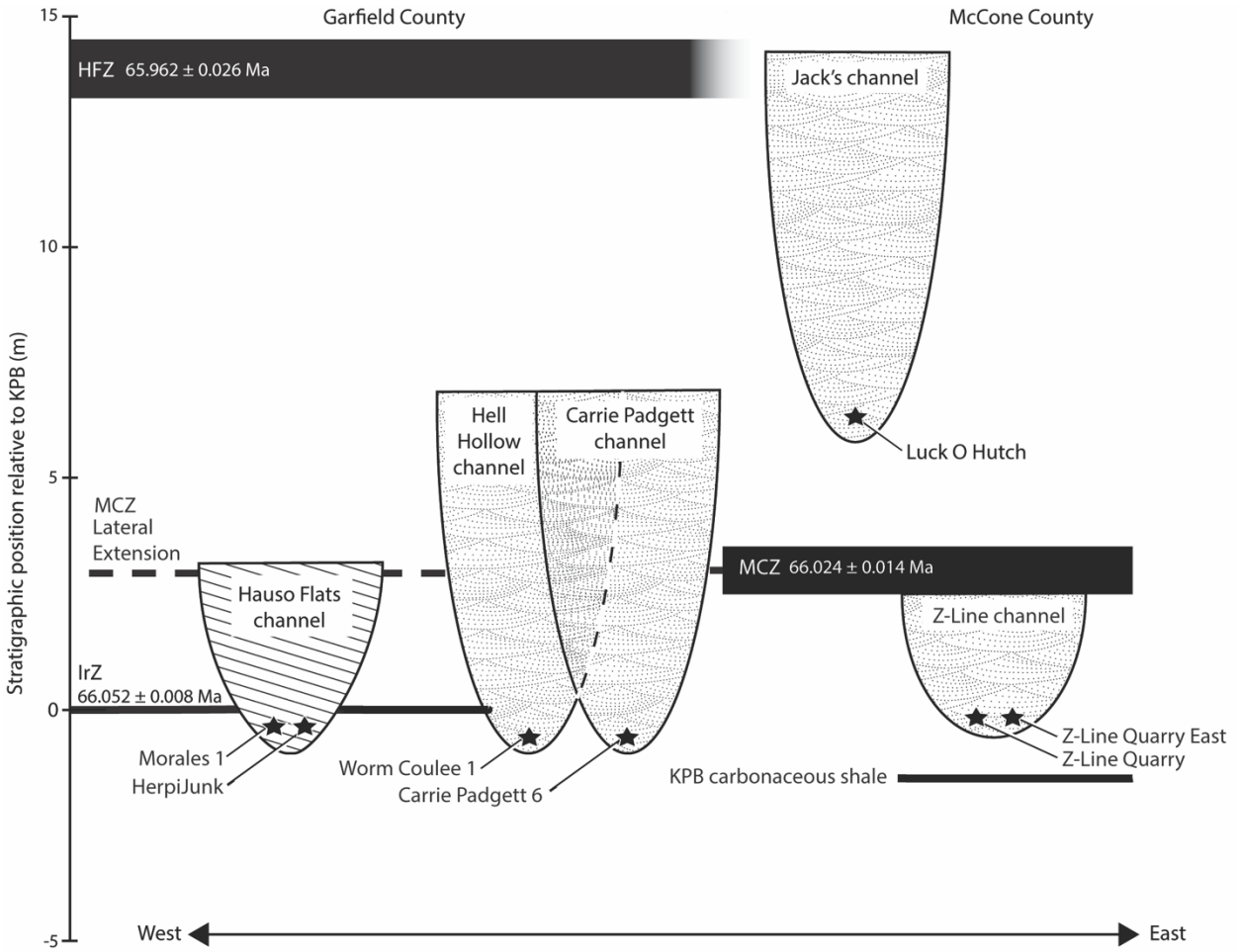

Figure 2.8 A schematic of the stratigraphic relationships among Tullock Member channel deposits from the Hell Creek region discussed in this paper. The thickness of each channel deposit and each coal layer is to scale, but the breadth of each channel deposit is not. The ages of the coals are from Sprain et al. (2018) and are presented as the weighted mean age with uncertainties, excluding systematic sources. The entire represented section is in magnetochron C29r (Sprain et al., 2018; Smith et al., 2018). The diagonal hatching of the Hauso Flats channel represents the lateral accretion beds. The overlapping of the Carrie Padgett channel on the Hell Hollow channel represents the temporal sequence of the deposition of Hell Hollow channel sediments first, followed by an erosive regime, and then the deposition of the Carrie Padgett channel sands (Weaver et al., 2022a). The KPB carbonaceous shale is a ~10 cm layer that coincides with a negative carbon isotope excursion that was interpreted by Arens et al. (2014) as marking the KPB. The stratigraphy bracketing Jack's channel differs from that depicted for the other sections because the upper bracket is not represented (see Smith et al. [2018] for a more detailed explanation).

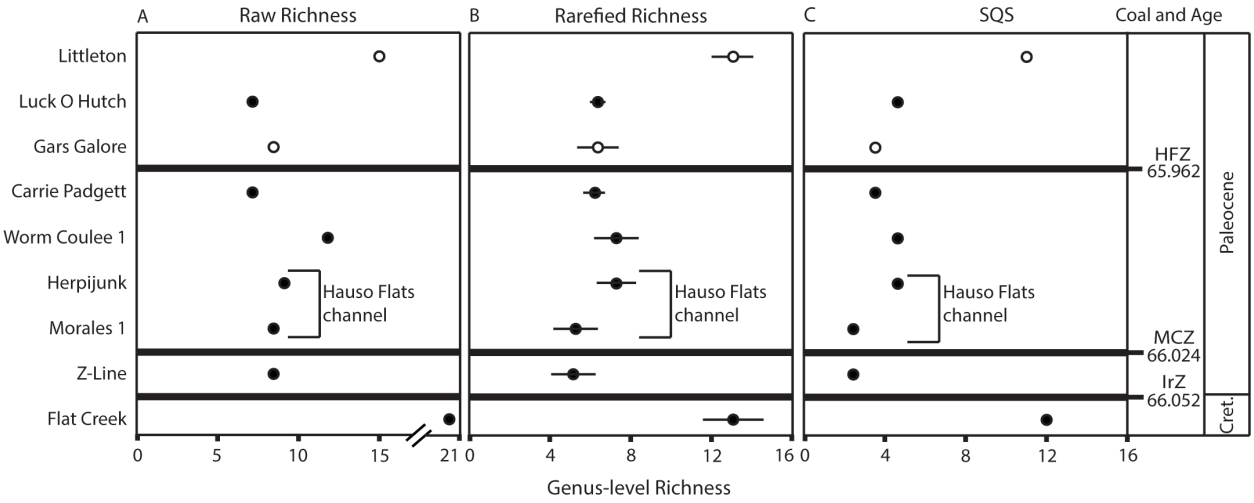

Figure 2.9 Genus-level richness estimates for select Hell Creek region (filled circles) and Denver Basin (open circles) mammalian assemblages. The vertical sequence of localities reflects the depositional age of each locality, which may differ from the age of the associated fossil assemblage. Morales 1 and Herpijunk are bracketed to reflect that they are from the same channel (the Hauso Flats channel) and in turn likely the same age. The Denver Basin locality ages are based on published ages (Dahlberg et al., 2016; Lyson et al., 2019), which we have re-calibrated to the age used for the KPB in the Hell Creek region. The ages of coals are in millions of years ago and reflect the weighted mean ages without uncertainties (see Sprain et al., 2018). **A**, Raw richness values. **B**, Rarefied richness values are shown with 95% confidence intervals (calculated using standard error). **C**, Shareholder quorum subsampling (SQS) richness values calculated using Alroy's (2010) methodology. Note the relatively stable levels of richness across the Pu1 local faunas with the exception of the Littleton local fauna. Cret.—Cretaceous

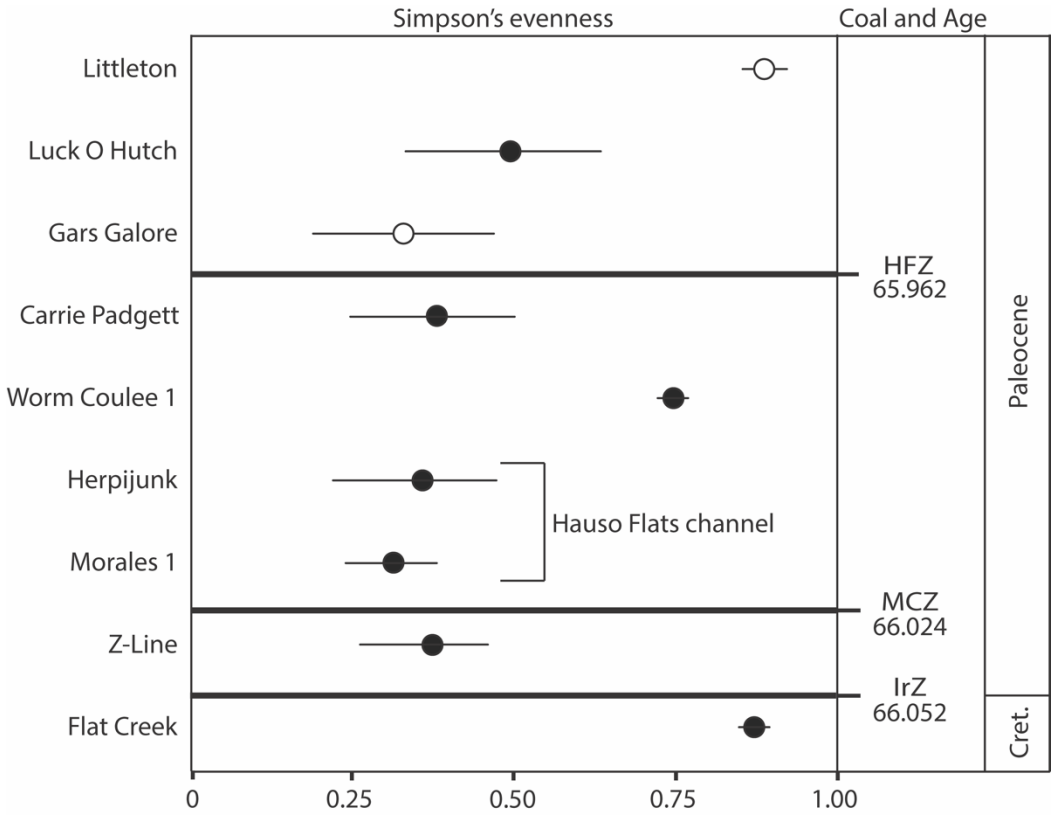

Figure 2.10 Simpson's evenness values for select Hell Creek region (filled circles) and Denver Basin (open circles) mammalian assemblages calculated at the genus level. Values are expressed as the inverse of the dominance measures (1–D) with 95% confidence intervals obtained from 9,999 bootstrap replicates. The vertical sequence of localities reflects the depositional age of each locality, which may differ from the age of the associated fossil assemblage. Morales 1 and Herpijunk are bracketed to reflect that they are from the same channel (the Hauso Flats channel) and in turn likely the same age. The Denver Basin locality ages are based on published ages (Dahlberg et al., 2016; Lyson et al., 2019), which we have re-calibrated to the age used for the KPB in the Hell Creek region. The ages of coals are in millions of years ago and reflect the weighted mean ages without uncertainties (see Sprain et al., 2018). Note the relatively low and stable levels of evenness during the Pu1 with the exception of Worm Coulee 1 and Littleton local faunas. Cret.—Cretaceous

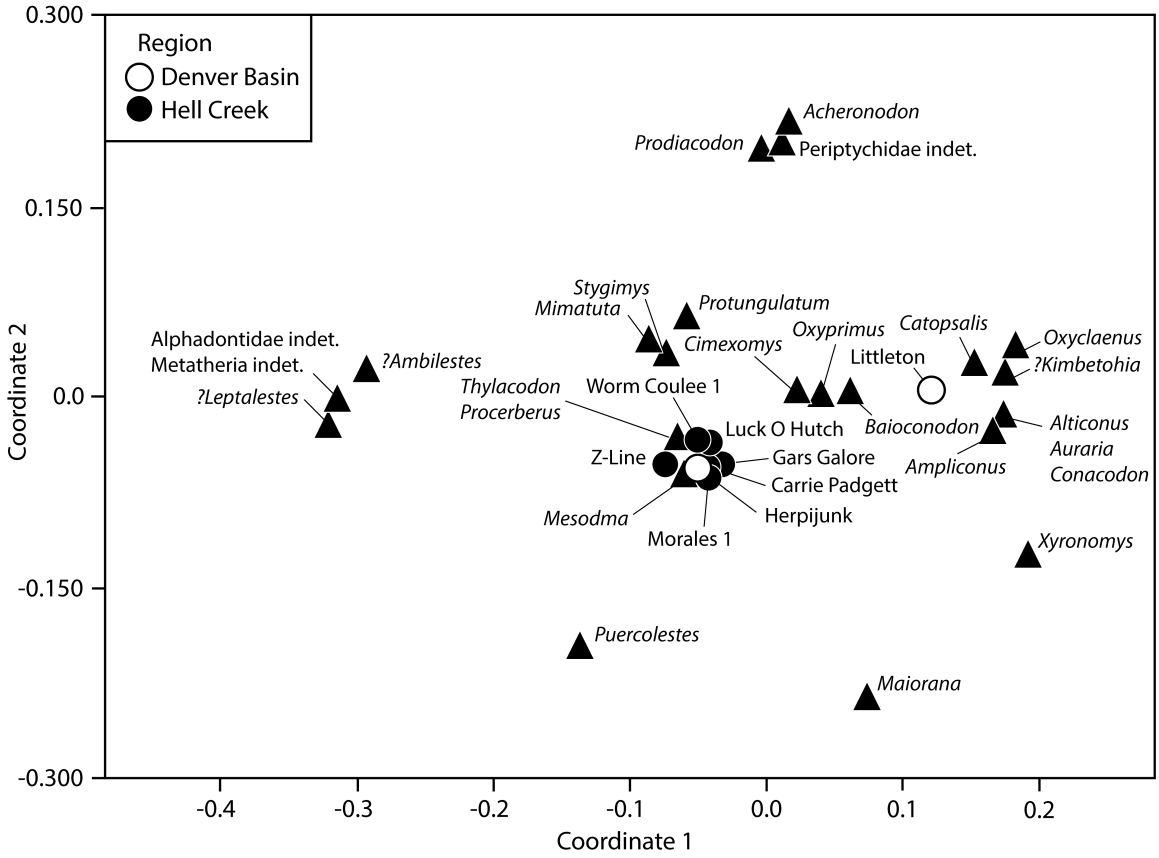

Figure 2.11.Plot of Coordinate 1 and 2 of the non-metric multidimensional scaling (NMDS) analysis of select Pu1 mammalian local faunas using the Bray Curtis genus-level dissimilarity matrix. Circles indicate local faunas from the Hell Creek region (filled circles) and Denver Basin (open circles). Triangles indicate select genera present within the local faunas. Note that the Littleton local fauna plots farthest away from all localities along Coordinate 1, whereas CA2 axis primarily separates singleton taxa on the margins from more common taxa in a central cluster.

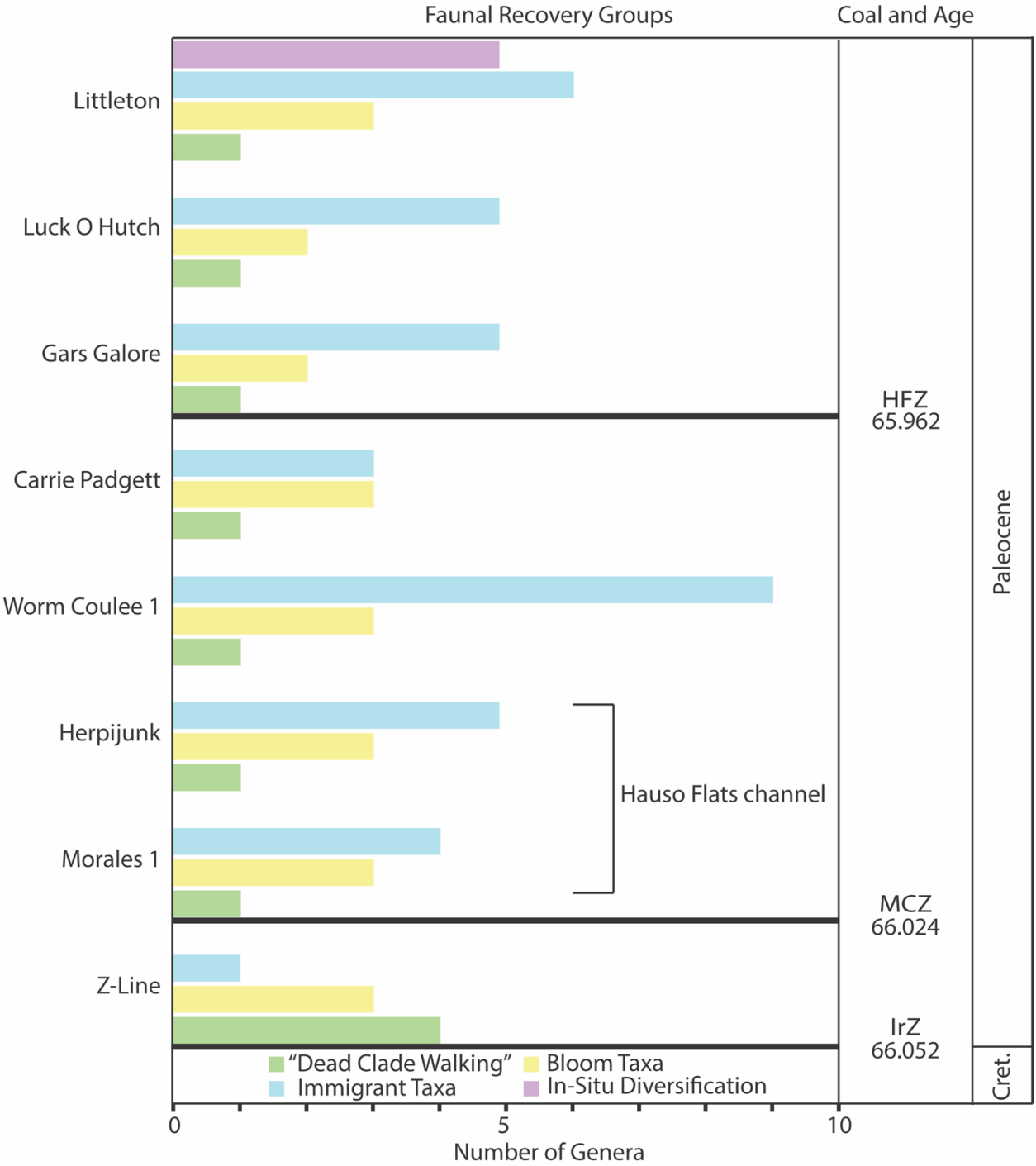

Figure 2.12 The number of genera in each faunal recovery group for each of the included local faunas. The vertical sequence of localities reflects the depositional age of each locality, which may differ from the age of the associated fossil assemblage. Morales 1 and Herpijunk are bracketed to reflect that they are from the same channel (the Hauso Flats channel) and in turn likely the same age. The Denver Basin locality ages are based on published ages (Dahlberg et al., 2016; Lyson et al., 2019), which we have re-calibrated to the age used for the KPB in the Hell Creek region. The ages of coals are in millions of years ago and reflect the weighted mean ages without uncertainties (see Sprain et al., 2018). We classified each taxon into one of four faunal

recovery groups: ‘dead clade walking’ (DCW), bloom taxon, immigrant taxon, or a byproduct of in-situ diversification (Table 2.2; see Methods and Supplemental Information for a more detailed explanation).

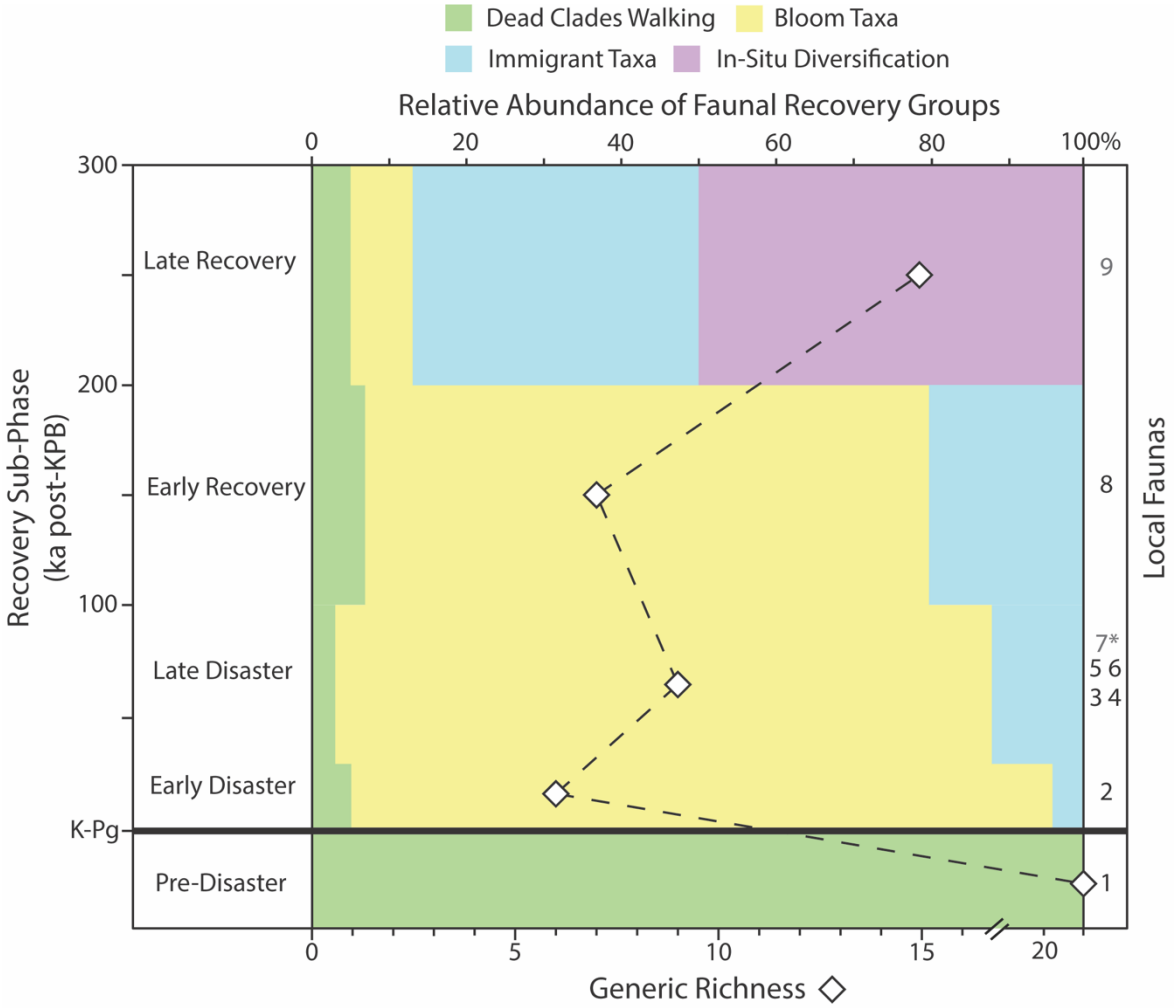

Figure 2.13 Proposed model of post-KPB mammalian recovery patterns in the Western Interior of North America based on local faunas of the Hell Creek region and Denver Basin. Local faunas represented by numbers: 1—Flat Creek; 2—Z-Line; 3—Morales 1; 4—Herpijunk; 5—Carrie Padgett; 6—Worm Coulee 1; 7—Gars Galore; 8—Luck O Hutch; 9—Littleton. Black numbers represent local faunas from the Hell Creek region, gray numbers represent local faunas from the Denver Basin. Each local fauna was placed into a biotic recovery sub-phase based on its depositional age and similarity in community structure (see Discussion for more detailed explanations). The age range of each sub-phase is in thousands of years (ka) post-KPB and reflects the proposed age of the constituent local fauna. The asterisk for Gars Galore indicates there is a difference between the vertical placement on the timeline (100 ka) and its estimated age (128 ka). The generic richness for each sub-phase (open diamonds) is based on the corresponding value of the local fauna or the mean value for the five local faunas in the late disaster sub-phase (see Fig. 2.12 for generic richness values for each local fauna).We classified each taxon into one of four faunal recovery groups: ‘dead clade walking’ (DCW), bloom taxon, immigrant taxon, or a byproduct of in-situ diversification (Table 2.2; see Methods and

Supplemental Information for a more detailed explanation). For each sub-phase, the relative abundance of individuals of each faunal recovery group is represented by the width of its corresponding-colored bar. Note that the relative abundance of bloom taxa decreased while the relative abundance of immigrants increased from the early disaster through late recovery. Taxonomic richness also increased from early recovery into late recovery with the onset of in-situ diversification.

2.12 TABLES

Table 2.1 Taxonomic dissimilarity values of select Pu1 mammalian assemblages. The values in the top panels were calculated using Bray Curtis metric. Values in the left panels were calculated at the genus level, and those in the right panel at the species level.

	Genus Level								Species Level							
	M1	HJ	CP	WC	ZL	LH	GG	LF	M1	HJ	CP	WC	ZL	LH	GG	LF
M1	0	-	-	-	-	-	-	-	0	0.50	0.44	0.78	0.61	0.57	0.59	0.93
HJ	0.27	0	-	-	-	-	-	-	-	0	0.43	0.68	0.62	0.36	0.70	0.93
CP	0.17	0.31	0	-	-	-	-	-	-	-	0	0.79	0.58	0.54	0.56	0.93
WC	0.63	0.44	0.64	0	-	-	-	-	-	-	-	0	0.92	0.78	0.85	0.97
ZL	0.36	0.36	0.29	0.65	0	-	-	-	-	-	-	-	0	0.65	0.73	0.87
LH	0.28	0.41	0.29	0.67	0.47	0	-	-	-	-	-	-	-	0	0.69	0.89
GG	0.33	0.46	0.34	0.70	0.45	0.33	0	-	-	-	-	-	-	-	0	0.87
LF	0.71	0.67	0.76	0.74	0.81	0.72	0.77	0	-	-	-	-	-	-	-	0

Note: M1—Morales 1; HJ—Herpijunk, CP—(Carrie Padgett 1 and 6 combined), WC—Worm Coulee 1, ZL— (Z-Line Q and Z-Line-E combined); LH—Luck O Hutch; GG—Gars Galore; LF—Littleton Fauna

Table 2.2 Mammalian faunal lists for the Pu1 local faunas in the Hell Creek region used in this study. The number of specimens of each taxon and the corresponding percent relative abundance (in parentheses) are presented for each local fauna.

Local Fauna	Z-Line (V84193, V84194)	Morales 1 (V77128)	Herpijunk (V77129)	Worm Coulee 1 (V74111)	Carrie Padgett (V77124, V79100)	Luck O Hutch (V88036)
Taxon						
Multituberculata						
Mesodma hensleighi[B]	-	17 (6%)	3 (4%)	-	2 (3%)	1 (2%)
Mesodma formosa[B]	27 (23%)	104 (41%)	32 (40%)	-	28 (35%)	11 (20%)
Mesodma thompsoni[B]	42 (36%)	74 (29%)	18 (22%)	306 (32%)	22 (28%)	16 (29%)
Mesodma sp.[B]	17 (15%)	9 (3%)	11 (14%)	-	11 (13%)	9 (16%)
Cimexomys minor[D]	-	6 (2%)	2 (3%)	10 (1%)	3 (4%)	1 (2%)
Cimexomys gratus[D]	-	3 (1%)	-	8 (< 1%)	-	3 (5%)
Stygimys kuszmauli[I]	-	3 (1%)	2 (3%)	44 (4%)	2 (3%)	-
?*Stygimys kuszmauli*[I]	-	-	1 (1%)	-	-	-
Catopsalis alexanderi[I]	-	-	-	1 (< 1%)	-	-
Acheronodon garbani[I]	-	-	-	1 (< 1%)	-	-

Metatheria						
Thylacodon montanensis[B]	10 (9%)	5 (2%)	2 (3%)	168 (18%)	3 (4%)	-
?*Leptalestes cooki*[D]	1 (1%)	-	-	-	-	-
Alphadontidae indet.[D]	2 (2%)	-	-	-	-	-
Metatheria indet.[D]	4 (3%)	-	-	-	-	-
Eutheria						
Procerberus formicarum[B]	9 (8%)	19 (7%)	3 (4%)	294 (32%)	6 (8%)	1 (2%)
Procerberus cf. *P. grandis*[ID]	-	-	-	-	-	2 (4%)
?*Ambilestes cerberoides*[D]	1 (1%)	-	-	-	-	-
?*Prodiacodon crustulum*[I]	-	-	-	-	-	1 (2%)
Prodiacodon sp. A[I]	-	-	-	2 (< 1%) *	-	-
Puercolestes simpsoni[I]	-	-	1 (1%)	-	-	-
Protungulatum donnae[I]	-	-	-	18 (1%)	1 (1%)	4 (7%)
Oxyprimus erikseni[I]	-	4 (1%)	1 (1%)	21 (2%)	-	2 (4%)
Baioconodon nordicum[I]	-	-	2 (3%)	2 (< 1%)	-	-
Baioconodon engdahli[I]	-	1 (< 1%)	-	8 (< 1%)	-	-

Baioconodon sp.[I]	-	1 (< 1%)	-	-	-	1 (2%)
Mimatuta morgoth[I]	-	-	-	26 (2%)	-	1 (2%)
Mimatuta minuial[I]	-	1 (< 1%)	-	10 (1%)	1 (1%) *	-
Mimatuta sp.[I]	3 (3%)	1 (< 1%)	1 (1%)	-	-	1 (2%)
Periptychidae indet.[I]	-	-	-	1 (< 1%)	-	1 (2%)
TOTAL N	116	248	79	920	80	55

Note: N—number of specimens identifiable to genus or species level or that can be attributed to a taxon distinct from all others in the assemblage. The V-number below the locality name is the UCMP vertebrate locality number, [D]—taxa designated as a 'dead clade walking,' [B]—taxa designated as a bloom taxon, [I]—taxa designated as an immigrant, [ID]—taxa designated as the product of in-situ diversification, *—specimens whose identification has not been confirmed or has been questioned by previous work.

2.13 Supplemental Materials

Dental Terminology, Conventions, and Measurements We used dental terminology that follows Jepsen (1940), Archibald (1982), and Kielan-Jaworowska et al. (2004). Lower premolars and molars are denoted in text, tables, and figures with lowercase letters and numbers corresponding to their position in the series (e.g., m1 for a lower first molar). Upper premolars and molars are denoted with uppercase letters (e.g., M1 for an upper first molar). Cusp formulae for multituberculates are presented from buccal to lingual row (e.g., 7:8:6). "R" denotes the presence of a continuous ridge instead of a row of separate cusps (e.g., 7:8:R). Question marks are used to indicate uncertainty of the cusp count in the dental formula. The multituberculate

dental measurements that we used follow Novacek and Clemens (1977) and Eaton (1995) for premolars and molars, respectively. The therian dental measurements that we used follow Archibald (1982). The specimens were measured using a Leica MZ 9.5 binocular dissecting microscope, with a custom measuring stage precise to 0.001 mm.

Measurement Abbreviations We oriented specimens for measurements according to the protocol outlined in Wilson Mantilla et al. (2021). **DW**, greatest distal width of upper molar or talonid width of lower molar; **H**, crown height of multituberculate p4 measured at right angle from the baseline to the highest point of the apical curve of the tooth (Novacek and Clemens, 1977); **L**, mesiodistal length of crown; **L1**, length from mesial edge of multituberculate p4 crown to the highest point on the apical curve, parallel to the length (L) (Novacek and Clemens, 1977); **MW**, greatest mesial width of upper molar or trigonid width of lower molar; **N**, sample size; **W**, buccolingual width of crown; **X**, mean; . ***** indicates incomplete measurement due to damage.

SYSTEMATIC PALEONTOLOGY

Class MAMMALIA Linnaeus, 1758

Subclass ALLOTHERIA Marsh, 1880

Order MULTITUBERCULATA Cope, 1884

Suborder PTILODONTOIDAE Sloan and Van Valen, 1965

Family NEOPLAGIAULACIDAE Ameghino, 1890

Genus *MESODMA* Jepsen, 1940

MESODMA FORMOSA Marsh, 1889

(Fig. S1)

Referred material—

V77128: p4: UCMP 140296, UCMP 140294 m1: UCMP 140297, UCMP 140302, UCMP 140304, UCMP 140306, UCMP 140307, UCMP 140309, UCMP 140310, UCMP 140311, UCMP 140312, UCMP 140315, UCMP 140319, UCMP 140320, UCMP 140323, UCMP 140325, UCMP 140326, UCMP 140328, UCMP 294333, UCMP 294335, UCMP 294336 m2: UCMP 294341, UCMP 294347, UCMP 294348, UCMP 294349, UCMP 294350, UCMP 294351, UCMP 294352, UCMP 294354, UCMP 294355, UCMP 294356, UCMP 294357, UCMP 294358, UCMP 294360, UCMP 294364, UCMP 294366, UCMP 294368, UCMP 294369, UCMP 294370, UCMP 294382, UCMP 294383, UCMP 294384, UCMP 294385, UCMP 294387, UCMP 294389, UCMP 294390, UCMP 294391, UCMP 294392, UCMP 294397 P4: UCMP 140332, UCMP 140336, UCMP 140339, UCMP 140341, UCMP 140342, UCMP 140344, UCMP 140345, UCMP 140348, UCMP 140349, UCMP 140352, UCMP 294329 M1: UCMP 140356, UCMP 140360, UCMP 140362, UCMP 140363, UCMP 140365, UCMP 140367, UCMP 140368, UCMP 294343, UCMP 294344 M2: UWBM 114793, UCMP 294340, UCMP 294398, UCMP 294399, UCMP 294400, UCMP 294401, UCMP 294402, UCMP 294404, UCMP 294408, UCMP 294409, UCMP 294412, UCMP 294414, UCMP 294415, UCMP 294416, UCMP 294417, UCMP 294419, UCMP 294421, UCMP 294422, UCMP 294423, UCMP 294424, UCMP 294425, UCMP 294427, UCMP 294428, UCMP 294430, UCMP 294431, UCMP 294436, UCMP 294438, UCMP 294439, UCMP 294441, UCMP 294442, UCMP 294443, UCMP 294444, UCMP 294445, UCMP 294446, UCMP 294447; **V77129:** m1: UWBM 104573, UWBM 104579, UWBM 115321, UWBM 115338, m2: UWBM 112769, UWBM 104570, UWBM 112758, UWBM 112754, UWBM 112752, UWBM 104641, UWBM 104597, UWBM 112559, UWBM 115322, UWBM 115330, UWBM 115323, UWBM 115331 P4: UWBM 112747 M1: UWBM 104585, UWBM 114640 M2: UWBM 112760, UWBM 112759, UWBM 112766, UWBM 112772, UWBM 112762, UWBM 104589, UWBM 115291, UWBM 114792, UWBM 114669, UWBM 114666, UWBM 115309, UWBM 115348, UWBM 115304; **V77124:** p4: UWBM 114145 m1: UWBM 102342, UWBM 94919, UWBM 111137, UWBM 111136, UWBM 114665 m2: UWBM 105257, UWBM 102343, UWBM 111210, UWBM 111208, UWBM 111207, UWBM 111217, UWBM 114645 P4: UWBM 110682 M1: UWBM 114654, UWBM 112984, UWBM 114643 M2: UWBM 105272, UWBM 105279, UWBM 104615, UWBM 102345, UWBM 104614, UWBM 102344, UWBM 110670, UWBM 115358, UWBM 115360; **V79100:** M1: UCMP 294522 M2: UCMP 294526

DESCRIPTION

The specimens match published descriptions of the crown morphology and cusp formula of *Mesodma* (Clemens, 1964; Novacek and Clemens, 1977; Archibald, 1982). Specimens

identified as p4's were attributed to *M. formosa* on the basis of size rather than shape based on the results of Smith and Wilson (2017). Using linear measurements outlined in Archibald (1982), specimens were plotted along with data from Smith and Wilson (2017). All of the referred specimens unambiguously fit within the *M. formosa* size range (Clemens, 1964; Lillegraven, 1969; Archibald, 1982). Width measurements were unavailable for specimens UCMP 110682 – UCMP 294329.

TABLE S1. Dental measurements (in mm) of p4s from *Mesodma formosa*

Tooth Position	Specimen	L	L1	H
p4	UWBM 114145	__	1.40*	__
p4	UCMP 140296	__	__	1.56
p4	UCMP 140294	__	1.33*	1.65

TABLE S2. Dental measurements (in mm) of *Mesodma formosa*

Tooth Position	Specimen	L	W	Cusp Formula
m1	UWBM 104573	1.53*	1.09	3+:3+

m1	UWBM 104579	1.73*	1.04	5+:3+
m1	UWBM 115321	2.54	1.11	7:4
m1	UWBM 115338	2.39	1.02	7:5
m1	UWBM 102342	2.11	1.04	6:4
m1	UWBM 94919	2.44	1.12	6:4
m1	UWBM 111137	2.53	1.03	6:4
m1	UWBM 111136	2.31	0.96	6:4
m1	UWBM 114665	2.46	1.03	6:5
m1	UCMP 140297	2.27	0.99	6:4
m1	UCMP 140302	2.39	1.17	6:4
m1	UCMP 140304	2.32	1.04	6:4

m1	UCMP 140306	2.30	0.99	7:5
m1	UCMP 140307	2.55	0.99	6:4
m1	UCMP 140309	2.23	1.01	6:4
m1	UCMP 140310	2.27	0.96	?:4
m1	UCMP 140311	2.38	1.02	6:4
m1	UCMP 140312	2.14	1.07	6:4
m1	UCMP 140315	2.26	0.93	6:4
m1	UCMP 140319	2.30	0.96	6:4?
m1	UCMP 140320	2.22	1.07	6:4
m1	UCMP 140323	2.36	1.01	6:4
m1	UCMP 140325	2.36	0.92	6:4

m1	UCMP 140326	2.36	0.89	7:5
m1	UCMP 140328	2.30	0.89	6:4
m1	UCMP 294333	2.30	1.04	6?:?
m1	UCMP 294335	2.18	0.94	6:4
m1	UCMP 294336	2.04	0.79	5:?
m2	UWBM 112769	1.39	1.27	2:3
m2	UWBM 104570	1.31	1.20	2:3
m2	UWBM 112758	1.32	1.23	2:3
m2	UWBM 112754	1.35	1.22	4:2
m2	UWBM 112752	1.35	1.16	3:2
m2	UWBM 104641	1.30	1.20	3:2

m2	UWBM 104597	1.37	1.18	3:2
m2	UWBM 112559	1.32	1.16	3:2
m2	UWBM 115322	1.40	1.05	3+:2
m2	UWBM 115330	1.37	1.17	4:2
m2	UWBM 115323	1.42	1.23	3:2
m2	UWBM 115331	1.47	1.35	4+:2
m2	UWBM 105257	1.27	1.15	3:2
m2	UWBM 102343	1.52	1.20	4:2
m2	UWBM 111210	1.34	1.21	1+:2
m2	UWBM 111208	1.61	1.16	3:2
m2	UWBM 111207	1.59	1.11	3:2

m2	UWBM 111217	1.34	1.23	3:2
m2	UWBM 114645	1.38	1.24	4:2
m2	UCMP 294341	1.41	1.22	2:3
m2	UCMP 294347	1.38	1.16	4:3
m2	UCMP 294348	1.41	1.22	4:2
m2	UCMP 294349	1.37	1.10	3:2
m2	UCMP 294350	1.31	1.00	4:2
m2	UCMP 294351	1.48	1.20	3+:2
m2	UCMP 294352	1.42	1.14	4:2
m2	UCMP 294354	1.53	1.17	3:2
m2	UCMP 294355	1.34	1.06	3:2

m2	UCMP 294356	1.33	1.08	4:2
m2	UCMP 294357	1.31	1.11	4:2
m2	UCMP 294358	1.29	1.16	4:2
m2	UCMP 294360	1.44	1.06	0+:2
m2	UCMP 294364	1.49	1.17	3:2
m2	UCMP 294366	1.37	1.16	0+:2
m2	UCMP 294368	1.27	1.13	4:2
m2	UCMP 294369	1.44	1.18	4:2
m2	UCMP 294370	1.41	1.03	4:2
m2	UCMP 294382	1.31	1.09	3:2
m2	UCMP 294383	1.35	1.04	4:2

m2	UCMP 294384	1.31	1.02	4:2
m2	UCMP 294385	1.40	1.14	4:2
m2	UCMP 294387	1.34	1.05	3:2
m2	UCMP 294389	1.36	1.22	3:2+
m2	UCMP 294390	1.32	0.91	0+:0+
m2	UCMP 294391	1.56	1.19	4:2
m2	UCMP 294392	1.25	1.12	4:2
m2	UCMP 294397	1.32	1.19	4:2
P4	UWBM 112747	2.12*	1.08*	0+:5
P4	UWBM 110682	2.30		1:7
P4	UCMP 140332	2.41		3:7

P4	UCMP 140336	2.38		2:7
P4	UCMP 140339	2.32		2:6
P4	UCMP 140341	2.28		2:7
P4	UCMP 140342	2.28		2:7
P4	UCMP 140344	2.37		3:7
P4	UCMP 140345	2.22		3:7
P4	UCMP 140348	2.21		2:7
P4	UCMP 140349	2.23		2:7
P4	UCMP 140352	2.38		3:7
P4	UCMP 294329	2.169*		0:7
M1	UWBM 104585	2.87	1.38	7:8:6

M1	UWBM 114640	3.01	1.41	7:8:4
M1	UWBM 114654	2.03*	1.42	4+:5+:4+
M1	UWBM 112984	3.02	1.46	7:8:5
M1	UWBM 114643	1.90	1.41	4+:5+:4+
M1	UCMP 140356	3.18	1.31	7:8:4
M1	UCMP 140360	3.23	1.28	7:8:4
M1	UCMP 140362	3.08	1.22	7:8:4
M1	UCMP 140363	2.98	1.15	7:8:4
M1	UCMP 140365	3.14	1.22	7:8:5
M1	UCMP 140367	3.28	1.19	7:8:4
M1	UCMP 140368	3.30	1.22	7:8:4

M1	UCMP 294343	3.11	1.32	0+:0+:0+
M1	UCMP 294344	3.02	1.33	6:7:2+
M1	UCMP 294522	2.85	1.39	5+:5+:1+
M2	UWBM 112760	1.54	1.37	1:3:4
M2	UWBM 112759	1.41	1.42	1:2:3
M2	UWBM 112766	1.41	1.39	1:3:3
M2	UWBM 112772	1.60	1.47	1:3:3
M2	UWBM 112762	1.48	1.44	1:3:3
M2	UWBM 104589	1.43	1.42	1:3:3
M2	UWBM 115291	1.47	1.51	1:3:3
M2	UWBM 114792	1.38	1.32	1:3:3

M2	UWBM 114669	1.42	1.36	1:3:3
M2	UWBM 114666	1.41	1.43	1:3:3+
M2	UWBM 115309	1.46	1.38	
M2	UWBM 115348	1.46	1.45	1:3:3
M2	UWBM 115304	1.43	1.42	1:3:3
M2	UWBM 114793	1.55	1.42	1:3:0+
M2	UWBM 105272	1.46	1.45	1:2:3
M2	UWBM 105279	1.32	1.31	1:3:3
M2	UWBM 104615	1.44	1.43	1:3:3
M2	UWBM 102345	1.44	1.44	1:3:3+
M2	UWBM 104614	1.38	1.37	1:3:3

M2	UWBM 102344	1.48	1.47	1:3:3
M2	UWBM 110670	1.49	1.33	1:3:3
M2	UWBM 115358	1.36	1.38	1:3:3
M2	UWBM 115360	1.41	1.48	1:3:3
M2	UCMP 294340	1.31	1.38	1:3:3
M2	UCMP 294398	1.47	1.09	1:3:3
M2	UCMP 294399	1.51	1.23	1:3:3
M2	UCMP 294400	1.44	1.29	1:3:3
M2	UCMP 294401	1.30	1.27	1:3:3
M2	UCMP 294402	1.49	1.22	1:3:3
M2	UCMP 294404	1.34	1.15	1:3:3

M2	UCMP 294408	1.51	1.28	1:3:3
M2	UCMP 294409	1.46	1.25	1:3:3
M2	UCMP 294412	1.36	1.14	1:3:3
M2	UCMP 294414	1.53	1.32	1:3:3
M2	UCMP 294415	1.52	1.21	1:3:3+
M2	UCMP 294416	1.41	1.26	1:3:3
M2	UCMP 294417	1.48	1.24	1:3:3
M2	UCMP 294419	1.42	1.18	0+:2:3+
M2	UCMP 294421	1.43	1.16	1:2:3
M2	UCMP 294422	1.40	1.25	1:2:0+
M2	UCMP 294423	1.54	1.24	1:0+:2+

M2	UCMP 294424	1.41	1.28	1:3:3
M2	UCMP 294425	1.43	1.24	1:3:3
M2	UCMP 294427	1.34	1.25	1:3:3
M2	UCMP 294428	1.32	1.17	1:1+:0+
M2	UCMP 294430	1.41	1.13	1:3:3
M2	UCMP 294431	1.30	1.22	1:3:3
M2	UCMP 294436	1.30	1.31	1:3:3
M2	UCMP 294438	1.37	1.21	1:3:3
M2	UCMP 294439	1.28	1.21	1:3:3
M2	UCMP 294441	1.30	1.23	1:3:3
M2	UCMP 294442	1.28	1.23	1:3:3

M2	UCMP 294443	1.38	1.20	1:3:3
M2	UCMP 294444	1.43	1.22	1:3:3
M2	UCMP 294445	1.31	1.16	1:3:3
M2	UCMP 294446	1.42	1.26	1:3:3
M2	UCMP 294526	1.60	1.27	1:3:3
M2	UCMP 294447	1.44	1.28	1:3:3

FIGURE S1. **A,** Left m2 of *Mesodma formosa* (UWBM 104641) in stereo occlusal view. **B,** Right M2 of *Mesodma formosa* (UWBM 104589) in stereo occlusal view. Both specimens are oriented with the mesial face upwards. Scale bar equals 1 mm.

MESODMA THOMPSONI Clemens, 1964

(Fig. S2)

Referred material— **V77128:** p4: UCMP 140295, UCMP 140289, UCMP 140290, UCMP 140291, UCMP 140292 m1: UCMP 140298, UCMP 140299, UCMP 140300, UCMP 140301, UCMP 140303, UCMP 140305, UCMP 140308, UCMP 140313, UCMP 140314, UCMP 140316, UCMP 140317, UCMP 140318, UCMP 140321, UCMP 140322, UCMP 140324, UCMP 140327, UCMP 140330, UCMP 140331, UCMP 294332, UCMP 294337, UCMP 294338 m2: UCMP 294359, UCMP 294361, UCMP 294362, UCMP 294363, UCMP 294365, UCMP 294367, UCMP 294377, UCMP 294388, UCMP 294394, UCMP 294396 P4: UWBM 114796, UCMP 140333, UCMP 140335, UCMP 140337, UCMP 140338, UCMP 140340, UCMP 140343, UCMP 140346, UCMP 140347, UCMP 140351, UCMP 140353, UCMP 294324, UCMP 294326, UCMP 294328 M1: UWBM 115289, UCMP 140355, UCMP 140358, UCMP 140359, UCMP 140361, UCMP 140364, UCMP 140366, UCMP 140370, UCMP 140371, UCMP 294342 M2: UCMP 294405, UCMP 294406, UCMP 294407, UCMP 294410,

UCMP 294411, UCMP 294413, UCMP 294426, UCMP 294429, UCMP 294432, UCMP 294434, UCMP 294437, UCMP 294440, UCMP 294448; **V77129:** p4: UWBM 104586 m1: UWBM 114676, UWBM 114668, UWBM 114790, UWBM 115329, UWBM 115339, UWBM 115299, UWBM 104588 P4: UWBM 103772, UWBM 114667, UWBM 114786, UWBM 114670, UWBM 115315, UWBM 115307 M1: UWBM 112750, UWBM 112748, UWBM 104580; **V77124:** m1: UWBM 110683, UWBM 114651, UWBM 114656, UWBM 115352 P4: UWBM 107348, UWBM 105259, UWBM 105258, UWBM 104646, UWBM 103323, UWBM 105273, UWBM 111213 M1: UWBM 111201, UWBM 111135, UWBM 114677, UWBM 105256, UWBM 114655 M2: UWBM 114662, UWBM 114671; **V79100:** m2: UCMP 294523 M1: UCMP 294527

DESCRIPTION

The specimens match published descriptions of the crown morphology and cusp formula of *Mesodma* (Clemens, 1964; Novacek and Clemens, 1977; Archibald, 1982). All referred specimens within the published size range of *M. thompsoni* and its junior synonym *M. garfieldensis* (Clemens, 1964; Lillegraven, 1969; Archibald, 1982; Smith and Wilson, 2017). Width measurements were unavailable for specimens UWBM 105273–UCMP 294328.

TABLE S3. Dental measurements (in mm) of p4's from *Mesodma thompsoni*.

Tooth Position	Specimen	L	L1	H
p4	UWBM 104586	3.69	1.16	1.82
p4	UCMP 140295	__	__	1.88
p4	UCMP	4.04	1.08	1.83

	140289			
p4	UCMP 140290	4.15	1.20	1.97
p4	UCMP 140291	4.14	__	1.77
p4	UCMP 140292	3.36	1.182	1.95

TABLE S4. Dental measurements (in mm) of *Mesodma thompsoni*.

Tooth Position	Specimen	L	W	Cusp Formula
m1	UWBM 114676	2.57	1.05	7:5
m1	UWBM 114668	2.59	1.08	6:4
m1	UWBM 114790	2.62	1.09	6:4
m1	UWBM 115329	3.06	1.33	6:4
m1	UWBM 115339	2.40	1.21	6+:4
m1	UWBM 115299	2.58	1.07	6:4

m1	UWBM 104588	2.73	1.11	7:5
m1	UWBM 110683	3.17	1.42	7:5
m1	UWBM 114651	2.56	0.85*	6:4
m1	UWBM 114656	2.69	1.15	6:4
m1	UWBM 115352	2.60	1.18	6:4
m1	UCMP 140298	2.76	1.12	6:4
m1	UCMP 140299	2.59	1.16	6:4
m1	UCMP 140300	2.41	1.00	6:4
m1	UCMP 140301	2.46	1.19	6:4
m1	UCMP 140303	2.81	1.32	6:4
m1	UCMP 140305	2.54	1.04	6:4

m1	UCMP 140308	2.55	1.09	6:4
m1	UCMP 140313	2.80	1.04	6:4
m1	UCMP 140314	2.54	1.08	6:4
m1	UCMP 140316	2.44	0.89	6:4
m1	UCMP 140317	2.60	1.08	6:4
m1	UCMP 140318	2.34	0.90	6:4
m1	UCMP 140321	2.46	1.00	6:4
m1	UCMP 140322	2.49	1.04	6:4
m1	UCMP 140324	2.90	1.29	6:4
m1	UCMP 140327	2.65	1.04	6:4
m1	UCMP 140330	2.69	1.05	6:4

m1	UCMP 140331	2.59	0.92*	6:4
m1	UCMP 294332	2.93	0.74*	6:4
m1	UCMP 294337	2.49	0.89*	6:4
m1	UCMP 294338	2.42	1.15	6:4
m2	UCMP 294359	1.33	1.25	4:2
m2	UCMP 294361	1.50	1.37	4:2
m2	UCMP 294362	1.52	1.06	4:2
m2	UCMP 294363	1.37	1.24	4:2
m2	UCMP 294365	1.41	1.26	4:2
m2	UCMP 294367	1.57	1.20	4+:2
m2	UCMP 294377	1.47	1.21	4:2

m2	UCMP 294388	1.15	1.31	4:2
m2	UCMP 294394	1.44	1.33	4:2
m2	UCMP 294396	1.34	1.29	4:2
m2	UCMP 294523	1.53	1.46	3:2
P4	UWBM 103772	2.53	1.13	2:7
P4	UWBM 114786	2.58	1.04	2:7
P4	UWBM 114667	2.83	1.23	2:7
P4	UWBM 114670	2.81	1.14	2:7
P4	UWBM 115315	2.62	1.23	1:7
P4	UWBM 115307	2.82		2:7
P4	UWBM 114796	2.87	1.31	4:7

P4	UWBM 107348	1.76*	1.03*	0+:3+
P4	UWBM 107348	2.67	1.15	2:7
P4	UWBM 105259	2.71	1.32	2:7
P4	UWBM 105258	2.97	1.28	2:6+
P4	UWBM 104646	2.78	1.37	2:7
P4	UWBM 103323	2.82	1.26	4:7
P4	UWBM 105273	2.67	__	2:7
P4	UWBM 111213	2.51	__	3:7
P4	UCMP 140333	2.91	__	2:7
P4	UCMP 140335	2.56	__	3:7
P4	UCMP 140337	2.56	__	2:4+

P4	UCMP 140338	2.53	__	2:7
P4	UCMP 140340	2.95	__	3:7
P4	UCMP 140343	2.77	__	2:7
P4	UCMP 140346	2.61	__	2:7
P4	UCMP 140347	2.87	__	3:7
P4	UCMP 140351	2.55	__	3:7
P4	UCMP 140353	2.79	__	3:7
P4	UCMP 294324	2.44	__	3:7
P4	UCMP 294326	2.48	__	3:7?
P4	UCMP 294328	2.51	__	3:5?
M1	UWBM 111201	3.11	1.36	8:9:6

M1	UWBM 111135	3.20	1.40	5+:10:5+
M1	UWBM 114677	2.06*	1.46	0+:0+:5
M1	UWBM 112750	3.25	1.22	8:10:0+
M1	UWBM 112748	3.16	1.42	8:9:7
M1	UWBM 104580	2.06*	1.33	3+:5+:5
M1	UWBM 115289	2.10	1.56	4+:5+:2
M1	UWBM 105256	3.42	1.33*	7:9:0+
M1	UWBM 114655	2.3*	1.45	4+:6+:4+
M1	UCMP 294339	3.19	1.41	7:8:5
M1	UCMP 140355	3.40	1.29	7:8:4
M1	UCMP 140358	3.32	1.39	8:9:4

M1	UCMP 140359	3.26	1.39	7:9:4
M1	UCMP 140361	3.45	1.39	7:8:4
M1	UCMP 140364	3.21	1.36	7:8:5
M1	UCMP 140366	3.30	1.49	7:8:4
M1	UCMP 140370	3.46	1.28	6:8:4
M1	UCMP 140371	3.64	1.42	7:8:4
M1	UCMP 294342	3.47	1.59	7+0+:0+
M1	UCMP 294527	3.37	1.37	7:8:4
M2	UWBM 114662	1.48	1.68	1:3:3
M2	UWBM 114671	1.52	1.41	1:3:3
M2	UCMP 294405	1.62	1.51	1:3:3

M2	UCMP 294406	1.67	1.28	1:3:4
M2	UCMP 294407	1.70	1.40	1:3:3
M2	UCMP 294410	1.82	1.30	1:3:4
M2	UCMP 294411	1.71	1.28	1:3:3
M2	UCMP 294413	1.73	1.39	1:3:3
M2	UCMP 294426	1.62	1.41	0+:0+:3
M2	UCMP 294429	1.51	1.30	1:3:3
M2	UCMP 294432	1.43	1.33	1:3:3
M2	UCMP 294434	1.59	1.35	1:3:3+
M2	UCMP 294437	1.40	1.40	1:3:3
M2	UCMP 294440	1.56	1.45	1:3:3

M2	UCMP 294448	1.57	1.33	1:3:3

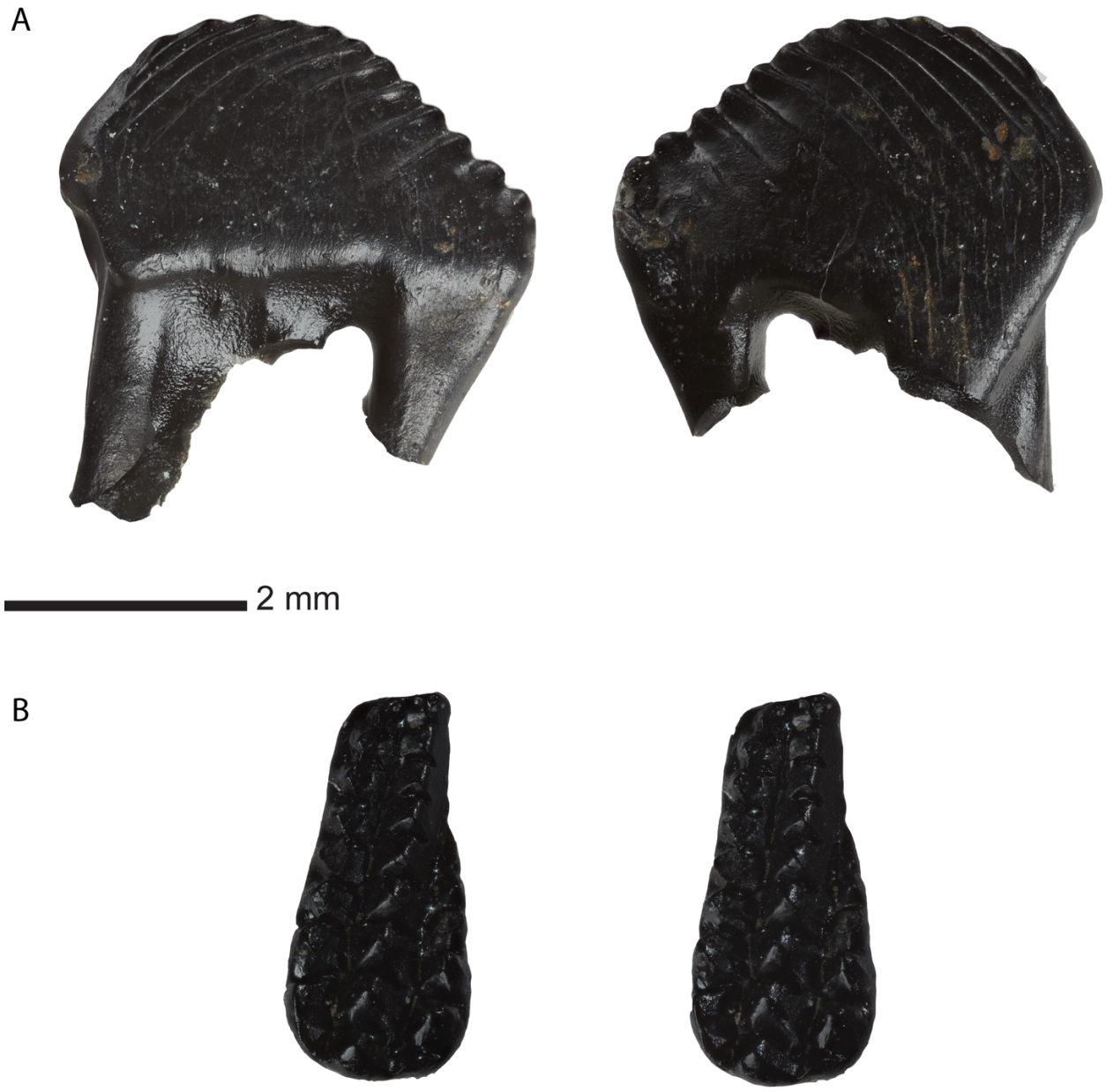

FIGURE 2. **A,** Left p4 of *Mesodma thompsoni* (UWBM 111209) in lingual (left) and buccal (right) views. **B,** Right M1 of *Mesodma thompsoni* (UWBM 111201) in stereo occlusal view with the mesial face upwards. Scale bar equals 2 mm.

MESODMA HENSLEIGHI Lillegraven, 1969

(Fig. S3)

Referred material— **V77128:** m2: UCMP 294353, UCMP 294371, UCMP 294372, UCMP 294373, UCMP 294374, UCMP 294375, UCMP 294378, UCMP 294379, UCMP 294381, UCMP 294386, UCMP 294393, UCMP 294395 P4: UCMP 140334, UCMP 294327 M1: UCMP 140369 M2: UCMP 294403, UCMP 294420; V**77129:** m1: UWBM 114678 m2: UWBM 112764, UWBM 112751; **V77124:** M1: UWBM 114146, UWBM 111216

DESCRIPTION

Description: The specimens are identified to the genus *Mesodma* based on overall morphology and cusp number. *M. hensleighi* differs from other species of *Mesodma* primarily on the basis of its smaller size (Lillegraven, 1969; Novacek and Clemens 1977; Smith and Wilson, 2017). All referred specimens within the published size range of *M. hensleighi*.

TABLE S5. Dental measurements (in mm) of *Mesodma hensleighi*

Tooth Position	Specimen	L	W	Cusp Formula
m1	UWBM 114678	2.35	0.99	6:4
m2	UWBM 112764	1.19	1.08	4:2
m2	UWBM 112751	1.13	1.11	3:2

m2	UCMP 294353	1.26	1.00	4:2
m2	UCMP 294371	1.22	1.05	3:2
m2	UCMP 294372	1.01	1.15	3:2
m2	UCMP 294373	1.13	1.00	3:2
m2	UCMP 294374	1.17	1.03	3:2
m2	UCMP 294375	1.08	0.97	4:2
m2	UCMP 294378	1.11	0.92	0+:2
m2	UCMP 294379	1.05	1.05	4:2
m2	UCMP 294381	1.04	0.97	4:2
m2	UCMP 294386	1.00	0.79	3:2
m2	UCMP 294393	1.21	1.04	4:2

m2	UCMP 294395	1.21	1.02	3:2
P4	UCMP 140334	1.91	__	3:7
P4	UCMP 294327	2.10	__	0+:5+
M1	UWBM 114146	1.92*	1.33	3:4+:4+
M1	UWBM 111216	2.22*	1.17	4+:6:2+
M1	UCMP 140369	2.90	1.13	6:6:2
M2	UCMP 294403	1.28	1.20	1:3:3
M2	UCMP 294420	1.18	1.10	1:3:0+

FIGURE S3. Right m2 of *Mesodma hensleighi* (UWBM 112764) in stereo occlusal view with the mesial face upwards. Scale bar equals 1 mm [stereo pair; print exact size].

MESODMA SP.

Referred material— **V77128:** p4: UWBM 114797, UCMP 294498 P4: UCMP 294325, UCMP 294330 M1: UCMP 294503, UCMP 294505, UCMP 294507, UCMP 294508, UCMP 294509; **V77129:** p4: UWBM 115292 m1: UWBM 104576, UWBM 115300, UWBM 115324, UWBM 115308 m2: UWBM 114788 P4: UCMP 294511 M1: UWBM 104594, UWBM 115319, UWBM 115340, UWBM 115341, UWBM 115346; **V77124:** p4: UWBM 103322 m1: UWBM 99771, UWBM 104613, UWBM 103215,103216 P4: UWBM 111214 M1: UWBM 115359, UWBM 115355, UWBM 115354; **V79100:** P4: UCMP 294524, UCMP 294525

DESCRIPTION

The specimens match published descriptions of the crown morphology and cusp formula of *Mesodma* (Clemens, 1964; Novacek and Clemens, 1977; Archibald, 1982). However, because the specimens are fragmentary or have measurements that overlap with published measurements of

more than one species, we refrain from referring them to species (Clemens, 1964; Lillegraven, 1969; Archibald, 1982).

Family EUCOSMODONTIDAE Jepsen, 1940

Genus *STYGIMYS* Sloan and Van Valen, 1965

STYGIMYS KUSZMAULI Sloan and Van Valen, 1965

(Fig. 4)

Referred material— **V77128:** m2: UCMP 294456 M1: UCMP 294462 M2: UCMP 294457; **V77129:** M2: UWBM 112763; **V77124:** M2: UWBM 114653, UWBM 114659

DESCRIPTION

Lower Molar— UCMP 294456 is a right m2. Cusps are worn forming two mesial-distal ridges with slight subcresecentic apices, the cusp formula is 4:2. The two internal cusps are conical in shape, with the mesial-most being the larger. The external cusps equal in size to each other but are smaller than the internal cusps.

Upper Molars— UCMP 294455 is a right M1. Entire tooth is present; however, majority of cusps are worn to the base with an estimated cusp formula of ?:7:3. Square base of the cusps implies a conical shape when unworn. UWBM 112763 is well preserved left M2. All three cusp rows are preserved with minimal damage with cusp formula 1:3:3. The buccal cusp row is formed by a mesial-distal ridge. UWBM 112763 lacks additional distal cusps found in the buccal row of other specimens. The middle row is comprised of three conical cusps with grooves separating each. The distal cusp merges slightly with the buccal cusp ridge. The groove

separating the first and second cusps of the middle row is more pronounced than that separaring the second and third cusps. The lingual cusp row is comprised of three similarly sized conical cusps. The second cusp of the lingual row is distinctly sub-crescentic with visible indentation on the tip. The groove between the distal cusp and medial is less distinct than between medial and mesial. The tooth tapers slightly on the buccal end. Specimens were identified to *S. kuszmauli* primarily based on size, cusp formula and morphology (Johnston, 1984; Archibald 1982). The specimens were distinguished from other multituberculate genera by their large size and conical-shaped cusps.

TABLE S6. Dental measurements (in mm) of *Stygimys kuszmauli*.

Tooth Position	Specimen	L	W	Cusp Formula
m2	UCMP 294456	2.20	1.92	4:2
M1	UCMP 294462	5.04	2.53	?:7:3
M2	UWBM 114653	2.78	2.48	1:3:3
M2	UWBM 114659	2.54	1.97*	1:3:?
M2	UWBM 112763	2.53	2.40	1:3:3

M2	UCMP 294457	2.19	2.10	1:3:3

FIGURE S4. Left M2 of *Stygimys kuszmauli* (UWBM 114653) in stereo occlusal view with the mesial face upwards. Scale bar equals 1 mm.

"PARACIMEXOMYS GROUP"

Genus *CIMEXOMYS* Sloan and Van Valen, 1965

CIMEXOMYS MINOR Sloan and Van Valen 1965

(Fig. S5)

Referred material— **V77128:** m1: UWBM 114794, UWBM 115290 M1: UCMP 294458, UCMP 294459, UCMP 294460, UCMP 294497; **V77129:** m2: UWBM 104574 M2: UWBM 104642; **V77124:** m1: UWBM 111134, UWBM 111215 m2: UWBM 111203

DESCRIPTION

Lower Molars— UWBM 111134 is a complete m1 with cusp formula 6:4. The cusp formula and overall morphology matches Sloan and Van Valen's (1965) description of *C. minor.* UWBM 111134 can be distinguished from *Stygimys* due to its smaller size and from similarly sized species of *Mesodma* due to the pyramidal shape of the cusps (Clemens, 1964; Archibald, 1982).

Upper Molars— UCMP 294458 is a complete M1 with cusp formula 4:6:R. Both buccal and medial cusp rows are comprised of distinct subcrescentic apexes. The lingual cusp row is best described as a ridge, which runs 50% of the tooth margin (Sloan and Van Valen 1965). There is no distinction between cusp apexes similar to Archibald's (1982) description of *C. hausoi.* UCMP 294458 is distinguished from *C. hausoi* based on size, falling outside published size ranges (Archibald, 1982; Lofgren, 1995).

m2's and M2's— The pyramidal shape of the cusps distinguishes these specimens from the similarly sized m2's of *Mesodma sp.* There is debate over the ability to discriminate m1's, m2's and M2's of *C. minor* from other similarly sized multituberculates i.e., *Mesodma sp.* (Archibald, 1982; Lofgren, 1995; Weaver et al., 2021). The identification of these teeth is primarily based off the subcrescentic, pyramidal morphology of the cusps and lingual ridge when present compared to the crescentic, distal apexes of *Mesodma sp.* (Clemens, 1964 & 1973; Sloan and Van Valen, 1965; Archibald 1982).

Tooth Position	Specimen	L	W	Cusp Formula
m1	UWBM 114794	2.35	1.02	6:4
m1	UWBM 115290	1.47*	1.13	3+:2+
m1	UWBM 111134	2.44	1.09	6:4
m1	UWBM 111215	2.15	1.08	6:4
m2	UWBM 104574	1.5	1.25	3:2
m2	UWBM 111203	1.47	1.19	3:2
M1	UCMP 294458	2.36	1.22	4:6:1
M1	UCMP 294459	2.32	1.14	4:6:1
M1	UCMP 294460	2.61	1.26	4:6:1

TABLE S7. (Continued)

M1	UCMP 294497	2.52	1.15	4:6:R

M2	UWBM 104642	1.45	1.44	1:3:3

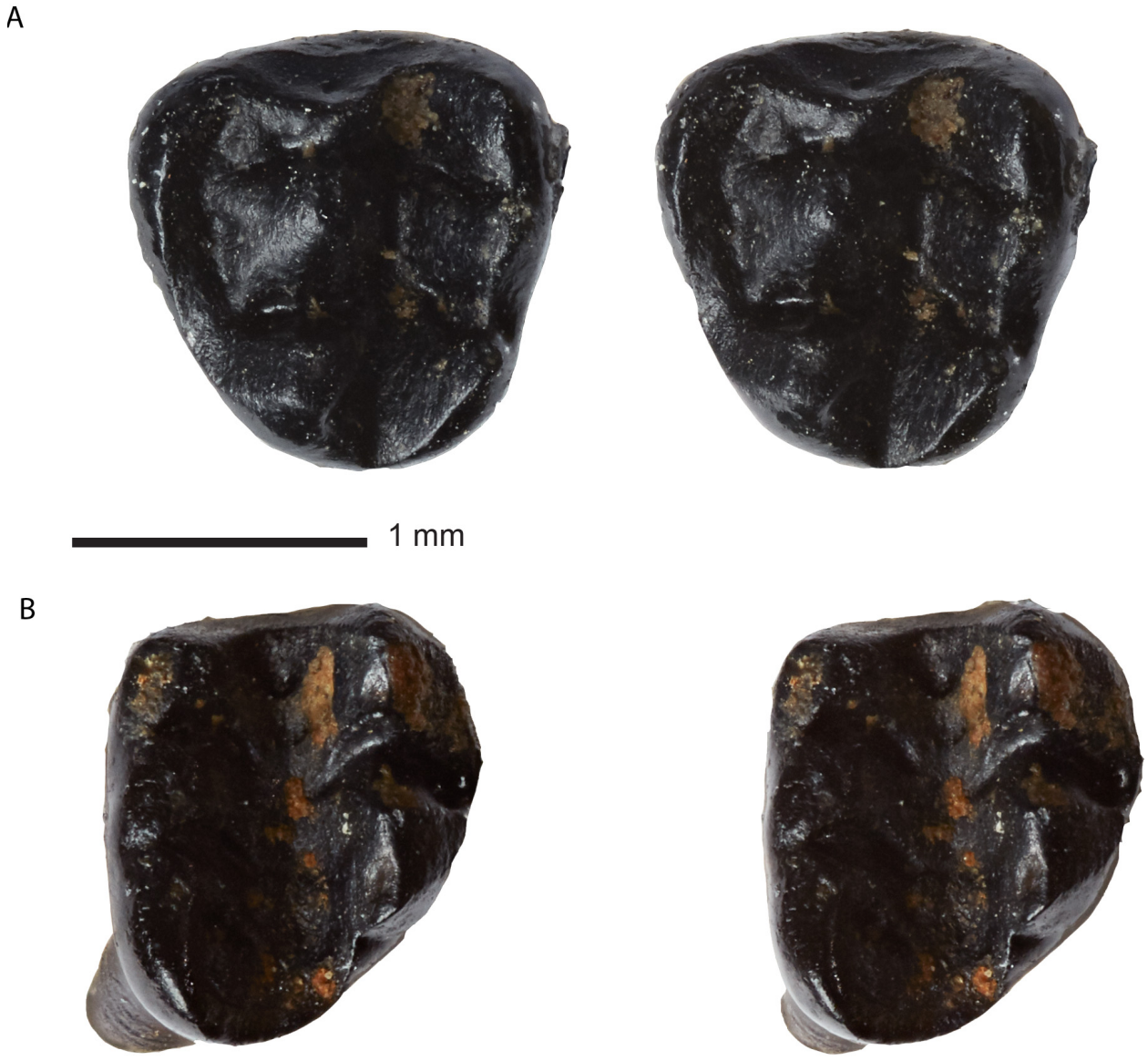

FIGURE S5. **A,** Right M2 of *Cimexomys minor* (UWBM 104642) in stereo occlusal view with the mesial face upwards. **B, Left** m2 of *Cimexomys minor* (UWBM 104574) in stereo occlusal view with the mesial face upwards. Scale bar equals 1 mm [stereo pair; print exact size].

CIMEXOMYS GRATUS Jepson 1930

Cimexomys hausoi Archibald 1982

Referred material— **V77128**: m1: UCMP 294461 m2: UCMP 294463 M1: UCMP 294462

DESCRIPTION

Lower Molars— UCMP 294461 is a complete left m1 with cusp formula 6:4. The cusps in both rows have a pyramidal morphology but are larger in the lingual row. The overall tooth margin tapers toward the distal end. Specific traits that support the identification include the pyramidal shaped cusps, and the presence of grooves on the lingual cusps. Distinguished from *S. kuszmauli* primarily on size and number of cusps in lingual row (Lofgren, 1995). Additionally, UCMP 294461 is too large to represent *C. judithae* (now referred to as *Filikomys primaevus*) or *M. thompsoni* (Archibald, 1982; Montellano et al. 2000; Weaver et al., 2021). UCMP 294463 is a lower m2. The overall morphology of UCMP 294463 similar to that of *C. minor* or *F. primaevus* but differentiated based on large size and additional buccal cusp (Archibald, 1982; Montellano et al., 2000; Weaver et al., 2021). The cusp formula is 4:2, the lingual cusps show evidence of wear on the apexes following the pattern of wear outlined in Archibald (1982).

Upper Molar— UCMP 294462 is a complete right M1 with cusp formula 5:6:R. Buccal and medial cusp rows possess large pyramidal cusps. Lingual cusp forms ridge that is less than half the total tooth margin similar to Archibald's (1982) description. Overall morphology, similar to

that of *C. minor* or *F. primaevus* but larger in size. Differs from *S. kuszmauli* in size, the presence of a distinct lingual ridge and cusp formula (Lofgren, 1995).

TABLE S8. Dental measurements (in mm) of *Cimexomys hausoi*.

Tooth Position	Specimen	L	W	Cusp Formula
m1	UCMP 294461	3.12	1.41	6:4
m2	UCMP 294463	2.08	1.64	5:6:1
M1	UCMP 294462	3.41	1.69	4:2

Subclass METATHERIA Huxley, 1880

Family HERPETOTHERIIDAE Trouessart, 1879

Genus *THYLACODON* Matthew and Granger, 1921

THYLACODON MONTANENSIS Williamson et al., 2012

(Fig. S6)

Referred material— **V77128:** M3: UCMP 294500 M4: UCMP 294483, UCMP 294487, UCMP 294489, UCMP 294490; **V77129:** m1: UWBM 115313 mx: UWBM 115342; **V77124:** M1: UWBM 114664 M2: UWBM 105261 M4: UWBM 110684

DESCRIPTION

Lower molars— UWBM 115313 is missing the entirety of the talonid basin, though the mesial end of the cristid obliqua is present. The trigonid of UWBM 115313 is similar to the description in Archibald (1982). UWBM 115313 can be distinguished from other metatherians, particularly *Alphadon* by the inferred location of the cristid obliqua below the protoconid (Archibald, 1982; Clemens, 2006).

Upper molars— UWBM 114664 is a fragmentary upper left M1 preserving the stylar shelf and paracone. UWBM 114664 can be distinguished from other small metatherian like *Alphadon* due to the parallel position of the stylar cups and lack of ectoflexus indentation (Archibald, 1982). UWBM 105261 is a fragmentary upper right M2 similar in appearance to UWBM 114664. The metacone of UWBM 105261 is larger than the paracone (Archibald, 1982; Lofgren, 1995). The stylar shelf cusps of UWBM 105261 are parallel, similar to UWBM 114664. UCMP 294500 is an upper M3, that differs from UWBM 105261 due to the less developed, and more angular parastylar shelf. UCMP 294483 is a complete upper M4, identified based on the mesially extended parastylar shelf. Compared to UWBM 105261 the metacone is reduced and smaller than the paracone. UCMP 294487, 294489 and 294490 are all similar in appearance to UWBM 105261. *Thylacodon montanensis* is the only metatherian present in our sample, in contrast to Smith and Wilson (2018) who describe specimens potentially representing Lancian metatherian holdovers.

TABLE S9. Dental measurements (in mm) of *Thylacodon montanensis*.

Tooth Position	Specimen	L	DW	MW
m1	UWBM 115313	1.145*	__	1.44
mx	UWBM 115342	1.72*	1.38	__
M1	UWBM 114664	1.92*	__	__
M2	UWBM 105261	2.265	__	__
M3	UCMP 294500	2.79	__	__
M4	UWBM 110684	1.51	1.9	2.66
M4	UCMP 294483	1.77	2.47	3.05
M4	UCMP 294487	1.65	2.27	3.04
M4	UCMP 294489	2.04	2.86	3.23
M4	UCMP 294490	__	2.05*	__

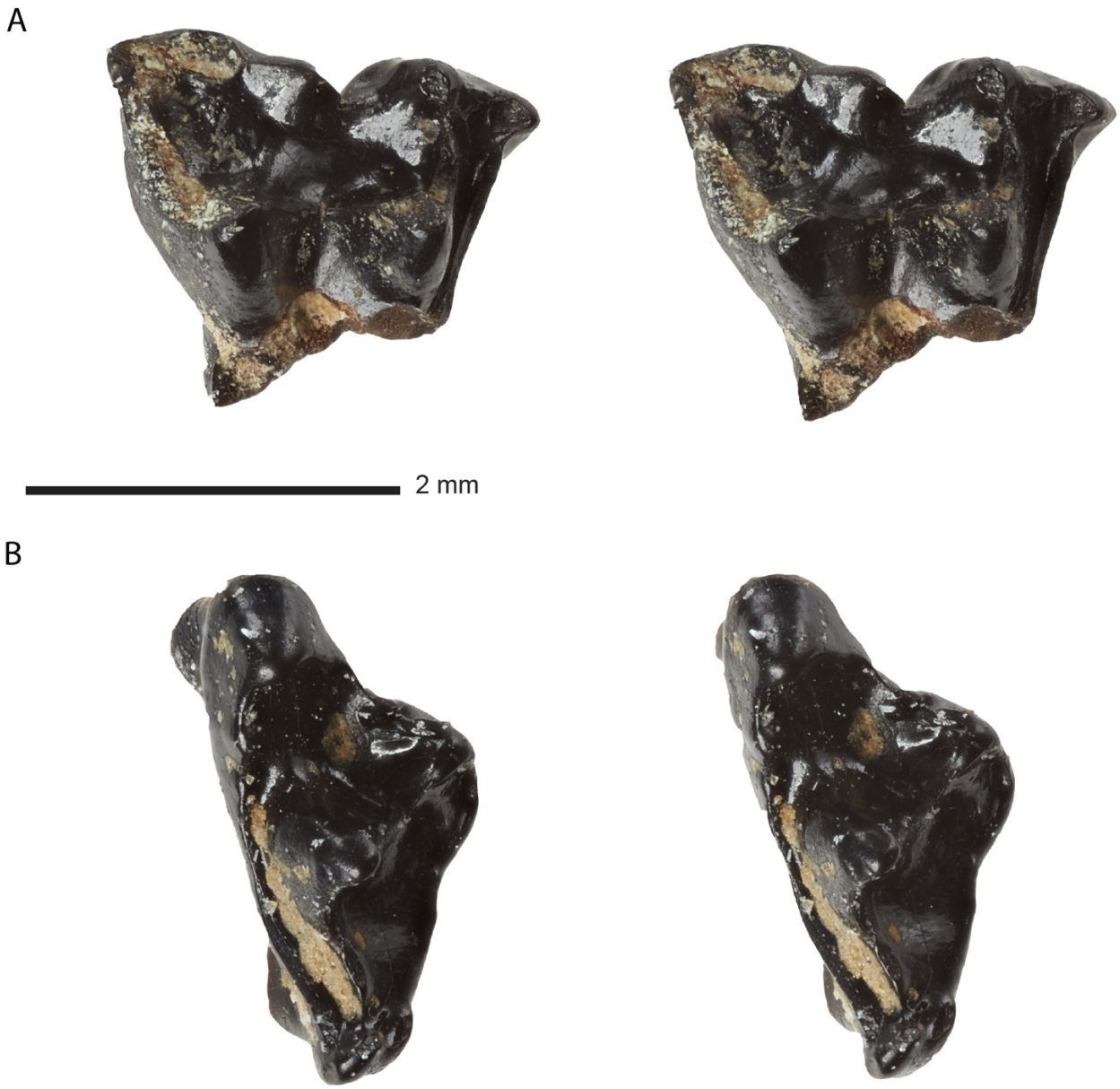

FIGURE S6. **A,** Buccal fragment of a right M2 of *Thylacodon montanensis* (UWBM 105261) in stereo occlusal view with the buccal face upwards. **B,** Fragment of a left M4 of *Thylacodon montanensis* (UWBM 110684) in stereo occlusal view with the buccal face upwards. Scale bar equals 2 mm [stereo pair; print exact size].

Subclass EUTHERIA Huxley, 1880

Order CIMOLESTA McKenna, 1975

Family CIMOLESTIDAE Marsh, 1889

Genus *PROCERBERUS* Sloan and Van Valen, 1965

PROCERBERUS FORMICARUM Sloan and Van Valen, 1965

(Fig. S7)

Referred material— **V77128:** p3: UCMP 294468, UCMP 294469, UCMP 294470 p4**:** UCMP 294474, UCMP 294478 m1: UCMP 294473, UCMP 294476 m2: UCMP 294471, UCMP 294475, UCMP 294477 m3: UCMP 294471 m?: UWBM 114795 P4: UCMP 139013 M1: UCMP 294466, UCMP 294496 M2: UCMP 294465 M3:UWBM 114798, UCMP 294464, UCMP 294467; **V77129:** m2: UWBM 114789, UWBM 115302, UWBM 115295; **V77124:** m1: UWBM 111219 m2: UWBM 111205, UWBM 114639 m3: UWBM 100541, UWBM 114646 m?: UWBM 100541; **V79100** UCMP 150007

DESCRIPTION

Lower Premolars— UCMP 294468, 294469 and 294470 represent lower p3's. All three are similar in appearance with a small mesial cusp, large protoconid and smaller distal cusps. UCMP 294468 features an addition cuspule not mentioned in previous descriptions (Archibald, 1982; Clemens, 2017). UCMP 294478 and 294474 both represent lower p4's of *P. formicarum.* Their overall appearance matches descriptions outlined in Lillegraven (1969) and Clemens (2017). On both specimens, the protoconid the tallest cusp followed by the metaconid and paraconid. The paraconid is distinctly separated from the protoconid on both UCMP 294478 and 294474. There is no mesial cingulum present on either specimen. A deep ridge separates the narrower talonid from the more mesial-distal extended trigonid. Both specimens can be distinguished from other cimolestids based on large paraconid (i.e., *Cimolestes cerberoides*), presence of the metaconid (i.e., *Cimolestes cerberoides* and *Puerolestes simpsoni*) and lack of a mesial cingulum (i.e., *Gypsonictops sp.*) (Lillegraven, 1969; Clemens, 2017; Clemens, 2019). Both specimens also fit within reported size ranges in Archibald (1982) and Clemens (2017).

Lower Molars— UWBM 114789 is fragmentary lower m1 missing the entirety of the talonid. All three cusps on the trigonid are preserved. The protoconid is the largest and tallest cusp, followed by the metaconid and then paraconid. The protoconid is positioned on the same plane as the metaconid. The paraconid is substantially smaller than the other two cusps and points buccally with respect to the metaconid. UWBM 114789 has a precingulid ridge, and the paracristid notch is the deepest on the trigonid. The hypoflexid region is missing from the specimen, along with the rest of the talonid. The trigonid fall is flat and likely forms a 90-degree angle with the missing talonid basin. UWBM 114789 was identified as *Procerberus formicarum* based on the height of the trigonid cusps, small metacristid notch, angle of protoconid notch and is in the size range reported in Archibald (1982) and Clemens (2017). UCMP 294471 is a right dentary fragment comprised of the m2 and m3. The m2 trigonid basin is smaller than UWBM 114789 but the arrangement of cusps is similar matching the description in Clemens (2017). The protoconid and metaconid are about equal in size and height whereas the paraconid is much smaller matching description from Sloan and Van Valen (1965) and Lillegraven (1969).. The trigonid basin on the m3 is similar to the m2, with no enlarged precingulum as described in Clemens (2017). The hypoconulid of the m3 is larger and more distally positioned then on the m2 or published descriptions of *Gypsonictops illuminatus* (Lillegraven 1969). UCMP 150007 is referred to as a *Procerberus formicarum* m2 however the identification has not been confirmed by JRC or GPWM.

Upper Premolar— UCMP 139013 represents an upper right P4. The protocone of UCMP 139103 is the largest cup in both mesiodistral length and buccolingual width and height. There

appear to be no cuspules visible between the protocone and stylar shelf region. The paracone is larger than the metacone. When compared to Clemens (2017), the morphology is similar except for the distal end where UCMP 139013 has less tapered distal end than reference specimen.

Upper Molars— UCMP 294466 represents a fragment of an upper right M1. The lingual portion of the tooth is missing just lingual of the meta- and paraconules. The paracone is larger than the metacone, the two cusps are confluent at their base. The ectoflexus is shallow, and the stylar shelf forms a horizontal plain (Lillegraven, 1969; Clemens, 2017). UCMP 294465 represents a fragment of an upper M2 missing the lingual end and part of parastylar lobe. UCMP 294465 differs from UCMP 294466 in having a deep ectoflexus, forming a bilobate buccal end. Similarly, to UCMP 294466, the paracone is larger than the metacone on UCMP 294465. The paraconule and metaconule are both small. UCMP 294464 and 294467 represent upper right M3s. UCMP 294464 is a complete tooth, that matches the descriptions outline in Clemens (2017). The protocone is shifted mesially and is parallel to the paracone. The parastylar lobe is large and possess a smaller cuspule. There is no metastylar lobe present. UCMP 294467 is missing the paracone and lingual portion of the tooth. When compared to UCMP 294464, it is slightly larger but overall morphology is similar.

TABLE S10. Dental measurements (in mm) of *Procerberus formicarum*.

Tooth Position	Specimen	L	DW	MW
p3	UCMP 294468	2.64	__	__

p3	UCMP 294469	2.34	__	__
p3	UCMP 294470	2.34	__	__
p4	UCMP 294474	3.00	__	__
p4	UCMP 294478	2.57	__	__
m1	UWBM 111219	1.56*	__	1.73
m1	UCMP 294473	2.34	1.20	1.54
m1	UCMP 294476	2.52	1.49	1.59
m2	UWBM 114789	1.62*	__	1.40
m2	UWBM 115302	1.38*	__	1.55
m2	UWBM 115295	2.15*	1.26	1.3*
m2	UWBM 111205	2.44	1.55	1.57

m2	UWBM 114639	1.19*	__	1.76
m2	UCMP 294471	2.30	1.74	1.40
m2	UCMP 294475	2.76	1.63	1.85
m2	UCMP 294477	2.19*	1.25*	1.57*
m3	UWBM 100541	1.33*	__	1.74
m3	UWBM 114646	1.64*	__	1.33
m3	UCMP 294471	2.53	1.44	1.27
mx	UWBM 114795	1.02*	__	1.56
mx	UWBM 100541	__	__	1.74
P4	UCMP 139013	2.2	__	__
M1	UCMP 294466	2.56	2.16*	1.80*

M1	UCMP 294496	2.43	1.92*	2.00*
M2	UCMP 294465	1.82*	__	1.80*
M3	UWBM 114798	1.69*	2.94	2.81
M3	UCMP 294464	2.14	2.93	3.64
M3	UCMP 294467	2.96	2.57*	2.70*


A
2 mm
B

FIGURE S7. **A,** Fragment of a right m2 of *Procerberus formicarum* (UWBM 114789) in stereo occlusal view with the mesial face upwards. **B,** Fragment of a left M3 of *Procerberus formicarum (*UWBM 114798) missing the buccal margin in stereo occlusal view with the buccal face upwards. Scale bar equals 2 mm.

PUERCOLESTES Reynolds, 1936

PUERCOLESTES SIMPSONI Reynolds, 1936

(Fig. S8)

Referred material— **V77129:** m1: UWBM 112746

DESCRIPTION

Lower Molar— UWBM 112746 is well preserved, lower left m1. All three of the cusps in the trigonid are equally worn with the protoconid being the largest followed by the metaconid and a substantially shorter paraconid. The protoconid is positioned buccal to, but on the same plane as the metaconid. There is a distinctive protocristid notch between the protoconid and metaconid forms a wider angle than present in *P. formicarum* (Clemens, 2017). The metaconid is positioned buccally, with a distinctive metacristid ridge between the metaconid and paraconid. The paraconid is positioned lingually, the paracristid ridge between the paraconid and protoconid is the widest ridge on the trigonid. Mesial to the paracristid ridge is a precingulid, which forms a short, low ridge along the mesial edge. The talonid is substantially shorter than the trigonid, with the hypoconid and hypoconulid exhibiting signs of wear. All the major cusps are similar in size with the hypoconid being slightly larger which differs Clemens (1973) description of *Cimolestes incisus*. The hypoconid is extended buccally, with a thin cristid obliqua connecting it to the mesoconid. There is a ridge that connects the hypoconid and hypoconulid. The hypoconulid is

positioned on the buccodistal margin of the tooth. The postcristid ridge is the deepest ridge on the talonid, with no ridge connecting the two cusps. The entoconid is the only unworn cusp on the tooth. There is a small entoconulid visible in lingual view. The lack of upper and lower P4's prevents us from commenting on the Williamson et al., (2011) revised diagnosis of the genus and the relationship with *Cimolestes incisus.*

FIGURE S8. Left m1 of *Puercolestes simpsoni* (UWBM 112746) in stereo occlusal view with the mesial face upwards. Scale bar equals 2 mm.

TABLE 11. Dental measurements (in mm) of *Puercolestes simpsoni.*

Tooth Position	Specimen	L	DW	MW

TABLE S11. (Continued)

m1	UWBM 112746	4.095	2.57	2.16

UNGULATA Linnaeus, 1766

Family ARCTOCYONIDAE Giebel, 1855

Genus *PROTUNGULATUM* Sloan and Van Valen, 1965

PROTUNGULATUM DONNAE Sloan and Van Valen, 1965

(Fig. S9)

Referred material— **V77124:** M2: UWBM 111132

DESCRIPTION

Upper Molar— UWBM 111132 represents an upper M2 fragment. The buccal margin is missing the parastylar shelf, whereas the lingual portion of the crown is missing from the paraconule and metaconule until the edge of the tooth margin. The paracone and metacone are distinct and positioned close to the buccal margin. The paraconule and metaconules are similar and size and directly lingual to the respective para/metacone. There is evidence of both a pre- and post-cingulum, however the damage prevents us from determining the extent the cingulae extend buccally. UWBM 111132 can be distinguished from the similar sized genus *Mimatuta* based on the buccally positioned paracone and metacone relative to the protocone, and overall, less bulbous appearance of the cusps. The lack of a protocone prevents us from comparing the placement to that of *Mimatuta* as described in Archibald (1982). The overall size of the fragment

fits within reported ranges from Archibald (1982) and Lofgren (1995) and differentiates the specimen from *Oxyprimus erikseni* (Luo, 1991).

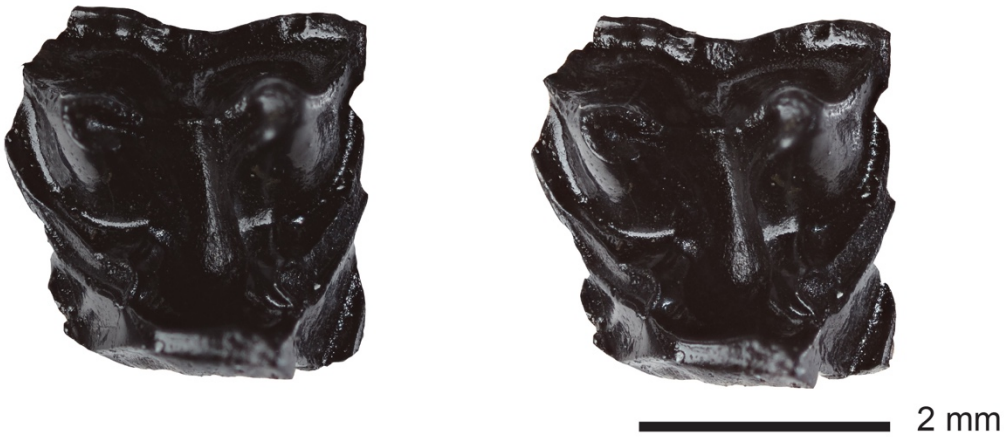

FIGURE S9. Buccal fragment of a left M2 of *Protungulatum donnae* (UWBM 111132) in stereo occlusal view with buccal margin upwards. Scale bar equals 2 mm.

TABLE S12. Dental measurements (in mm) of *Protungulatum donnae.*

Tooth Position	Specimen	L
M2	UWBM 111132	2.86

Genus *OXYPRIMUS* Van Valen, 1978

OXYPRIMUS ERIKSENI Van Valen, 1978

(Fig. S10)

Referred material— **V77128:** m1: UCMP 139015 m2: UWBM 104578 m3: UCMP 139014 M2: UCMP 139019 M3: UCMP 139018

DESCRIPTION

Lower Molars— UCMP 139015 is a complete right m1. The protoconid is the largest cusp followed closely by distally shifted metaconid. The lingually shifted paraconid is the smallest cups in height and area. A small precingulid is present. The talonid basin is buccolingually wide matching the description from Archibald (1982) in contrast to Luo (1991). The hypoconid and hypoconulid are subequal in size possibly due to wear, whereas the entoconid is slightly smaller. UCMP 139015 is attributed to *O. erikseni* primarily based on size which has been identified as the major differentiating factor with other Puercan 1 artocyonids (i.e., *Protungulatum sp.*; Luo, 1991). Furthermore, the lingually shifted paraconid and small cingulum also ally the specimen with previous descriptions of *O. erikseni* (Archibald, 1982; Luo, 1991). UWBM 104578 is a left m2 trigonid fragment. The overall morphology is similar to UCMP 139015, except the metaconid is parallel to the protoconid. UCMP 139014 is a right m3. The protoconid and metaconid are similar in size, with the metaconid shifted distally compared to the protoconid. The paraconid of UCMP 139014 is similar to UCMP 139015 in that it is the smallest trigonid cusp and is shifted lingually from the midline. The talonid is extended distally and longer than the trigonid. The hypoconulid is extended distally and is the largest of talonid cusp. Similar to UCMP 139015, UCMP 139014 is attributed to *O. erikseni* on the basis of its small size and lingually positioned paraconid (Archibald, 1982).

Upper Molars— UCMP 139019 is a complete right M2, with an overall buccolingually rectangular shape. The parastylar and metastylar shelves are subequal in size, with a rounded ectoflexus between the two lobes. The paracone and metacone are similar in size as well. The

paracone is positioned more buccally than the metacone. A small paraconule is visible, the lack of metaconule is likely due to post-mortem damage. The protocone is large and shifted buccally. The lingual face of the protocone is steep and long as it slopes to the base of the tooth. A small precingulum is present running from the base of the paracone until the slope of the protocone. A much larger post-cingulum is present and possess a small cusp, potentially a hypocone. UCMP 139018 is a right M3. The parastylar lobe is substantially larger than UCMP 139019 whereas the metastylar shelf is smaller. The paracone is larger than the metacone and possess a small wear facet on its apex. The metacone is positioned distally on the edge of the metastylar shelf. The paraconule is larger in size and height than the metaconule. The protocone is positioned more lingually than UCMP 139019, with a smaller, less steep lingual face. The pre- and post-cingulum are similar in size and lack any addition cusps. Both UCMP 139019 and UCMP 139018 are primarily identified as *O. erikseni* on the basis of size and steep lingual face of UCMP 139018's protocone (Luo, 1991).

TABLE S13. Dental measurements (in mm) of *Oxyprimus erikseni.*

Tooth Position	Specimen	L	DW	MW
m1	UCMP 139015	3.32	2.24	2.26
m2	UWBM 104578	__	__	2.73
m3	UCMP 139014	3.93	1.92	2.55

TABLE S13. (Continued)				
M2	UCMP 139019	3.13	4.76	4.72
M3	UCMP 139018	3.15	3.96	4.60

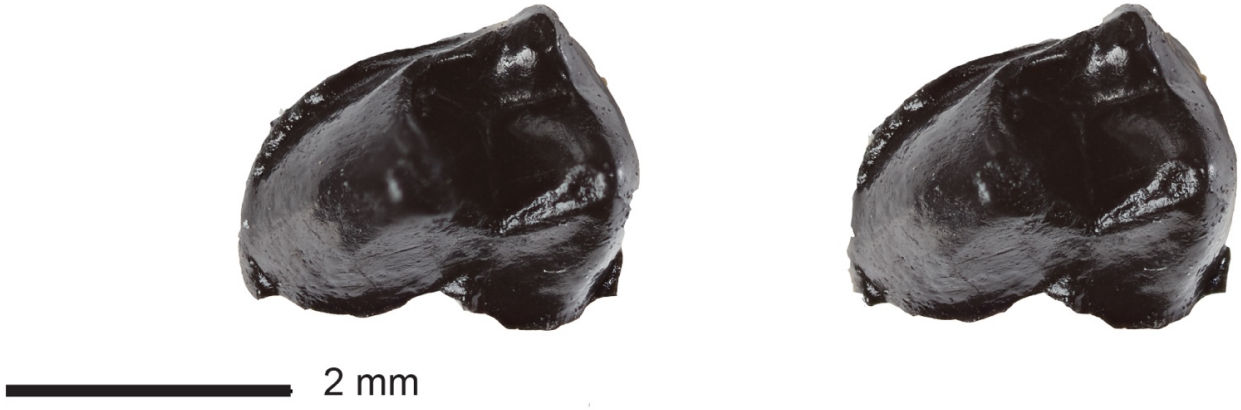

FIGURE S10. Trigonid fragment of a left m1 of *Oxyprimus erikseni* (UWBM 104578) in stereo occlusal view with the mesial face upwards. Scale bar equals 2 mm.

Genus *BAIOCONODON* Gazin, 1941

BAIOCONODON NORDICUM Jepsen, 1930

(Fig. S11)

Ragnorak nordicum Jepsen, 1930b:501

Referred material—V77129: Dentary Fragment with m1 and m2: UCMP 121791

DESCRIPTION

Dentary Fragment— UCMP 121791 represents three edentulous dentary fragments (two of which are questionable in nature see Archibald [1982]) and two associated teeth, a left m1 and right m2. The roots of the m1 are attached, along with the roots of the trailing p4. Compared to the associated right m2, the m1 is substantially smaller. All the major trigonid cusps are broken, leaving only the bases. The base of the protoconid is the largest, followed closely by the metaconid. The paraconid the smallest trigonid cusps and appear to be positioned lingually to the midline There is no evidence of a precingulid at the base of the trigonid. The talonid is shorter and slightly narrower mesiodistally than the trigonid. The entoconid is large and positioned close to the hypoconulid. The tooth matches the descriptions and size range reported in Archibald (1982) and Lofgren (1995). Many of the features, including the mesiodistally narrower talonid and closely positioned entoconid and hypoconulid, were also noted by Dahlberg (2016). As mentioned before, the m2 is substantially larger than the m1 a characteristic noted by Archibald (1982) when describing the now synonymized species *Ragnarok harbichti.* Similar to the m1, the protoconid is the largest trigonid cusp followed closely by the metaconid. The paraconid, whereas the smallest cusp, doesn't appear reduced and is affix closely to the metaconid, shifted lingually. There is no precingulid present. The trigonid is mesiodistally wider than the talonid basin. The trigonid is similar in appearance to the associated m1. UWBM 104581 is a complete left m2. Its appearance is similar to UCMP 121791, with less wear present on the cups. UWBM 104581 was identified as *Baioconodon nordicum* based on fitting the reported size range, overall low, bulbous cusps and wide trigonid (Archibald, 1982; Lofgren, 1995; Dahlberg, 2016).

TABLE S14. Dental measurements (in mm) of *Baioconodon nordicum.*

Tooth Position	Specimen	L	DW	MW
m1	UCMP 121791	5.54	3.33	3.55
m2	UCMP 121791	6.33	3.82	4.48

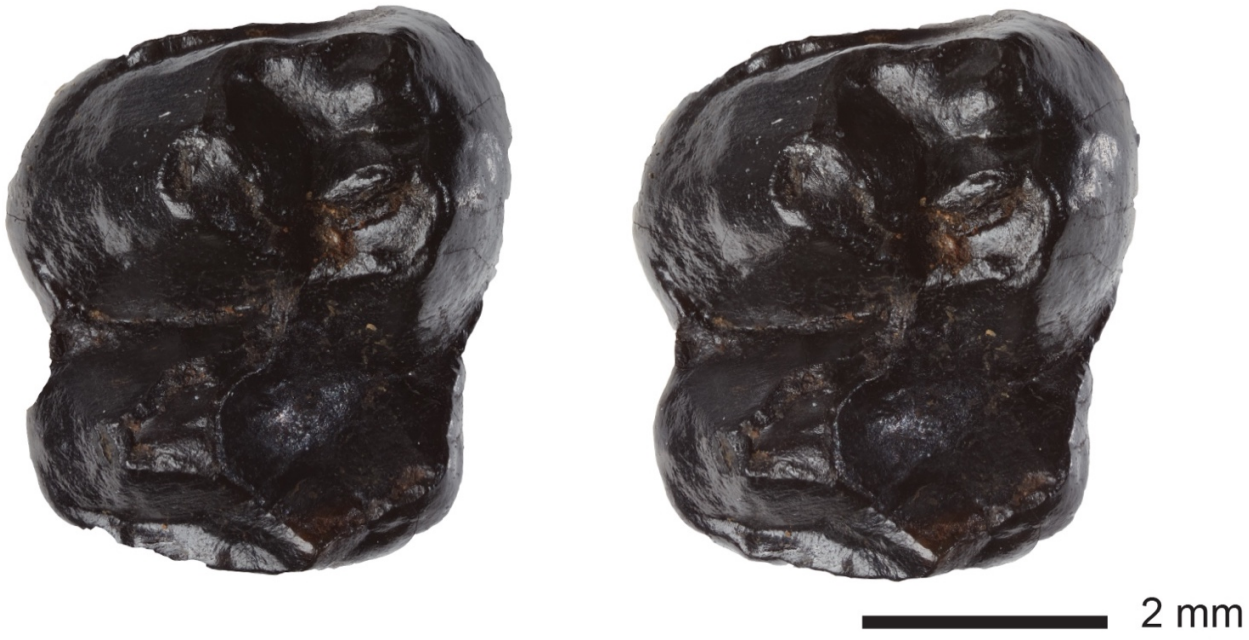

FIGURE 11. Left m1 of *Baioconodon nordicum* (UWBM 104581) in stereo occlusal view with the mesial face upwards. Scale bar equals 2 mm.

BAIOCONODON ENGDAHLI Archibald, 1982

Ragnarok engdahli Archibald, 1982:183, fig. 56

Referred material— **V77128:** p4: UCMP 139011

DESCRIPTION

Lower Premolar— UCMP 139011 is a left p4. The protoconid is the largest cusp with a bulbous appearance. The paraconid is distinct, but smaller than the protoconid, and positioned lingual to the midline. There is a smaller metaconid present, affixed to the base of the protoconid. The talonid basin is small. A ridge runs from the protoconid to the single talonid cusp. The morphology and size of UCMP 139011 match to the description of *Ragnarok engdahli* in Archibald (1982). It can be distinguished from other archaic ungulates primarily due to the large size and differs from other species of *Baioconodon* due to the small size of the metaconid relative to the other trigonid cusps (Archibald, 1982).

TABLE S13. Dental measurements (in mm) of *Baioconodon engdahli.*

Tooth	Specimen	L	DW
p4	UCMP 139011	4.73	3.06

BAIOCONODON SP.

Referred material— **V77128:** M2: UCMP 139017

DESCRIPTION:

Upper Molar— UCMP 139017 refers a left M2 fragment. The lingual portion of the tooth is missing from the para and metaconules. The parastyle is absent, the metastyle is rounded. The

paracone and metacone are parallel, subequal in size and shifted lingually from the tooth margin. There are equally sized wear facets on the paracone and metacone as well. 139017 is attributed to *Baioconodon* on the basis of size. The fragment is as large or larger than the upper molars of the other reported Puercan 1 archaic ungulates including *Protungulatum gorgun* (Archibald, 1982; Lofgren, 1995). However, the fragmentary nature prevents us from making a species designation.

TABLE S15. Dental measurements (in mm) of *Baioconodon sp.*

Tooth Position	Specimen	L
M2	UCMP 139017	4.96

Family PERIPTYCHIDAE Cope, 1882

Genus *MIMATUTA* Van Valen, 1978

MIMATUTA MINUIAL Van Valen, 1978

Referred material: **V77128**: p4: UCMP 139012; **V79100:** M1/2 UCMP 150027

DESCRIPTION

Lower Premolar— The lower p4 of *Mimatuta* is often considered the most diagnostic tooth position (Van Valen, 1978). UCMP 139012 is a complete left p4. The bulbous protoconid is the largest of the cusps. Affixed to the protoconid is the large, well developed metaconid. The large

metaconid was noted in the original species description Van Valen (1978) and subsequent descriptions Archibald (1982) and Lofgren (1995) as the major distinguishing featuring between *M. morgoth* and *M. minuial.* UCMP 139012 possess a very small mesially leaning paraconid. The talonid basin is featureless and about subequal width to the trigonid, which differs from the similarly sized *Protungulatum donnae.* UCMP 150007 is referred to as *Mimatuta minuial* M1 or M2 however the identification has not been confirmed by JRC or GPWM.

TABLE S16. Dental measurements (in mm) of *Mimatuta minuial.*

Tooth Position	Specimen	L	DW
p4	UCMP 139012	3.91	1.97

MIMATUTA SP.

(Fig. S12)

Referred material— **V77128:** M3: UCMP 139020; **V77129:** M2: UWBM 112753

DESCRIPTION

Upper Molars— UWBM 112753 is a damaged M2 with the vast majority of the lingual portion missing. The stylar shelf is rounded and flattened. The metacone is positioned slightly buccal to the paracone. The ectocingulum ridge is distinct and raised. The paracone and metacone are

equal in height. The preparacrista ridge is oriented buccally towards the paracone and is shorter than the ectocingulum. The postparacrista is rounded and curves in towards the paraconule similar to the specimens depicted in Luo (1991). The paraconule is large and conular in shape making the description of Luo (1991) and differentiating it from the similarly size *Protungulatum donnae*. Both the metaconule and protocone are missing from the specimen due to damage. Distal to the paraconule there is evidence for the beginning of the precingulum, which would extend lingually down the tooth. UCMP 139020 is a left upper M3. The parastylar shelf is larger and more distinct than the metastylar shelf. The paracone is larger than the metacone and shifted more buccally. The paraconule and metaconule are positioned closed to each other, forming a small trigon basin a featured noted for other upper molar tooth positions by Luo (1991). The protocone is positioned close to the para- and metaconules, matching the descriptions of *Mimatuta sp.* uppers by Archibald (1982) and Lofgren (1995). The lingual slope of the protocone is missing due to damage.

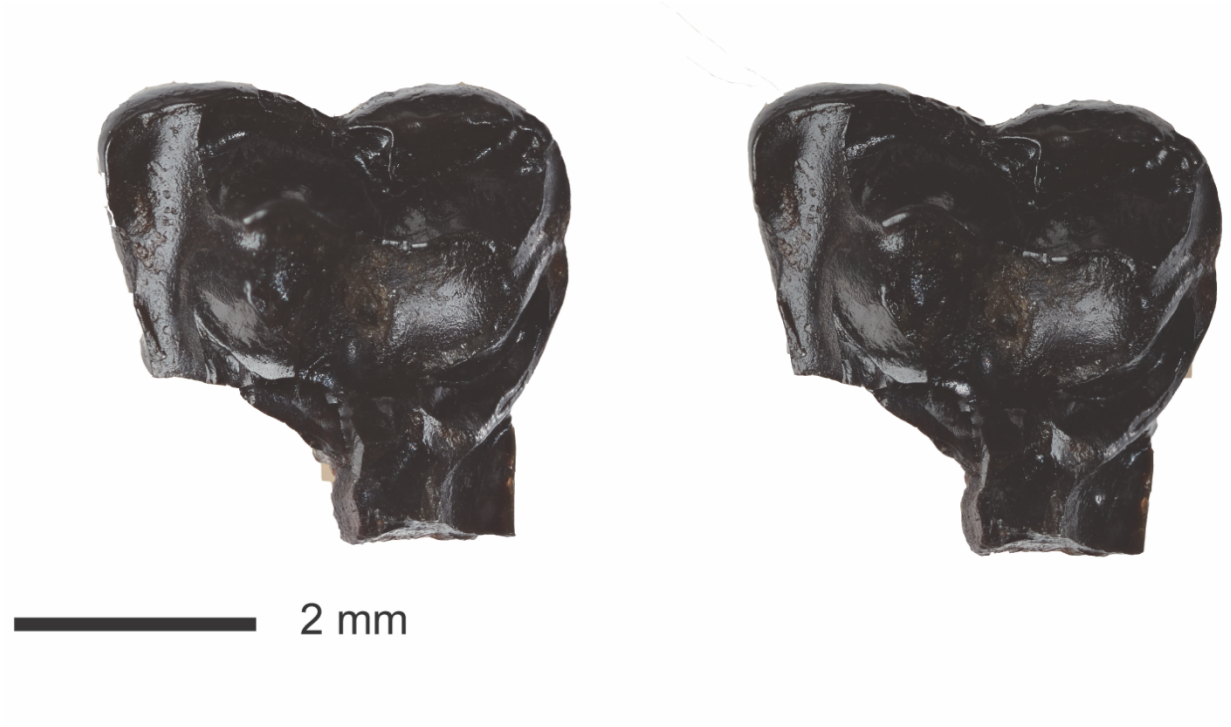

FIGURE S12. Buccal fragment of a left M2 of *Mimatuta sp.* (UWBM 112753) in stereo occlusal view with the buccal face upwards. Scale bar equals 2 mm.

TABLE S17. Dental measurements (in mm) of *Mimatuta sp.*

Tooth Position	Specimen	L
M2	UWBM 112753	3.83
M3	UCMP 139020	2.773

Class MAMMALIA Linnaeus, 1758

Gen.et sp. indet.

Referred material— **V77128:** UWBM 115285, UWBM 115286, UWBM 115288, UWBM 115287, UWBM 115284, UCMP 294331, UCMP 294334, UCMP 294345, UCMP 294346, UCMP 294376, UCMP 294380, UCMP 294418, UCMP 294433, UCMP 294435, UCMP 294449, UCMP 294451, UCMP 294452, UCMP 294453, UCMP 294454, UCMP 294479, UCMP 294480, UCMP 294481, UCMP 294482, UCMP 139016, UCMP 294484, UCMP 294485, UCMP 294486, UCMP 294488, UCMP 294491, UCMP 294492, UCMP 294493, UCMP 294494, UCMP 294495, UCMP 294499, UCMP 294501, UCMP 294502, UCMP 294504, UCMP 294506; **V77129:** UWBM 112749, UWBM 104584, UWBM 114673, UWBM 114675, UWBM 114674, UWBM 114672, UWBM 112563, UWBM 112564, UWBM 112562, UWBM 112561, UWBM 114787, UWBM 114791, UWBM 114641, UWBM 114642, UWBM 115318, UWBM 115317, UWBM 115316, UWBM 115326, UWBM 115314, UWBM 115320, UWBM 115327, UWBM 115298, UWBM 115306, UWBM 115337, UWBM 115343, UWBM 115344, UWBM 115345, UWBM 115332, UWBM 115334, UWBM 115335, UWBM 115336, UWBM 115347, UWBM 115303, UWBM 115310, UWBM 115305, UWBM 115328, UWBM 115312, UWBM 115301, UWBM 115311, UWBM 115349, UCMP 294450, UCMP 294510, UCMP 294512, UCMP 294513, UCMP 294514 **V77124:** UWBM 110669, UWBM 105271, UWBM 105362, UWBM 105260, UWBM 105274, UWBM 105264, UWBM 105270, UWBM 105276, UWBM 105277, UWBM 103103, UWBM 104373, UWBM 105267, UWBM 105268,

UWBM 105269, UWBM 105263, UWBM 114140, UWBM 114143, UWBM 111202, UWBM 114650, UWBM 114652, UWBM 114649, UWBM 114648, UWBM 114661, UWBM 114663, UWBM 114660, UWBM 114658, UWBM 115356, UWBM 114657, UWBM 112985, UWBM 112982, UWBM 114647, UWBM 114644, UWBM 114638, UWBM 1153500, UWBM 115353, UWBM 115357, UWBM 114141

These specimens represent canine, incisors, or unidentifiable fragments of teeth referred to as Mammalia indet.

RESULTS

TABLE S19. Species Level Richness and Taxonomic Diversity Metrics

	M1	HJ	CP	WC	ZL	LH	GG	LF
Raw Species Richness	14	13	10	15	10	13	11	20
Rarefied Richness	8.78 ± 1.33	11.12 ± 1.1	9.00 ± 0.82	8.04 ± 1.34	7.93 ± 1.01	12.88 ± 0.32	9.75 ± 0.94	15.88 ± 1.39
SQS	4.6	6.4	5.1	3.9	4.7	7.6	5.5	13.1
SQS Corrected	4.6	6.4	4.4	3.2	3.4	7.1	5	11.8
Simpson's Index	0.72	0.76	0.77	0.75	0.75	0.82	0.77	0.89
Pielou's Evenness	0.63	0.72	0.76	0.62	0.77	0.80	0.74	0.86

Note: M1—Morales 1; HJ—Herpijunk, CP—Carrie Padgett 6, WC—Worm Coulee 1, ZL— (Z-Line Q and Z-Line-E combined); LH—Luck O Hutch; GG—Gars Galore; LF—Littleton Fauna

TABLE S20. Genus Level Richness and Taxonomic Diversity Metrics

	M1	HJ	CP	WC	ZL	LOH	GG	LF

Raw Generic Richness	8	9	7	12	8	7	8	15
Rarefied Richness	5.44 ± 1.1	7.59 ± 0.97	6.13 ± 0.77	7.49 ± 1.1	5.93 ± 1.01	6.98 ± 0.13	6.75 ± 0.94	13.27 ± 0.93
SQS	2.6	4.7	3.4	4.9	2.9	4.4	3.2	11.4
SQS Corrected	2.1	4.2	2.7	1.7	1.8	2.7	2.8	6.4
Simpson's Index	0.32	0.35	0.37	0.75	0.37	0.50	0.33	0.89
Pielou's Evenness	0.36	0.41	0.44	0.66	0.45	0.58	0.39	0.89

Note: M1—Morales 1; HJ—Herpijunk, CP—Carrie Padgett 6, WC—Worm Coulee 1, ZL— (Z-Line Q and Z-Line-E combined); LH—Luck O Hutch; GG—Gars Galore; LF—Littleton Fauna

TABLE S21. Faunal Designations for post-KPB recovery scheme

Genus	Species*	Faunal Designation	Study Region
Mesodma		Bloom Taxon	Both
Stygimys		Immigrant	HC Only
Cimexomys		Dead Clade Walking	Both
Acheronodon		Immigrant	HC Only
Catopsalis		Immigrant	Both
?Kimbetohia		Immigrant	DB Only
Xyronomys		Immigrant	DB Only
Thylacodon		Bloom Taxa	Both
?Leptalestes		Dead Clade Walking	HC Only

Procerberus	*formicarum*	Bloom Taxon	HC Only
Procerberus	*andesiticus*	Bloom Taxon	DB Only
Procerberus	*cf. grandis*	In-Situ Diversification	Both
Puercolestes		Immigrant*	HC Only
Prodiacodon		Immigrant	HC Only
?Ambilestes		Dead Clade Walking	HC Only
Mimatuta		Immigrant	HC Only
Baioconodon		Immigrant	Both
Protungulatum		Immigrant	Both
Oxyprimus		Immigrant	Both
Maiorana		Immigrant	DB Only
Ampliconus		Immigrant	DB Only
Oxyclaenus		In-Situ Diversification	DB Only
Oxyacodon		In-Situ Diversification	DB Only
Conacodon		In-Situ Diversification	DB Only
Auraria		In-Situ Diversification	DB Only
Alticonus		In-Situ Diversification	DB Only

Note: HC—Hell Creek region, DB—Denver Basin region, * see Williamson et al. (2011) for different interpretation.

References Cited

Ameghino, F. (1890). Los Plagionlacídeos argentinos y sus relaciones zoológicas, geológicas y geográficaso. *Boletín Del Instituto Geográfico Argentino*, *11*, 143–208.

Archibald, J. D. (1982). *A Study of Mammalia and Geology Across the Cretaceous-tertiary Boundary in Garfield County, Montana*. University of California Press.

Clemens, W. (2006). Early Paleocene (Puercan) peradectid marsupials from northeastern Montana, North American Western Interior. *Palaeontographica, Abteilung A: Palaozoologie - Stratigraphie*, *277*, 19–31. https://doi.org/10.1127/pala/277/2006/19

Clemens, W. A. (1964). *Fossil mammals of the type Lance Formation, Wyoming. Part I. Introduction and Multituberculata* (Vol. 48). University of California Publications in Geological Sciences.

Clemens, W. A. (1973). *Fossil mammals of the type Lance Formation, Wyoming. Part 3. Eutheria and summary* (Vol. 94). University of California Publications in Geological Sciences. https://cir.nii.ac.jp/crid/1572824498958062208

Clemens, W. A. (2017). Procerberus (Cimolestidae, Mammalia) from the Latest Cretaceous and Earliest Paleocene of the Northern Western Interior, USA. *PaleoBios*, *34*. https://doi.org/10.5070/P9341034494

Clemens, W. A. (2019). Puercolestes and Betonnia (Cimolestidae, Mammalia) from the early Paleocene (Puercan 3 Interval Zone) of northeastern Montana, U.S.A. *PaleoBios*, *36*. https://doi.org/10.5070/P9361042705

Cope, E. D. (1884). The Vertebrata of the Tertiary Formations of the West. By E. D. Cope. Book 1. (Rep. U. S. geol. Surv. Terr., Vol. Iii.). *Science*, *3*(122), 1–1009. https://doi.org/10.1126/science.ns-5.122.467

Dahlberg, E. L., Eberle, J. J., Sertich, J. J. W., & Miller, I. M. (2016). A new earliest Paleocene (Puercan) mammalian fauna from Colorado's Denver Basin, U.S.A. *Rocky Mountain Geology*, *51*(1), 1–22. https://doi.org/10.2113/gsrocky.51.1.1

Giebel, C. (1855). *Die Säugethiere in zoologischer, anatomischer und palæontologischer Beziehung*. A. Abel.

Huxley, T. H. (1880). On the application of the laws of evolution to the arrangement of the Vertebrata and more particularly of the Mammalia. *Proceedings of the Zoological Society of London*, *1880*, 649–662.

Jepsen, G. L. (1930). Stratigraphy and Paleontology of the Paleocene of Northeastern Park County, Wyoming. *Proceedings of the American Philosophical Society*, *69*(1), 463–528.

Jepsen, G. L. (1940). Paleocene Faunas of the Polecat Bench Formation, Park County, Wyoming: Part I. *Proceedings of the American Philosophical Society*, *83*(2), 217–340.

Kielan, Z. (2004). A new reconstruction of multituberculate endocranial casts and encephalization quotient of Kryptobaatar. *ACTA PALAEONTOLOGICA POLONICA*, 12.

Lillegraven, J. A. (1968). Latest Cretaceous mammals of upper part of Edmonton formation of Alaerta, Canada, and review of marsupial-placental dichotomy in mammalian evolution. *Univ. Kansas. Paleont. Contrib.*, *50*, 1–122.

Linnaeus, C. von. (1758). *Systema naturae, per regna tria naturae: Secundum classes, ordines, genera, species cum characteribus, differentiis, synonymis, locis* (Ed. 13., Vol. 1–1, pp. 1–533). Typis Ioannis Thomae. https://doi.org/10.5962/bhl.title.559

Luo, Z. (1991). Variability of dental morphology and the relationships of the earliest arctocyonid species. *Journal of Vertebrate Paleontology*, *11*(4), 452–471. https://doi.org/10.1080/02724634.1991.10011415

Marsh, O. C. (1880). Notice of Jurassic mammals representing two new orders. *American Journal of Science*, *s3-20*(117), 235–239. https://doi.org/10.2475/ajs.s3-20.117.235

Marsh, O. C. (1889). Discovery of Cretaceous Mammalia; Part II. *American Journal of Science*, *s3-38*(224), 177–180. https://doi.org/10.2475/ajs.s3-38.224.177

Matthew, W. D., & Granger, W. (1921). *New genera of Paleocene mammals* (Vol. 13). By order of the Trustees of The American Museum of Natural History.

McKenna, M. C. (1975). Toward a Phylogenetic Classification of the Mammalia. In W. P. Luckett & F. S. Szalay (Eds.), *Phylogeny of the Primates: A Multidisciplinary Approach* (pp. 21–46). Springer US. https://doi.org/10.1007/978-1-4684-2166-8_2

Montellano, M., Weil, A., & Clemens, W. A. (2000). An exceptional specimen of Cimexomys judithae (Mammalia: Multituberculata) from the Campanian Two Medicine Formation of Montana, and the phylogenetic status of Cimexomys. *Journal of Vertebrate Paleontology*, *20*(2), 333–340. https://doi.org/10.1671/0272-4634(2000)020[0333:AESOCJ]2.0.CO;2

Novacek, M., & Clemens, W. A. (1977). Aspects of Intrageneric Variation and Evolution of Mesodma (Multituberculata, Mammalia). *Journal of Paleontology*, *51*(4), 18.

Reynolds, T. E. (1936). Two New Insectivores from the Lower Paleocene of New Mexico. *Journal of Paleontology*, *10*(3), 202–209.

Sloan, R. E., & Van Valen, L. (1965). Cretaceous Mammals from Montana. *Science*, *148*(3667), 220–227. https://doi.org/10.1126/science.148.3667.220

Smith, S. M., Sprain, C. J., Clemens, W. A., Lofgren, D. L., Renne, P. R., & Wilson, G. P. (2018). Early mammalian recovery after the end-Cretaceous mass extinction: A high-resolution view from McGuire Creek area, Montana, USA. *GSA Bulletin*, *130*, 2000–2014. https://doi.org/10.1130/B31926.1

Smith, S., & Wilson Mantilla, G. (2017). Species Discrimination of Co-Occurring Small Fossil Mammals: A Case Study of the Cretaceous-Paleogene Multituberculate Genus Mesodma. *Journal of Mammalian Evolution*, *24*. https://doi.org/10.1007/s10914-016-9332-2

Trouessart, E. (1878). Catalogue de mammiferes vivants et fossils. Ordo III. Chiroptera. *Revue et Magasin de Zoologie, 3e Série*, *6*, 204–254.

Van Valen, L. (1978). The beginning of the Age of Mammals. *Evolutionary Theory*, *4*, 45–80.

Williamson, T. E., Brusatte, S. L., Carr, T. D., Weil, A., & Standhardt, B. R. (2012). The phylogeny and evolution of Cretaceous–Palaeogene metatherians: Cladistic analysis and description of new early Palaeocene specimens from the Nacimiento Formation, New Mexico. *Journal of Systematic Palaeontology*, *10*(4), 625–651. https://doi.org/10.1080/14772019.2011.631592

Williamson, T. E., Weil, A., & Standhardt, B. (2011). Cimolestids (Mammalia) from the early Paleocene (Puercan) of New Mexico. *Journal of Vertebrate Paleontology*, *31*(1), 162–180. https://doi.org/10.1080/02724634.2011.539649

Wilson Mantilla, G. P., Chester, S. G. B., Clemens, W. A., Moore, J. R., Sprain, C. J., Hovatter, B. T., Mitchell, W. S., Mans, W. W., Mundil, R., & Renne, P. R. (2021). Earliest Palaeocene purgatoriids and the initial radiation of stem primates. *Royal Society Open Science*, *8*(2), rsos.210050, 210050. https://doi.org/10.1098/rsos.210050

CHAPTER 3: INVESTIGATING THE POTENTIAL DECOUPLING OF MAMMALIAN TAXONOMIC AND ECOLOGICAL RECOVERY FOLLOWING THE CRETACEOUS-PALEOGENE MASS EXTINCTION

3.1 INTRODUCTION

Biotic recovery comprises the evolutionary and ecological processes that follow large-scale disasters like mass extinction events (Kirchner and Weil, 2000; Erwin, 1998, 2001; Hull, 2015). Although there is a lack of a single definition for biotic recovery, it is often broadly prescribed as the return to pre-mass-extinction or similar conditions (Kauffman and Harries, 1996; Erwin, 1998, 2001). The process has traditionally been broken down into a three-phase model: (1) "lag" or "disaster," (2) "recovery," and (3) "recovered," each with distinct characteristics (Harries and Kauffman, 1990; Erwin, 1998). The disaster phase, often described as a "pause" after the extinction, is characterized by the high abundance of ecological generalist bloom taxa and the appearance of immigrant taxa from refugia. Communities from the disaster interval typically have both low evenness and taxonomic richness values compared to pre-mass-extinction biotas (Harries and Kauffman, 1990; Schindler, 1990; Schubert and Bottjer, 1992; Erwin, 1993; Kauffman and Harries, 1996; Erwin, 1998; Smith et al., 2018). The recovery phase is marked by the onset of in-situ diversification, continued immigration, and a decrease in the abundance of bloom taxa. Recovery phase communities typically have both higher evenness and richness values compared to disaster faunas but still lower than pre-mass-extinction values (Kauffman

and Harries, 1996; Erwin, 1998). The recovered phase is the final phase of the recovery process and is characterized by a return to pre-mass-extinction levels of both evenness and richness. Most studies have analyzed and characterized biotic recovery using taxonomic proxies (i.e., taxonomic richness and evenness; Niklas et al., 1983; Benton, 1995; Wilson, 2014) and, to a lesser extent, ecological proxies (i.e., ecological diversity and disparity, or morphospace occupation; Sahney and Benton, 2008; Wilson, 2013; Grossnickle and Newham, 2016). However, many of these analyses investigated taxonomic recovery and ecological recovery separately rather than exploring how these patterns differ and potentially influence each other.

The few studies that compared taxonomic and ecological aspects of recovery showed that these aspects have often been temporally decoupled (Foote, 1999; Erwin, 2007; Bapst et al., 2012; Ruta et al., 2013; Song et al., 2018; Edie et al., 2018; Cole and Hopkins, 2021), although the relative sequence varies between studies (Fig. 3.1). Under the Ecological-lag hypothesis, taxonomic recovery outpaced ecological recovery, sometimes by an order of magnitude (Fig. 3.1; Wing and Boucher, 1998; Chen and Benton, 2012; Wilson, 2013; Dineen et al., 2014; Ezcurra and Butler, 2018; Song et al., 2018). This temporal lag in ecological recovery might be due to the nature of the process of rebuilding complex ecological interactions in ecosystems (Kirchner and Weil, 2000; Erwin, 2007). Mass extinctions not only remove species, but depending on selectivity, can also reduce or eliminate entire ecological guilds; in turn, associated ecological interactions can be weakened or broken. It would stand to reason that the processes of recovery, such as immigration and in-situ diversification, replenish numbers of species in a community more rapidly than they rebuild complex ecological interactions, which might involve the coordinated evolution of novel morphologies (Kirchner and Weil, 2000; Erwin, 2008; Chen and Benton, 2012; Song et al., 2018). Thus, ecological recovery might be the rate-limiting step

(Chen and Benton, 2012). Under the Taxonomic-lag hypothesis, ecological recovery outpaced taxonomic recovery (Fig. 3.1; Foote, 1994; Wagner, 2010; Bapst et al., 2012; Wright, 2017; Edie et al., 2018; Lowery and Fraass, 2019). The temporal lag in taxonomic recovery might be due to how morphospace is initially colonized (Chen and Benton, 2012; Wright, 2017; Lowery and Fraass, 2019). In these scenarios, morphospace is colonized first by a limited number of progenitors, either survivors or immigrants. These progenitors occupy different regions of morphospace, resulting in high ecological disparity and low taxonomic richness during the initial stages of recovery (Foote and Gould, 1992). These taxa then diversify and begin to refill regions of ecospace, resulting in a slow increase in taxonomic richness (Chen and Benton, 2012; Wright, 2017; Lowery and Fraass, 2019). Under the In-step hypothesis, taxonomic and ecological recovery occurred in lockstep until pre-mass-extinction levels are reached again (Foote, 1993; Payne et al., 2011; Cole and Hopkins, 2021; Fig. 3.1). Understanding the potential temporal offset of taxonomic and ecological recovery is critical to our understanding of biotic recovery. If these two facets of biotic recovery are decoupled, then previous interpretations of recovery patterns based solely on taxonomic proxies may be failing to capture the full picture (Foote, 1993, 1997). Understanding these dynamics may also inform us about the origin and maintenance of diversity and the assembly of communities more generally (Erwin, 2006; Hull, 2015).

Here, we test these competing hypotheses for community recovery using the mammalian biotic recovery following the Cretaceous-Paleogene (K-Pg) mass extinction event. We chose the K/Pg event due to its importance in the development of modern, mammalian-dominated terrestrial ecosystems. The Paleocene biotic recovery of mammals set the stage for the evolutionary radiation that allowed mammals to become one of the most ecologically diverse

vertebrate groups (Simpson, 1937). The Western Interior of North America hosts several regions that preserve vertebrate micro- and macrofossil assemblages that sample the intervals immediately before and after the K-Pg boundary (KPB). Among them, the Hell Creek region in northeastern Montana in the Williston Basin offers arguably the best opportunity to study biotic recovery following the K-Pg mass extinction. It preserves numerous, well-sampled mammalian assemblages from the Hell Creek Formation and the Tullock Member of the Fort Union Formation (Archibald, 1982; Lofgren, 1995; Clemens, 2002; Wilson, 2005, 2014; Clemens and Wilson, 2009; Smith et al., 2018; Claytor et al., In Review). Those assemblages have been integrated into a local, high-resolution temporal framework representing a ca. 3-Ma window spanning the KPB that constructed from magneto-, litho-, chemo-, and biostratigraphic- and radioisotopic data and continues to be refined (Swisher et al., 1993; Archibald et al., 1982; Wilson, 2005, 2014; LeCain et al., 2014; Renne et al., 2013; Moore et al., 2014; Hartman et al., 2014; Ickert et al., 2015; Sprain et al., 2015, 2018; Smith et al., 2018; Weaver et al. 2022). The most recent description and analyses of mammalian assemblages from the Hell Creek region (Smith et al., 2018; Claytor et al., In Review) provided an even more granular view of post-KPB biotic recovery and thus led to the subdivision of both the disaster and recovery phases into sub-phases (i.e., Early disaster, Late disaster, Early recovery, and Late recovery). This new model was based on taxonomic recovery only (i.e., richness, evenness, and taxonomic composition) and did not consider measures of ecological recovery. Here, we apply ecological richness and disparity metrics to this established sequence of mammalian faunal assemblages from the first ~1 million years of the Paleocene in the Hell Creek region (Sprain et al., 2018) to investigate the timing and patterns of mammalian ecological recovery relative to taxonomic recovery.

To reconstruct the ecological recovery of mammals following the K-Pg mass extinction event, we created two-dimensional ecospace models. Compared to studies of ecology that focus on a singular aspect of an organism's ecology (e.g., diet, body size, or locomotor mode), ecospace analyses allow for the evaluations of how the combination of different ecological factors contribute to the patterns of ecospace occupation in a community (Bambach, 1983; Bambach et al., 2007; Bush et al., 2007; Bush and Bambach, 2011; Dineen et al., 2014 Oliviera et al., 2016; Chen et al., 2019; Fraser et al., 2021; Fraser and Lyons, 2021). This multivariate approach allows for a more nuanced interpretation of how ecological variables interact in space and time (e.g., do body size and diet evolve independently through time). Previous studies investigating the ecospace occupation of mammals have typically focused on three aspects of their ecology that are more readily inferred in the fossil record: diet, body size, and locomotor mode (Gilbert, 2005; Louys et al., 2014; Chen et al., 2019). We acknowledge the importance of locomotion and its influence on an organism's habitat preference; however, due to both the nature of North America's Late Cretaceous and Paleocene record of mammals, which consists mainly of isolated teeth and jaw fragments, and the difficulty of assigning species-level identifications to the limited isolated postcranial materials, we focus our analyses on diet and body size. Dietary ecology can be inferred through a wide array of techniques, including gross dental morphology, dental topographic analyses, dental microwear analyses, and morphology-free proxies (i.e., stable isotopes) each with a varying degree of precision and accuracy (Scott and Ungar, 2006; Evans et al., 2007; Wilson et al., 2012; Wilson, 2013; DeSantis, 2016). Body mass can be estimated using taxon- and morphology-appropriate formulae resulting from regression analyses in extant mammals and serve as a proxy for body size (Conroy, 1987; Bloch et al., 1998; Smits and Wilson, 2011; Wilson et al., 2012). Using estimated body size and

reconstructed diet for each taxon in each community in our study system, we developed a temporal sequence of two-dimensional ecospace models to investigate changes in ecospace occupation during the post-K-Pg recovery.

3.2 MATERIALS AND METHODS

Institutional Abbreviations UCMP, the University of California Museum of Paleontology, Berkeley, California, U.S.A.; UWBM, the University of Washington Burke Museum of Natural History and Culture, Seattle, Washington, U.S.A.

Temporal Sequence of Mammalian Faunal Assemblages We used the model of K-Pg biotic recovery of Claytor et al. (In Review) along with chronostratigraphic framework of the Hell Creek region to establish a temporal sequence of early Paleocene local faunas, between the Pre-mass-extinction phase and the Post-recovery phase. These local faunas sample the Early disaster, Late disaster, and Early recovery sub-phases. The Late recovery sub-phase has only been sampled by the Littleton local fauna from the Denver Basin of Colorado (Middleton, 1983; Middleton and Dewar, 2004). To minimize the influence of spatial differences, we excluded the Late recovery sub-phase (Littleton local fauna) from our analyses. We acknowledge that the absence of the Late recovery sub-phase may obscure important aspects of the taxonomic and ecological recovery patterns, including the true timing of certain changes (e.g., if ecospace occupation increased during the Late Recovery sub-phase but we only note the change in the Recovered phase).

We used the Flat Creek local fauna (Archibald, 1982; Wilson, 2014) for the Pre-mass-extinction phase. For the Early disaster sub-phase, we used the Z-Line local fauna (UCMP locs. V84193 and V84194). The Z-Line localities have been dated to be within the first 28 ka

following the KPB, bracketed through previous geochronological studies between a carbonaceous shale interpreted as the KPB and a spatially adjacent coal layer (Smith et al., 2018; Sprain et al., 2018). The Morales 1 (UCMP V77128), Herpijunk (UCMP V77129), Carrie Padgett (UCMP locs. V77124 and V79100), and Worm Coulee 1 (UCMP V74111) local faunas represent the Late disaster sub-phase (Wilson, 2014; Claytor et al., In Review). All four of those local faunas have been bracketed to between 28–80 ka following the KPB, though they sample three distinct channel complexes (Sprain et al., 2018; Weaver et al., 2022; Claytor et al., In Review). The Luck O Hutch local fauna, which has been bracketed temporally to between 28–328 ka post-KPB, though it is interpreted as likely younger than the Late-disaster local faunas, represent the Early recovery sub-phase (Smith et al., 2018; Sprain et al., 2018). We acknowledge the potential impact of the incomplete sampling of the Luck O Hutch local fauna, which may influence the patterns of taxonomic or ecological recovery. Although there are other localities in the study region that sample the Early recovery subphase, they have not been studied in detail and comprehensive faunal lists are not yet available (Sprain et al., 2018; Wilson Mantilla et al., 2021). We used the Garbani channel local fauna, which is assigned to the Pu3 interval of the Puercan North American Land Mammal 'age,' (hereafter NALMA; Clemens, 2013), to represent the Recovered phase of biotic recovery. The Garbani channel assemblage is bracketed temporally between 500–900 ka following the KPB (Weaver et al., 2022). We also sampled a Post-recovery phase represented by the earliest Torrejonian (To1) Horsethief and Farrand Channel local faunas, both of which have been bracketed between ~934 ka–1.011 Ma following the KPB (Clemens and Wilson, 2009; Hovatter and Wilson, 2015).

We compiled faunal lists for each of the local faunas from previous studies (Archibald, 1982; Clemens and Wilson, 2009; Wilson, 2014; Smith et al., 2018; Clemens, Personal

Communication 2019; Claytor et al., In Review; Hovatter and Wilson, 2015). Due to the discrepancies in sample sizes, the large number of singleton taxa in the Late disaster local faunas, and stratigraphic relationships between the Late disaster sub-phases localities we removed all taxa not unaccounted for in more than two of the local faunas. As such, the results for both taxonomic and ecological proxies for the Late disaster sub-phase may differ slightly from the true patterns. The faunal list for the Recovered phase is compiled from assemblages of multiple, spatially adjacent localities that we interpret them as one local fauna because they derive from the same channel complex. The Post-recovery faunal list is currently undergoing study, but the contents are up-to-date.

Body Size Estimations and Dietary Categories We mapped ecospace occupation during the Pre-mass-extinction interval through the post-K-Pg recovery interval using two-dimensional ecospace models with estimates for both body mass and dietary ecology for each taxon in each local fauna. We used body mass estimates from either previously studies (Wilson et al., 2013; Smith, 2017) or our own calculations using taxon- and morphology-appropriate formulae based on regression analyses of extant mammals (Bloch et al., 1998 for eutherians excluding primates; Conroy, 1987 for primates; Smits and Wilson, 2011 for metatherians; Wilson et al., 2012 for multituberculates). We acknowledge that body mass estimates for extinct taxa have uncertainties (Fortelius, 1990; Damuth, 1990), but we have taken measures to minimize their impact on this study. Whenever possible, we estimated body mass using linear measurements of the lower first molar (m1). For taxa without m1 measurements, we utilized the measurements from an available molar tooth position, with a preference for the lower second molar (m2s) for therians. For taxa represented by only upper molars (some eutherians), we utilized the formula developed by Bloch et al. (1987) for upper M1s. Several taxa from the faunal list lacked species-level identifications;

to calculate their body masses, we used the average body mass of the other species within the genus known from that same temporal interval. The body mass estimate for each taxon was placed into one of five body-size bins (see Table 3.1). The body mass estimate and body-size categorization for each taxon are in Tables 3.2–3.6.

We inferred dietary preference for each taxon using either previous interpretations (e.g. gross morphology, OPC, dental microwear analyses) of that taxon or extrapolations from closely related or morphologically similar taxa. With these data, we categorized each taxon into one of four ordered dietary categories: (one) herbivore, (two) plant-dominated omnivore, (three) animal-dominated omnivore, and (four) faunivore. We utilized broad categorizations due to the mixture of different techniques for dietary reconstructions or inferences and the different resolutions for dietary classifications available. The herbivore category represents a range of diets that included folivores, granivores, and frugivores. The faunivore category is primarily represented by both soft and hard invertivores, in addition to mammals that feed on other vertebrates. We note that the dietary categories utilized are coarse and potentially obscure the true dietary preferences for the included taxa, as mammals can exhibit varying degrees of dietary plasticity due to factors including resource availability, seasonality, and many more (Rivals and Semprebon, 2011). Finer-scale dietary categories may better illustrate the true nature of ecospace occupation; however, due to the varying levels of dietary analyses available for the included taxa, we default to the broader dietary categories. The dietary category assignment for each taxon and their justifications are in Tables 3.2–3.6. Each taxon was mapped to one of the 20 eco-cells in the 5 x 4 ecospace using the combination of its body size category and dietary category as coordinates. Note that more than one taxon can map to the same eco-cell.

Ecological Richness, Disparity, and Mean To quantify ecospace occupation patterns, we calculated ecological richness, functional evenness, and disparity for each ecospace plot. Ecological richness (ERich) represents the number of different ecologies in the local fauna and is a count of the eco-cells occupied in the ecospace. Functional evenness (FEven) represents the distribution of taxa across each ecospace plot and was calculated using Simpson's evenness (1-D; Simpson, 1949); 95% confidence intervals for FEven were estimated by resampling (9,999 bootstraps). Ecological disparity (EDisp) is the magnitude of differences in ecologies in the community and is calculated using the function avgdist() from the R package *vegan* as the Manhattan pairwise distance between the taxa in ecospace. We assessed95% confidence intervals for EDisp by resampling (1,000 bootstraps). To compare determine if there were statistically significant differences in EDisp and FEven through time, we used multiple *t*-tests in R.

3.3 RESULTS

Ecospace Occupation Through the study interval, 15 out of the 20 available ecocells were occupied by at least one taxon (Fig. 3.2). The most common ecology (hereafter, mode) for the Pre-mass-extinction local fauna was the small-bodied, animal-dominated omnivore eco-cell, with 8 spp. present. The mode remained relatively consistent in the small-bodied, animal-dominated omnivore or faunivore ecocells throughout the entire study interval. Generally, ecospace occupation was restricted to the lower left quadrant characterized by smaller body sizes and animal-based diets until the Recovered phases (Fig. 3.2). Following the Early disaster sub-phase, eutherians and multituberculates experienced shifts both towards more herbivorous diets and larger body sizes, although not in tandem. Multituberculates expanded into the herbivore dietary category prior to eutherians, in the Late disaster sub-phase and Recovered phases, respectively.

Moreover, multituberculates expanded into larger body sizes than eutherians during the Recovered phase. The patterns of ecospace occupation showed clustering within certain ecocells along with a gradual expansion towards the upper right quadrant, characterized by larger-body sizes and more plant-based diets.

Taxonomic and Ecological Richness

Taxonomic and ecological richness followed similar trends to each other throughout the study interval. The latest Cretaceous (Lancian) Pre-mass-extinction local fauna had high taxonomic richness (29 spp.) and ecological richness (ERich = 11; Figs. 3.2 and 3.3). Multituberculates and metatherians had the highest ERich values (ERich = six) compared to eutherians (ERich = three). Both taxonomic and ecological richness fell substantially across the KPB and remained low (<15 spp., ERich <7) through the Early recovery sub-phase and less than 328 ka after the KPB (Figs. 3.2 and 3.3). Eutherians had the highest ERich values for both the Late disaster (ERich = four) and Early recovery (ERich = three), primarily driven by the appearance of archaic ungulate immigrants (Fig. 3.2). Taxonomic and ecological richness exceeded Pre-mass-extinction levels (≥34 spp., ERich = 13) by the Recovered phase and possibly as early as the Late recovery sub-phase, which is not represented in our study. Eutherians continued to have the highest ERich followed by the multituberculates and then the metatherians (ERich = nine, seven, and one, respectively; Fig. 3.2). Taxonomic richness remained stable during the Post-recovery phase (≥ 34 spp.), but ecological richness declined (ERich = 10; Figs. 3.2 and 3.3). Despite declines in total ERich, eutherian ERich remained stable, yet multituberculate ERich declined (ERich = nine and three, respectively). The trends in both taxonomic and ecological richness followed the previously established patterns of biotic recovery, with increases through each sub-phase, though taxonomic richness appears to have increased at a faster rate.

Functional Evenness Functional evenness (FEven) remained relatively stable and high with no significant differences for any of the subphases or phases through the study interval. FEven during the Pre-mass-extinction phase was 0.85 and only dropped slightly during the Early disaster sub-phase to 0.75 (Fig. 3.4). FEven increased for both the Late disaster and Early recovery sub-phases (0.80 and 0.81 respectively; Fig. 3.4). FEven returned to Pre-mass-extinction levels during the recovered phase and continued to increase in the Post-recovery (0.85 and 0.88 respectively).

Ecological Disparity Although the mean value for EDisp remained relatively consistent across the KPB, there are notable differences. There was a significant drop in EDisp between the Pre-mass-extinction phase (1.53) and Early disaster sub-phase (1.40; $p = 0.001$; Fig. 3.5). EDisp rose significantly (1.51; $p = 0.018$), to near Pre-mass-extinction levels, in the Late disaster sub-phase before significantly dropping again in the Early recovery sub-phase (1.42; $p = 0.040$; Fig. 3.5). EDisp then rose significantly again to higher than pre-mass extinction levels during the Recovered phase (1.58; $p = 1.135 \times 10^{-6}$). EDisp dropped significantly again during the Post-recovery phase (1.51; $p = 0.004$).

3.4 DISCUSSION

Overall, our results support the In-step hypothesis that taxonomic and ecological recovery occurred in lockstep, both reaching pre-mass-extinction levels between 500–900 ka following the KPB in the Hell Creek region (Wilson, 2013 and 2014; Weaver et al., 2021; Figs. 3.1 and 3.3). Taxonomic and ecological richness both experienced marginal increases from the KPB to the Early recovery subphases, roughly 80–328 ka post-KPB (Sprain et al., 2018; Claytor et al., In Review). The increases in richness occur in tandem with increases in both FEven and EDisp

(Figs. 3.4 and 3.5). FEven and EDisp were lowest during the Early disaster sub-phase which follows trends reported in previous works investigating biotic recovery (Mouillot et al., 2013; Wilson, 2013). The decrease in both metrics was likely due to increased redundancy following the KPB, with more than 50% of the Early disaster taxa occupying only two ecocells (Fig. 3.2). The extinction selectivity of the causal mechanism and its subsequent effects selected against ecological specialists, including specialized faunivores, taxa with plant based diets (i.e., plant-dominated omnivores and herbivores), and larger body sizes, thus limiting ecospace occupation and resulting in a more homogeneous community (Fig. 3.2; Mouillot et al., 2013; Wilson, 2013; Dineen et al., 2014; Wilson, 2014). This pattern has also been demonstrated in other tetrapod families other than mammals, with small omnivores and insectivores having higher survivorship than larger herbivores and carnivores (Fara, 2000). Following the Early disaster sub-phase FEven and EDisp both increased, likely because of a decrease in redundancy as more taxa occupied new regions of ecospace, though certain ecocells remain highly occupied (i.e., small, animal-dominated, or faunivore cells). All four metrics reached Pre-mass extinction levels during the Recovered phase suggesting a period of intensive immigration and/or in situ diversification during the currently unsampled Late recovery sub-phase, roughly 328–500 ka post-KPB (Figs. 3.3, 3.4 and 3.55).

Our study focuses on a higher-resolution temporal framework, on the order of tens of thousands to hundreds of thousand of years, compared to other studies that utilize coarser temporal frameworks, on the order of millions of years (Foote, 1994, 1999). As such, the more limited temporal window may explain the temporal concordance between ecological and taxonomic recovery compared to other studies that identified offsets. The temporal concordance between ecological and taxonomic recovery has previously been explained as being consistent

with diffusion through ecospace that is non-selective with respect to morphology, based on the diversification models proposed by Foote (1993, 1997; Cole and Hopkins, 2021). For our study system, a mixture of abiotic and biotic factors potentially influenced the diffusion across ecospace, including the co-evolution of angiosperms and mammals, along with the timing of Deccan Traps volcanism which may be associated with subsequent stabilization of the local environment.

Crown-group angiosperms first radiated during the Early Cretaceous, though they only became significant components of Mesozoic ecosystems towards the end of the Cretaceous or early Paleogene (Wing and Boucher, 1998; Magallón et al., 2013, 2015; Crifò et al., 2014). Angiosperms provided not only novel food resources (i.e., fruit and seeds) but also stratified forested ecosystems, creating new habitats for animals (Eriksson, 2014). Thus, the ecological diversification of angiosperms has been suggested as a possible trigger for the ecomorphological diversification of numerous mammal groups, including multituberculates and therians, during the Late Cretaceous (Wilson et al., 2012; Grossnickle and Polly, 2013; Eriksson, 2014; Grossnickle and Newham, 2016; Chen et al., 2019; Grossnickle et al., 2019). Moreover, taxa like archaic ungulates, which lack a Late Cretaceous fossil record (though see Archibald et al., 2011, and Kelly, 2014 for possible pre-KPB records of certain archaic ungulates), possessed dental characteristics that imply a shift towards more herbivorous diets pre-KPB. Multituberculates along with the eutherian archaic ungulates and plesiadapiform primates were the primary drivers of the increases observed in ERich, specifically in the direction of more plant-based diets and larger body size categories, although not in tandem (Wilson, 2013 and 2014; Fig. 3.6). The ecological richness of archaic ungulates and plesiadapiform primates peaked during the Post-recovery phase (ERich = eight); however, multituberculate occupation peaked during the

Recovered phase (ERich = seven), suggesting the expansion of archaic ungulates and plesiadapiform primates may have driven a reduction in ecospace occupation for multituberculates or the expansion may have represented a non-competitive replacement by the eutherian clades (Benton 1991; Fig. 3.6). The reduction in multituberculate occupation coincides with a documented reduction in their taxonomic richness as well (Van Valen and Sloan, 1966; Krause, 1986; Wilson, 2014). The reduction in multituberculate diversity, both ecologically and taxonomically, may be an artifact of differences in sampling intensities between the Post-recovery and Recovered localities (see Materials and Methods for a more detailed explanation) or reflect a biologically meaningful trend. Continued sampling of our Post-recovery localities and detailed descriptions of the local faunas will help us better understand the decline.

The transitions between different phases of recovery may have been influenced by abiotic factors, including Deccan Traps volcanism and climatic swings. The length of the Disaster phase, roughly 80 ka in the Hell Creek region, has been posited to correspond to a pulse in Deccan Trap volcanism that roughly coincides with this interval (Schoene et al., 2019, 2021; Claytor et al., In Review; but see Sprain et al., 2019 for a different interpretation). Deccan Traps volcanism has been suggested as a causal mechanism in the destabilization of mammalian communities prior to the KPB (Wilson, 2014). As such, the continued eruptions in the Paleocene may have resulted in persistent ecosystem instability. Moreover, the timing of the taxonomic recovery, a return to pre-extinction levels of richness of floral communities also coincides with this interval (Wilson Deibel, 2022).The timing of the Deccan Traps volcanism and floral taxonomic recovery suggest unstable environmental conditions that may have prevented any significant changes in both taxonomic and ecological richness during the first 80 ka after the KPB within the Hell Creek region. The low productivity and unstable environments of the first 80 ka likely could not

support larger-bodied, plant-dominated omnivores or herbivores controlling the rate at which mammals could diffuse through those regions of ecospace (Wilf and Johnson, 2004; Wilson, 2014). Moreover, high functional redundancy, as seen in the Early disaster sub-phase, may have increased the resilience of mammalian communities during the period of environmental instability (Walker, 1992; Harris, 1993; Fonesca and Ganade, 2001; Rosenfeld, 2002; Palumbi et al., 2008; Dineen et al., 2014). As such, we would not expect mammals to expand into unoccupied regions of ecospace until environmental perturbations caused by Deccan Traps volcanism had ceased, allowing environmental stability to return to the ecosystem, delaying the transition from the Disaster to Recovery phases. However, the recovery of floral communities likely took longer elsewhere in the Western Interior of North America, up to 300 ka after the KPB in the Denver Basin (Lyson et al., 2019) and up to 10 million years in the Williston Basin of North Dakota (Wilf and Johnson, 2004), suggesting the concordance between these factors may be a local signal within the Hell Creek region. Additionally, the transition between the Recovery and Recovered phase may have also coincided with environmental changes. A warming interval detected in the Denver Basin of Colorado dated to roughly 700 ka following the KPB, based on the local sediment accumulation rate derived by Clyde et al. (2016), may have influenced the transition from the currently unsampled Late recovery sub-phase into the Recovered phase (Lyson et al., 2019). The warming occurred in tandem with the appearance of two large-bodied mammals (*Taeniolabis taoensis* and *Eoconodon coryphaeus*) and the first appearance of legumes in the Denver Basin. Lyson et al. (2019) suggest the warming pulse helped facilitate immigration and/or in situ diversification. Although this warming interval has not been detected within the Hell Creek region, the timing suggests it may have influenced the rapid taxonomic and ecological diversification that occurs during the currently undescribed Late

recovery sub-phase (Figs. 2 and 3). Overall, we hypothesize that a mix of both abiotic and biotic factors influenced the patterns and rate of mammalian biotic recovery in the Hell Creek region.

3.5 CONCLUSION

Taken together, our results support the In-step hypothesis and a temporal concordance between ecological and taxonomic recovery for mammals within the Hell Creek region. We demonstrate that the revised model of biotic recovery proposed by Claytor et al. (In Review) can be utilized for investigations into both the taxonomic and ecological aspects of biotic recovery. The model was originally tested using local faunas from the Denver Basin and taxonomic proxies, the results of which suggested that mammalian recovery was not spatially uniform (Claytor et al. In Review). For this reason, we are unable to determine the applicability of the model to other regions within the Western Interior. Differences in the taxonomic richness and abundance of certain mammal groups including archaic ungulates and plesiadapiforms, suggest regional differences in how mammals occupied ecospace during the early phases of recovery (Silcox and Williamson, 2012). These regional differences may be a result of the formation of geographic barriers, climatic gradients, or even be related to the spatial pattern of the recovery of angiosperms (Boyd and Lillegraven, 2011; Smith et al., 2018; Wilson Mantilla et al., 2021). Comparison with other regions within the Western Interior, including the Denver Basin of Colorado, the Hanna and Great Divide basins of Wyoming, and the San Juan Basin of New Mexico, will help in our understanding of the ecological recovery of mammals and whether provinciality impacts how mammals occupied ecospace.

3.6 REFERENCES CITED

Archibald, J. D. (1982). *A Study of Mammalia and Geology Across the Cretaceous-tertiary Boundary in Garfield County, Montana*. University of California Press.

Archibald, J. D., Gingerich, P. D., Lindsay, E. H., Clemens, W. A., Krause, D. W., & Rose, K. D. (1987). First North American Land Mammal Ages of the Cenozoic Era. In *Cenozoic Mammals of North America*. University of California Press,.

Archibald, J. D., Zhang, Y., Harper, T., & Cifelli, R. L. (2011). Protungulatum, Confirmed Cretaceous Occurrence of an Otherwise Paleocene Eutherian (Placental?) Mammal. *Journal of Mammalian Evolution*, *18*(3), 153–161. https://doi.org/10.1007/s10914-011-9162-1

Bambach, R. K. (1983). Ecospace Utilization and Guilds in Marine Communities through the Phanerozoic. In M. J. S. Tevesz & P. L. McCall (Eds.), *Biotic Interactions in Recent and Fossil Benthic Communities* (pp. 719–746). Springer US. https://doi.org/10.1007/978-1-4757-0740-3_15

Bambach, R. K., Bush, A. M., & Erwin, D. H. (2007). Autecology and the Filling of Ecospace: Key Metazoan Radiations. *Palaeontology*, *50*(1), 1–22. https://doi.org/10.1111/j.1475-4983.2006.00611.x

Bapst, D. W., Bullock, P. C., Melchin, M. J., Sheets, H. D., & Mitchell, C. E. (2012). Graptoloid diversity and disparity became decoupled during the Ordovician mass extinction. *Proceedings of the National Academy of Sciences*, *109*(9), 3428–3433. https://doi.org/10.1073/pnas.1113870109

Benton, M. J. (1991). Extinction, Biotic Replacements, and Clade Interactions. *The Unity of Evolutionary Biology*, 89–102.

Benton, M. J. (1995). Diversification and Extinction in the History of Life. *Science*, *268*(5207), 52–58. https://doi.org/10.1126/science.7701342

Bloch, J. I., Rose, K. D., & Gingerich, P. D. (1998). New Species of Batodonoides (Lipotyphla, Geolabididae) from the Early Eocene of Wyoming: Smallest Known Mammal? *Journal of Mammalogy*, *79*(3), 804. https://doi.org/10.2307/1383090

Boyd, D. W., & Lillegraven, J. A. (2011). Persistence of the Western Interior Seaway: Historical background and significance of ichnogenus Rhizocorallium in Paleocene strata, south-central Wyoming. *Rocky Mountain Geology*, *46*(1), 43–69. https://doi.org/10.2113/gsrocky.46.1.43

Bush, A. M., & Bambach, R. K. (2011). Paleoecologic Megatrends in Marine Metazoa. *Annual Review of Earth and Planetary Sciences*, *39*(1), 241–269. https://doi.org/10.1146/annurev-earth-040809-152556

Bush, A. M., Bambach, R. K., & Daley, G. M. (2007). Changes in theoretical ecospace utilization in marine fossil assemblages between the mid-Paleozoic and late Cenozoic. *Paleobiology*, *33*(1), 76–97. https://doi.org/10.1666/06013.1

Chen, M., Strömberg, C. A. E., & Wilson, G. P. (2019). Assembly of modern mammal community structure driven by Late Cretaceous dental evolution, rise of flowering plants, and dinosaur demise. *Proceedings of the National Academy of Sciences*, *116*(20), 9931–9940. https://doi.org/10.1073/pnas.1820863116

Chen, Z.-Q., & Benton, M. J. (2012). The timing and pattern of biotic recovery following the end-Permian mass extinction. *Nature Geoscience*, *5*(6), Article 6. https://doi.org/10.1038/ngeo1475

Claytor, J. R., Weaver, L. N., Tobin, T. S., & Wilson Mantilla, G. (n.d.). *New mammalian local faunas from the first ca. 80 ka of the Paleocene in northeastern Montana and a revised model of biotic recovery from the Cretaceous-Paleogene mass extinction*.

Clemens, W. A. (2002). Evolution of the mammalian fauna across the Cretaceous-Tertiary boundary in northeastern Montana and other areas of the Western Interior. In J. H. Hartman, K. R. Johnson, & D. J. Nichols, *The Hell Creek Formation and the Cretaceous-Tertiary boundary in the northern Great Plains: An Integrated continental record of the end of the Cretaceous*. Geological Society of America. https://doi.org/10.1130/0-8137-2361-2.217

Clemens, W. A. (2013). Cf. Wortmania from the early Paleocene of Montana and an evaluation of the fossil record of the initial diversification of the Taeniodonta (Mammalia). *Canadian Journal of Earth Sciences*, *50*(3), 341–354. https://doi.org/10.1139/e2012-055

Clemens, W. A., & Hartman, J. H. (2014). From Tyrannosaurus rex to asteroid impact: Early studies (1901–1980) of the Hell Creek Formation in its type area. In G. P. Wilson, W. A. Clemens, J. R. Horner, & J. H. Hartman, *Through the End of the Cretaceous in the Type Locality of the Hell Creek Formation in Montana and Adjacent Areas*. Geological Society of America. https://doi.org/10.1130/2014.2503(01)

Clemens, W. A., & Wilson, G. P. (2009). Early Torrejonian mammalian local faunas from northeastern Montana, U.S.A. *Museum of Northern Arizona Bulletin 65*.

Clyde, W. C., Ramezani, J., Johnson, K. R., Bowring, S. A., & Jones, M. M. (2016). Direct high-precision U–Pb geochronology of the end-Cretaceous extinction and calibration of Paleocene astronomical timescales. *Earth and Planetary Science Letters*, *452*, 272–280. https://doi.org/10.1016/j.epsl.2016.07.041

Cole, S. R., & Hopkins, M. J. (2021). Selectivity and the effect of mass extinctions on disparity and functional ecology. *Science Advances*, *7*(19), eabf4072. https://doi.org/10.1126/sciadv.abf4072

Conroy, G. C. (1987). Problems of body-weight estimation in fossil primates. *International Journal of Primatology*, *8*(2), 115–137. https://doi.org/10.1007/BF02735160

Crifò, C., Currano, E. D., Baresch, A., & Jaramillo, C. (2014). Variations in angiosperm leaf vein density have implications for interpreting life form in the fossil record. *Geology*, *42*(10), 919–922. https://doi.org/10.1130/G35828.1

Damuth, J. (1990). Problems in estimating body masses of archaic ungulates using dental measurements. *Body Size in Mammalian Paleobiology: Estimation and Biological Implications*, *229*(381), tables 16.9-16.10).

DeSantis, L. R. G. (2016). Dental microwear textures: Reconstructing diets of fossil mammals. *Surface Topography: Metrology and Properties*, *4*(2), 023002. https://doi.org/10.1088/2051-672X/4/2/023002

Dineen, A. A., Fraiser, M. L., & Sheehan, P. M. (2014). Quantifying functional diversity in pre- and post-extinction paleocommunities: A test of ecological restructuring after the end-Permian mass extinction. *Earth-Science Reviews*, *136*, 339–349. https://doi.org/10.1016/j.earscirev.2014.06.002

Edie, S. M., Jablonski, D., & Valentine, J. W. (2018). Contrasting responses of functional diversity to major losses in taxonomic diversity. *Proceedings of the National Academy of Sciences*, *115*(4), 732–737. https://doi.org/10.1073/pnas.1717636115

Eriksson, O. (2016). Evolution of angiosperm seed disperser mutualisms: The timing of origins and their consequences for coevolutionary interactions between angiosperms and frugivores. *Biological Reviews*, *91*(1), 168–186. https://doi.org/10.1111/brv.12164

Erwin, D. (2001). Lessons from the past: Biotic recoveries from mass extinctions. *Proceedings of the National Academy of Sciences of the United States of America*, *98*, 5399–5403. https://doi.org/10.1073/pnas.091092698

Erwin, D. H. (1993). *The Great Paleozoic Crisis: Life and Death in the Permian*. Columbia University Press.

Erwin, D. H. (1998). The end and the beginning: Recoveries from mass extinctions. *Trends in Ecology & Evolution*, *13*(9), 344–349. https://doi.org/10.1016/S0169-5347(98)01436-0

Erwin, D. H. (2007). Disparity: Morphological Pattern and Developmental Context. *Palaeontology*, *50*(1), 57–73. https://doi.org/10.1111/j.1475-4983.2006.00614.x

Erwin, D. H. (2008). Macroevolution of ecosystem engineering, niche construction and diversity. *Trends in Ecology & Evolution*, *23*(6), 304–310. https://doi.org/10.1016/j.tree.2008.01.013

Evans, A. R., Wilson, G. P., Fortelius, M., & Jernvall, J. (2007). High-level similarity of dentitions in carnivorans and rodents. *Nature*, *445*(7123), 78–81. https://doi.org/10.1038/nature05433

Ezcurra, M. D., & Butler, R. J. (2018). The rise of the ruling reptiles and ecosystem recovery from the Permo-Triassic mass extinction. *Proceedings of the Royal Society B: Biological Sciences*, *285*(1880), 20180361. https://doi.org/10.1098/rspb.2018.0361

Fara, E. (2000). Diversity of Callovian-Ypresian(Middle Jurassic-Eocene) tetrapod families and selectivity of extinctions at the K/T boundary. *Geobios*, *33*(3), 387–396. https://doi.org/10.1016/S0016-6995(00)80166-7

Fonseca, C. R., & Ganade, G. (2001). Species Functional Redundancy, Random Extinctions and the Stability of Ecosystems. *Journal of Ecology*, *89*(1), 118–125.

Foote, M. (1993). Discordance and concordance between morphological and taxonomic diversity. *Paleobiology*, *19*(2), 185–204. https://doi.org/10.1017/S0094837300015864

Foote, M. (1994). Morphological Disparity in Ordovician-Devonian Crinoids and the Early Saturation of Morphological Space. *Paleobiology*, *20*(3), 320–344.

Foote, M. (1997). The Evolution of Morphological Diversity. *Annual Review of Ecology and Systematics*, *28*(1), 129–152. https://doi.org/10.1146/annurev.ecolsys.28.1.129

Foote, M. (1999). Morphological diversity in the evolutionary radiation of Paleozoic and post-Paleozoic crinoids. *Paleobiology*, *25*(sp1), 1–116. https://doi.org/10.1666/0094-8373(1999)25[1:MDITER]2.0.CO;2

Foote, M., Gould, S. J., Lee, M. S. Y., Briggs, D. E. G., Fortey, R. A., & Wills, M. A. (1992). Cambrian and Recent Morphological Disparity. *Science*, *258*(5089), 1816–1818.

Fortelius, M. (1990). Problems with using fossil teeth to estimate body sizes of extinct mammals. *Body Size in Mammalian Paleobiology Estimation and Biological Implications.*, 207–228.

Fraser, D., & Lyons, S. K. (2020). Mammal Community Structure through the Paleocene-Eocene Thermal Maximum. *The American Naturalist*, *196*(3), 271–290. https://doi.org/10.1086/709819

Fraser, D., Soul, L. C., Tóth, A. B., Balk, M. A., Eronen, J. T., Pineda-Munoz, S., Shupinski, A. B., Villaseñor, A., Barr, W. A., Behrensmeyer, A. K., Du, A., Faith, J. T., Gotelli, N. J., Graves, G. R., Jukar, A. M., Looy, C. V., Miller, J. H., Potts, R., & Lyons, S. K. (2021). Investigating Biotic Interactions in Deep Time. *Trends in Ecology & Evolution*, *36*(1), 61–75. https://doi.org/10.1016/j.tree.2020.09.001

Gilbert, C. C. (2005). Dietary ecospace and the diversity of euprimates during the Early and Middle Eocene. *American Journal of Physical Anthropology*, *126*(3), 237–249. https://doi.org/10.1002/ajpa.20036

Grossnickle, D. M., & Newham, E. (2016). Therian mammals experience an ecomorphological radiation during the Late Cretaceous and selective extinction at the K–Pg boundary. *Proceedings of the Royal Society B: Biological Sciences*, *283*(1832), 20160256. https://doi.org/10.1098/rspb.2016.0256

Grossnickle, D. M., & Polly, P. D. (2013). Mammal disparity decreases during the Cretaceous angiosperm radiation. *Proceedings of the Royal Society B: Biological Sciences*, *280*(1771), 20132110. https://doi.org/10.1098/rspb.2013.2110

Grossnickle, D. M., Smith, S. M., & Wilson, G. P. (2019). Untangling the Multiple Ecological Radiations of Early Mammals. *Trends in Ecology & Evolution*, *34*(10), 936–949. https://doi.org/10.1016/j.tree.2019.05.008

Harries, P. J., & Kauffman, E. G. (1990). Patterns of survival and recovery following the Cenomanian-Turonian (Late Cretaceous) mass extinction in the Western Interior Basin, United States. In E. G. Kauffman & O. H. Walliser (Eds.), *Extinction Events in Earth History* (pp. 277–298). Springer. https://doi.org/10.1007/BFb0011152

Harris, J. (1993). Ecosystem structure and growth of the African savanna. *Global and Planetary Change*, *8*(4), 231–248. https://doi.org/10.1016/0921-8181(93)90011-C

Hartman, J., Butler, R., Weiler, M., & Schumaker, K. (2014). Context, naming, and formal designation of the Cretaceous Hell Creek Formation lectostratotype, Garfield County, Montana. *Special Paper of the Geological Society of America*, *503*, 89–121. https://doi.org/10.1130/2014.2503(02)

Hovatter, B. T., & Wilson, G. P. (2015). Faunal analysis of earliest Torrejonian (To1) mammals from northeastern Montana, USA. *Journal of Vertebrate Paleontology, Programs and Abstracts, 75th Annual Meeting of the Society of Vertebrate Paleontology, Dallas, TX*, 14–17.

Hull, P. (2015). Life in the Aftermath of Mass Extinctions. *Current Biology*, *25*(19), R941–R952. https://doi.org/10.1016/j.cub.2015.08.053

Ickert, R. B., Mulcahy, S. R., Sprain, C. J., Banaszak, J. F., & Renne, P. R. (2015). Chemical and Pb isotope composition of phenocrysts from bentonites constrains the chronostratigraphy around the Cretaceous-Paleogene boundary in the Hell Creek region, Montana: CHEMISTRY OF BENTONITES AT HELL CREEK. *Geochemistry, Geophysics, Geosystems*, *16*(8), 2743–2761. https://doi.org/10.1002/2015GC005898

Kauffman, E. G., & Harries, P. J. (1996). The importance of crisis progenitors in recovery from mass extinction. *Geological Society, London, Special Publications*, *102*(1), 15–39. https://doi.org/10.1144/GSL.SP.1996.001.01.02

Kelly, T. S. (2014). Preliminary report on the mammals from Lane's Little Jaw site quarry: a latest Cretaceous (earliest Puercan?) Local fauna, Hell Creek Formation, southeastern Montana. *Paludicola*, *10*(1), 50–91.

Kirchner, J. W., & Weil, A. (2000). Delayed biological recovery from extinctions throughout the fossil record. *Nature*, *404*(6774), 177–180. https://doi.org/10.1038/35004564

Krause, D. W. (1986). Competitive exclusion and taxonomic displacement in the fossil record; the case of rodents and multituberculates in North America. *Rocky Mountain Geology*, *24*(special_paper_3), 95–117. https://doi.org/10.2113/gsrocky.24.special_paper_3.95

LeCain, R., Clyde, W., Wilson Mantilla, G., & Riedel, J. (2014). Magnetostratigraphy of the Hell Creek and lower Fort Union Formations in northeastern Montana. *Special Paper of the Geological Society of America*, *503*, 137–147. https://doi.org/10.1130/2014.2503(04)

Lillegraven, J. A., & Eberle, J. J. (1999). Vertebrate faunal changes through Lancian and Puercan time in southern Wyoming. *Journal of Paleontology*, *73*(4), 691–710. https://doi.org/10.1017/S0022336000032510

Lofgren, D. L. (1995). *The Bug Creek Problem and the Cretaceous-Tertiary Transition at McGuire Creek, Montana*. University of California Press.

Louys, J., Meloro, C., Elton, S., Ditchfield, P., & Bishop, L. C. (2015). Analytical framework for reconstructing heterogeneous environmental variables from mammal community structure. *Journal of Human Evolution*, *78*, 1–11. https://doi.org/10.1016/j.jhevol.2014.11.001

Lowery, C. M., & Fraass, A. J. (2019). Morphospace expansion paces taxonomic diversification after end Cretaceous mass extinction. *Nature Ecology & Evolution*, *3*(6), 900–904. https://doi.org/10.1038/s41559-019-0835-0

Lyson, T. R., Miller, I. M., Bercovici, A. D., Weissenburger, K., Fuentes, A. J., Clyde, W. C., Hagadorn, J. W., Butrim, M. J., Johnson, K. R., Fleming, R. F., Barclay, R. S., Maccracken, S. A., Lloyd, B., Wilson, G. P., Krause, D. W., & Chester, S. G. B. (2019). Exceptional continental record of biotic recovery after the Cretaceous–Paleogene mass extinction. *Science*, *366*(6468), 977–983. https://doi.org/10.1126/science.aay2268

Magallón, S., Gómez-Acevedo, S., Sánchez-Reyes, L. L., & Hernández-Hernández, T. (2015). A metacalibrated time-tree documents the early rise of flowering plant phylogenetic diversity. *New Phytologist*, *207*(2), 437–453. https://doi.org/10.1111/nph.13264

Magallón, S., Hilu, K. W., & Quandt, D. (2013). Land plant evolutionary timeline: Gene effects are secondary to fossil constraints in relaxed clock estimation of age and substitution rates. *American Journal of Botany*, *100*(3), 556–573. https://doi.org/10.3732/ajb.1200416

Middleton, M. D. (1983). *Early Paleocene Vertebrates of the Denver Basin, Colorado* [Ph.D., University of Colorado at Boulder]. https://www.proquest.com/docview/303134256/abstract/56608BA2E973479FPQ/1

Middleton, M. D., & Dewar, E. W. (2004). New mammals mrom the early Paleocene Littleton Fauna (Denver Formation, Colorado). *New Mexico Museum of Natural History and Science Bulletin*, *26*.

Moore, J. R., Wilson, G. P., Sharma, M., Hallock, H. R., Braman, D. R., Renne, P. R., Clemens, W. A., Horner, J. R., & Hartman, J. H. (2014). Assessing the relationships of the Hell Creek–Fort Union contact, Cretaceous-Paleogene boundary, and Chicxulub impact ejecta horizon at the Hell Creek Formation lectostratotype. *Montana, USA, in Wilson, GP, Clemens, WA, Horner, JR, and Hartman, JH, Eds., Through the End of the Cretaceous in the Type Locality of the Hell Creek Formation in Montana and Adjacent Areas: Geological Society of America Special Paper*, *503*, 123–135.

Mouillot, D., Graham, N. A. J., Villéger, S., Mason, N. W. H., & Bellwood, D. R. (2013). A functional approach reveals community responses to disturbances. *Trends in Ecology & Evolution*, *28*(3), 167–177. https://doi.org/10.1016/j.tree.2012.10.004

Niklas, K. J., Tiffney, B. H., & Knoll, A. H. (1983). Patterns in vascular land plant diversification. *Nature*, *303*(5918), Article 5918. https://doi.org/10.1038/303614a0

Oliveira, B. F., Machac, A., Costa, G. C., Brooks, T. M., Davidson, A. D., Rondinini, C., & Graham, C. H. (2016). Species and functional diversity accumulate differently in mammals. *Global Ecology and Biogeography*, *25*(9), 1119–1130. https://doi.org/10.1111/geb.12471

Palumbi, S. R., McLeod, K. L., & Grünbaum, D. (2008). Ecosystems in Action: Lessons from Marine Ecology about Recovery, Resistance, and Reversibility. *BioScience*, *58*(1), 33–42. https://doi.org/10.1641/B580108

Payne, J. L., Summers, M., Rego, B. L., Altiner, D., Wei, J., Yu, M., & Lehrmann, D. J. (2011). Early and Middle Triassic trends in diversity, evenness, and size of foraminifers on a carbonate platform in south China: Implications for tempo and mode of biotic recovery from the end-Permian mass extinction. *Paleobiology*, *37*(3), 409–425. https://doi.org/10.1666/08082.1

Renne, P. R., Deino, A. L., Hilgen, F. J., Kuiper, K. F., Mark, D. F., Mitchell, W. S., Morgan, L. E., Mundil, R., & Smit, J. (2013). Time Scales of Critical Events Around the Cretaceous-Paleogene Boundary. *Science*, *339*(6120), 684–687. https://doi.org/10.1126/science.1230492

Rivals, F., & Semprebon, G. M. (2011). Dietary plasticity in ungulates: Insight from tooth microwear analysis. *Quaternary International*, *245*(2), 279–284. https://doi.org/10.1016/j.quaint.2010.08.001

Rosenfeld, J. S. (2002). Functional redundancy in ecology and conservation. *Oikos*, *98*(1), 156–162. https://doi.org/10.1034/j.1600-0706.2002.980116.x

Ruta, M., Angielczyk, K. D., Fröbisch, J., & Benton, M. J. (2013). Decoupling of morphological disparity and taxic diversity during the adaptive radiation of anomodont therapsids.

Proceedings of the Royal Society B: Biological Sciences, *280*(1768), 20131071. https://doi.org/10.1098/rspb.2013.1071

Sahney, S., & Benton, M. J. (2008). Recovery from the most profound mass extinction of all time. *Proceedings of the Royal Society B: Biological Sciences*, *275*(1636), 759–765. https://doi.org/10.1098/rspb.2007.1370

Schindler, E. (1990). The late Frasnian (Upper Devonian) Kellwasser Crisis. In E. G. Kauffman & O. H. Walliser (Eds.), *Extinction Events in Earth History* (pp. 151–159). Springer. https://doi.org/10.1007/BFb0011143

Schoene, B., Eddy, M. P., Keller, C. B., & Samperton, K. M. (2021). An evaluation of Deccan Traps eruption rates using geochronologic data. *Geochronology*, *3*(1), 181–198. https://doi.org/10.5194/gchron-3-181-2021

Schoene, B., Eddy, M. P., Samperton, K. M., Keller, C. B., Keller, G., Adatte, T., & Khadri, S. F. R. (2019). U-Pb constraints on pulsed eruption of the Deccan Traps across the end-Cretaceous mass extinction. *Science*, *363*(6429), 862–866. https://doi.org/10.1126/science.aau2422

Schubert, J. K., & Bottjer, D. J. (1992). Early Triassic stromatolites as post-mass extinction disaster forms. *Geology*, *20*(10), 883–886. https://doi.org/10.1130/0091-7613(1992)020<0883:ETSAPM>2.3.CO;2

Scott, R. S., Ungar, P. S., Bergstrom, T. S., Brown, C. A., Childs, B. E., Teaford, M. F., & Walker, A. (2006). Dental microwear texture analysis: Technical considerations. *Journal of Human Evolution*, *51*(4), 339–349. https://doi.org/10.1016/j.jhevol.2006.04.006

Silcox, M. T., & Williamson, T. E. (2012). New discoveries of early Paleocene (Torrejonian) primates from the Nacimiento Formation, San Juan Basin, New Mexico. *Journal of Human Evolution*, *63*(6), 805–833. https://doi.org/10.1016/j.jhevol.2012.09.002

Simpson, E. H. (1949). Measurement of Diversity. *Nature*, *163*(4148), Article 4148. https://doi.org/10.1038/163688a0

Simpson, G. G. (1937). The Beginning of the Age of Mammals. *Biological Reviews*, *12*(1), 1–46. https://doi.org/10.1111/j.1469-185X.1937.tb01220.x

Smith, S. M. (2017). *Mammalian faunal recovery following the Cretaceous-Paleogene mass extinction: A multifaceted investigation* [Thesis]. https://digital.lib.washington.edu:443/researchworks/handle/1773/40850

Smith, S. M., Sprain, C. J., Clemens, W. A., Lofgren, D. L., Renne, P. R., & Wilson, G. P. (2018). Early mammalian recovery after the end-Cretaceous mass extinction: A high-resolution view from McGuire Creek area, Montana, USA. *GSA Bulletin*, *130*, 2000–2014. https://doi.org/10.1130/B31926.1

Smits, P. D., & Wilson, G. P. (2011). *Estimates and trends in body size of Laurasian Cretaceous mammals.* 13th conference on Australasian Vertebrate Evolution Paleontology and Systematics, Perth.

Song, H., Wignall, P. B., & Dunhill, A. M. (2018). Decoupled taxonomic and ecological recoveries from the Permo-Triassic extinction. *Science Advances*, *4*(10), eaat5091. https://doi.org/10.1126/sciadv.aat5091

Sprain, C. J., Renne, P. R., Clemens, W. A., & Wilson, G. P. (2018). Calibration of chron C29r: New high-precision geochronologic and paleomagnetic constraints from the Hell Creek region, Montana. *GSA Bulletin*, *130*(9–10), 1615–1644. https://doi.org/10.1130/B31890.1

Sprain, C. J., Renne, P. R., Wilson, G. P., & Clemens, W. A. (2015). High-resolution chronostratigraphy of the terrestrial Cretaceous-Paleogene transition and recovery interval in the Hell Creek region, Montana. *Geological Society of America Bulletin*, *127*(3–4), 393–409. https://doi.org/10.1130/B31076.1

Swisher III, C. C., Dingus, L., & Butler, R. F. (1993). 40Ar/39Ar dating and magnetostratigraphic correlation of the terrestrial Cretaceous–Paleogene boundary and Puercan Mammal Age, Hell Creek – Tullock formations, eastern Montana. *Canadian Journal of Earth Sciences*, *30*(9), 1981–1996. https://doi.org/10.1139/e93-174

Van Valen, L., & Sloan, R. E. (1966). The Extinction of the Multituberculates. *Systematic Zoology*, *15*(4), 261–278. https://doi.org/10.2307/2411985

Wagner, P. J. (2010). Paleontological perspectives on morphological evolution. *Evolution since Darwin: The First 150 Years*.

Walker, B. H. (1992). Biodiversity and Ecological Redundancy. *Conservation Biology*, *6*(1), 18–23.

Weaver, L. N., Tobin, T. S., Claytor, J. R., Wilson Deibel, P. K., Clemens, W. A., & Wilson Mantilla, G. P. (2022). Revised Stratigraphic Relationships Within the Lower Fort Union Formation (Tullock Member, Garfield County, Montana, U.S.A.) Prodive a New Framework for Examining Post-KPG Mammalian Recovery Dynamics. *PALAIOS*, *37*(4), 104–127. https://doi.org/10.2110/palo.2021.011

Wilf, P., & Johnson, K. R. (2004). Land plant extinction at the end of the Cretaceous: A quantitative analysis of the North Dakota megafloral record. *Paleobiology*, *30*(3), 347–368. https://doi.org/10.1666/0094-8373(2004)030<0347:LPEATE>2.0.CO;2

Wilson Deibel, P. (2022). *Vegetation and Environmental Changes Across the Cretaceous-Paleogene (K-Pg) Boundary in Northeastern Montana* [Thesis]. https://digital.lib.washington.edu:443/researchworks/handle/1773/48392

Wilson, G. P. (2005). Mammalian Faunal Dynamics During the Last 1.8 Million Years of the Cretaceous in Garfield County, Montana. *Journal of Mammalian Evolution*, *12*(1–2), 53–76. https://doi.org/10.1007/s10914-005-6943-4

Wilson, G. P. (2013). Mammals across the K/Pg boundary in northeastern Montana, U.S.A.: Dental morphology and body-size patterns reveal extinction selectivity and immigrant-fueled ecospace filling. *Paleobiology*, *39*(3), 429–469. https://doi.org/10.1666/12041

Wilson, G. P. (2014). Mammalian extinction, survival, and recovery dynamics across the Cretaceous-Paleogene boundary in northeastern Montana, USA. In G. P. Wilson, W. A. Clemens, J. R. Horner, & J. H. Hartman, *Through the End of the Cretaceous in the Type Locality of the Hell Creek Formation in Montana and Adjacent Areas*. Geological Society of America. https://doi.org/10.1130/2014.2503(15)

Wilson, G. P., Evans, A. R., Corfe, I. J., Smits, P. D., Fortelius, M., & Jernvall, J. (2012). Adaptive radiation of multituberculate mammals before the extinction of dinosaurs. *Nature*, *483*(7390), 457–460. https://doi.org/10.1038/nature10880

Wilson Mantilla, G. P., Chester, S. G. B., Clemens, W. A., Moore, J. R., Sprain, C. J., Hovatter, B. T., Mitchell, W. S., Mans, W. W., Mundil, R., & Renne, P. R. (2021). Earliest Palaeocene purgatoriids and the initial radiation of stem primates. *Royal Society Open Science*, *8*(2), rsos.210050, 210050. https://doi.org/10.1098/rsos.210050

Wing, S. L., & Boucher, L. D. (1998). Ecological aspects of the Cretaceous flowering plant radiation. *Annual Review of Earth and Planetary Sciences*, *26*(1), 379–421. https://doi.org/10.1146/annurev.earth.26.1.379

Wright, D. F. (2017). Phenotypic Innovation and Adaptive Constraints in the Evolutionary Radiation of Palaeozoic Crinoids. *Scientific Reports*, *7*(1), Article 1. https://doi.org/10.1038/s41598-017-13979-9

3.7 FIGURES

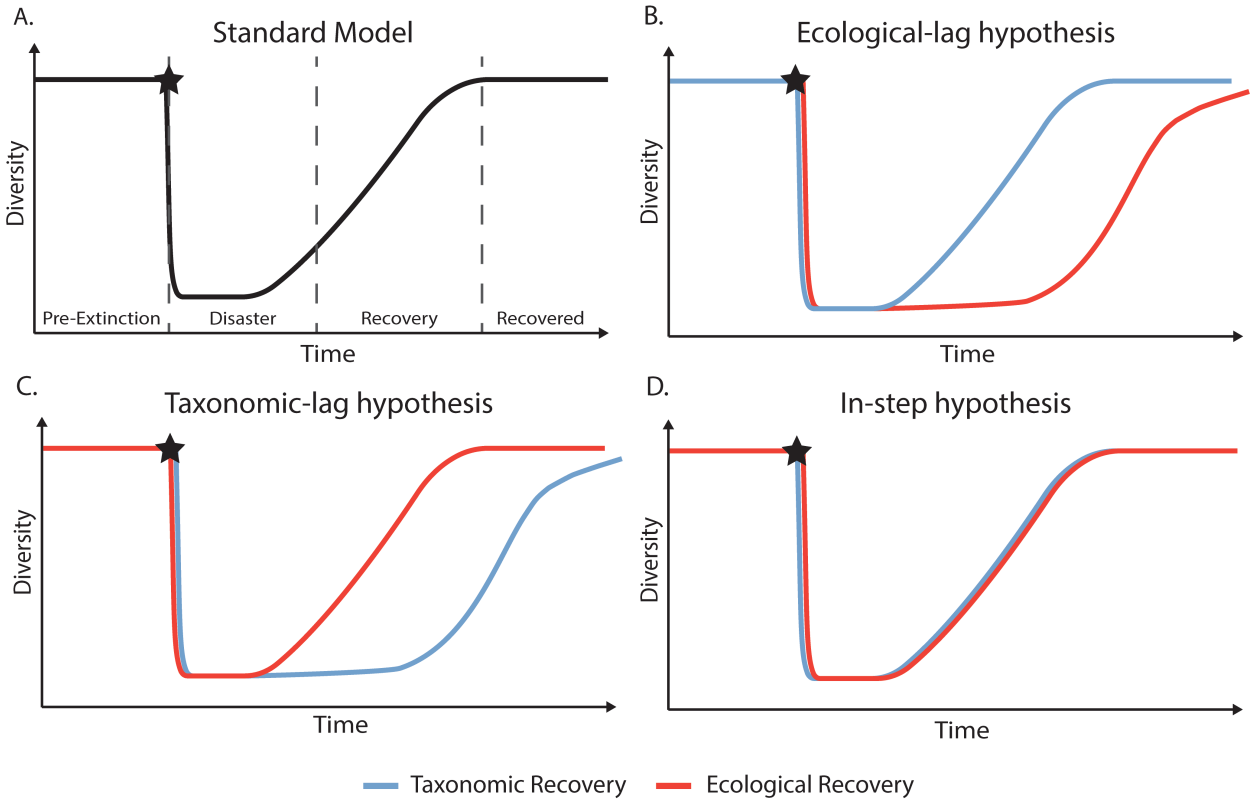

Figure 3.1 A. A generalized schematic of the three-phase model of biotic recovery modified from Erwin (2001). The black line represents the recovery curve based on a diversity metric (e.g., taxonomic richness) and how it changes through the recovery process. **B.** In Hypothesis 1 (Ecological-lag hypothesis), taxonomic recovery (blue) progresses faster than ecological recovery (red). **C.** In Hypothesis 2 (Taxonomic-lag hypothesis), ecological recovery progresses faster than taxonomic recovery. **D.** In Hypothesis 3 (In-step hypothesis), taxonomic and ecological recovery progress concurrently. The black star represents the onset of the extinction event.

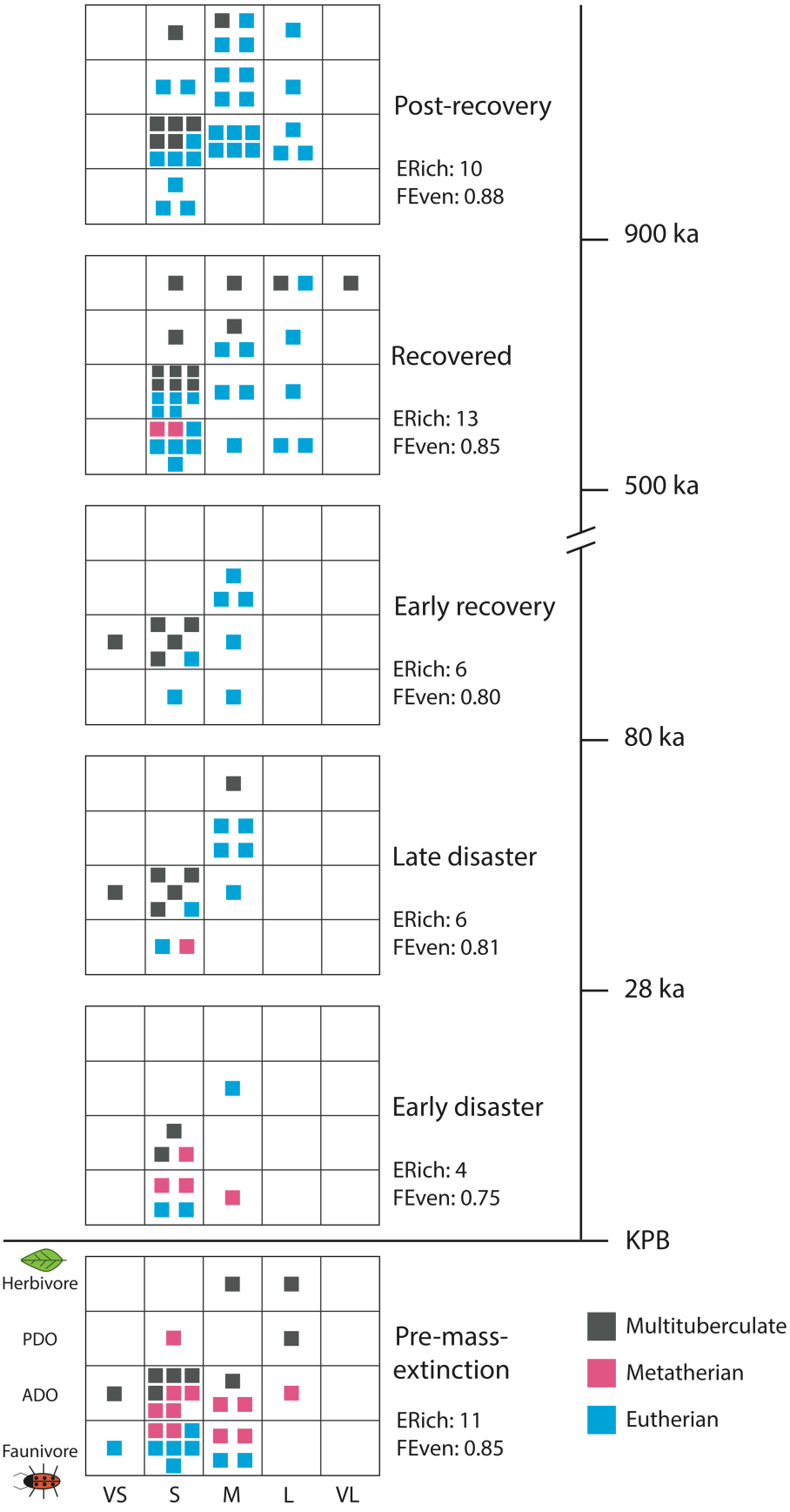
Post-recovery
ERich: 10
FEven: 0.88
900 ka
Recovered
ERich: 13
FEven: 0.85
500 ka
Early recovery
ERich: 6
FEven: 0.80
80 ka
Late disaster
ERich: 6
FEven: 0.81
28 ka
Early disaster
ERich: 4
FEven: 0.75
KPB
Herbivore
PDO
ADO
Faunivore
Pre-mass-extinction
ERich: 11
FEven: 0.85
VS
S
M
L
VL
Multituberculate
Metatherian
Eutherian

Figure 3.2 Ecological occupation of mammalian communities across the K-Pg boundary and through the first 1 Ma of the Paleocene in the Hell Creek region. Sub-phases/phases and their ages are according to Claytor et al. (In Review). Note that the listed ages represent the depositional age of the constituent localities and may differ from the age of the corresponding fossil assemblages. Each marker color represents a major clade of mammals present in the Hell Creek region during our study interval. Each square marker represents each taxon, primarily different species or genera, present in each sub-phase or phase. PDO—Plant-dominated omnivore; ADO—Animal-dominated omnivore; VS—Very Small, S—Small; M—Medium; L—Large; VL—Very Large.

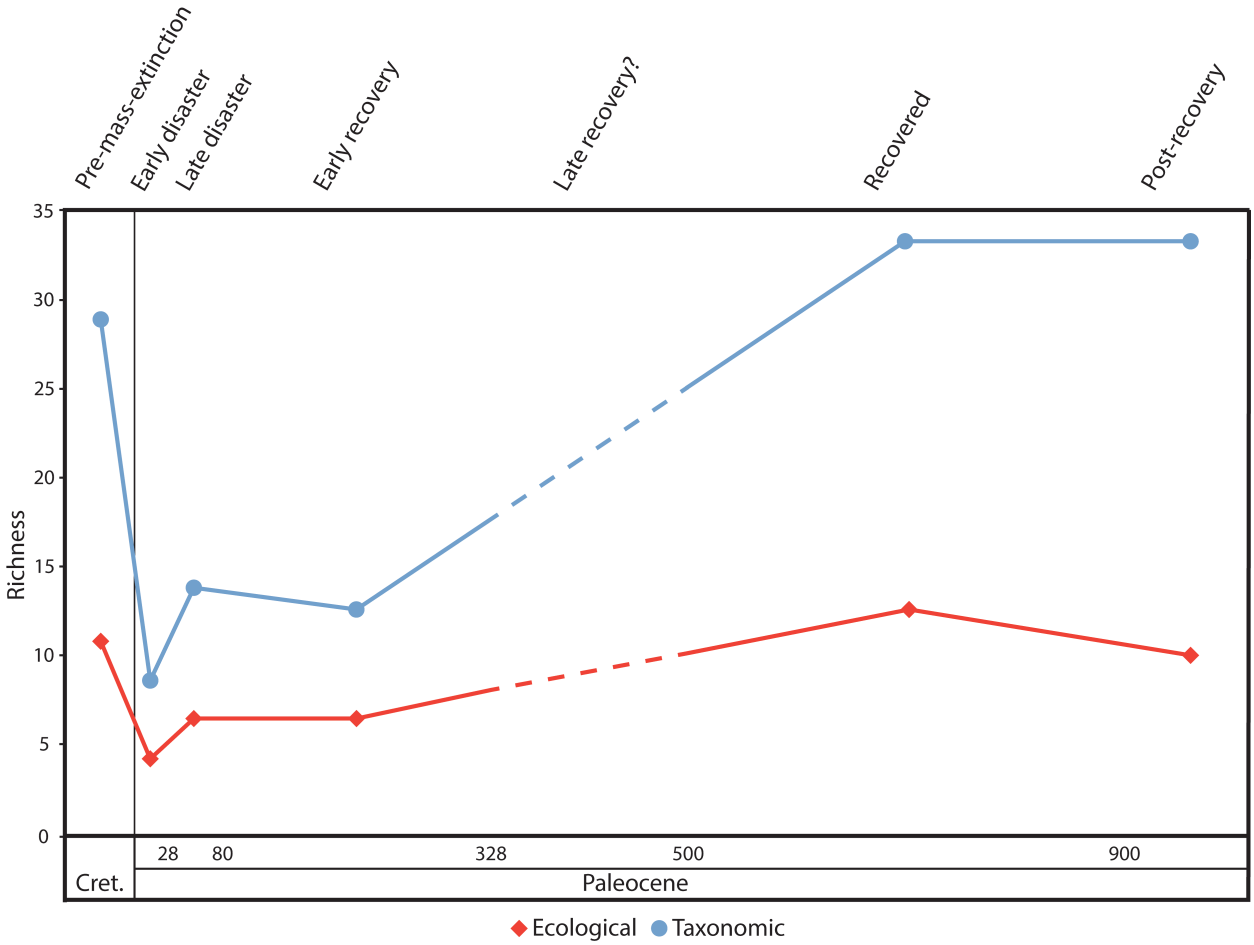

Figure 3.3 Taxonomic (blue) and ecological richness (red) of mammalian communities across the K-Pg boundary and through the first 1 Ma of the Paleocene in the Hell Creek region. Sub-phases/phases and their ages in thousands of years, represented by the numbers below, are according to Claytor et al. (In Review). Note that the represent the depositional age of the constituent localities and may differ from the age of the corresponding fossil assemblages. The dashed line for the Late recovery sub-phase indicates the lack of a representative local fauna from the Hell Creek region. Cret.—Cretaceous

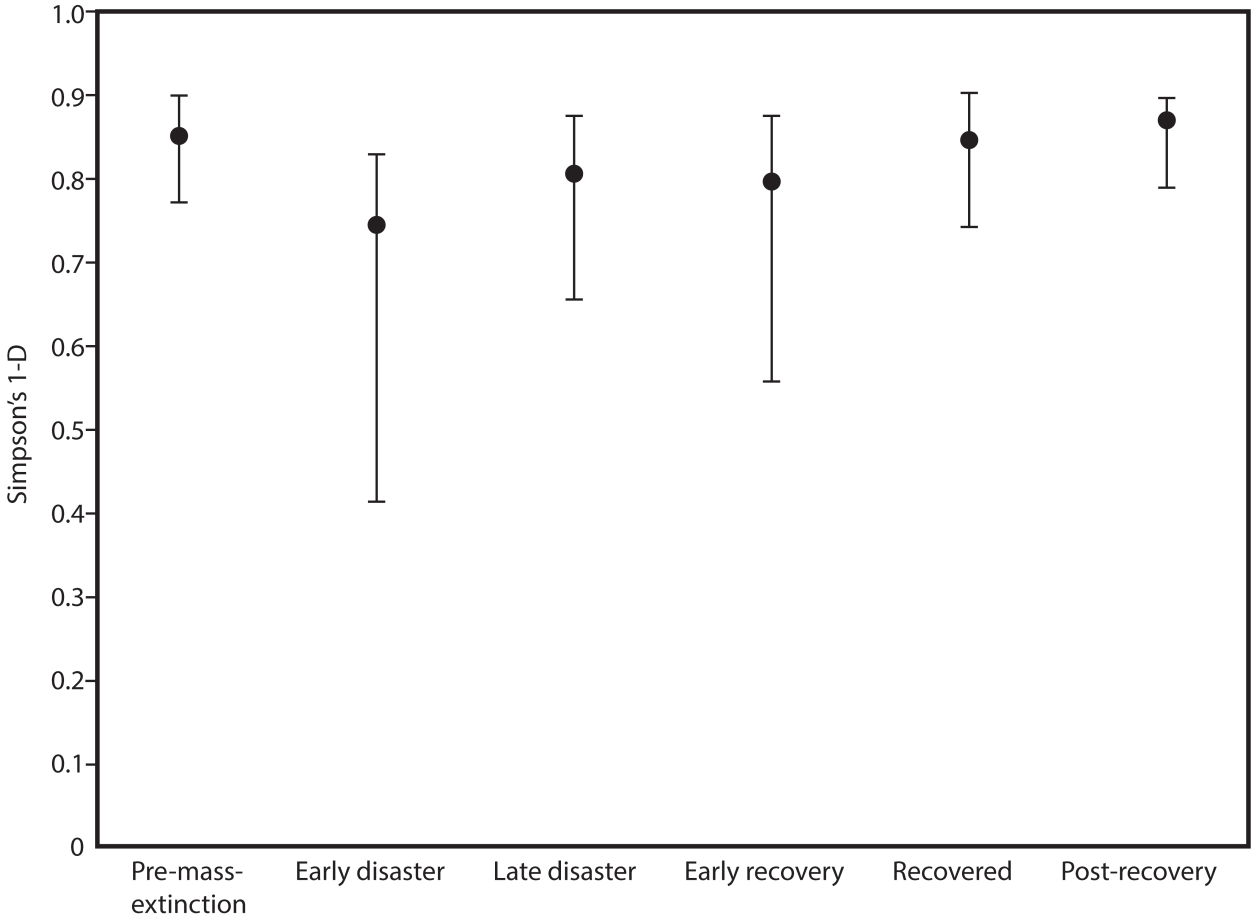

Figure 3.4 Functional evenness (FEven) and 95% confidence intervals of mammalian communities across the K-Pg boundary and through the first 1 Ma of the Paleocene in the Hell Creek region. Sub-phases/phases and their sequence are according to Claytor et al. (In Review).

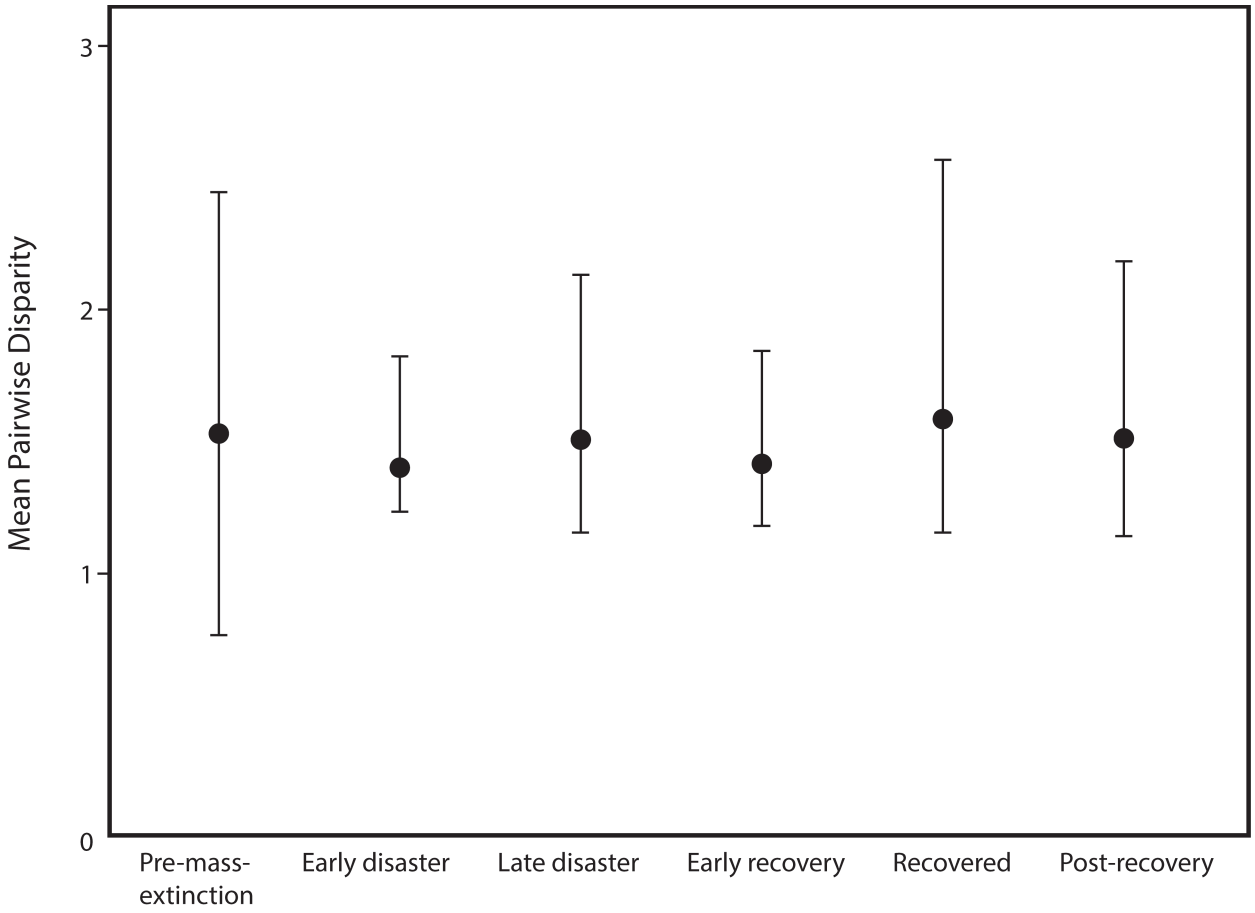

Figure 3.5 Mean pairwise ecological disparity (EDisp) and 95% confidence interval of mammalian communities across the K-Pg boundary and through the first 1 Ma of the Paleocene in the Hell Creek region. Sub-phases/phases and their sequence are according to Claytor et al. (In Review).

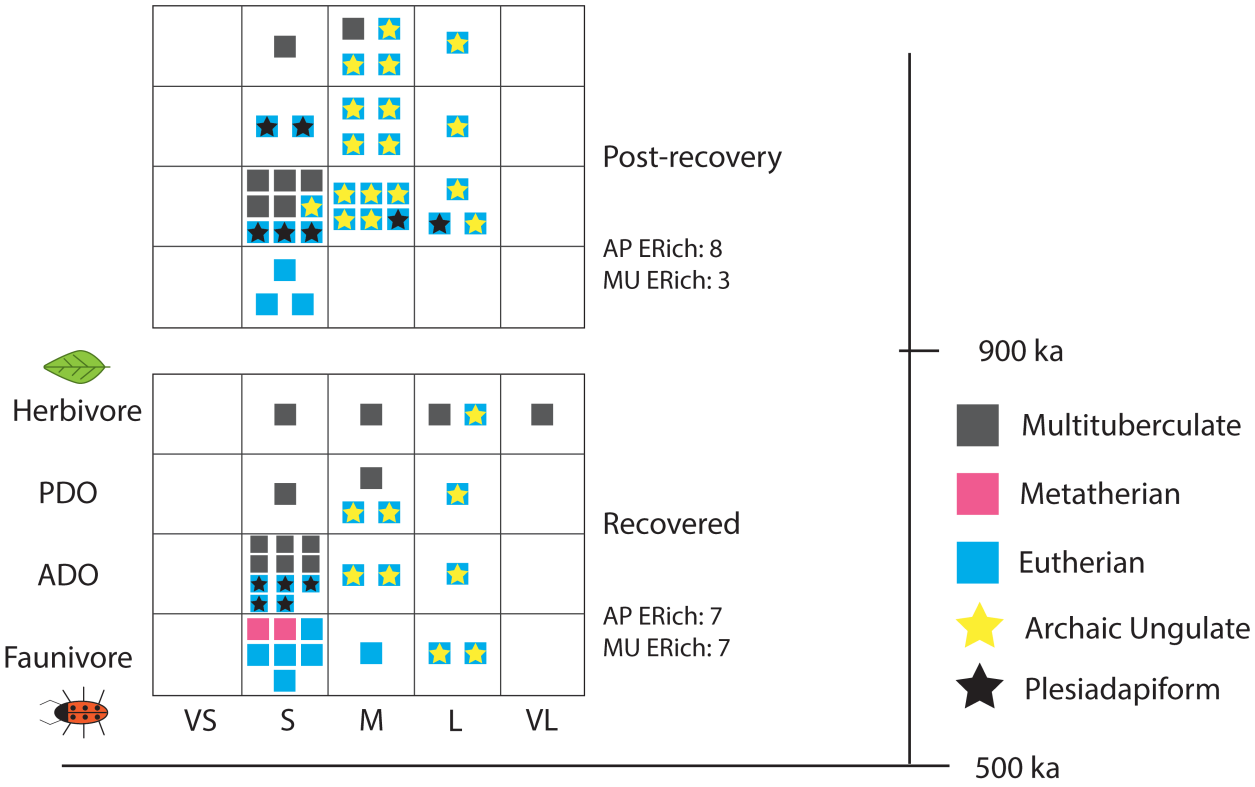

Figure 3.6 Ecological occupation of mammalian communities during the Recovered and Post-Recovery phases. Phases and their ages are according to Claytor et al. (In Review). Note that the listed ages represent the depositional age of the constituent localities and may differ from the age of the corresponding fossil assemblages. Each marker color represents a major clade of mammals present in the Hell Creek region during our study interval. Each square marker represents each taxon, primarily different species or genera, present in each phase. Yellow stats represent archaic ungulates, black stars represent plesiadapiform primates. AP ERich—Archaic ungulate and plesiadapiform primate ecological richness; MU—Multituberculate ecological richness; PDO—Plant-dominated omnivore; ADO—Animal-dominated omnivore; VS—Very Small, S—Small; M—Medium; L—Large; VL—Very Large.

3.8 TABLES

Table 3.1 Body size categories and the corresponding range of body masses in both natural log grams (ln g) and grams (g).

Size Category	Body Mass estimate (ln g)	Body Mass estimate (g)
Very Small	1.00–3.00	2.72–20.09
Small	3.01–5.00	20.29–148.41
Medium	5.01–7.00	149.90–1096.63
Large	7.01–9.00	1107.65–8103.08
Very Large	> 9.00	> 8184.52

Table 3.2 Summary table of estimated body masses, dietary category, and EcoCell for the pre-extinction subphase fauna. All body mass estimated were compiled from Wilson et al. (2013)

Taxa	Body Mass (ln g)	Size Category	Dietary Category	Dietary Justification	EcoCell
Cimolodon nitidus	5.19	Medium	Animal-Dominated Omnivore	Wilson et al. (2012)	M:ADO
Cimolomys gracilis	5.66	Medium	Herbivore	Wilson et al. (2012)	M:H
Meniscoessus robustus	7.10	Large	Plant-Dominated Omnivore	Wilson et al. (2012)	L:PDO
Essonodon browni	7.21	Large	Herbivore	Wilson et al. (2012)	L:H
Paracimexomys priscus	4.25	Small	Animal-Dominated Omnivore	Wilson et al. (2012)	S:ADO
Mesodma hensleighi	2.86	Very Small	Animal-Dominated Omnivore	Wilson et al. (2012)	VS:ADO
Mesodma formosa	3.55	Small	Animal-Dominated Omnivore	Wilson et al. (2012)	S:ADO
Mesodma thompsoni	3.98	Small	Animal-Dominated Omnivore	Wilson et al. (2012)	S:ADO
Cimexomys minor	3.93	Small	Animal-Dominated Omnivore	Wilson et al. (2012)	S:ADO
Nanocuris improvida	6.26	Medium	Faunivore	Wilson and Riedel (2010)	M:F
Didelphodon vorax	7.45	Large	Animal-Dominated Omnivore	Smith (2017)	L:ADO
Pediomys elegans	3.94	Small	Animal-Dominated Omnivore	Smith (2017)	S:ADO
?Leptalestes cooki	4.39	Small	Animal-Dominated Omnivore	Smith (2017)	S:ADO
Leptalestes krejcii	3.13	Small	Faunivore	Smith (2017)	S:F
Protolambda hatcheri	5.46	Medium	Animal-Dominated Omnivore	Smith (2017)	M:ADO
Protolambda florencae	5.80	Medium	Animal-Dominated Omnivore	Smith (2017)	M:ADO
Protalphadon foxi	3.42	Small	Faunivore	Smith (2017)	S:F
Turgidodon rhaister	5.82	Medium	Faunivore	Smith (2017)	M:F
Alphadon marshi	4.47	Small	Faunivore	Smith (2017)	S:F
Nortedelphys jasoni	3.99	Small	Faunivore	Smith (2017)	S:F
Glasbius twitchelli	3.98	Small	Plant-Dominated Omnivore	Smith (2017)	S:PDO
Gypsonictops hypoconus	3.48	Small	Animal-Dominated Omnivore	Smith (2017)	S:ADO
Gypsonictops illuminatus	4.12	Small	Animal-Dominated Omnivore	Smith (2017)	S:ADO
Cimolestes stirtoni	5.74	Medium	Faunivore	Smith (2017)	M:F
Altacreodus magnus	6.34	Medium	Faunivore	Smith (2017)	M:F
Ambilestes cerberoides	4.84	Small	Faunivore	Based on similar morphology with *Cimolestes stirtoni*	S:F
Scollardius propalaeorcytes	3.89	Small	Faunivore	Smith (2017)	S:F

Cimolestes incisus	4.89	Small	Faunivore	Based on similar morphology with *Cimolestes stirtoni*	S:F
Batodon tenuis	1.55	Very Small	Faunivore	Based on similar morphology with other cimolestids	VS:F

Table 3.3 Summary table of estimated body masses, dietary category, and EcoCell for the early disaster subphase fauna.

Taxa	Body Mass (ln g)	Body Mass Citation	Size Category	Dietary Category	Dietary Justification	EcoCell
Mesodma formosa	3.55	Wilson et al. (2013)	Small	Animal-Dominated Omnivore	Wilson et al. (2012)	S:ADO
Mesodma thompsoni	3.98	Wilson et al. (2013)	Small	Animal-Dominated Omnivore	Wilson et al. (2012)	S:ADO
Thylacodon montanensis	3.93	Wilson et al. (2013)	Small	Animal-Dominated Omnivore	Wilson (2013,14)	S:ADO
?Leptalestes cooki	4.39	Wilson et al. (2013)	Small	Faunivore	Smith (2017)	S:F
Alphadontidae indet.	3.87	Smith (2017)	Small	Faunivore	Based on similar morphology with *Nortedelphys* sp. Smith (2017)	S:F
Metatheria indet.	6.34	Smith (2017)	Medium	Faunivore	Based on similar morphology to Lancian metatherians. Smith (2017)	M:F
Procerberus formicarum	4.34	Wilson et al. (2013)	Small	Faunivore	Smith (2017)	S:F
?Ambilestes cerberoides	4.84	Lillegraven (1969)	Small	Faunivore	Based on similar morphology with *Cimolestes stirtoni*	S:F
Mimatuta sp.	5.77	Wilson et al. (2013)	Medium	Plant Dominated Omnivore	Smith (2017)	M:PDO

Table 3.4 Summary table of estimated body masses, dietary category, and EcoCell for the late disaster subphase fauna. All body mass estimated were compiled from Wilson et al. (2013)

Taxa	Body Mass (ln g)	Size Category	Dietary Category	Dietary Justification	EcoCell

Mesodma hensleighi	2.86	Very Small	Animal-Dominated Omnivore	Wilson et al. (2012)	VS:ADO
Mesodma formosa	3.55	Small	Animal-Dominated Omnivore	Wilson et al. (2012)	S:ADO
Mesodma thompsoni	3.98	Small	Animal-Dominated Omnivore	Wilson et al. (2012)	S:ADO
Cimexomys minor	3.93	Small	Animal-Dominated Omnivore	Wilson et al. (2012)	S:ADO
Cimexomys gratus	4.72	Small	Animal-Dominated Omnivore	Wilson et al. (2012)	S:ADO
Stygimys kuszmauli	5.35	Medium	Herbivore	Wilson et al. (2012)	M:H
Thylacodon montanensis	3.93	Small	Animal-Dominated Omnivore	Wilson (2013,14)	S:ADO
Procerberus formicarum	4.34	Small	Faunivore	Smith (2017)	S:F
Mimatuta morgoth	5.72	Medium	Plant-Dominated Omnivore	Smith (2017)	M:PDO
Mimatuta minuial	5.81	Medium	Plant-Dominated Omnivore	Smith (2017)	M:PDO
Baioconodon nordicum	6.56	Medium	Plant-Dominated Omnivore	Smith (2017)	M:PDO
Baioconodon engdahli	6.27	Medium	Plant-Dominated Omnivore	Smith (2017)	M:PDO
Protungulatum donnae	5.42	Medium	Animal-Dominated Omnivore	Smith (2017)	M:ADO
Oxyprimus erikseni	4.86	Small	Animal-Dominated Omnivore	Smith (2017)	S:ADO

Table 3.5 Summary table of estimated body masses, dietary category, and EcoCell for the early recovery subphase fauna. *—Denotes a tooth position other than m1 was utilized, m2 and M1 respectively.

Taxa	Body Mass (ln g)	Body Mass Citation	Size Category	Dietary Category	Dietary Justification	EcoCell
Mesodma hensleighi	2.86	Wilson et al. (2013)	Very Small	Animal-Dominated Omnivore	Wilson et al. (2012)	VS:ADO
Mesodma formosa	3.55	Wilson et al. (2013)	Small	Animal-Dominated Omnivore	Wilson et al. (2012)	S:ADO
Mesodma thompsoni	3.98	Wilson et al. (2013)	Small	Animal-Dominated Omnivore	Wilson et al. (2012)	S:ADO
Cimexomys minor	3.93	Wilson et al. (2013)	Small	Animal-Dominated Omnivore	Wilson et al. (2012)	S:ADO
Cimexomys gratus	4.72	Wilson et al. (2013)	Small	Animal-Dominated Omnivore	Wilson et al. (2012)	S:ADO

Procerberus formicarum	4.34	Wilson et al. (2013)	Small	Faunivore	Smith (2017)	S:F
Procerberus cf. *grandis*	6.63*	Clemens (2017)	Medium	Faunivore	Based on similar morphology with *Procerberus formicarum*	M:F
Mimatuta morgoth	5.72	Wilson et al. (2013)	Medium	Plant-Dominated Omnivore	Smith (2017)	M:PDO
Baioconodon sp.	6.42	Wilson et al. (2013)	Medium	Plant-Dominated Omnivore	Smith (2017)	M:PDO
Protungulatum donnae	5.42	Wilson et al. (2013)	Medium	Animal-dominated Omnivore	Smith (2017)	M:ADO
Oxyprimus erikseni	4.86	Wilson et al. (2013)	Small	Animal-dominated Omnivore	Smith (2017)	S:ADO
Periptychidae indet.	5.96*	Smith (2017)	Medium	Plant-dominated Omnivore	Based on similar morphology with *Mimatuta* sp.	M:PDO
Purgatorius sp.	3.68	Clemens (1974), Smith (2017), Wilson Mantilla et al. (2021)	Small	Animal-dominated Omnivore	Smith (2017)	S:ADO

Table 3.7 Summary table of estimated body masses, dietary category, and EcoCell for the recovered subphase fauna. *—Denotes a tooth position other than m1 was utilized, m2 and M1 respectively.

Taxa	Body Mass (ln g)	Body Mass Citation	Size Category	Dietary Category	Dietary Justification	EcoCell
Mesodma thompsoni	3.98	Wilson et al. (2013)	Small	Animal-Dominated Omnivore	Wilson et al. (2012)	S:ADO
Cimexomys minor	3.93	Wilson et al. (2013)	Small	Animal-Dominated Omnivore	Wilson et al. (2012)	S:ADO
Cimexomys gratus	4.72	Wilson et al. (2013)	Small	Animal-Dominated Omnivore	Wilson et al. (2012)	S:ADO
Catopsalis foliatus	7.80	Wilson et al. (2013)	Large	Herbivore	Wilson et al. (2012)	L:H
Ptilodus cf. P. *tsosiensis*	3.30	Simpson (1937)	Small	Plant-Dominated Omnivore	Wilson et al. (2012)	S:PDO

Stygimys cf. S. *camptorhiza*	5.35	Johnston (1980)	Medium	Herbivore	Wilson et al. (2012)	M:H
Parectypodus armstrongi	3.44	Simpson (1937)	Small	Herbivore	Wilson et al. (2012)	S:H
Taeniolabis lamberti	9.30	Williamson et al. (2016)	Very Large	Herbivore	Wilson et al. (2012)	VL:H
Eucosmodon cf. *E. americanus*	6.17	Wilson et al. (2012)	Medium	Plant-Dominated Omnivore	Wilson et al. (2012)	M:PDO
Neoplagiaulax kremnus	3.82	Scott (2003)	Small	Animal-Dominated Omnivore	Wilson et al. (2012)	S:ADO
Micrcosmodon arcuatus	3.51	Krause (1980)	Small	Animal-Dominated Omnivore	Wilson et al. (2012)	S:ADO
Microcosmodon harleyi	3.51	Krause (1980)	Small	Animal-Dominated Omnivore	Wilson et al. (2012)	S:ADO
Thylacodon montanensis	4.63	Wilson et al. (2013)	Small	Faunivore	Wilson (2013,14)	S:F
Peradectes minor	3.47	Williamson et al. (2012)	Small	Faunivore	Modified from Smith (2017)	S:F
Procerberus formicarum	4.34	Wilson et al. (2013)	Small	Faunivore	Smith (2017)	S:F
Puercolestes simpsoni	5.27	Clemens (2019)		Faunivore	Based on similar morphology with other cimolestids	M:F
Prodiacodon crustulum	4.70	Smith (2017)	Small	Faunivore	Smith (2017)	S:F
Loxolophus schizoophrenus	8.71	Tomida (1981)	Large	Plant-Dominated Omnivore	Based on similar morphology with other *Oxyclaenus spp.*	L:PDO
Bubogonia saskia	8.13*	Scott and Garner (2013)	Large	Animal-Dominated Omnivore	Inferenced based of morphology	L:ADO
Oxyclaenus corax	6.17	Kondrashow and Lucas (2004)	Medium	Animal-Dominated Omnivore	Smith (2017)	M:ADO
Litomylus orthronepius	4.78	Simpson (1937)	Small	Animal-Dominated Omnivore	Based on similar morphology with other *Oxytomodon spp.*	S:ADO
Oxyacodon ferronensis	5.03	Archibald et al. (1983)	Medium	Plant-Dominated Omnivore	Modified from Smith (2017)	M:PDO
Carcinodon aquilonius	6.17	Archibald (1998)	Medium	Animal-Dominated Omnivore	Based on other *Carcinodon spp.* Smith (2017)	M:ADO

Purgatorius janisae	3.40	Clemens (1974)	Small	Animal-Dominated Omnivore	Smith (2017)	S:ADO
Purgatorius unio	3.14	Smith (2017)	Small	Animal-Dominated Omnivore	Smith (2017)	S:ADO
Purgatorius mckeeveri	4.49	Wilson Mantilla et al. (2021)	Small	Animal-Dominated Omnivore	Based on other *Purgatorius* spp. Smith (2017)	S:ADO
Pandemonium dis	4.70	Fox et al. (2014)	Small	Animal-Dominated Omnivore	Smith (2017)	S:ADO
Eoconodon hutchisoni	8.36	Clemens (2011)	Large	Faunivore	Modified from Smith (2017)	L:F
Eoconodon nidhoggi	7.59	Clemens (2011)	Large	Faunivore	Modified from Smith (2017)	L:F
Crustulus fontanus	6.98*	Clemens (2018)		Plant-Dominated Omnivore	Clemens (2018)	M:PDO
cf. *Wortmania*	8.57	Williamson and Brusatte (2013)	Large	Herbivore	Based on inferences in Clemens (2013)	L:H
Nyctithere sp.A	2.9-3.38	Clemens (Personal Communication 2019)	Small	Faunivore	Clemens (Personal Communication 2019)	S:F
Eutherian sp. A	< 5.00	Clemens (Personal Communication 2019)	Small	Faunivore	Clemens (Personal Communication 2019)	S:F
Eutherian sp. B	< 5.00	Clemens (Personal Communication 2019)	Small	Faunivore	Clemens (Personal Communication 2019)	S:F

Table 3.8 Summary table of estimated body masses, dietary category, and EcoCell for the post-recovery subphase fauna. *—Denotes a tooth position other than m1 was utilized. *Litalestes* cf. *L. sternbergi* body mass was estimated using an M2, *Anisonchus* cf. *A. athelas* body mass was estimated using an m2, *Chriacus* cf. *calenancus* body mass was estimated using an m2, ?Promioclaenus sp. body mass was estimated using an m3, ?Goniacodon sp. body mass was estimated using an M1.

Taxa	Body Mass (ln g)	Body Mass Citation	Size Category	Dietary Category	Dietary Justification	EcoCell

Stygimys sp.	5.35	Wilson et al. (2013)	Medium	Herbivore	Wilson et al. (2012)	M:H
Microcosmodon cf. *M. harleyi*	3.51	Krause (1980)	Small	Animal-Dominated Omnivore	Wilson et al. (2012)	S:ADO
?Ectypodus/Parectypodus sp.	3.44	Simpson (1937)	Small	Herbivore	Wilson et al. (2012)	S:H
Mesodma formosa	3.55	Wilson et al. (2013)	Small	Animal-Dominated Omnivore	Wilson et al. (2012)	S:ADO
Mesodma thompsoni	3.98	Wilson et al. (2013)	Small	Animal-Dominated Omnivore	Wilson et al. (2012)	S:ADO
Neoplagiaulax kremnus	3.82	Scott (2003)	Small	Animal-Dominated Omnivore	Wilson et al. (2012)	S:ADO
Neoplagiaulax sp.	3.59	Scott (2005)	Small	Animal-Dominated Omnivore	Wilson et al. (2012)	S:ADO
Litalestes cf. *L. disjunctus*	5.92	Smith (2017)	Medium	Plant-Dominated Omnivore	Smith (2017)	M:PDO
Litalestes cf. *L. sternbergi*	6.16*	Clemens and Wilson (2009)	Medium	Plant-Dominated Omnivore	Based on other *Litalestes* spp. Smith (2017)	M:PDO
Anisonchus cf. *A. athelas*	5.69*	Clemens and Wilson (2009)	Medium	Plant-Dominated Omnivore	Wilson Mantilla (Personal Communication 2019)	M:PDO
?Eoconodon sp.	7.95	Clemens (2011)	Large	Animal-Dominated Omnivore	Smith (2017)	L:ADO
?Betonnia sp.	3.92	Williamson (2011)	Small	Faunivore	Based on similar morphology with *Procerberus*	S:F
?Procerberus sp.	4.34	Wilson et al. (2013)	Small	Faunivore	Smith (2017)	S:F
Prodiacodon cf. *P. crustulum*	4.70	Smith (2017)	Small	Faunivore	Smith (2017)	S:F
Pandemonium dis	4.70	Fox et al. (2014)	Small	Plant-Dominated Omnivore	Smith (2017)	S:PDO
Paromomys farrandi	3.98	Clemens and Wilson (2009)	Small	Plant-Dominated Omnivore	Smith (2017)	S:PDO
Purgatorius cf. *pinecreeensis*	3.94	Scott et al. (2016)	Small	Animal-Dominated Omnivore	Based on other *Purgatorius* spp.	S:ADO
Purgatorius sp. indet.	3.54	Scott et al. (2016), Smith (2017)	Small	Animal-Dominated Omnivore	Based on other *Purgatorius* spp.	S:ADO
Purgatorius unio	3.14	Smith (2017)	Small	Animal-Dominated Omnivore	Smith (2017)	S:ADO

Ursolestes cf. *perpetior*	5.34	Personal measurements	Medium	Animal-Dominated Omnivore	Based on similar morphology with *Purgatorius*	M:ADO
Ursolestes n. sp.	8.91	Personal measurements	Large	Animal-Dominated Omnivore	Based on similar morphology with *Purgatorius*	L:ADO
Loxolophus schizophrenus	8.71	Yukimitsu Tomida (1981)	Large	Plant-Dominated Omnivore	Based on similar morphology with other *Oxyclaenus spp.*	L:PDO
?Carcinodon sp.	6.08	Smith (2017)	Medium	Animal-Dominated Omnivore	Smith (2017)	M:ADO
?Oxyprimus sp.	4.86	Wilson et al. (2013)	Small	Animal-Dominated Omnivore	Smith (2017)	S:ADO
Chriacus ?punitor	6.53	Scott et al. (2012)	Medium	Herbivore	Based on other *Chriacus* spp.Smith (2017)	M:H
Chriacus baldwani	6.72	Smith (2017)	Medium	Herbivore	Smith (2017)	M:H
Chriacus cf. *calenancus*	6.95*	Van Valen (1978)	Medium	Herbivore	Based on other *Chriacus* spp. Smith (2017)	M:H
Mimotricentes subtrigonus	7.25	Smith (2017)		Herbivore	Smith (2017)	L:H
Oxyclaenus cf. *O. simplex*	6.22	Kondrashow and Lucas (2004))	Medium	Animal-Dominated Omnivore	Smith (2017)	M:ADO
Oxyclaenus cf. *O. subbituminus*	5.86	Smith (2017)	Medium	Animal-Dominated Omnivore	Smith (2017)	M:ADO
Prothryptacodon albertensis	5.62	Clemens and Wilson (2009)	Medium	Animal-Dominated Omnivore	Based on similar morphology with *Oxyprimus* spp.	M:ADO
Oxytomodon cf. *O. perissum*	5.42	Smith (2017)	Medium	Animal-Dominated Omnivore	Smith (2017)	M:ADO
?Promioclaenus sp.	6.16*	Clemens and Wilson (2009)	Medium	Plant-Dominated Omnivore	Based on similar morphology with *Litalestes* spp.	M:PDO
?Goniacodon sp.	7.38*	Scott et al. (2012)	Large	Animal-Dominated Omnivore	Hovatter (Personal Communication 2022)	L:ADO

CHAPTER 4: INSIGHTS INTO THE ECOLOGY OF THE LATE CRETACEOUS METATHERIAN *DIDELPHODON* USING STABLE ISOTOPE ANALYSES ($\delta^{18}O$ and $\delta^{13}C$)

4.1 ABSTRACT

Didelphodon, known from the Judithian through Lancian of the northern Western Interior of North America, was a member of the metatherian clade, Stagodontidae, possesses dentocranial characteristics that imply a durophagous diet, along with isolated postcranial elements that suggest a possible semiaquatic ecology. However, due to the nature of the Mesozoic fossil record in North America, consisting of primarily isolated elements, there is a degree of uncertainty about past inferences about the ecology of *Didelphodon.* Here we report on the first stable isotope analyses of *Didelphodon*, from the Hell Creek region of northeastern Montana, providing morphology-independent insights into its ecology. Specifically, we utilized the well-established offset in $\delta^{18}O$ values for terrestrial and aquatic taxa to test whether *Didelphodon* was semiaquatic. Moreover, we examined the $\delta^{13}C$ values from *Didelphodon* for potential insights into its dietary ecology. We sampled carbonate from enamel of *Didelphodon* along with contemporaneous members of both Crocodylia and Theropoda to serve as the semiaquatic and terrestrial baselines, respectively. The $\delta^{18}O$ values for *Didelphodon* closely align with those of the semiaquatic crocodilians, both exhibiting 2–3‰ lower values than the terrestrial theropods. *Didelphodon* also had lower $\delta^{13}C$ values than both the crocodilians and theropods, potentially suggesting a different diet, including mollusks and plant materials. Our

results support the hypothesis that *Didelphodon* was semiaquatic, potentially making it the earliest semiaquatic therian known. In addition, our results add to the growing literature suggesting that mammals were diversifying ecologically prior to the Cretaceous-Paleogene mass extinction.

4.2 INTRODUCTION

The Cretaceous-Paleogene mass extinction (K-Pg) has historically been viewed as a major turning point in mammalian evolution from the limited diversity of Mesozoic mammals into the incredible diversity seen in the Cenozoic (Simpson, 1937). The recovery and subsequent evolutionary radiation of mammals following the K-Pg mass extinction is associated with not only increases in taxonomic richness (Lillegraven, 1972; Maas and Krause, 1994; Wilson, 2014; Wilson et al., 2021) but also increases in ecological diversity (i.e., ecological disparity, body mass, diet; Alroy, 1999; Smith et al., 2010; Wilson, 2013; Grossnickle and Newham, 2016; Halliday and Goswami, 2016; Chen et al., 2019; Grossnickle et al., 2019). However, recent fossil discoveries and large-scale clade-level analyses suggest that the ecological radiation of mammals began prior to the K-Pg (Luo, 2007; Wilson et al., 2012; dos Reis et al., 2014). One clade in particular that experienced a pre-K-Pg diversification is the metatherians, the stem-based clade that includes marsupials and their closest relatives (Clemens, 1968; Szalay, 2004; Rougier et al., 1998; Williamson et al. 2014). During the Late Cretaceous, metatherians were taxonomically rich, occupying all northern landmasses, and ecologically more diverse than their eutherian counterparts (Rougier et al., 1998; Vullo et al., 2009; Williamson et al., 2014; Goin et al., 2016; Brannick et al., in review). Representatives from one clade of metatherians, the Stagodontidae, possess dentocranial characteristics that imply a unique dietary ecology among Mesozoic

mammals, durophagy (Clemens, 1966; Lofgren, 1992; Fox and Naylor, 2006; Wilson et al., 2016; Cohen, 2017; Brannick and Wilson, 2020). Specifically, *Eodelphis cutleri* and *Didelphodon vorax* have both been interpreted as durophagous predator-scavengers, suggesting durophagy evolved twice within the clade (Brannick and Wilson, 2020). Moreover, *Didelphodon* has been interpreted as a semiaquatic mammals based on the morphology of isolated postcranial elements, including the tarsal bones and caudal vertebrae (Salazy, 2004; Longrich, 2004; Borths, 2008). However, other authors reject this hypothesis due to difficulties referring the isolated postcranial elements to *Didelphodon* and similarities between the postcranial bone morphologies with other non-aquatic taxa (Fox and Naylor, 2006). For example, Chen and Wilson (2015) established that semiaquatic and semifossorial small mammals have similar postcranial morphology despite differences in ecology due to the high biomechanical demands incurred during both types of locomotion. This ambiguity combined with the fragmentary Mesozoic mammalian fossil record in North America, which consists mainly of isolated teeth, jaws, and postcranial elements, makes it unlikely that morphology alone will help inform us about the autecology of *Didelphodon.* Instead, utilizing morphology-independent methods (i.e., stable isotopes, and dental macro- and microwear) become necessary. Understanding the ecology of *Didelphodon* is crucial to not only to our understanding of the Stagodontidae, but also to further assess the ecological diversity of Mesozoic mammals. Here we report results from the first stable isotope analysis ($\delta^{18}O$ and $\delta^{13}C$) of *Didelphodon* with implications for our understanding of the ecology of the genus.

Stable isotope analyses have been undertaken broadly across extant and extinct mammals as a means to better infer their autecology and the environment around them, utilizing the established relationships between the stable isotope composition of sampled materials and

different biological and environmental factors (Koch et al., 1989; Bocherens et al., 1996; Cerling and Ehleringer, 2000; Clemenz and Koch, 2001; Thewissen et al., 2007; Secord et al., 2008; Amiot et al., 2010; Cullen et al., 2019, 2020). Studies that investigate extinct mammals tend to focus on the most diagenetically resistant materials, including bone, enamel, dentin, and diagenetically resistant isotopes of oxygen ($\delta^{18}O$) and carbon ($\delta^{13}C$) (Kohn and Cerling, 2002). Bone, enamel, and dentin are partially composed of the mineral hydroxyapatite, often referred to as bioapatite (Krueger, 1991; Kohn and Cerling, 2002; Koch, 2007; Sponheimer and Cerling, 2014). The crystal structure of bioapatite allows the substitution of the PO_4^{3-} and OH- ions with numerous other ions, most importantly CO_3^{2-} (carbonate), which is believed to be diagenetically resistant (LeGeros, 1991; Elliot, 1994; Kohn and Cerling, 2002). Enamel is particularly resistant to diagenetic changes due to its larger crystals, lower porosity, and more compact structure compared to bone or dentin (Lowen and Weiner, 1989; LeGeros, 1991). As a result, the vast majority of studies that investigate $\delta^{18}O$ and $\delta^{13}C$ rely on the carbonate substitutions in enamel (Sponheimer and Cerling, 2014). Investigating both $\delta^{18}O$ and $\delta^{13}C$ can provide key insights into the ecology of extinct mammals and their environment.

The oxygen isotopic composition of enamel has been primarily utilized as a proxy for understanding paleoclimates and habitat use (Koch et al., 1989, 1995; Bryant et al., 1996; Clementz and Koch, 2001). For terrestrial mammals, the $\delta^{18}O$ of enamel is influenced by the oxygen composition of the food and water, along with physiological processes. The $\delta^{18}O$ values obtained from enamel tend to reflect the values of the meteoric water, which varies depending on temperature and precipitation (Kohn, 1996; Koch 2007). For this reason, $\delta^{18}O$ can be used to determine different aspects of the paleoclimate, including temperature and precipitation (Schoeninger et al., 2003). Moreover, all things being equal, the oxygen isotopic composition of

enamel varies due to differences in habitat use, specifically between semiaquatic or aquatic and terrestrial vertebrates (Bocherens et al., 1996; Clemenz and Koch, 2001; Thewissen et al., 2007; Amiot et al., 2010). For both living and fossil communities, semiaquatic or aquatic vertebrates tend to have lower $\delta^{18}O$ values (2–3‰ shift) than the coexisting terrestrial animals (Thewissen et al., 2007; Cerling et al., 2008; Amiot et al., 2010). The depletion of $\delta^{18}O$ in semiaquatic or aquatic vertebrates is caused by reduced daily aerial evapotranspiration, which typically results in an enrichment in $\delta^{18}O$ for terrestrial vertebrates compared to meteoric water (Kohn, 1996; Cerling et al., 2008). As a result, $\delta^{18}O$ values can be used to investigate the habitat use of extinct vertebrates.

The carbon isotopic composition of enamel has been widely utilized as a proxy for understanding the dietary ecology of extant and extinct mammals (Bocherens et al., 1996; Cerling and Ehleringer, 2000; Secord et al., 2008; Cullen et al., 2019, 2020). Many of these analyses are based on differences in the photosynthetic pathway of plants consumed by herbivores, specifically CO_2 fixation in C_3 and C_4 plants (Thorp et al., 1989). During photosynthesis in C_3 plants, the heavier carbon isotope ^{13}C is discriminated against and the lighter isotope ^{12}C is preferentially incorporated into its tissues (Farquhar et al., 1982; Cerling and Ehleringer, 2000). In contrast, during the C_4 photosynthetic pathway, nearly all of the carbon, including the heavier isotope, is incorporated into the plant's tissues (Cerling and Ehleringer, 2000). As a result, the $\delta^{13}C$ values for C_4 plants more closely match the atmospheric values, ranging between -9 and -14‰, whereas C_3 plants are typically depleted in ^{13}C resulting in lower values, ranging between -20 and -35‰ (Cerling and Ehleringer, 2000; Condron et al., 2005; Sponheimer and Cerling, 2014). When plants are consumer and digested, carbon is then incorporated into mammalian tissues, including enamel, with an enrichment factor of 9–14‰

depending on the clade (Cerling and Harris, 1999; Tejada et al., 2020). The bimodal distribution in $\delta^{13}C$ values between C_3 and C_4 plants carries over to the $\delta^{13}C$ values for the mammals that eat them, a phenomenon that is called the trophic enrichment factor (TEF, hereafter), allowing for dietary reconstructions. For ecosystems that lack or predate the evolution of the C_4 photosynthetic pathway differences in dietary ecology can still be distinguished by $\delta^{13}C$ values in an exclusively C_3 community (Cerling and Ehleringer, 2000; McFadden and Higgins, 2004; Secord et al., 2008; Tejada et al., 2020). Due to the nature of carbonate analyses, both $\delta^{18}O$ and $\delta^{13}C$ values are recorded, allowing for detailed investigations into mammal ecology and overall community structure.

Here we report on the stable carbon and oxygen composition of tooth enamel from *Didelphodon* from the Hell Creek region of NE Montana. The Hell Creek region is among the best places in the world to study mammals during the last ca. 2-Ma of the Cretaceous due to the large number of known mammalian assemblages integrated into a high-resolution temporal framework (Clemens, 2002; Wilson, 2005 and 2014; LeCain et al., 2014; Hartman et al., 2014; Sprain et al., 2015, 2018). To investigate whether *Didelphodon* was primarily terrestrial or semiaquatic, we also sampled coeval taxa, also from the Hell Creek region, from known terrestrial (small theropods) or semiaquatic (crocodilians) ecologies. If *Didelphodon* was primarily semiaquatic, we predict it's $\delta^{18}O$ to align with the other semiaquatic taxa more closely than the terrestrial taxa. If *Didelphodon* was primarily terrestrial, we predict its $\delta^{18}O$ to align with those of the terrestrial taxa. Moreover, the $\delta^{13}C$ values may provide insights into feeding ecology of *Didelphodon*. Although the exposures in the Hell Creek region preserve a temporal interval that predates the evolution of C_4 plants, we are still able to explore aspects of *Didelphodon* dietary ecology. This analysis represents the first of its kind to report on the stable carbon and

oxygen values from *Didelphodon* and the first to use $\delta^{18}O$ values to test for semiaquatic ecology amongst Mesozoic mammals.

4.3 INSTITUTIONAL ABBREVIATIONS—UWBM, University of Washington Burke Museum of Natural History and Culture, Seattle, Washington, USA.; **DMNH**, Denver Museum of Nature and Science, Denver, Colorado, USA.

4.4 MATERIALS AND METHODS

4.4.1 Specimen Selection and Enamel Preparation

Specimens were collected from the Hell Creek region by UWBM and DMNH field crews. To minimize the potential influence of differences (i.e., climatic changes) among localities, we restricted our sample to specimens from only a few lower Hell Creek localities (UWBM C1111, C1116, C1115 and C1126 and DMNH 3310). We utilized isolated teeth of *Didelphodon*, along with teeth from members of both Crocodylia and Theropoda to serve as the semiaquatic and terrestrial baselines, respectively. Each specimen was molded and cast at UWBM to provide a record of its surface features. Enamel samples were collected, roughly 6–9 mg, from each specimen using a Kupa ManiPro Passport Portable Nail Filing System with a medium grit carbide drill bit. Any larger pieces of enamel were then crushed into a powder using a mortar and pestle. Pretreatment followed the methodology outlined in Miller et al. (2018). The powdered enamel samples were first treated with 1.5 mL of a 30% hydrogen peroxide solution, agitated, and left to rest for 10 minutes. The samples were then centrifuged for four minutes, and the hydrogen peroxide solution was removed. Following the removal of the hydrogen peroxide solution, the samples were treated with 0.1 mL of 0.1 M acetic acid (per 1 mg of enamel),

agitated, and left for a period of less than four hours. The samples were centrifuged for four minutes, and the acetic acid solution was removed and replaced with 1.5 mL of ultrapure water. After this, the samples were then centrifuged for four minutes, and the solution was replaced with new ultrapure water; this step was repeated twice to ensure neutrality. Following the last rinse with ultrapure water, the solution was removed, the samples were covered with Parafilm, and they were left in a drying oven (60 °C) overnight. Once dried, the samples were weighed, with the ideal mass being 2–4 mg per sample as because the mass spectrometer requires 0.1 mg of pure carbonate and enamel on average is 2–5% carbonate (Xu et al., 2014). Due to the small size of some of the sampled teeth, several specimens failed to yield at least 2 mg of enamel; these samples were still included but were further examined for possible issues resulting from the low enamel mass. On the other hand, several teeth yielded more than 4 mg of enamel and were divided into multiple samples whose $\delta^{18}O$ and $\delta^{13}C$ values were averaged together post-analysis.

4.4.2 Mass Spectrometry

Replicates of three internal reference materials (C1, C2, and CQS2) were included with the enamel samples in each mass spectrometer run to help with calibrating the results. The enamel samples and standards were loaded into the Kiel III Carbonate Device coupled to a Finnigan Delta Plus isotope ratio mass spectrometer for dual-inlet based $\delta^{18}O$ and $\delta^{13}C$ measurements. We utilized acid-prep mass spectrometry rather than laser ablation due to issues regarding access, differing levels of accuracy for oxygen isotope data, and potentially CO_2 contamination. The University of Washington IsoLab does not have a laser ablation system, and due to limitations related to the ongoing COVID-19 pandemic, I was unable to travel to other institutions. Laser ablation analyses tend to yield less accurate $\delta^{18}O$ values than more traditional

methodologies due to potential contamination with diagenetically altered oxygen from the enamel (Cerling and Sharp, 1996; Kohn et al., 1999). Moreover, laser ablation is prone to CO_2 contamination for large samples, which could potentially obscure small differences in both $\delta^{18}O$ and $\delta^{13}C$ values (Cerling and Sharp, 1996). The established difference in values of $\delta^{13}C$ for C_3 and C_4 diets is still present, but differences for C_3 communities may be obscured (Cerling and Sharp, 1996). Due to the nature of this study, which is based in an exclusively C_3 ecosystem and is dependent on small differences in $\delta^{18}O$, we decided to utilize acid-prep mass spectrometry. All $\delta^{18}O$ and $\delta^{13}C$ values are reported on the VPDB scale. We used standard methods for running the Kiel and post-process of data (see University of Washington IsoLab website https://isolab.ess.washington.edu/SOPs/kiel.php). Post-processing was completed in MatLab.

4.4.3 Data Analysis

$\delta^{18}O$ values were converted from VPDB to VSMOW using the methodology outlined in Kim et al. (2015). The $\delta^{18}O$ and $\delta^{13}C$ values were averaged for specimens with multiple samples and a square root of the pooled variance was calculated to aggregate the standard deviations. Multiple two-tailed *t*-tests were run in R using the package *vegan* to compare the $\delta^{18}O$ and $\delta^{13}C$ values across the three sample taxa (six in total). We acknowledge the limitations associated with the small sample sizes and the impacts on any interpretations of *t*-test results. The carbon isotope composition of diet ($\delta^{13}C_{diet}$) was calculated using trophic enrichment factor (TEF) values from Cullen et al. (2020). For *Didelphodon*, we used both the faunivore and herbivore mammalian TEF as Didelphodon has been interpreted as potentially omnivorous (12.80 and 10.50‰, respectively; Wilson et al. 2016). For Crocodylia, we used the faunivore reptilian TEF (8.40‰). For the theropods, we used three different formulas for faunivores: the mammalian, reptilian, and

avian (12.80, 8.40, and 8.30 respectively) following the protocol outline in Cullen et al. (2020). To calculate $\delta^{13}C_{diet}$, we subtracted the TEF from the observed $\delta^{13}C$ value.

4.5 RESULTS

4.5.1 $\delta^{18}O$ and $\delta^{13}C$ Average Values

Didelphodon has the lowest average $\delta^{18}O$ values, followed closely by the crocodilians, and then the theropods (19.18, 19.64, and 22.76‰, respectively; Figure 4.1 and Table 4.1). The theropods have the largest range, between 20.71 and 24.73‰ followed by *Didelphodon*, and then the crocodilians (16.94 and 20.88‰, 17.12 and 20.59‰, respectively; Table 4.1). On average, the sampled theropods had the highest $\delta^{13}C$ value, followed by the crocodilians and then *Didelphodon* (-5.98, -7.44, and -9.12‰, respectively; Figure 4.1 and Table 4.1). *Didelphodon* has the largest range of $\delta^{13}C$ values between -11.25 and -7.12‰ followed by the theropods and then the crocodilians (-8.34 and -5.88‰, -7.58 and -4.01‰, respectively; Table 4.1).

4.5.2. t-test Results

To quantitatively compare the $\delta^{18}O$ and $\delta^{13}C$ values of our sample taxa, we ran multiple *t*-tests (Table 4.2). For $\delta^{18}O$, there is a significant difference ($p \leq 0.05$; Table 4.2) between the values of *Didelphodon* and the crocodilians compared to the theropods ($p = 0.02$ and 0.03, respectively; Table 4.2). There is no significant difference between the $\delta^{18}O$ values for *Didelphodon* and the crocodilians ($p = 0.66$; Table 342). For $\delta^{13}C$, there is a significant difference between the values of *Didelphodon* and the theropods ($p = 0.04$; Table 4.2). However,

there is no significant difference between the $\delta^{13}C$ values of the crocodile with either *Didelphodon* or the theropods ($p = 0.15$ for both; Table 4.2).

4.5.3 Diet

$\delta^{13}C_{diet}$ was calculated using four different TEFs depending on the taxa: either the mammalian faunivore or herbivore, reptilian faunivore, or avian faunivore (Table 4.3). For the theropod, three different TEFs were used to determine $\delta^{13}C_{diet}$ ranged between -14.28‰ (avian faunivore), -14.38‰ (reptilian faunivore), and -18.78‰ (mammalian faunivore; Figure 3.2), depending on the TEF used. For *Didelphodon*, two different TEFs were used resulting in -21.92‰ (mammalian faunivore) and -19.62‰ (mammalian herbivore) for $\delta^{13}C_{diet}$ (Figure 4.2). For the crocodilians, the reptilian faunivore TEF (8.40‰) was used. Crocodilians had a $\delta^{13}C_{diet}$ -15.84‰ on average (Figure 4.2). Overall, *Didelphodon* had the lowest $\delta^{13}C_{diet}$ values, followed by the crocodile and theropods.

4.6 DISCUSSION

4.6.1 Didelphodon: Aquatic or Terrestrial?

To test the hypothesis that *Didelphodon* was semiaquatic, we compared the $\delta^{18}O$ values from the enamel of known aquatic (crocodilians) and terrestrial taxa (theropods) from the same localities. We would expect the $\delta^{18}O$ values for the aquatic taxa to be 2–3‰ lower on average than the terrestrial taxa (Thewissen et al., 2007; Cerling et al., 2008; Amiot et al., 2010). Moreover, we would expect less intra-taxon variation for aquatic taxa compared to terrestrial (Clementz and Koch, 2001). Unlike other studies of Late Cretaceous stable isotopes, we

recovered a clear 2–3‰ difference ($p = 0.03$) between mean $\delta^{18}O$ values for our sample of crocodilians and theropods (Cullen et al., 2020). The difference may be a result of the use of laser ablation in Cullen et al., (2020) compared to standard acid-prep (Cerling and Sharp, 1996). On average, the crocodilians have lower $\delta^{18}O$ values and less inter-individual variation than the theropods (Figure 4.1 and Table 4.1). These results support the already established relationship between habitat usage and $\delta^{18}O$ values and confirm the presence of this relationship in the deep past in the Hell Creek region (Clementz and Koch, 2001; Thewissen et al., 2007; Cerling et al., 2008; Amiot et al., 2010). The $\delta^{18}O$ values for *Didelphodon* are significantly different than those of the theropods but not the crocodilians ($p = 0.02$ and $p = 0.66$, respectively; Table 4.2). On average, the $\delta^{18}O$ values for *Didelphodon* are 2–3‰ lower than those of the theropods, similar to the results for the crocodilians. *Didelphodon* also exhibits lower inter-individual variation compared to the theropods, although it is higher than crocodilians (Table 4.1). The sample size for each of our taxa is small (4–6 individuals), but it is nonetheless comparable to previous work investigating the stable isotope composition of both extinct and extant small mammals (Thewissen et al., 2007; Cullen et al., 2019, 2020). We also acknowledge that the difference in $\delta^{18}O$ values may be related to differences in the environment because $\delta^{18}O$ also tracks changes in temperature or precipitation (Kohn, 1996; Schoeninger et al., 2003; Koch 2007). However, because most of the specimens were collected from spatially or temporally adjacent localities in the lower Hell Creek Formation, the bottom 30 meters of formation (Hartman et al., 2014; Wilson, 2014) during a time of relatively stable paleotemperatures (as determined by carbonate-clumped isotope palaeothermometry; Tobin et al., 2015), we deem this explanation less likely. Therefore, observed differences are likely due to differences in habitat usage rather than differences in temperature or precipitation.

Previous researchers have attempted to illuminate the paleoecology of *Didelphodon* by investigating postcranial elements tentatively referred to this taxon. The morphology of the tarsals, including the nearly spherical calcaneocuboid joint, differs from the primitive metatherian condition, allowing for an increased rotational ability of the foot. Moreover, the morphology of the astragalus indicates extensive mobility between the cuboid and astragalus (Szalay, 1994). Both traits were interpreted to reflect changes in motility necessary for movement in aquatic habitats (Szalay, 1994). Moreover, caudal vertebrae referred to as *Eodelphis* spp., the possible progenitor of *Didelphodon*, along with those assigned to *Didelphodon*, exhibit traits similar to those of a beaver or platypus. The vertebrae are usually large in both length and width and dorsoventrally flattened (Longrich, 2004; Borths, 2008). These features suggest a flattened, oarlike tail that helps with movement in aquatic habitats (Longrich, 2004). However, due to the nature of the Mesozoic mammal fossil record, which consists of primarily isolated bones and teeth, the assignment of the post-cranial remains to *Didelphodon* has been questioned (Fox and Naylor, 2006). In addition, the circular shape of the calcaneocuboid joint appears to neither be exclusive to, no necessary for, aquatic mammalian taxa. Thus, it has also been identified in extant gliding mammals (Szalay and Drawhorn, 1980) and the extant aquatic metatherian *Chironectes minimus* lacks the spherical calcaneocuboid joint and is instead crescentic (Szalay, 1994). Moreover, many postcranial features associated with semiaquatic locomotion are often also linked to semi-fossorial locomotion as well due to the high biomechanical loads incurred (Chen and Wilson, 2015). The uncertainty involved with the morphological characteristics has limited the ability of researchers to infer the paleoecology of *Didelphodon*; however, stable isotope analyses, which are not morphology-based, provide an independent line of evidence supporting the aquatic hypothesis. Acknowledging the limitations

of our study and the post-cranial interpretations, our results support the morphology-based hypothesis that *Didelphodon* was semiaquatic, potentially making it the earliest semiaquatic therian known.

4.6.2 Didelphodon Dietary Inferences

To explore the dietary ecology of *Didelphodon*, we examined the $\delta^{13}C_{diet}$ using taxon appropriate TEFs. Out of the three sampled taxa, *Didelphodon* has the lowest average $\delta^{13}C_{diet}$ out of the sampled taxa, suggesting a different diet than both the crocodilians and the theropods (Figure 3.2; Table 3.3). Based on a suite of craniodental features, including both dorsoventral and mediolateral buttressing and increased canine bending strength, *Didelphodon* has been interpreted as durophagous (Wilson et al., 2016; Brannick and Wilson, 2018). Interestingly, microwear analyses were unable to match the diet of *Didelphodon* to a modern analog due to its shared wear patterns with modern carnivores, along with animal and plant-dominated omnivores. For this reason, *Didelphodon* was interpreted as an omnivore feeding upon hard-shelled invertebrates, vertebrates, and plants (Wilson et al., 2016). The $\delta^{13}C_{diet}$ supports this interpretation of the dietary ecology, suggesting *Didelphodon* fed upon hard-shell invertebrates, potentially benthic, along with plant material all of which would result in lower $\delta^{13}C_{diet}$ than the crocodilians and theropods. Benthic organisms tend to have lower $\delta^{13}C$ values than their pelagic or littoral counterparts due to the increased uptake of respired CO_2 by benthic algae (Rau, 1978, 1980; Zanden and Rasmussen, 1999). As a result, organisms that feed on benthic food sources often have depleted $\delta^{13}C_{diet}$ values compared to other aquatic taxa (Zanden and Rasmussen, 1999; Cullen et al., 2019, 2020). Conversely, freshwater phytoplankton are typically depleted in ^{13}C relative to other aquatic producers (Cloern et al., 2002; Thewissen et al., 2007). The

depletion at the base of the food chain would again result in an overall shift in the $\delta^{13}C_{diet}$ values through the food chain. The $\delta^{13}C_{diet}$ values for *Didelphodon* also fall within the range of C_3 plants (-20 and -35‰; Cerling and Ehleringer, 2000; Condron et al., 2005; Sponheimer and Cerling, 2014); therefore, we cannot rule out the possibility that *Didelphodon* fed upon plant materials. Comparisons with other aquatic, durophagous taxa (i.e., *Champsosaurus* or *Myledaphus*) may help illuminate whether the depleted $\delta^{13}C_{diet}$ values in *Didelphodon* are a result of feeding on bivalves or plant materials (Cullen et al., 2020).

4.6.3 Broader Implications

Metatherians experienced an ecological diversification during the Late Cretaceous that has only recently started to be described and includes arboreal, scansorial, and terrestrial taxa (Szalay, 1994; Luo et al., 2003; Williamson et al., 2014; Chen and Wilson, 2015) (Williamson et al., 2014; Wilson et al., 2014; Goin et al., 2016; Grossnickle and Newham, 2016; Wilson et al., 2016; Grossnickle et al., 2019; Brannick et al., in review). Our reconstructed autecology of of *Didelphodon* adds to this newly recognized ecomorphological diversity of Mesozoic mammals, with *Didelphodon* and possibly earlier members of the Stagodontidae representing the earliest evidence of a semiaquatic ecology within therians (Longrich, 2004; Chen and Wilson, 2015). Along with a diversity of locomotor modes, metatherians also had a range of dietary ecologies during the Cretaceous, including carnivory (soft and hard-bodied insectivores), omnivory, herbivory, and durophagy (molluscivores; Wilson and Riedel, 2010; Wilson, 2013; Williamson et al., 2014; Goin et al., 2016; Grossnickle and Newham, 2016; Grossnickle et al., 2019). *Didelphodon* was not the first mammal to explore a semiaquatic ecology; there are several examples of semiaquatic taxa, including the docodonts *Castorocauda* and *Haldanodon* and the

eutricondonts *Liaoconodon* and *Yanoconodon* (Ji et al., 2006; Chen and Wilson, 2015). However, the Stagodontidae appear to be the only clade of Mesozoic mammals to have expanded into a durophagous dietary category, suggesting that *Didelphodon* had a unique ecology for semiaquatic Mesozoic mammals. Taken together, our results help to further our understanding of the true diversity of Mesozoic mammals and provide a framework for future analyses.

4.7 CONCLUSION

In this study, we report on the first stable isotope analysis of *Didelphodon*, with implications for the ecology of *Didelphodon* and Mesozoic mammals more broadly. Our results suggest that *Didelphodon* represents the earliest known semiaquatic therian mammal, indicating that a semiaquatic ecology evolved independently multiple times among Mesozoic mammals (Ji et al., 2006; Luo, 2007; Chen and Wilson, 2015). The appearance of several of these taxa corresponds to periods of ecological radiation during the Late Jurassic (*Castorocauda* and *Haldanodon*) and Late Creaceous (*Didelphodon*; Ji et al., 2006; Luo, 2007; Grossnickle et al., 2019). The Late Jurassic and Late Cretaceous radiations have been linked to different causal mechanisms, the breakup of Pangea and the radiation of angiosperms, respectively (Close et al., 2015; Grossnickle et al., 2019). As such, the evolution of a semiaquatic ecology appears not to be linked to any specific driver, environmentally or ecologically, but may serve as an avenue to avoid competition with other diversifying terrestrial mammals.

Along with adding to our growing understanding of the ecological diversity of Mesozoic mammals, our results provide a framework for future investigations. For example, *Eodelphis cutleri* has been hypothesized as the progenitor of *Didelphodon* due to similarities in dentocranial characteristics that appear transitional between non-durophagous and durophagous

diets (Brannick and Wilson, 2020). However, the caudal vertebrae referred to *Eodelphis* spp. already exhibit traits similar to those of modern semiaquatic mammals and *Didelphodon* (Longrich, 2004; Borths, 2008). This suggests that Stagodontids evolved a semiaquatic ecology prior to the evolution of durophagy. Stable isotope analyses of *E. cutleri* may provide insights into the timing and order of the acquisition of these unique ecological traits. More broadly, stable isotope analyses should be utilized more widely in ecological studies of Mesozoic mammals, as they constitute an approach that is less impacted by the fragmentary nature of the fossil record than most of morphology-based techniques.

4.8 ACKNOWLEDGEMNTS

We acknowledge that the fossils in this paper were collected on lands that are the traditional territory of the Fort Belknap Assiniboine & Gros Ventre Tribes and Fort Peck Assiniboine & Sioux Tribes. Future field trips will be respectful to the original peoples and sovereignty.

We also thank the people of Jordan, Montana for welcoming us into their community each summer for field collection, current and former members of the Wilson Mantilla Lab (A. Brannick, B. Hovatter, E. Armstrong, K. Meltesen, J. Silviria, I. Newbins, D. DeMar, and E. Augustine) for feedback on the project, former undergraduate assistants K. Sanderson for help with specimen preparation, David Krause for providing access to DMNH specimens, Katherine Anderson for providing access to UWBM specimens, Andrew Schauer for IsoLab assistance and guidance, Katherine Huntington for access to her lab space, the UW PaleoPod for fruitful discussions and support, Thure Cerling and James Ehleringer for IsoCamp training and productive discussions, the U.S. Bureau of Land Management and the Montana State Department of Natural Resources and Conservation for providing paleontological permits, and Greg Liggett, Doug Melton, and Patrick

Rennie for facilitating those permits. Financial support of the Hell Creek Project was provided by the Myhrvold and Havranek Charitable Family Fund, the David B. Jones Foundation, the University of Washington Department of Biology, and the Burke Museum of Natural History and Culture. Financial support was also provided to JRC through National Science Foundation Graduate Research Fellowships, Paleontological Society H. Richard Lane Award, and the Colorado Scientific Society Memorial Research Fund .

4.9 REFERENCES CITED

Amiot, R., Buffetaut, E., Lécuyer, C., Wang, X., Boudad, L., Ding, Z., Fourel, F., Hutt, S., Martineau, F., Medeiros, M. A., Mo, J., Simon, L., Suteethorn, V., Sweetman, S., Tong, H., Zhang, F., & Zhou, Z. (2010). Oxygen isotope evidence for semi-aquatic habits among spinosaurid theropods. *Geology*, *38*(2), 139–142. https://doi.org/10.1130/G30402.1

Bennett, C. V., Upchurch, P., Goin, F. J., & Goswami, A. (2018). Deep time diversity of metatherian mammals: Implications for evolutionary history and fossil-record quality. *Paleobiology*, *44*(2), 171–198. https://doi.org/10.1017/pab.2017.34

Bocherens, H., Koch, P. L., Mariotti, A., Geraads, D., & Jaeger, J.-J. (1996). Isotopic Biogeochemistry (13C, 18O) of Mammalian Enamel from African Pleistocene Hominid Sites. *PALAIOS*, *11*(4), 306–318. https://doi.org/10.2307/3515241

Borths, M. R. (2008). *Digging Past the Dinosaurs?: Locomotor Trends and Mammalian Survivorship at the K–Pg (Cretaceous/Paleogene) Boundary* [Thesis, The Ohio State University]. https://kb.osu.edu/handle/1811/32196

Brannick, A. L., & Wilson, G. P. (2020). New Specimens of the Late Cretaceous Metatherian *Eodelphis* and the Evolution of Hard-Object Feeding in the Stagodontidae. *Journal of Mammalian Evolution*, *27*(1), 1–16. https://doi.org/10.1007/s10914-018-9451-z

Cerling, T. E., & Ehleringer, J. R. (2000). Welcome to the C4 World. *The Paleontological Society Papers*, *6*, 273–286. https://doi.org/10.1017/S1089332600000802

Cerling, T. E., & Harris, J. M. (1999). Carbon isotope fractionation between diet and bioapatite in ungulate mammals and implications for ecological and paleoecological studies. *Oecologia*, *120*(3), 347–363. https://doi.org/10.1007/s004420050868

Cerling, T. E., Harris, J. M., Hart, J. A., Kaleme, P., Klingel, H., Leakey, M. G., Levin, N. E., Lewison, R. L., & Passey, B. H. (2008). Stable isotope ecology of the common hippopotamus. *Journal of Zoology*, *276*(2), 204–212. https://doi.org/10.1111/j.1469-7998.2008.00450.x

Chen, M., & Wilson, G. P. (2015). A multivariate approach to infer locomotor modes in Mesozoic mammals. *Paleobiology*, *41*(2), 280–312. https://doi.org/10.1017/pab.2014.14

Clemens, W. A. (1966). *Fossil Mammals, Type Lance Formation, Wyoming. Part II. Marsupialia*. University of California Publications in Geological Sciences.

Clemens, W. A. (1968). Origin and Early Evolution of Marsupials. *Evolution*, *22*(1), 1–18. https://doi.org/10.2307/2406645

Clementz, M. T., & Koch, P. L. (2001). Differentiating aquatic mammal habitat and foraging ecology with stable isotopes in tooth enamel. *Oecologia*, *129*(3), 461–472. https://doi.org/10.1007/s004420100745

Cloern, J. E., Canuel, E. A., & Harris, D. (2002). Stable carbon and nitrogen isotope composition of aquatic and terrestrial plants of the San Francisco Bay estuarine system. *Limnology and Oceanography*, *47*(3), 713–729. https://doi.org/10.4319/lo.2002.47.3.0713

Close, R. A., Friedman, M., Lloyd, G. T., & Benson, R. B. J. (2015). Evidence for a Mid-Jurassic Adaptive Radiation in Mammals. *Current Biology*, *25*(16), 2137–2142. https://doi.org/10.1016/j.cub.2015.06.047

Codron, J., Codron, D., Lee-Thorp, J. A., Sponheimer, M., Bond, W. J., de Ruiter, D., & Grant, R. (2005). Taxonomic, anatomical, and spatio-temporal variations in the stable carbon and nitrogen isotopic compositions of plants from an African savanna. *Journal of Archaeological Science*, *32*(12), 1757–1772. https://doi.org/10.1016/j.jas.2005.06.006

Cohen, J. E. (2018). Earliest Divergence of Stagodontid (Mammalia: Marsupialiformes) Feeding Strategies from the Late Cretaceous (Turonian) of North America. *Journal of Mammalian Evolution*, *25*(2), 165–177. https://doi.org/10.1007/s10914-017-9382-0

Cullen, T. M., Longstaffe, F. J., Wortmann, U. G., Goodwin, M. B., Huang, L., & Evans, D. C. (2019). Stable isotopic characterization of a coastal floodplain forest community: A case study for isotopic reconstruction of Mesozoic vertebrate assemblages. *Royal Society Open Science*, *6*(2), 181210. https://doi.org/10.1098/rsos.181210

Cullen, T. M., Longstaffe, F. J., Wortmann, U. G., Huang, L., Fanti, F., Goodwin, M. B., Ryan, M. J., & Evans, D. C. (2020). Large-scale stable isotope characterization of a Late Cretaceous dinosaur-dominated ecosystem. *Geology*, *48*(6), 546–551. https://doi.org/10.1130/G47399.1

Daniel Bryant, J., Koch, P. L., Froelich, P. N., Showers, W. J., & Genna, B. J. (1996). Oxygen isotope partitioning between phosphate and carbonate in mammalian apatite. *Geochimica et Cosmochimica Acta*, *60*(24), 5145–5148. https://doi.org/10.1016/S0016-7037(96)00308-0

dos Reis, M., Donoghue, P. C. J., & Yang, Z. (2014). Neither phylogenomic nor palaeontological data support a Palaeogene origin of placental mammals. *Biology Letters*, *10*(1). https://doi.org/10.1098/rsbl.2013.1003

Elliot, J. C. (1994). Structure and Chemistry of the Apatites and Other Calcium Orthophosphates. *Studies in Inorganic Chemistry*, *18*, 68.

Farquhar, G. D., O'Leary, M. H., & Berry, J. A. (1982). On the Relationship Between Carbon Isotope Discrimination and the Intercellular Carbon Dioxide Concentration in Leaves. *Functional Plant Biology*, *9*(2), 121–137. https://doi.org/10.1071/pp9820121

Fox, R. C., & Naylor, B. G. (2006). Stagodontid marsupials from the Late Cretaceous of Canada and their systematic and functional implications. *Acta Palaeontologica Polonica*, *51*(1). https://bibliotekanauki.pl/articles/23125

Goin, F. J., Woodburne, M. O., Zimicz, A. N., Martin, G. M., & Chornogubsky, L. (2016). Dispersal of Vertebrates from Between the Americas, Antarctica, and Australia in the Late Cretaceous and Early Cenozoic. In F. Goin, M. Woodburne, A. N. Zimicz, G. M. Martin, & L. Chornogubsky, *A Brief History of South American Metatherians* (pp. 77–124). Springer Netherlands. https://doi.org/10.1007/978-94-017-7420-8_3

Hartman, J., Butler, R., Weiler, M., & Schumaker, K. (2014). Context, naming, and formal designation of the Cretaceous Hell Creek Formation lectostratotype, Garfield County, Montana. *Special Paper of the Geological Society of America*, *503*, 89–121. https://doi.org/10.1130/2014.2503(02)

Ji, Q., Luo, Z.-X., Yuan, C.-X., & Tabrum, A. R. (2006). A Swimming Mammaliaform from the Middle Jurassic and Ecomorphological Diversification of Early Mammals. *Science*, *311*(5764), 1123–1127. https://doi.org/10.1126/science.1123026

Kim, S.-T., Coplen, T. B., & Horita, J. (2015). Normalization of stable isotope data for carbonate minerals: Implementation of IUPAC guidelines. *Geochimica et Cosmochimica Acta*, *158*, 276–289. https://doi.org/10.1016/j.gca.2015.02.011

Koch, P. L. (2007). Isotopic Study of the Biology of Modern and Fossil Vertebrates. In R. Michener & K. Lajtha (Eds.), *Stable Isotopes in Ecology and Environmental Science* (pp. 99–154). Blackwell Publishing Ltd. https://doi.org/10.1002/9780470691854.ch5

Koch, P. L., Fisher, D. C., & Dettman, D. (1989). Oxygen isotope variation in the tusks of extinct proboscideans: A measure of season of death and seasonality. *Geology*, *17*(6), 515–519. https://doi.org/10.1130/0091-7613(1989)017<0515:OIVITT>2.3.CO;2

Koch, P. L., Zachos, J. C., & Dettman, D. L. (1995). Stable isotope stratigraphy and paleoclimatology of the Paleogene Bighorn Basin (Wyoming, USA). *Palaeogeography, Palaeoclimatology, Palaeoecology*, *115*(1), 61–89. https://doi.org/10.1016/0031-0182(94)00107-J

Kohn, M. J. (1996). Predicting animal δ18O: Accounting for diet and physiological adaptation. *Geochimica et Cosmochimica Acta*, *60*(23), 4811–4829. https://doi.org/10.1016/S0016-7037(96)00240-2

Kohn, M. J., & Cerling, T. E. (2002). Stable Isotope Compositions of Biological Apatite. *Reviews in Mineralogy and Geochemistry*, *48*(1), 455–488. https://doi.org/10.2138/rmg.2002.48.12

Krueger, H. W. (1991). Exchange of carbon with biological apatite. *Journal of Archaeological Science*, *18*(3), 355–361. https://doi.org/10.1016/0305-4403(91)90071-V

Lee-Thorp, J. A., Sealy, J. C., & van der Merwe, N. J. (1989). Stable carbon isotope ratio differences between bone collagen and bone apatite, and their relationship to diet. *Journal of Archaeological Science*, *16*(6), 585–599. https://doi.org/10.1016/0305-4403(89)90024-1

LeGeros, R. Z. (n.d.). Calcium Phosphates in Oral Biology and Medicine (1991). *Search In*.

Lofgren, D. L. (1992). Upper Premolar Configuration of Didelphodon vorax (Mammalia, Marsupialia, Stagodontidae). *Journal of Paleontology*, *66*(1), 162–164.

Longrich, N. (2004). Aquatic specialization in mammals from the Late Cretaceous of North America. *Journal of Vertebrate Paleontology*, *24*(3), 84A-85A.

Lowenstam, H. A., & Weiner, S. (1989). *On Biomineralization*. Oxford University Press.

Luo, Z.-X. (2007). Transformation and diversification in early mammal evolution. *Nature*, *450*(7172), 1011–1019. https://doi.org/10.1038/nature06277

Luo, Z.-X., Ji, Q., Wible, J. R., & Yuan, C.-X. (2003). An Early Cretaceous Tribosphenic Mammal and Metatherian Evolution. *Science*, *302*(5652), 1934–1940. https://doi.org/10.1126/science.1090718

MacFadden, B. J., & Higgins, P. (2004). Ancient ecology of 15-million-year-old browsing mammals within C3 plant communities from Panama. *Oecologia*, *140*(1), 169–182. https://doi.org/10.1007/s00442-004-1571-x

Morales-García, N. M., Gill, P. G., Janis, C. M., & Rayfield, E. J. (2021). Jaw shape and mechanical advantage are indicative of diet in Mesozoic mammals. *Communications Biology*, *4*(1), Article 1. https://doi.org/10.1038/s42003-021-01757-3

Rau, G. (1978). Carbon-13 Depletion in a Subalpine Lake: Carbon Flow Implications. *Science*, *201*(4359), 901–902. https://doi.org/10.1126/science.201.4359.901

Rau, G. H. (1980). Carbon-13/Carbon-12 Variation in Subalpine Lake Aquatic Insects: Food Source Implications. *Canadian Journal of Fisheries and Aquatic Sciences*, *37*(4), 742–746. https://doi.org/10.1139/f80-098

Rougier, G. W., Wible, J. R., & Novacek, M. J. (1998). Implications of Deltatheridium specimens for early marsupial history. *Nature*, *396*(6710), Article 6710. https://doi.org/10.1038/24856

Schoeninger, M. J., Reeser, H., & Hallin, K. (2003). Paleoenvironment of Australopithecus anamensis at Allia Bay, East Turkana, Kenya: Evidence from mammalian herbivore enamel stable isotopes. *Journal of Anthropological Archaeology*, *22*(3), 200–207. https://doi.org/10.1016/S0278-4165(03)00034-5

Scott, C. S., & Fox, R. C. (2015). Review of Stagodontidae (Mammalia, Marsupialia) from the Judithian (Late Cretaceous) Belly River Group of southeastern Alberta, Canada. *Canadian Journal of Earth Sciences*, *52*(8), 682–695. https://doi.org/10.1139/cjes-2014-0170

Secord, R., Wing, S. L., & Chew, A. (2008). Stable isotopes in early Eocene mammals as indicators of forest canopy structure and resource partitioning. *Paleobiology*, *34*(2), 282–300. https://doi.org/10.1666/0094-8373(2008)034[0282:SIIEEM]2.0.CO;2

Sereno, P. C. (2006). Shoulder girdle and forelimb in multituberculates: Evolution of parasagittal forelimb posture in mammals. *Amniote Paleobiology: Perspectives on the Evolution of Mammals, Birds, and Reptiles*, 315–366.

Sponheimer, M., & Cerling, T. E. (2014). Investigating Ancient Diets Using Stable Isotopes in Bioapatites. In *Treatise on Geochemistry* (pp. 341–355). Elsevier. https://doi.org/10.1016/B978-0-08-095975-7.01222-5

Sprain, C. J., Renne, P. R., Clemens, W. A., & Wilson, G. P. (2018). Calibration of chron C29r: New high-precision geochronologic and paleomagnetic constraints from the Hell Creek region, Montana. *GSA Bulletin*, *130*(9–10), 1615–1644. https://doi.org/10.1130/B31890.1

Sprain, C. J., Renne, P. R., Wilson, G. P., & Clemens, W. A. (2015). High-resolution chronostratigraphy of the terrestrial Cretaceous-Paleogene transition and recovery interval in the Hell Creek region, Montana. *Geological Society of America Bulletin*, *127*(3–4), 393–409. https://doi.org/10.1130/B31076.1

Szalay, F. S. (1994). *Evolutionary History of the Marsupials and an Analysis of Osteological Characters*. Cambridge University Press.

Szalay, F. S., & Drawhorn, G. (1980). Evolution and Diversification of the Archonta in an Arboreal Milieu. In W. P. Luckett (Ed.), *Comparative Biology and Evolutionary Relationships of Tree Shrews* (pp. 133–169). Springer US. https://doi.org/10.1007/978-1-4684-1051-8_4

Tejada, J. V., Flynn, J. J., Antoine, P.-O., Pacheco, V., Salas-Gismondi, R., & Cerling, T. E. (2020). Comparative isotope ecology of western Amazonian rainforest mammals. *Proceedings of the National Academy of Sciences*, *117*(42), 26263–26272. https://doi.org/10.1073/pnas.2007440117

Thewissen, J. G. M., Cooper, L. N., Clementz, M. T., Bajpai, S., & Tiwari, B. N. (2007). Whales originated from aquatic artiodactyls in the Eocene epoch of India. *Nature*, *450*(7173), 1190–1194. https://doi.org/10.1038/nature06343

Tobin, T. S., Wilson, G. P., Eiler, J. M., & Hartman, J. H. (2014). Environmental change across a terrestrial Cretaceous-Paleogene boundary section in eastern Montana, USA, constrained by carbonate clumped isotope paleothermometry. *Geology*, *42*(4), 351–354. https://doi.org/10.1130/G35262.1

Ventresca Miller, A., Fernandes, R., Janzen, A., Nayak, A., Swift, J., Zech, J., Boivin, N., & Roberts, P. (2018). Sampling and Pretreatment of Tooth Enamel Carbonate for Stable Carbon and Oxygen Isotope Analysis. *Journal of Visualized Experiments*, *138*, 58002. https://doi.org/10.3791/58002

Vullo, R., Gheerbrant, E., de Muizon, C., & Néraudeau, D. (2009). The oldest modern therian mammal from Europe and its bearing on stem marsupial paleobiogeography. *Proceedings of the National Academy of Sciences*, *106*(47), 19910–19915. https://doi.org/10.1073/pnas.0902940106

Weil, A. (2002). Upwards and onwards. *Nature*, *416*(6883), Article 6883. https://doi.org/10.1038/416798a

Williamson, T. E., Brusatte, S. L., & Wilson, G. P. (2014). The origin and early evolution of metatherian mammals: The Cretaceous record. *ZooKeys*, *465*, 1–76. https://doi.org/10.3897/zookeys.465.8178

Wilson, G. P. (2013). Mammals across the K/Pg boundary in northeastern Montana, U.S.A.: Dental morphology and body-size patterns reveal extinction selectivity and immigrant-fueled ecospace filling. *Paleobiology*, *39*(3), 429–469. https://doi.org/10.1666/12041

Wilson, G. P. (2014). Mammalian extinction, survival, and recovery dynamics across the Cretaceous-Paleogene boundary in northeastern Montana, USA. In G. P. Wilson, W. A. Clemens, J. R. Horner, & J. H. Hartman, *Through the End of the Cretaceous in the Type*

Locality of the Hell Creek Formation in Montana and Adjacent Areas. Geological Society of America. https://doi.org/10.1130/2014.2503(15)

Wilson, G. P., Ekdale, E. G., Hoganson, J. W., Calede, J. J., & Vander Linden, A. (2016). A large carnivorous mammal from the Late Cretaceous and the North American origin of marsupials. *Nature Communications*, *7*(1), Article 1. https://doi.org/10.1038/ncomms13734

Wilson, G. P., Evans, A. R., Corfe, I. J., Smits, P. D., Fortelius, M., & Jernvall, J. (2012). Adaptive radiation of multituberculate mammals before the extinction of dinosaurs. *Nature*, *483*(7390), 457–460. https://doi.org/10.1038/nature10880

Wilson, G. P., & Riedel, J. A. (2010). New Specimen Reveals Deltatheroidan Affinities of the North American Late Cretaceous Mammal Nanocuris. *Journal of Vertebrate Paleontology*, *30*(3), 872–884.

Xu, C., Reed, R., Gorski, J. P., Wang, Y., & Walker, M. P. (2012). The Distribution of Carbonate in Enamel and its Correlation with Structure and Mechanical Properties. *Journal of Materials Science*, *47*(23), 8035–8043. https://doi.org/10.1007/s10853-012-6693-7

Zanden, M. J. V., & Rasmussen, J. B. (1999). Primary consumer delta13C and delta15N and the trophic position of aquatic consumers. *Ecology*, *80*(4), 1395–1396.

4.10 FIGURES

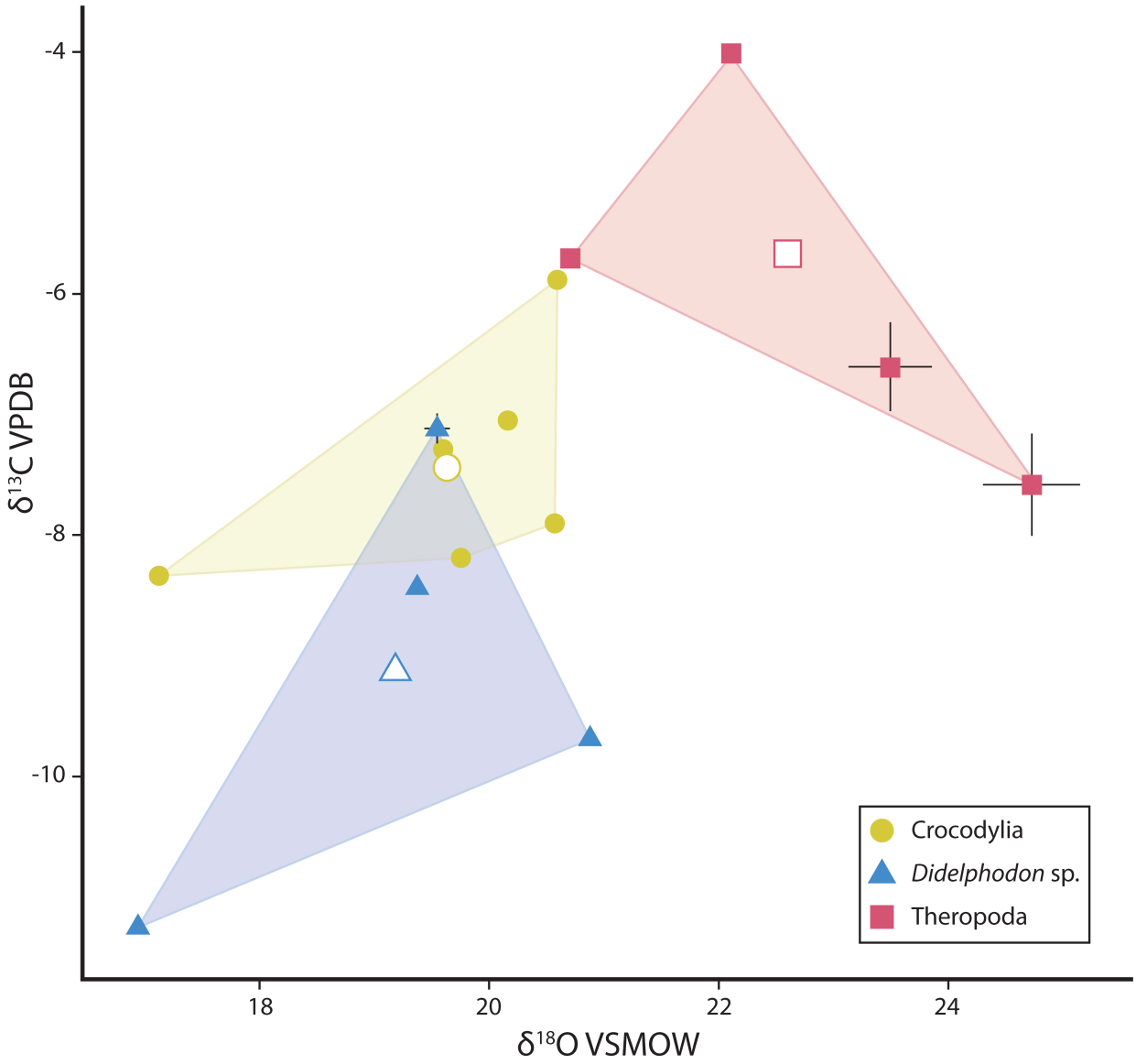

Figure 4.1 Scatterplot with the average $\delta^{18}O$ and $\delta^{13}C$ values for each specimen (colored symbol) along with average for each taxon (white symbol). Although standard deviation was calculated for each specimen, only three values are large enough to be visible.

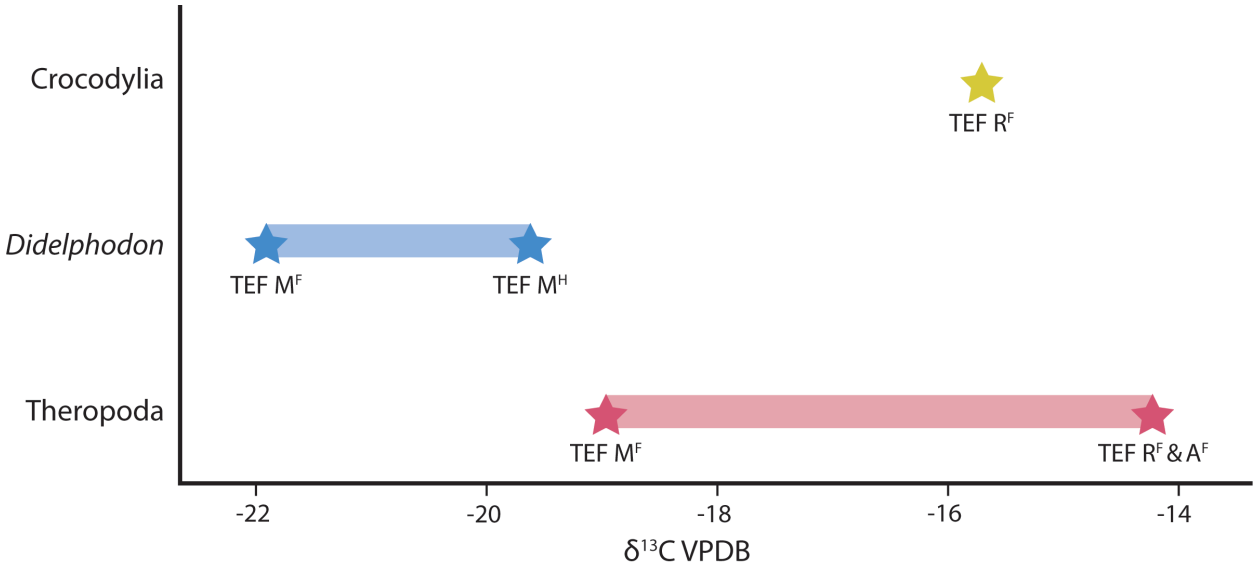

Figure 4.2 Summary plot of the and $\delta^{13}C_{diet}$ calculated using TEF values from Cullen et al. (2020). TEF— Trophic enrichment factor; M^F— Mammalian faunivore; M^H— Mammalian herbivore; R^F— Reptilian faunivore; A^F— Avian faunivore

4.11 TABLES

Table 4.1 Summary table of the average $\delta^{18}O$ and $\delta^{13}C$ values for each specimen and total average for each taxon. $\delta^{18}O$ VSMOW was calculated using the methodology outlined in Kim et al. (2015). N— The number of samples per specimen.

Specimen Number	Taxa	N	$\delta^{13}C$ VPDB	Standard Deviation (C)	$\delta^{18}O$ VPDB	Standard Deviation (O)	$\delta^{18}O$ VSMOW
UWBM 107336	Crocodylia	2	-8.19	0.016	-10.83	0.049	19.77
UWBM 196159	Theropoda	2	-4.01	0.029	-8.55	3.315	22.11
DMNH 55218	*Didelphodon*	1	-11.25	0.056	-13.56	0.350	16.94
UWBM 94405	Crocodylia	3	-7.05	0.027	-10.43	0.031	20.16
UWBM 91435	*Didelphodon*	3	-9.69	0.037	-9.74	0.052	20.88
UWBM 94694	Crocodylia	1	-7.29	0.030	-10.98	0.039	19.60
UWBM 107364	Crocodylia	1	-8.34	0.024	-13.38	0.032	17.12
UWBM 89829	Crocodylia	3	-5.88	0.037	-10.02	0.080	20.59
UWBM 91434	*Didelphodon*	2	-8.44	0.016	-11.20	0.036	19.37

UWBM 105143	Theropoda	1	-5.71	0.013	-9.91	0.043	20.71
UWBM 105835	Crocodylia	1	-7.90	0.043	-10.04	0.026	20.57
UWBM 115538	*Didelphodon*	1	-7.12	0.102	-11.03	0.090	19.55
UWBM 93092	Theropoda	1	-7.58	0.414	-6.00	0.061	24.73
UWBM 115481	Theropoda	3	-6.61	0.350	-7.20	0.041	23.49
Average	Crocodylia	6	-7.44	0.913	-10.95	1.257	19.63
Average	*Didelphodon*	4	-9.12	1.762	-11.38	1.591	19.18
Average	Theropoda	4	-5.98	1.520	-7.91	1.685	22.76

Table 4.2 Summary table of the *t*-test results.

Isotope	Taxa 1	Taxa 2	*p*-value
$\delta^{13}C$	*Didelphodon*	Crocodylia	0.152
$\delta^{13}C$	*Didelphodon*	Theropoda	0.036
$\delta^{13}C$	Crocodylia	Theropoda	0.151
$\delta^{18}O$	*Didelphodon*	Crocodylia	0.662
$\delta^{18}O$	*Didelphodon*	Theropoda	0.024
$\delta^{18}O$	Crocodylia	Theropoda	0.026

Table 4.3 Summary table of the $\delta^{13}C_{diet}$ calculated using TEF values from Cullen et al. (2020).

Specimen Number	Taxa	$\delta^{13}C$ VPDB	$\delta^{13}C_{diet}$ Mammalian Faunivore	$\delta^{13}C_{diet}$ Mammalian Herbivore	$\delta^{13}C_{diet}$ Reptilian Faunivore	$\delta^{13}C_{diet}$ Avian Faunivore
UWBM 107336	Crocodylia	-8.19	-	-	-16.59	-
UWBM 196159	Theropoda	-4.01	-16.81	-	-12.41	-12.31
DMNH 55218	*Didelphodon*	-11.25	-24.05	-21.75	-	-
UWBM 94405	Crocodylia	-7.05	-	-	-15.45	-
UWBM 91435	*Didelphodon*	-9.69	-22.49	-20.19	-	-
UWBM 94694	Crocodylia	-7.29	-	-	-15.69	-
UWBM 107364	Crocodylia	-8.34	-	-	-16.74	-
UWBM 89829	Crocodylia	-5.88	-	-	-14.28	-
UWBM 91434	*Didelphodon*	-8.44	-21.24	-18.94	-	-
UWBM 105143	Theropoda	-5.71	-18.51	-	-14.10	-14.01
UWBM 105835	Crocodylia	-7.90	-	-	-16.30	-
UWBM 115538	*Didelphodon*	-7.12	-19.92	-17.62	-	-
UWBM 93092	Theropoda	-7.58	-20.38	-	-15.98	-15.88
UWBM 115481	Theropoda	-6.61	-19.41	-	-15.01	-14.91
Average	Crocodylia	-7.44	-	-	-15.84	-
Average	*Didelphodon*	-9.12	-21.92	-19.62	-	-
Average	Theropoda	-5.98	-18.78	-	-14.38	-14.28

CHAPTER 5: CONCLUDING REMARKS

The studies presented in this dissertation use interdisciplinary data and quantitative analyses to assess (i) the biotic recovery of mammals following the Cretaceous-Paleogene (K-Pg) mass extinction, both the taxonomic and ecological aspects; and (ii) the unique ecology of the metatherian *Didelphodon* and its implications for the ecological diversity of Mesozoic mammals. Here, I summarize the major conclusions from each study.

Chapter 2

- Utilizing the new mammalian faunal data along with new stratigraphic observations, we proposed a new model for mammalian recovery following the K-Pg mass extinction event. Specifically, we subdivided the established 'disaster' and 'recovery' into early and late sub-phases to allow for a more granular view of biotic recovery in mammalian communities.
- Our results suggest differences in the length of the disaster phase of recovery between the Hell Creek region and the Denver Basin (80 ka and up to 128 ka following the Cretaceous-Paleogene boundary (KPB), respectively). The length of the disaster phase may be related to a number of abiotic and biotic factors, including environmental instability related to Deccan Trap volcanism, the timing of recovery of the angiosperms, and the potential spatial variation in angiosperm recovery.
- The transition between the disaster phase and recovery phase occurred between the first 100 ka and 300 ka following the KPB.

- Immigrant taxa began to colonize the post-extinction ecosystems immediately after the KPB, during the early disaster sub-phase. However, they do not become fully established until the late disaster sub-phase, likely as a result of the disappearance of most ‘dead clades walking’. In-situ diversification of taxa lagged behind, beginning after the first 300 ka following the KPB.

Chapter 3

- The taxonomic and ecological recovery of mammals from the Hell Creek region likely occurred in tandem, with both reaching Pre-mass-extinction levels of richness roughly 500–900 ka following the KPB.
- The diversification of angiosperms may have influenced the patterns of ecospace reoccupation, specifically for the archaic ungulate eutherians and multituberculates. However, our results suggest that archaic ungulates may have driven a reduction in ecospace occupation for multituberculates.
- The timing of the transition between the Disaster and Recovery phases was likely influenced by both abiotic and biotic factors, including Deccan Traps volcanism and the recovery of angiosperms. However, the concordance between the recovery of angiosperms and the end of the Disaster phase is potentially a local signal within the Hell Creek region.
- The transition between the Recovery and Recovered phases was potentially influenced by a warming interval that may have facilitated increased immigration and in situ diversification.

Chapter 4

- The $\delta^{18}O$ values obtained from the enamel of *Didelphodon* are more closely aligned with the values from aquatic crocodilians than terrestrial theropods, suggesting a semiaquatic ecology. This interpretation is also supported by previous analyses of postcranial elements.
- *Didelphodon* has the lowest average $\delta^{13}C_{diet}$ suggesting a different diet than the sampled crocodilians and theropods. Potential food sources for *Didelphodon* include hard-shell invertebrates, either benthic or those that feed upon freshwater phytoplankton, or plant material.
- Our results suggest that *Didelphodon* is the earliest evidence of a semiaquatic ecology within therian mammals, adding to the diversity of Mesozoic mammal ecologies. Although *Didelphodon* was not the first mammal to explore a semiaquatic ecology, the combination of a durophagous diet suggests a unique ecology of *Didelphdon* compared to other semiaquatic Mesozoic mammals.
- Future investigations into the ecology of Mesozoic mammals should utilize stable isotopes as a means to combat the paucity of postcranial elements.